AGARD-CP-573

AGARD

ADVISORY GROUP FOR AEROSPACE RESEARCH & DEVELOPMENT
7 RUE ANCELLE, 92200 NEUILLY-SUR-SEINE, FRANCE

AGARD CONFERENCE PROCEEDINGS 573

Environmental Factors in Electronic Warfare Related to Aerospace Systems

(Les facteurs d'environnement en guerre électronique relatifs aux systèmes aérospatiaux)

Papers presented at the Sensor and Propagation Panel Symposium, held at Pratica di Mare AFB (Rome), Italy 8-11 May 1995.

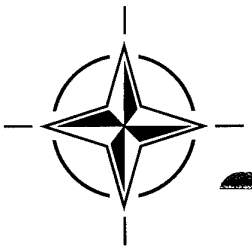

NORTH ATLANTIC TREATY ORGANIZATION

Published January 1996

Distribution and Availability on Back Cover

DISCLAIMER NOTICE

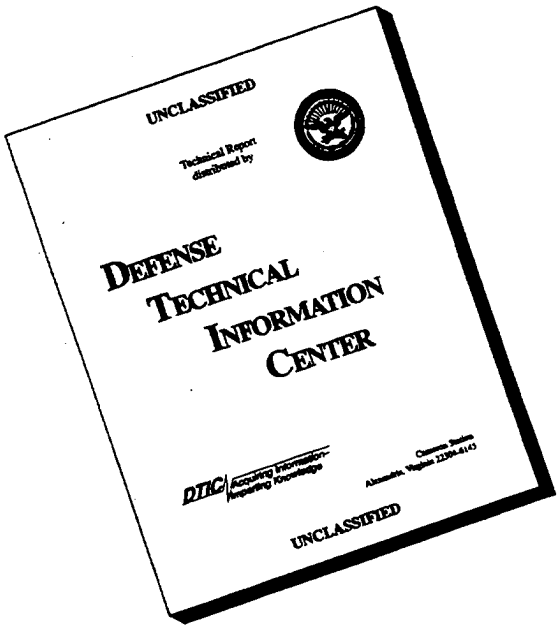

THIS DOCUMENT IS BEST QUALITY AVAILABLE. THE COPY FURNISHED TO DTIC CONTAINED A SIGNIFICANT NUMBER OF PAGES WHICH DO NOT REPRODUCE LEGIBLY.

AGARD-CP-573

AGARD

ADVISORY GROUP FOR AEROSPACE RESEARCH & DEVELOPMENT
7 RUE ANCELLE, 92200 NEUILLY-SUR-SEINE, FRANCE

AGARD CONFERENCE PROCEEDINGS 573

Environmental Factors in Electronic Warfare Related to Aerospace Systems

(Les facteurs d'environnement en guerre électronique relatifs aux systèmes aérospatiaux)

Papers presented at the Sensor and Propagation Panel Symposium, held at Pratica di Mare AFB (Rome), Italy 8-11 May 1995.

North Atlantic Treaty Organization
Organisation du Traité de l'Atlantique Nord

The Mission of AGARD

According to its Charter, the mission of AGARD is to bring together the leading personalities of the NATO nations in the fields of science and technology relating to aerospace for the following purposes:

- Recommending effective ways for the member nations to use their research and development capabilities for the common benefit of the NATO community;
- Providing scientific and technical advice and assistance to the Military Committee in the field of aerospace research and development (with particular regard to its military application);
- Continuously stimulating advances in the aerospace sciences relevant to strengthening the common defence posture;
- Improving the co-operation among member nations in aerospace research and development;
- Exchange of scientific and technical information;
- Providing assistance to member nations for the purpose of increasing their scientific and technical potential;
- Rendering scientific and technical assistance, as requested, to other NATO bodies and to member nations in connection with research and development problems in the aerospace field.

The highest authority within AGARD is the National Delegates Board consisting of officially appointed senior representatives from each member nation. The mission of AGARD is carried out through the Panels which are composed of experts appointed by the National Delegates, the Consultant and Exchange Programme and the Aerospace Applications Studies Programme. The results of AGARD work are reported to the member nations and the NATO Authorities through the AGARD series of publications of which this is one.

Participation in AGARD activities is by invitation only and is normally limited to citizens of the NATO nations.

Published January 1996

ISBN 92-836-1028-8

Printed by Canada Communication Group
45 Sacré-Cœur Blvd., Hull (Québec), Canada K1A 0S7

Environmental Factors in Electronic Warfare Related to Aerospace Systems

(AGARD CP-573)

Executive Summary

An in-depth knowledge of the characteristics of the propagation medium and how they should/could be modified is essential in order to obtain more efficient sensors for aerospace systems. During the symposium the effects of environmental factors on the different disciplines relating to EW were widely analyzed, and all relevant aspects were considered including among others:

— The effect of interference in the ionosphere on various satellite systems, and the propagation mechanisms affecting countermeasures against EO and laser systems.

— The layering of appropriate paints as a means of protecting airbase structures in more than one band, as well as camouflage as a measure against radar sensors.

— The disruptive potential of high-power microwaves, and the exploitation of SMART munitions.

Considering the problem of reduction of aircraft signature, evidence was provided that it is now possible to achieve this by an accurate definition of the mission profile. Finally, several solutions were offered to protect aircraft during peace-keeping operations, i.e. an active self protection laser system against optical seeker head missiles.

Les facteurs d'environnement en guerre électronique relatifs aux systèmes aérospatiaux

(AGARD CP-573)

Synthèse

L'amélioration de l'efficacité des senseurs des systèmes aérospatiaux passe par l'acquisition de connaissances très complètes concernant les caractéristiques du milieu de propagation, ainsi que par la définition des modifications qu'il serait faisable et souhaitable d'y apporter. Les effets des facteurs d'environnement sur les différentes disciplines se rapportant à la guerre électronique EW ont été largement analysés lors du symposium et tous les aspects connexes ont été examinés, y compris:

— les effets des perturbations ionosphériques sur les différents systèmes satellite, et les mécanismes de propagation ayant un impact sur les contremesures contre les systèmes électro-optiques et laser;

— l'application de couches de peinture appropriées comme moyen de protection des structures implantées sur les bases aériennes sur plusieurs bandes de fréquences, ainsi que le camouflage en tant que mesure de protection contre les senseurs radar;

— le potentiel perturbateur des micro-ondes de grande puissance et l'exploitation de munitions intelligentes SMART.

Concernant le problème de la réduction de la signature radar il a été soutenu qu'il est désormais possible d'y parvenir par la définition précise du profil de la mission. Enfin, différentes solutions ont été proposées pour la protection des aéronefs lors des opérations de maintien de la paix, le problème posé étant celui de l'auto-protection active d'un système laser contre les missiles à têtes chercheuses optiques.

Contents

* Published in the classified supplement, CP-573(S).

* Published in the classified supplement, CP-573(S).
† Paper 13 (unclassified) is printed in both volumes, as the discussion sheet relating to this paper is classified.

* Published in the classified supplement, CP-573(S).

Theme

Environmental factors have to be considered in all kinds of electronic warfare (EW) scenarios and with respect to the EW-performance of military systems in any part of the electromagnetic wave spectrum. Political changes have led or lead to appropriate modifications of EW-scenarios, and continuous progress is being achieved in EW-analysis and system technologies in the entire spectrum, from optical to extremely low frequencies.

Relevant environmental aspects of aerospace sensor technology include characteristics of the sensor near-field, or site effects, and the propagation path with natural or anthropogenic obstacles and attenuating elements in the atmosphere, such as obscurants and scatter elements (including chaff). An appropriate selection of frequencies and EW-performance is interrelated. Some propagation properties may be influenced by artificial modification. The adaptivity and thus the survivability of systems is of paramount importance; they depend on the prompt recognition of and reaction to EW-related changes in such environmental conditions. Electronic/optical counter-measures and counter-countermeasures (including, for example, camouflage, terrain masking, and emission control) as well as electronic support measures (including, for example, direction-finding) are to be considered. Examples of typical objectives may be high jamming efficiency, or on the other hand, good anti-jamming performance with low probability of exploitation (detection and interception).

With particular emphasis on aerospace systems, this symposium was therefore proposed to address recent progress and predicted future advancement in the areas mentioned; it offered the possibility to present and discuss new EW-concepts and related environmental effects. Characteristics and vulnerability of present-day and particularly future airborne and surface-support systems in surveillance, communications, command and control and navigation are taken into account. Attention was directed at adaptation of aerospace systems and mitigation of their vulnerability.

The symposium covered the following topics:

— Survey of threat and EW scenarios for aerospace systems.

— Relevant environmental effects with respect to aerospace systems in the applicable portions in the entire spectrum from optical/infrared frequencies to the ELF range.

— Environmental control (including artificial modification of propagation media).

— Aerospace system aspects.

— Advances in environment-oriented EW-analysis and modelling as related to aerospace systems.

— Environmental aspects of emerging EW-concepts and future outlook with the focus on aerospace systems.

Thème

Les facteurs d'environnement doivent être pris en compte dans tous les différents scénarios de guerre électronique (EW), ainsi que pour les performances EW des systèmes militaires dans tout le spectre des ondes électromagnétiques. Les scénarios EW ont été, et seront modifiés pour tenir compte de changements d'ordre politique. Des progrès sont réalisés en permanence dans le domaine de l'analyse EW et les technologies systèmes dans tout le spectre de fréquences, de l'optique jusqu'aux très basses fréquences.

Les aspects d'environnement relevant des technologies des senseurs aérospatiaux comprennent les caractéristiques du champ proche des senseurs, ou les effets de site, ainsi que les trajets de propagation avec obstacles naturels et anthropocentriques et les effets atténuants de l'atmosphère, tels que les obscurcissants et les éléments de diffusion (y compris les chaffs).

La corrélation est faite entre un certain nombre de fréquences représentatives et les performances du système EW. Certaines caractéristiques de propagation peuvent être influencées par des modifications artificielles. L'adaptation, et donc les capacités de survie des systèmes sont d'une importance capitale; l'obtention de ces qualités passe par la détection rapide des modifications. Les contre-mesures et les contre-contre-mesures électroniques/optiques (y compris, par exemple, le camouflage, le masquage du terrain et le contrôle des émissions), ainsi que les aides électroniques (y compris, par exemple, la goniométrie) doivent être prises en considération. Parmi les exemples des buts recherchés figurent le brouillage à hautes performances ou, inversement, l'antibrouillage performant à faible probabilité d'exploitation (détection et interception).

Ce symposium, qui a concerné particulièrement les systèmes aérospatiaux, a donc été proposé, afin d'examiner les progrès récents et les avancées prévues dans les domaines en question; il a permis la présentation et la discussion des nouveaux concepts EW et des effets d'environnement connexes. Le symposium a tenu compte des caractéristiques et de la vulnérabilité des systèmes, aéroportés et ceux servant au support logistique, en surveillance, en commandement et contrôle et en navigation. Une attention particulière a été portée sur l'adaptation des systèmes aérospatiaux et l'atténuation de leur vulnérabilité.

Le symposium a traité des sujets suivants:

— tour d'horizon de la menace et des scénarios pour systèmes EW

— les effets d'environnement par rapport aux systèmes aérospatiaux dans les secteurs applicables de l'ensemble du spectre, de l'optique/infrarouge jusqu'aux fréquences mégamétriques

— le contrôle de l'environnement (y compris la modification artificielle des moyens de propagation)

— les aspects systèmes aérospatiaux

— les progrès réalisés en analyse et modélisation EW de l'environnement du point de vue des systèmes aérospatiaux

— les aspects d'environnement des nouveaux concepts d'EW et les perspectives d'avenir, surtout en ce qui concerne des systèmes aérospatiaux.

Sensor and Propagation Panel

Chairman: Prof. D.H. HÖHN
FGAN
Forschungsinstitut für Optik
Schloss Kressbach
D-7400 Tübingen
Germany

Deputy Chairman: Mr. F. CHRISTOPHE
Dept. Micro-ondes
ONERA-CERT Toulouse
BP 4025
2, Avenue E. Belin
31055 Toulouse Cedex
France

TECHNICAL PROGRAMME COMMITTEE

Co-Chairmen:

Dr. H.J. Albrecht (GE)
Mr. G. Wyman (UK)

Programme Committee Members:

Dr. W.A. Flood (US)
L'ICA P. Fuerxer (FR)
Dr. P. Kossey (US)
Prof. J. Nitsch (GE)
Lt. Colonel P-L. Mancini (IT)
Dr. P. Hildebrand (SHAPE, NE)

PANEL EXECUTIVE

Lt. Colonel G. DEL DUCA, IAF

Mail from Europe:
AGARD-NATO
ATTN: SPP Executive
7, rue Ancelle
92200 Neuilly-sur-Seine
France

Phone: 33-1-47.38.57.68

from North America
AGARD-NATO/SPP
PSC 116
APO AE 09777

Fax: 33-1-47.38.57.99

Preface

Electronic Warfare (EW) Systems must operate in hostile environments in which the propagation medium can be modified by natural events and hostile action. The efficiency of sensors is dependent upon their ability to operate in all conditions requiring knowledge of the characteristics of the propagation medium. EW by definition covers a large number of disciplines and the theme of this symposium concerning the Environmental Factors reflected the same wide field of interests; particular attention was directed at Aerospace Systems and their essential surface support.

The meeting commenced with a lead session on Electronic Warfare and Aerospace Environment. Subsequent sessions addressed recent progress and possible future advancement in Environmental Effects and Control, Aspects of Radio-Frequency Systems, Aspects of Electro-Optical Systems, EW-Analysis, Simulation and Modelling, and concluded with a review session on Emerging EW-Concepts.

Forty-three papers were presented during the symposium; it was attended by more than 150 participants. In addition, the meeting represented a forum for fruitful discussions; this and the wide variety of disciplines may have provided the trigger for alternative solutions to known problems.

Gratefully acknowledged are the cooperation and assistance of all who have contributed to the success of the meeting, in particular the members of the Technical Programme Committee, authors, and session chairmen, and the AGARD staff led by Lt. Col. G. Del Duca.

Special thanks are offered to our Italian hosts for the local arrangements at Pratica di Mare and for the excellent support provided during the meeting.

H.J. Albrecht G. Wyman

Editors' Summary

The symposium commenced with a lead session on Electronic Warfare and Aerospace Environment. Subsequent sessions addressed recent progress and possible future advancement in Environmental Effects and Control, Aspects of Radio-Frequency Systems, Aspects of Electro-Optical Systems, EW-Analysis, Simulation and Modelling, and concluded with a review session on Emerging EW-Concepts.

The keynote paper was directed towards the progress made in the area of signal processing in the military context coupled with the aspirations of the users. The paper contains detail of signal processing in the millimeter and optical fields with an indication of the benefits which can accrue. The treatment of uncertainty, inherent in any sensor system, and the increase in the order of correlation leads potentially to higher confidence in the identification of signals.

The lead session continued with a review paper addressing the ionospheric environment and its impact on EW-systems. The paper provided detail of the physics involved and highlighted areas of the globe at which large scintillation effects can be present. Evidence of interference to various satellite systems used for communications, navigation, and surveillance was provided. The implication of exploiting various properties of the ionosphere were also given together with the limitations imposed on the modulation schemes. The second review paper represented the equivalent foundation for IR, UV and Optical bands by providing detail of the various propagation and background mechanisms relevant to countermeasures against electro-optical and laser systems. The paper included a discussion of background target signature, battle effects, sensor specifications, relevant signal processing, atmospheric transmittance and scattering, as well as presently available modelling tools. In addition, aspects of warning systems and target acquisition were dealt with.

Session II devoted to "Environmental Effects and Control" contained papers ranging from the effects of specific paints on the signature of aircraft to the prediction of antenna coupling. The paint aspects were particularly relevant to viewing the structure in more than one band simultaneously and considered the results of composites formed by layering different paints. Also represented were smoke effects on electro-optical systems. Examples of interference with RF navigation, surveillance and communication, with military EHF satellite communications, and possibilities of adaptive interference cancellation were given. Results of injecting antiphase signals were presented and the potential to encompass multiple sources was postulated. Several papers mentioned the impact of scintillation through the ionosphere whilst accessing satellites which consolidated the information given in the relevant review paper. Some extreme examples for the global positioning system (GPS) were cited. In addition, papers concerned the prediction of the shipboard environment, and camouflage measures on airbases against millimeter-wave radar sensors; here experimental results referred to hardened shelters.

Sessions IIIA and IIIB dealt with "Aspects of Radio Frequency Systems". Following a review on LPI radar (low probability of intercept) and a paper on electronic countermeasures (ECM) with synthetic aperture radar (SAR), digital RF memories were discussed together with the considerable benefits that the reduced necessary power brings on the system. The equipment was also part of systems which were addressed in other papers. Two ESM systems (electronic support measures) and their limitations were described. Two papers treated the disruptive potential of high power microwaves (HPM) and the significance of the modulation imposed in the case of guided missiles and other smart munitions. The selection of the excitation was mainly based on the interior resonances of the structure. The presentation inverted the analysis to harden the missiles. Another contribution concerned noise limitations with millimeter-wave seekers. Satellite systems were again discussed and in particular the global positioning system (GPS), where users should investigate the wider context of use and the region of deployment before establishing the error bounds for implementation.

Session IV, entitled "Aspects of Electro-Optical Systems" began with a paper describing the benefits of incorporating the seeker heads in any simulation. In this fashion the temporal reactions within the control loop and other characteristics of countermeasure effectiveness can be tested. In addressing the laser detectors, a novel means of measuring the angle of arrival was demonstrated which is essential if any narrow-beam counter is to be effective. The improved angular information allows the deployment of countermeasures to be optimized. A further presentation concerned missile plume experiments with the analysis of several motors using a spectroradiometer in the band 240 to 290 nm. Additional papers dealt with an active self-protection laser system for aircraft against missiles with optical seeker heads, and aspects of modelling an IR/UV scene in an electronic warfare scenario.

Session V covered "EW-Analysis, Simulation and Modelling". Concerning simulation, a number of papers reported on its fiscal benefits but with the caveat that some restricted flight trials will be necessary. The amount of realism which can now be injected is considerable, as was demonstrated from a recording. This trend is likely to continue with the increase in processing power available and thus the users can anticipate enhanced images for training. Papers dealt with a wide field within the subjects of this session, such as electro-optical and infrared countermeasures (EOCM, IRCM), performance of IR seekers, jamming and interception predictions of HF communications systems. Other subjects were detection of communication, navigation and identification signals, EW-related radar performance in operational environment, validation of EW-systems, and EW simulation integrated in an operative support centre.

Session VI — "Emerging EW-Concepts" — was an attempt to predict the relevant concepts in the near future. The review paper on camouflage of air vehicles provided evidence that reduction of object signatures is possible with the closer co-operation between engineers to discuss the various properties required to meet the aerodynamic and electronic systems. Emphasis was placed on defining the mission profile to determine which stealth concept is paramount during the various phases. Adaptive techniques were again discussed in relationship to jamming efficiency bringing together the digital RF memory and the antenna arrays but requiring a fast onboard processor. Trial results of overflying weapon sensors with a towed decoy were also presented and clearly showed the benefits of the countermeasures. In the IR and optical systems, the trend towards finer resolution on the seekers leads to a higher degree of refinement for the countermeasures. Several ideas were offered as potential counters with the prospect that they may be required to protect the aircraft in earnest as IR seekers proliferate and aircraft on peace keeping missions are subject to attack.

Forty-three papers were presented during the symposium; it was attended by more than 150 participants. In addition, the meeting represented a forum for fruitful discussions; this and the wide variation of disciplines may have provided the trigger for alternative solutions to known problems.

H.J. Albrecht G. Wyman

FUTURE MILITARY ELECTRONIC WARFARE - Where Will Modern Signal Processing Take Us?

Peter C J Hill
Ray C Saull

School of Electrical Engineering & Science
Cranfield University, RMCS
Shrivenham, Swindon, Wilts, SN6 8LA, UK

Tel: ++ 44 01793 785208
Fax: ++44 01793 782146

SUMMARY

Military electronic warfare (EW) is well recognised as a facilitating force multiplier in deciding the outcome of a conflict situation. Its operation depends very largely now on smart electronic signal processing. Modern developments in the fields of digital signal processing (DSP) algorithms, devices and systems and also in processing optical signals have been fast and a number of novel paradigms have emerged which will possibly have important repercussions in the EW arena. Selected cases are described together with research examples to show the progress and applicability of the new techniques. The main purpose of the paper is to focus on those hot signal processing developments which the EW community should be encouraged to monitor very closely.

1 INTRODUCTION & THEME

Recent military history from 1904 through World War 2 to the Persian Gulf Desert Storm operation has shown in no uncertain way that the use of electronic warfare (EW) techniques has been a decisive force multiplier for controlling the tactical battlespace and thus determining the outcome of the war. This multiplier is now preeminently based on the denial of battle information to the enemy whilst retaining and controlling it for friendly use. An example of the intensity of potential *information warfare* is demonstrated by Desert Storm military info-traffic. At its peak, the Allied Communications network managed more than 30,000 radio frequencies, 700,000 telephone calls and 150,000 messages *per day* and also some 500,00 photographs were received from defence satellite systems, U2/TR-1 platforms, AWACS(E-3s), Air Force JSTARS and miscellaneous UAVs during the course of the conflict [1]; moreover, the enemy was radar blinded with up to 2000 ARM missiles launched early on and their C3 centres taken out with smart weapons in the first few hours of the war. Needless to say, much of this technology depended on recent advances in *electronic digital signal processing* - hardware, algorithms and software. And we must not forget the propaganda battle carried out by both sides through the use of global television in order to dominate the perception of war.

So what of the future for EW and allied non-lethal technologies? We argue that information warfare will become pre-eminent and the interplay between 'safe kill' and 'hard kill' a cardinal factor in deciding the outcome.. It is generally agreed now that the battlefield will be digitised and 'all-knowing' through the use of multisensor/multimedia combination linked together through an information highway (infobahn) network. There would be less dependence on traditional land-based platforms such as tanks and much more on robotics and autonomous vehicles with smart and intelligent weapon systems operating from land, sea and air. Electronic protection of these assets would be of paramount importance and the use therefore of modern signal processing would be absolutely vital here. Any side gaining a tactical advantage in the use of modern signal processing technology would have the edge in quickly in determining the outcome of the conflict and this is the main theme of our paper.

We start by considering future threats and countermeasures in electronic information warfare as applied to C3/C4I and also smart weapons systems such as precision guided munitions focusing on emerging technology and techniques relevant to communications and non-communications EW. The potential use of 'hot' signal processing solutions which are emerging from the R&D laboratories will be described through one or two examples in the EW game and the talk will end with systems considerations and some final remarks on the way ahead.

2. THREATS & COUNTERMEASURES - THE EW GAME

EW is a surprise-element facilitator and force multiplier but not a battle winner as such. We need to have an advantage in areas such as,

- Strategic (pre-conflict) data collection
- Monitoring & control of the battlespace
- Overall digitisation of the battlefield
- Operation of C3/C4I networks
- Prevention of fratricide - forces & platforms
- Intercept of comms & non-comms signals
- Self-jamming protection of C3I systems
- Protection of weapon systems & platforms
- Defeat of enemy weapon systems
- Reduction in EA/EPM (development) cycle times

and finally and perhaps more importantly,

- *Integration* of all C2 and weapon platform assets

Paper presented at the AGARD SPP Symposium on "Environmental Factors in Electronic Warfare Related to Aerospace Systems" held in Pratica di Mare AFB (Rome) Italy, from 8-11 May 1995, and published in CP-573.

The key to dominating these areas is now recognised to be secure information handling through electronic data acquisition, signal processing, data fusion and final decision action suitably protected by the use of EW techniques, both EA(ECM) and EPM(ECCM).

An additional and growing threat here is not surprisingly that a fully digitised battlefield will result in an *infoglut* (information overload) and consequent network saturation operating from the level of integrated C3 systems right down to the future 'cyber-soldier' in the field! The solution to this data saturation syndrome is some form of *dimensionality reduction* at critical points in the chain and this will jointly depend on digital signal processing (DSP) techniques and also human computer interface (HCI) considerations. Does the General really want to observe in full the solders/pilots' view of the battlefield in *real-time* when they both operate in 'cyberspace' (and do either of them wish to reveal their electronic signatures)?

Data will have to be enormously compressed and selectively filtered for presentation and this requires rather intelligent signal processing. If this is not done, there will be observational confusion, ambiguous decisions and lack of trust which, in the final event, would lead the military to abandon 'high-tech' methods and revert instead to today's well-tested 'manual' methods.

An important feature of this information wargame scenario is the rapidly closing time gap between the EA and responsive EPM cycle as acted out in the theatre of smart weapons, countermeasures and counter-countermeasures. With the advent of fast-acting *adaptive* DSP techniques the technology edge will effectively disappear (Fig 1).

Finally, three lessons from Desert Storm stand out [2], viz, the IR GW missile is the greatest threat of the late 1990s; the RF countermeasures developed post-Vietnam experience actually work; and lastly, *stealth* if widely introduced, will 'force the re-writing of the RF EW handbook'. So what place signal processing in all this?

3. EMERGING SIGNAL PROCESSING TECHNOLOGY FOR EW

Solid state technology is still running with Moore's Law (processor speed doubles every 4 years) and there appears to be no limit until 0.1μm line widths are reached at the quantum bound. Microprocessor chips are emerging with 1200 MIPS and architectures moving from 64-bit to 128-bit databuses. Moreover 1Gb DRAMs are on the horizon with input/output bandwidths around 400 MHz; in other words performance is similar to available 4Mb/16Mb chips, but capacity 100 times greater. Estimated SPEC int/fp 92 figures are now in the region 300-600 for 64-bit chips with almost 10 million gates consuming around 30-50W. By the turn of the century SPEC int figures will reach 2000 and all key computer components will have vastly improved with typical systems having 7 Gb disk stores and 800 MIP processors, Fig 2 [3].

Generic DSP systems will offer comparable performance and dedicated chips such as neural processors will be 'off the shelf'. By the year 2000 computing will begin to go photonic rather than solely electronic and processor components could then be bussed by optical connections. Display technologies will be similarly advancing with techniques such as wide-angle view colour LCDs emerging.

The important EW-related electronic technologies and techniques can be summarised as

- Available electronic & photonic complexity
- Continued VHSIC and VLSIC technology
- Improved memory - capacity, speed & power
- Adaptability and reconfigurability
- Smart, assisted and intelligent processing
- Fast DSP devices & systems
- Robust algorithmic engineering
- Improved display technology
- Multisensor data fusion
- Parallel computer architectures
- Smart software & development tools
- Re-emergence of analogue techniques.

Applied to EW engineering, signal processing solutions and systems will be complexity and cost driven rather than purely technology led - just about any DSP 'silver bullet' should be possible in principle and automatically fine tuned in the field if necessary. We anticipate that these emerging technologies will strongly impact on many key areas in EW including, for example, battlefield automation, signal detection & intercept, responsive jamming, spoofing & platform protection, satellite remote sensing, weapon control & guidance and indeed the whole field of communications, radar, and laser EW systems.

4. THE HOT SIGNAL PROCESSING TECHNOLOGIES Application to EW

There is no generally agreed taxonomy for these hot technologies, but judging by the active research fields and their concomitant publication intensities, the following areas could perhaps provide EW winners in the future:

- Artificial neural networks (ANNs)
- Fuzzy logic systems (FLS)
- Genetic algorithms (GA)
- Higher order statistics (HOS)
- Wavelet transform processing (WT)
- Chaotic signal processing
- Speech & video coding
- Optical signal processing & switching
- Processing of optical signals

Let us examine these topics in turn and attempt to see where the techniques could be applied to enhancing EW engineering components and systems through various research investigations which have been carried out at RMCS and beyond.

4.1 Artificial neural networks

Artificial neural networks (ANNs) are becoming increasingly popular as a means for processing information. One of the main reasons for this is that their learning abilities for self-organisation make it possible to solve problems whilst avoiding the need to design complex algorithms [4]. An ANN derives its own internal representation of the input data by showing it the required input/output mapping over many training cycles - with or without supervision depending on the network type. Two pre-eminent ANN architectures are the (supervised) multilevel perceptron (MLP) and the (unsupervised) Kohonen self-organising topological map (SOTM), Fig 3. In microprocessor systems there is a clear separation of memory and processing units whilst in ANNs memory and processing capability are distributed across the neurons. Each neuron consists of a number of inputs, each associated with a weight (memory) and typically the product of inputs and weights is summed, passed through a squashing function to limit the output range, and sent on to the next layer of neuron(s). There are various learning paradigms.

The main thrust of applied ANN research is in the area of pattern recognition techniques applied to speech, vision, robotics and AI applications motivated by the desire to emulate biological neural networks with parallel neural net hardware classifiers. Such classifiers often outperform the classical Bayes approach and provide a selection of practical characteristics with trade offs in (memory) complexity, computation, training times, and adaptation requirements. There are very many uses in EW for such classifiers in both the ESM and EPM areas and also in weapon target recognition for GW systems, precision munitions and the like.

At RMCS we have been involved in various ANN EW signal processing investigations over the past ten years. An early study into automatic digital modulation recognition showed that, given suitable waveform moments, an MLP trained with back propagation performed quite as well as schemes based on multivariate analysis of variance (enhanced principal component analysis) and certainly outperformed existing competition for low SNR channels. Again using an MLP network there was a successful investigation into finger printing naval harbour radars; this required a modified training technique and also a method for circumventing the problem of very limited available input data.

The digital rf memory (DRFM) is now a most useful technology for radar platform protection (Fig 4) and, apart from its ECM use it can also be employed as an rf simulator for both simple and coded pulses across a wide spectrum; a 2-bit DRFM is normally sufficient for storing and replicating most currently used radar signals. We tackled the problem of using an ANN processor on a virtual radar threat platform to determine whether or not the return signals had been DRFM processed or were purely skin echoes; results showed we could get down to 3 bits with reasonable confidence in a modest noise environment.

A current doctoral study is investigating the application of various ANN schemes for estimating the direction of arrival (DOA) of radio waves at an antenna array. These schemes have been based on MLP, least-squares assisted ANNs, learning vector quantisation (LVQ) - SOTMs, and also radial basis functions (RBF) applied to both linear and circular arrays. Best results to date give $<1^{\circ}$ resolution down to 6 dB SNRs using LVQ or RBF ANNs with small circular arrays.

In a more recent project we are investigating the use of multiple Kohonen networks (SOTMs) for classifying earth land cover from remotely sensed satellite data; good texture and contour analysis prior to ANN processing is vital. The initial study used SAR image data but better performance is now being obtained from multi-spectral data analysis and even sub-pixel resolution has been reported in the literature. The military have interest in merging multiple-IR and visible band imagery together with terrain elevation data to achieve mission rehearsal simulation tools.

At RMCS we are also involved with an ANN image processing study in moving object recognition currently extending the research by combining with ANN acoustic signatures through techniques such as data fusion for the final decision process. Additionally ANNs have been used for digital image compression where SOTM processing with image sub-blocks can achieve 10-20:1 compression or better with Huffman coding.

Quite evidently, ANN signal processing has ubiquitous application in the EW arena and we have thrown up only a few examples here.

4.2 Fuzzy systems

Computers are excellent at executing highly structured, mathematically-based algorithms, but it is difficult for them to mimic the subtleties of human knowledge and judgement. The solution to this problem is fuzzy logic where specific system input values are mapped onto fuzzy sets with associated 'set-membership' values thus performing non linear mappings similar to an ANN processor [5]. Subject to certain restrictions it can be shown that the weights of an ANN are identical to confidence levels for the truth of individual rules in the corresponding fuzzy rule base. This correspondence becomes important for stability and learning convergence in certain types of fuzzy controller - vital for robust and safety critical applications.

The research thrust is currently with 'neurofuzzy systems' where the neural network can set up and improve rules in the fuzzy logic components (Fig 5) so that the system can modify its behaviour in response to variations in environmental conditions. In EW such a smart processor would be most useful in situations where background EA is used as a countermeasure to confuse friendly sensors, for target designations/recognisers, data fusion & decision systems and possibly also adaptive multimode airborne radars, to mention just a few examples. Progress in this area should be watched very closely by the EW community.

4.3 Genetic algorithms

Genetic algorithms (GAs) are search procedures, operating in the 'soft computing' area, which are based on the mechanics of natural selection and genetics [6]. GA processes resolve the Bellman 'curse of dimensionality' problem and create robust solutions to optimisation and search. Compared with traditional methods they work with a coding of the parameter set, not the parameters themselves; the search is from a population of points, not a single point; GAs use pay off information objectively and also probabilistic transition rules - not deterministics.

In the GA process there is a basic execution cycle which involves selecting candidate solutions according to fitness for reproduction followed by a random mating process through a 'crossover' partial

exchange procedure to produce offspring solutions and mutations. The performance of the new population is then evaluated, eliminating the weaker performers, and the entire process is then iterated. There must be some means to ensure the problem space is comprehensively searched and the population variation properly developed with the three idealised genetic operators of reproduction, crossover and mutation leading to a blind search which avoids analytical gradient techniques.

GAs are extremely flexible with I/O representing a wide variety of phenomena including combinatorial optimisation (e.g. fusion), image processing, software design and system learning. There is evidently great potential here for EW application in areas which require efficient domain independent search heuristics. For example, in the EW game of countermeasure (CM) versus countercountermeasure (CCM) the evolution of ideal CM/CCM solutions might nicely evolve using the GA approach. A more specific possible application here is to synthesise code generators to achieve certain desirable sequence properties such as bounded correlation metrics or interference suppression. At RMCS we intend to feasibility research such areas; we already have some experience in the application of GAs to soft control problems. Additionally the possibility exists of using GAs to adaptively optimise rules in neurofuzzy systems operating in varying environmental conditions as previously stated. Moreover, there is no reason why GA methods cannot be used to 'fine tune' existing solutions in a wide spectrum of optimisation problems. This is a young subject with enormous (gene!) potential.

4.4 Higher order statistical processing

Higher order moments (HOMs) and associated spectra (HOS) provide a correlation-based signal processing framework for studying non-gaussian processes and nonlinear systems without the limitation of phase blindness. HOM processing extends processing beyond second order correlation, power spectral density functions, least squares and eigendecomposition techniques. The techniques extract information due to deviations from gaussianity, recover signal phase characteristics, detect and quantify non-linearities in time series and provide high SNR domain detection, parameter estimation, signal classification and even reconstruction; importantly also, such processing suppresses gaussian noise in systems with unknown spectral characteristics [7]. HOS 'polyspectra' - bispectrum, trispectrum, and beyond - can detect and characterise the type of system nonlinearity from its output data alone.

Undoubtedly HOM processing offers great potential for EW particularly in the ESM/SIGINT area concerned with intercept operations; there may also be application to ELINT and radar pulse sorting but this has yet to be proved. Currently at RMCS we are studying the use of triple correlation techniques for detecting covert direct sequence spread spectrum (DS/SS) signals and estimating their generating functions in the presence of background noise and homomorphic interference such as CDMA channels (Fig 6); early results are encouraging. We have also used HOMs for preprocessing antenna data to enable an adaptive layered network, such as an MLP ANN, to estimate signal direction of arrival (Fig 7). Third order moments work well with circular arrays and compete well with HR techniques such as MUSIC, but considerable dimensionality reduction is required for input to the ANN and here we used principal component analysis (PCA). In such problems, an alternative to using PCA would be to somehow focus on high value HOM components selected from say a Volterra expansion of the complex array signals.

HOM/HOS signal processing is a very fertile area for further EW signal processing research.

4.5 Wavelet transform processing

The wavelet transform (WT) provides a time-scale (time-frequency) analysis of continuous and discrete signals with application to areas such as data compression, image processing and time-frequency spectral estimation [8]. The WT is a direct alternative to the short-time Fourier transform (STFT) and in a sense circumvents the Gabor uncertainty principle so that the analysis resolution is not solely controlled by the window function (Fig 8). The wavelet basis functions are all scaled versions of a common 'mother wavelet' whereas the basis functions of the STFT are all windowed sinusoids. The discrete WT can be conveniently implemented as successive sub-band decomposition using a digital filter bank tree.

The WT can perform better in some situations than the STFT, in particular for extracting signal information from a non-stationary process, but there is a distinct increase in complexity of interpretation of the results. Wavelets may offer advantage for signal intercept analysis in rapidly time-varying dense signal environments but this has yet to be researched. One area where WT processing has potential application is in 'pyramidal' video source encoding - this is a compression technique where users with various link and/or display channel capacities can access video frames accordingly from a single digital source. This could be a useful video format for conveying tactical military imagery through a hierarchical tree structure from high grade to lower grade users.

In general however, it is not yet clear what real advantage WT processing has over more conventional spectral analysis techniques so that application to EW areas such as Doppler radar processing for example, is somewhat uncertain for the time being.

4.6 Chaotic signal processing

Central to the idea of 'chaos' is the realisation that even very simple non-linearities in time series can lead to extremely complex behaviour where an apparently random process is taking place and exhibiting a near-white or coloured power spectrum. There is thus an element of unpredictability or chaos which turns out to be very sensitive to initial conditions and wordlength accuracy of the discretely mapped variables involved. Nevertheless, chaotic sequences can be predicted with some certainty over short timescales providing we have knowledge of the underlying dynamical system. A typical two-dimensional system is the Hénon map (Fig 9 shows one of the two sequences) which, as a 2D plot, would give a 'strange attractor' fractal type of image.

As with conventional autoregressive and moving average (ARMA) linear processing, chaotic time series estimation or prediction requires a suitable parametric model of the chaos generator. This can be estimated using a correlation technique based on a RBF approach [9]. Application to comms EW would include detection of weak signals in chaotic 'noise' such as multipath interference and, in radar and sonar, it may be possible to enhance SNRs and use the RBF technique for tracking. The process may also be useful for low grade cryptographic codes. At RMCS we have used chaotic sequences, inter alia, as DS/SS chip code reference signals in an investigation to enhance LPI performance against delay-and-multiply intercept receivers but, compared with other novel techniques explored, the results were a little disappointing.

There is certainly promise here and more work needs to be done on combining the new techniques with conventional (ARMA) methods so as to gain the best of both worlds.

4.7 Speech and video coding

This is now primarily civil rather than military led technology driven by the goal of achieving high definition multimedia services both at home and in the office [10].

In audio data compression the motivation is to achieve CD-quality digital audio broadcasting (DAB) and in land mobile radio to maximise the bandwidth efficiency (b/s/Hz) through smart speech coding. From the early 64 kb/s PCM systems there were successful ADM and ADPCM derivatives running at 16-32 kb/s but with the military concentrating more on linear predictive techniques such as LPC-10. Sub-band SBC/ATC coding has also been developed but comms EW planners should perhaps note that the choice for the pan European GSM cellular system was RPE-LTP (regular pulse excited - long term prediction) at 13 kb/s. The competition is with the half-rate code excited (CELP) codec at 6.5 kb/s which can get down to 4 kb/s (Fig 10). Coding delay and chip power are important selection criteria. Because redundancy is squeezed out in these codecs FEC channel coding is necessary through BCH, RS or convolutional codecs combined using interleaving and concatenation as necessary.

Speech recognition is an EW related technology which could be important for battlefield voiceprints for say C2; in development hidden Markov modelling (HMMs) is currently the most successful algorithm. Before year 2000 topic-specific, speaker independent recognition of large vocabulary will be available for specific highly structured applications. There will also be major advances in language modelling and, important to the military, voice C2 facilities will be available as software options on most PCs by 1996/97 in niche applications.

In video coding the main civil drivers seem to be the need to provide video on disk, digital terrestrial TV broadcasting and video-on-demand services. The goal is to bring down digital data rates to analogue bandwidths so that compression factors of around 8-20:1 are required. The standard basis codec is the MPEG (Motion Pictures Expert Group) algorithm which is applicable to a variety of video services. The basic MPEG model (there are two variations) is a coding loop involving a DCT variable length encoder with frame memory and motion estimator. Such systems are compatible with packet video streams as in B-ISDN and its progression to ATM circuits.

Much of this video compression technology will be relevant to battlefield information systems where overall communication channel capabilities will be at a premium, and where burst switching for EPM reasons is likely to be prevalent. There is also likely to be application to those precision guided munitions where fast video capture and processing is a cardinal component.

4.8 Optical signal processing and switching

Developments in production technology have brought about commercial integrated optical components for computing and also telecommunications switching [11]. The main benefits of photonic computing/signal processing accrue from the ability of optics to provide high-speed, high-bandwidth processing, parallel architectures/processing, and importantly, no interactions/crosstalk between intersecting beams. Integrated optics can provide efficient structures for complex signal calculations such as matrix multiplication and array processing, vector correlation and convolution and similar functions. Implementation of such operations using integrated optics together with optical fibres, configured as a systolic system, produces a compact and low power processing solution.

Electrical-optical interactions are used in computation . The acousto-optical effect can be used to mix (multiply) signals at a detector and a T-junction guide can effect addition between two beams as can a simple photodiode. Other guided-wave structures support logic-gate operations for all-optical signal processing. In telecommunications, nonlinear optical components in the form of parallel directional couplers have application to space/time division switching exchanges and will be offering an aggregate digital rate at an amazing 1 terabit/sec (10^{12} b/s) - a useful device in EW communications surveillance when densities reach up to 20,000 channels/sec!

Important aspects of processing of optical signals in areas such as EO & IR EW are dealt with below.

4.9 Processing of optical signals

The detection of optical (visual, IR, UV) signals is, to a large extent, still equivalent to the crystal video detector of the early days of RF systems, that is an amplitude detector. However, the optical threat, laser beam riding missiles, laser designators, LIDAR and LADAR as well as directed energy weapons, is upon us and there is a need to extract more information about the signal.

This information is best obtained by processing the signal while it is still photonic rather than after its conversion to electronic form by the detection process. The additional information available is the colour, spatial coherence, temporal coherence and also the polarisation of the signal. Work at RMCS has been concerned with the construction of temporal coherence filters to enable the detection of laser radiation in a high ambient illuminated background. The work was based on the use of a Fresnel Biprism with an optical delay on one side (Fig 11). Any process which produces interference by division of the wavefront thus allowing a delay to be inserted in one half of the wavefront will work.

Other research has been concerned with the measurement of the polarisation state of incoming IR radiation. When IR is emitted at any angle other than normal to the surface the radiation will have a polarisation signature which can be employed to distinguish man-made flat surfaces from naturally occurring ones. When surfaces are smooth and curved then the curvature can also be estimated by these techniques.

A general term for optical processing of the above type is Optical Transform Image Modulation (OTIM) and this holds out much promise for processing of optical signals and maybe signals at other frequencies as well.

5. CONCLUSIONS & FINAL REMARKS

There have recently been a number of important growth areas emerging in the signal processing arena - these include both electronic DSP & photonics and also optical processing of signals. On-going rapid developments in these fields will have enormous repercussions in the EW arena. In particular, there are a number of hot signal processing techniques, currently being researched, which will play a special part in future EW engineering and may even change the very nature of the EW game itself. In this respect, in the paper we have focused first, on the advantages of using statistical processing methods such as neurofuzzy systems

and higher order moments, together with novel ideas in chaotic and also wavelet transform processing; and second, pre-detector processing of optical signals to extract information normally lost in a simple detection process.

The motivation behind the paper is quite simple, viz; there are a number of smart signal processing developments currently active in the R&D laboratories which are potentially applicable to solving future EW engineering problems. The electronic warfare community should closely monitor these activities to ensure that they do not fall on the wrong side of the electronic and information technology edge in the foreseeable future.

April 1995 PCJH/RCS

6. REFERENCES

1. Herskovitz, S.B., "Farewell to Electronic Warfare - Special Report", Microwave Journal, September 92, pp28-42.

2. Streetly, M., "Does Electronic Warfare Work?" Proc. Int. Defence Conference '95, March 1995, Abu Dhabi,, pp720-729.

3. Lewis, T., "Where is Computing Headed", IEEE Computer, August 1994.

4. Lippmann, R.P., "An Introduction to Computing with Neural Nets", IEEE ASSP Magazine, April 1987, pp4-21.

5. Kosko, B., "Neural Networks and Fuzzy Systems", 1992, Prentice-Hall Inc., Englewood Cliffs, NJ.

6. Goldberg, D.E., "Genetic Algorithms in Search, Optimisation, and Machine Learning", 1989, Addison-Wesley Pub., Co., Inc.

7. Nikias, C.L. & Petropulu, A.P., "Higher-Order Spectra Analysis - a nonlinear signal processing framework", 1993, Prentice-Hall Inc., Englewood Cliffs, NJ.

8. Bentley, P.M. & McDonnell, J.T.E., "Wavelet Transforms - an introduction", IEE Els & Comms Eng Journal, 6, 4, August 1994, pp175-186.

9. Kearney, M.J., & Stark, J., "An Introduction to Chaotic Signal Processing", GEC Journal of Research, 1992, 10, 1, pp52-58.

10. Special Feature Issues of IEEE Comms Magazine, November 1993, 31, 11, (Speech Processing) & May 1994, 32, 5, (Video coding).

11. Scott Hinton, H., "Switching to Photonics", IEEE Spectrum, February 1992, 29, 2, pp42-45.

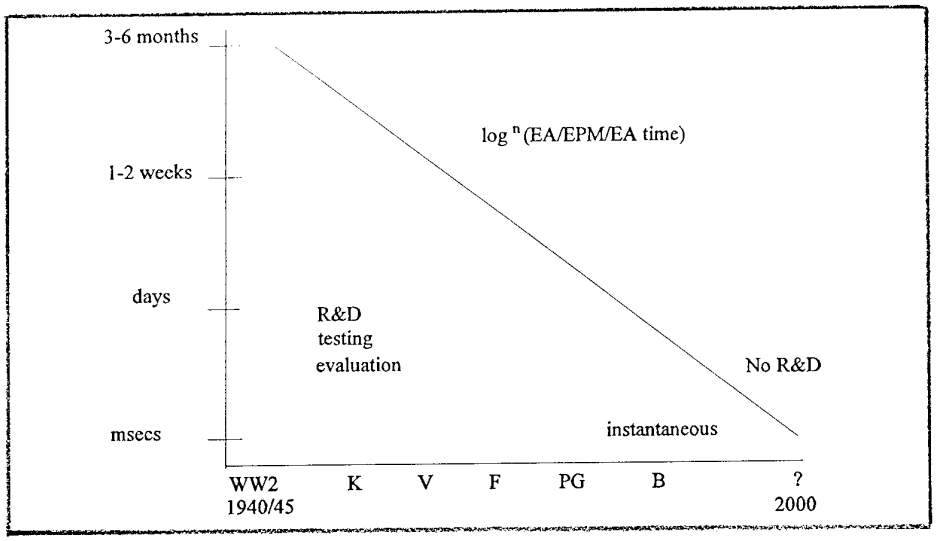

FIGURE 1: Evolution of the EA-EPM Development Cycle

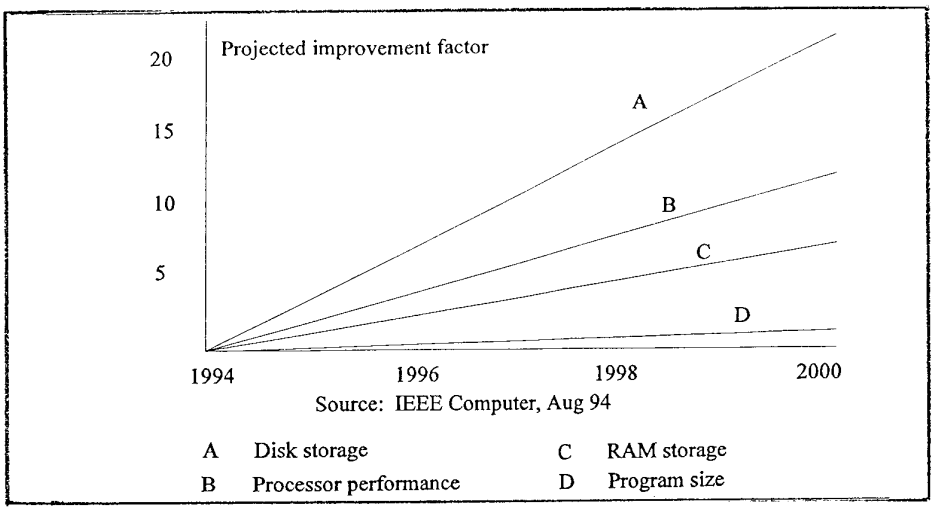

FIGURE 2: Future of Computer Components to Year 2000

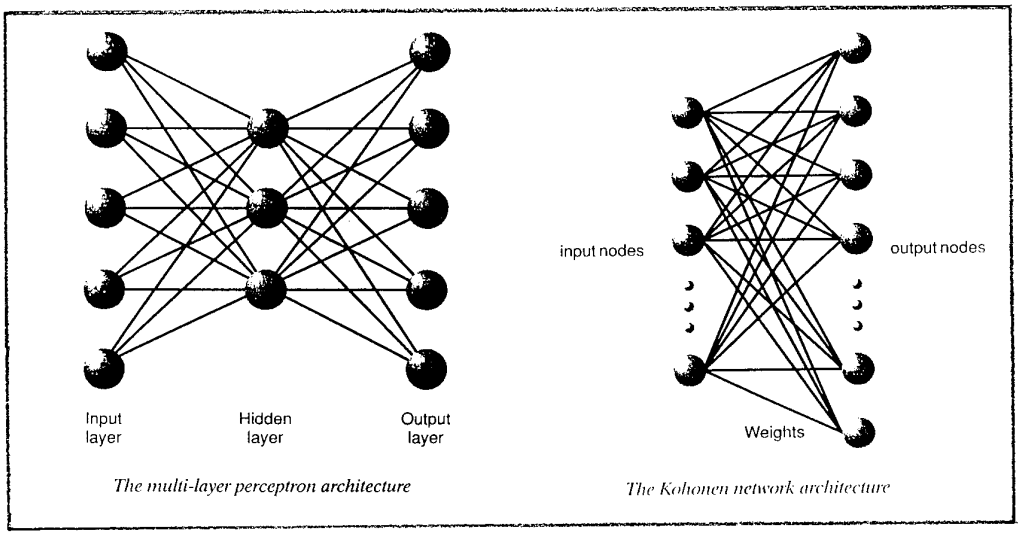

FIGURE 3: Basic Supervised & Unsupervised Neural Network Architectures (ANNs)

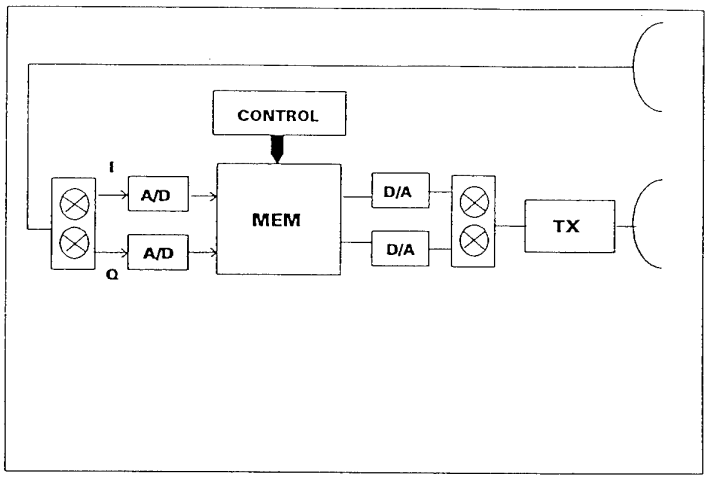

FIGURE 4: Block Schematic of Digital Radio-Frequency Memory (DRFM)

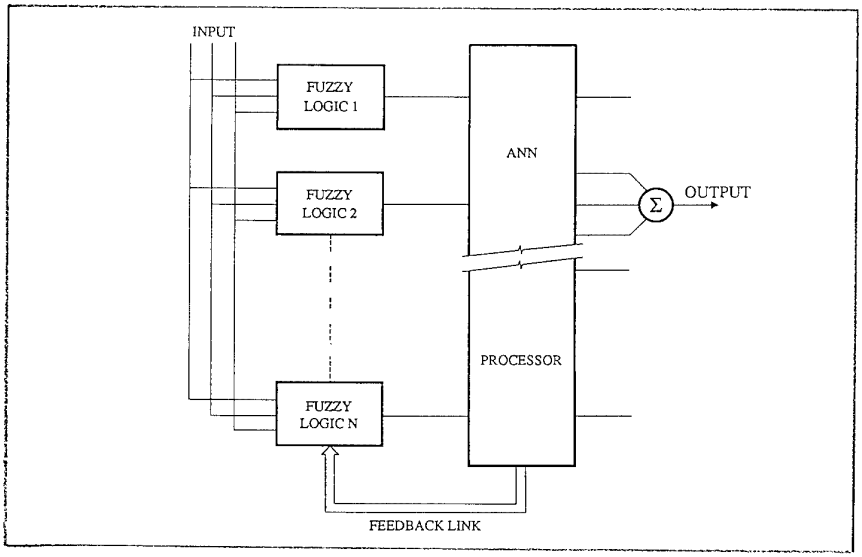

FIGURE 5: A Neuro-Fuzzy System Network

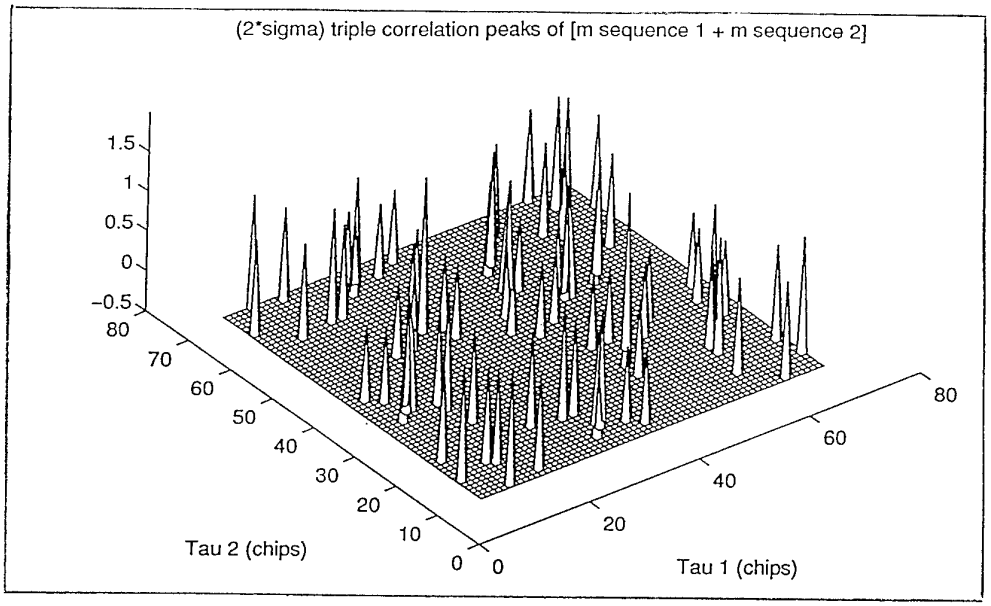

FIGURE 6: Triple Correlation of Two DS/SS Signals

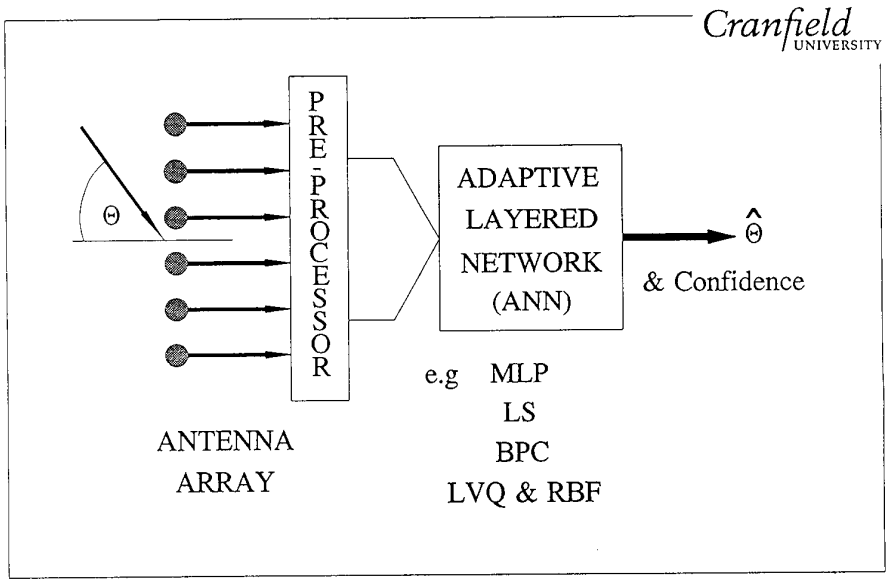

FIGURE 7: Modified ANN Processor for DOA Estimation

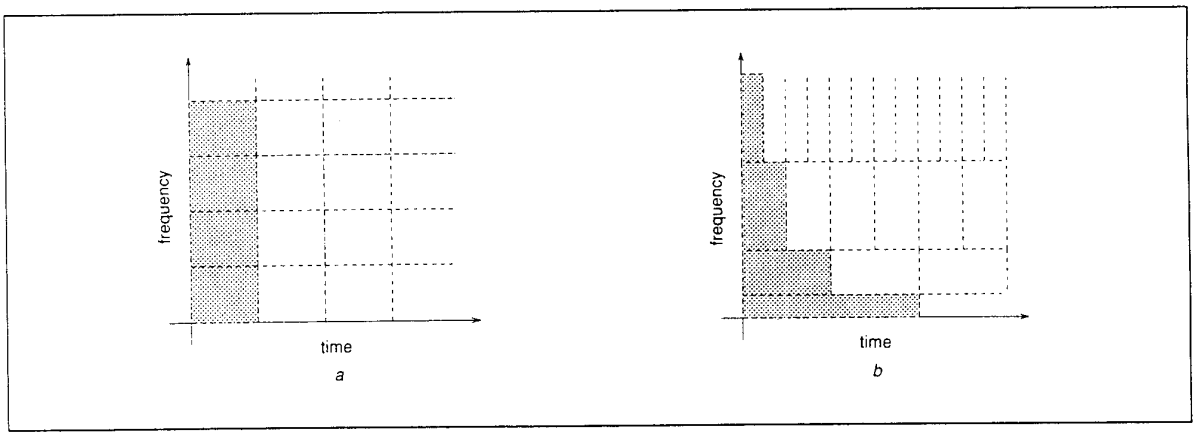

FIGURE 8A: Time-Frequency Resolution Cells for (a) SIFT and (b) WT

Ref [8]

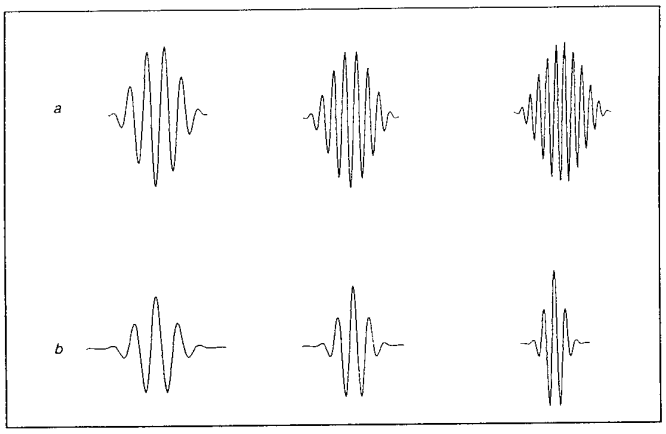

FIGURE 8B: Basis Functions for (a) SIFT and (b) Wavelets

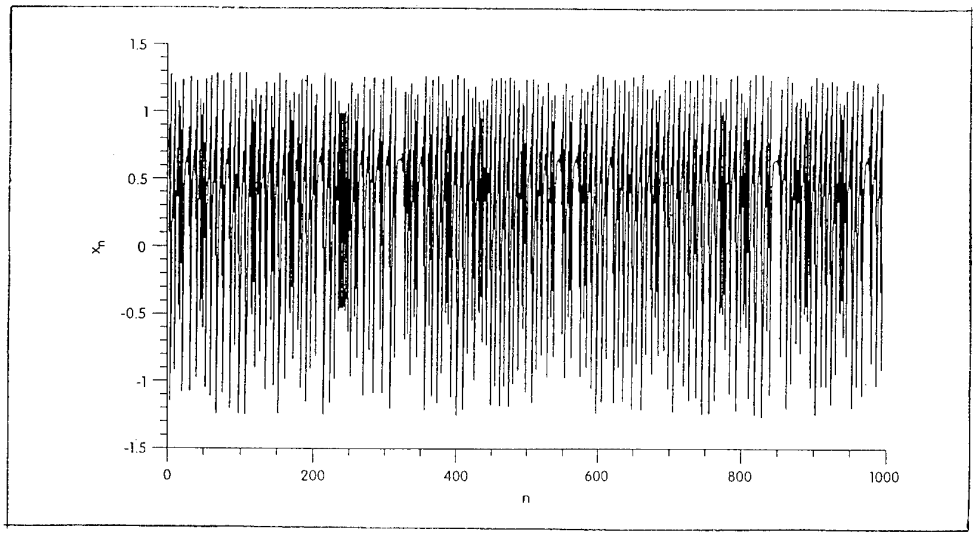

FIGURE 9: Chaotic Time Series from a Henon Map (Ref [9])

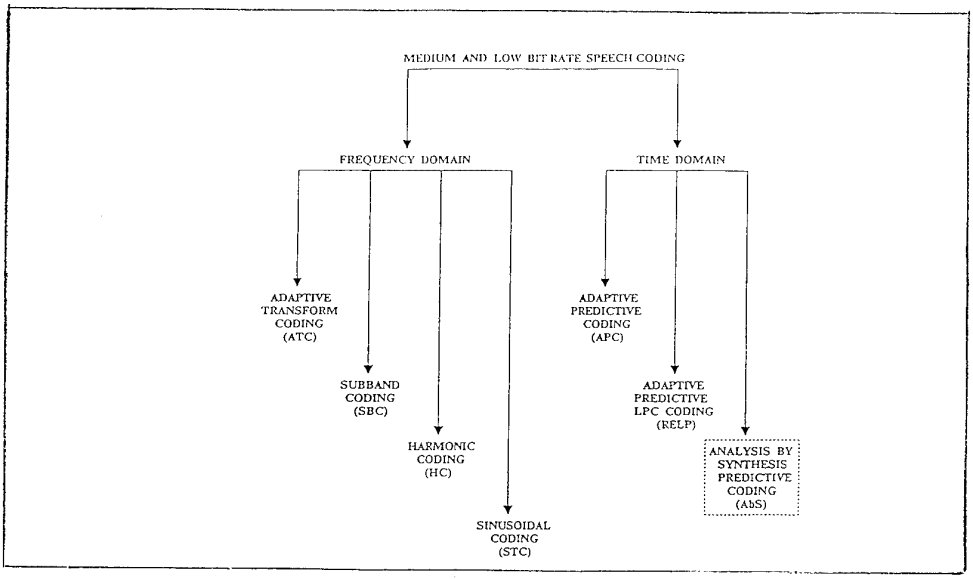

FIGURE 10: A Taxonomy of Speech Compression Codecs

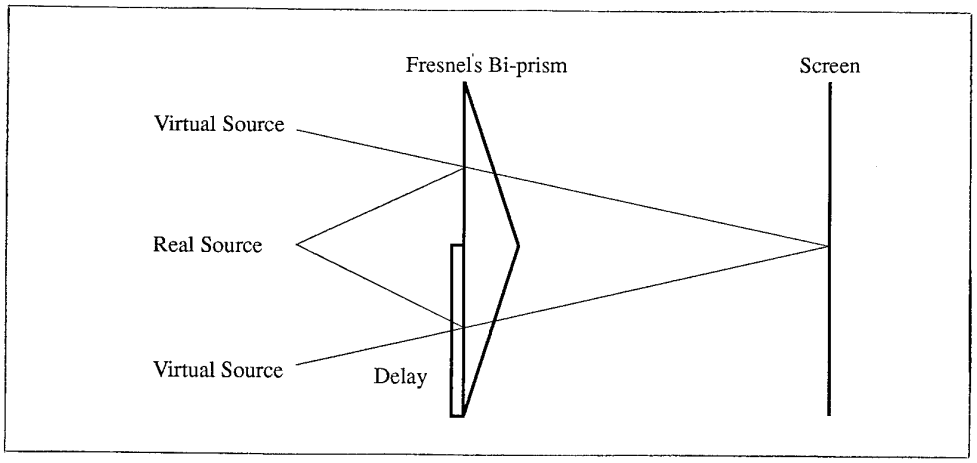

FIGURE 11: A Fresnel Biprism Temporal Coherence Filter

THE IONOSPHERIC FACTOR: EFFECTS AND MITIGATION IN RF NAVIGATION, SURVEILLANCE AND COMMUNICATION

Gregory. J. Bishop
Phillips Laboratory, U. S. Air Force Materiel Command
Geophysics Directorate, Ionospheric Effects Division
29 Randolph Road
Hanscom AFB, MA 01731-3010
USA

Andrew J. Mazzella and Elizabeth. A. Holland
NorthWest Research Associates
300 120th Avenue NE
Bellevue, WA 98005
USA

1. SUMMARY

The ionosphere is a factor in all RF systems that involve links between ground/air and space at or above 100 km altitude, and frequencies up to at least 4 GHz. Ionospheric scintillation can cause message errors in satellite communication links and reduced availability of satellites for GPS navigation. Ionospheric range errors can result in loss of accuracy or resolution in surveillance from space, or ground-based surveillance of space objects. The determination of whether the ionosphere will generate significant system degradation involves both environmental and system parameters. Environmental parameters include: earth-space weather, time of day, season, time of the solar activity cycle, and region of operation. System parameters include: frequency, noise thresholds, and performance requirements such as accuracy, resolution, or data rate. Mitigation, if possible, must be adapted to the function and specific mission of the aerospace system. Two-frequency GPS navigation incorporates ionospheric measurement for range error mitigation. However, single-frequency GPS must depend on statistical models or adjunct differential techniques. Ionospheric scintillation, through loss of lock, or reduced signal margins, can reduce availability of satellites for maintaining GPS navigation integrity. GPS navigation systems can be designed to monitor signal quality and employ adjunct inertial systems over intervals when GPS availability is compromised. In communication, for some systems, special equipment and signal formats can reduce message errors. Local measurement-warning systems can also be used to monitor onset and location of ionospheric disturbances, and identify satellite links that remain clear. When linked to a scintillation model, such warning systems can provide regional capability to identify "windows" for good operation of both surveillance and communication. Similarly, measuring systems that monitor ionospheric range error may be linked to region-adapted ionospheric models for surveillance correction. For systems with a wider mission, corrections outside the reach of a local monitor are required. These may be obtained from global networks of ionospheric sensors providing real-time input to global ionosphere and space weather models.

2. INTRODUCTION

The ionosphere is a major region of the earth-space environment, forming a layer of slightly ionized gas extending between 100 and 1000 km altitude. The most densely ionized region, typically between 300 and 400 km altitude, can produce important effects on radio frequency (RF) signals that traverse it, potentially impacting many aerospace electronic systems. The ionosphere exhibits temporal and regional variability in many ways analogous to tropospheric weather. Actually the ionosphere belongs to the regime of "space weather", being driven both by interaction from the lower atmosphere and from the space and interplanetary environment. The equatorial and polar ionospheric regions in particular exhibit disturbances and high values of ionization that tend to have the greatest impact on aerospace RF systems, Figure 1. Operators of radar surveillance, satellite navigation, and satellite communication systems traversing from the earth/air

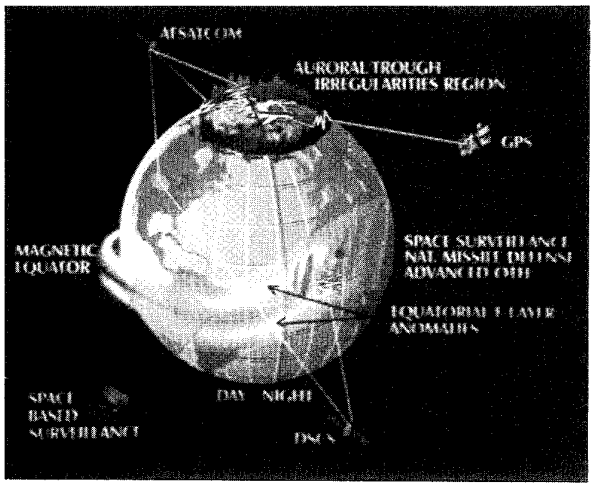

Figure 1. Global view of ionospheric regions that most effect RF Navigation, Surveillance and Communication.

Paper presented at the AGARD SPP Symposium on "Environmental Factors in Electronic Warfare Related to Aerospace Systems" held in Pratica di Mare AFB (Rome) Italy, from 8-11 May 1995, and published in CP-573.

to space environment need to assess and monitor ionospheric effects, just as a fighter pilot needs to consider tropospheric weather. The degree of any system impacts is highly dependent on individual system design and mission. Ionospheric effects may be overlooked or misjudged since the great variability of their character and occurrence can result in significant impacts at one time or region and none at another.

Any important ionospheric degradation of aerospace RF system function needs to be promptly detected, differentiated from other problem sources such as jamming or system failures, and mitigated if possible. Thus, when ionospheric degradation is recognized, some form of mitigation should be initiated. However, it has been noted that after such recognition *has* taken place, serious ionospheric impacts are often subsequently *ignored* by operators, because the source is "known". This inappropriate procedural change has two major negative consequences. First, the operators, in ignoring a known ionospheric effect, fail to record the magnitude and likelihood of occurrence of system degradation, information that is needed for system planning and mitigation development. Second, in ignoring an out-of-specification condition caused by the ionosphere, operators will eventually allow the ionosphere to *mask* the onset of system failures or jamming. Ultimately, system outage during a critical mission could result. Correction can be accomplished by operator training in identifying and logging ionospheric effects, and provision of ionospheric weather bulletins from forecasting centers. In future, operators of critical aerospace RF systems may be provided with ionospheric weather briefings prior to a mission, just as pilots are briefed on tropospheric weather.

3. TYPES OF IONOSPHERIC EFFECTS

The more important ionospheric effects on trans-ionospheric RF surveillance at typical system frequencies are [1]: signal delay, raypath refraction and Faraday rotation of linearly polarized signals due to ionospheric electron content; rapid changes in signal delay (phase) and signal fades and enhancements [2] due to ionospheric scintillation, and partial signal reflection, (either from irregularities at 95 to 125 km altitude [3] or enhanced backscatter from 400-1000 km [4]). The potential impact of any effect depends on the specific system design and mission, since that defines signal interaction with the ionosphere. The major ionospheric effects, their translation into systems effects, and their potential impacts are shown in Table 1. Some of the effects due to ionospheric total electron content and ionospheric irregularities in aerospace systems applications will be discussed below to illustrate the interaction of the ionosphere with RF systems.

3.1 Scintillation

Ionospheric "scintillation" results from the RF signal being disrupted in traversing a region of turbulence in the ionosphere [5]. Scintillation is observed as rapid changes in RF signal phase and amplitude, which may be perceived as extra "noise" in the system. However, scintillation has significant behaviors quite distinct from random noise phenomena. The ionospheric structures in the RF path as well as the relative velocity of the traverse through the structures control scintillation characteristics. For example, low velocity traverses through strong scattering structures can produce deep and sustained fades causing data loss in satellite communication links, or loss of signal lock for a GPS navigation satellite. High velocity traverses will have shorter sustained fades, but higher phase or fade rates that may cause loss of lock. The high frequency components of scintillation may effectively raise amplitude and phase noise levels in surveillance radars, reducing target discrimination and phase-coherent integration for imaging.

Table 1. The major ionospheric effects, their translation into systems effects, and their potential impacts.

Iono. Effect	**Radio (RF) Effect**	**Systems Effect**	**Potential Degradation of:**
Total electron content (TEC)	Signal delay Refraction Dispersion Faraday rotation (polarization	Range error Angle error Pulse distorts Signal loss fading)	Target location Target location Range resolution Coverage
Amplitude scintillation	Fades & enhancements	Signal fades Target fades	Comm thruput Target update
Phase scintillation	Rapid changes in signal delay	Rapid range-rate changes Phase noise	GPS lock Tracking Imaging
Clutter	Partial signal reflection	Anomalous signal returns	Detection Tracking

Ionospheric scintillation often is associated with particular ionospheric regions or boundaries (as discussed below) or with the onset of turbulence conditions. In either case, an RF system may experience nearly a step function onset of scintillation. Figure 2 [6] shows this effect observed by a surveillance radar in the northern mid-latitudes, while Figure 3 [7] shows an onset experienced by GPS near the equator. This particular scintillation sequence produced fades that reduced the signal level below GPS acquisition levels. This observation took place at a magnetically active period near the minimum of solar activity. Although no loss of lock took place in this instance, ionization levels and turbulence structures are typically much greater in the several years near the maximum of the solar activity cycle. Thus, equatorial GPS loss of lock events may be likely in magnetic storms near solar maximum.

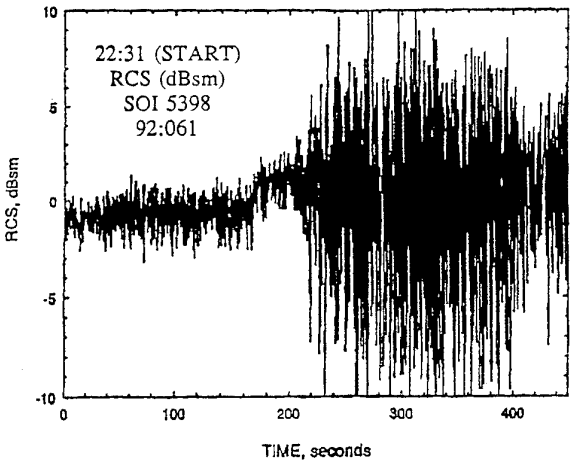

Figure 2. Severe scintillation observed by the Fylingdales U.K. radar as track crossed a "scintillation boundary" [6].

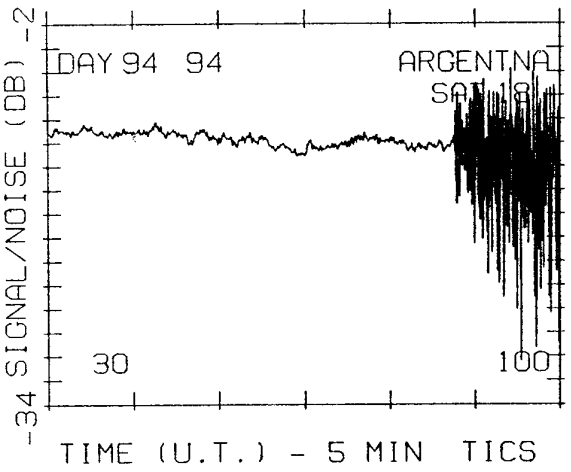

Figure 3. Tucuman, Argentina GPS observation showing ionospheric scintillation turn-on in a few seconds, with a peak-to-peak swing of 10 dB, increasing to ≈ 20 dB [7].

The spatial extent of scintillation occurrence is of significance to its effect on an RF system. Near the equator, scintillation is known to typically be associated with north-south aligned ionospheric features that span the magnetic equator and extend ten degrees or more on either side [8]. Figure 4 shows an observation of GPS satellite signals scintillating only when the signal path is within such a feature (shown as a dark region on the optical all-sky "fisheye" image in the figure). Until recently it was thought that the limited width of these ionospheric features implied that equatorial scintillation would only be an issue for small portions of the sky. However, observations during the hours subsequent to the data in Figure 3 revealed that nearly all GPS signal paths were simultaneously affected [7], Figure 11. The lower elevation angle observation geometry, coupled with the fact that the structures causing scintillation have a significant vertical extent can explain this occurrence. In Figure 5 we see that there is a "venetian-blind effect", when many structures are present, that can cause most signal paths to experience scintillation. (Exceptions are near overhead, and due north or south.) The observations in Figure 4 would be consistent with raypaths above 60 degrees elevation in Figure 5. This wide-area occurrence of equatorial scintil-

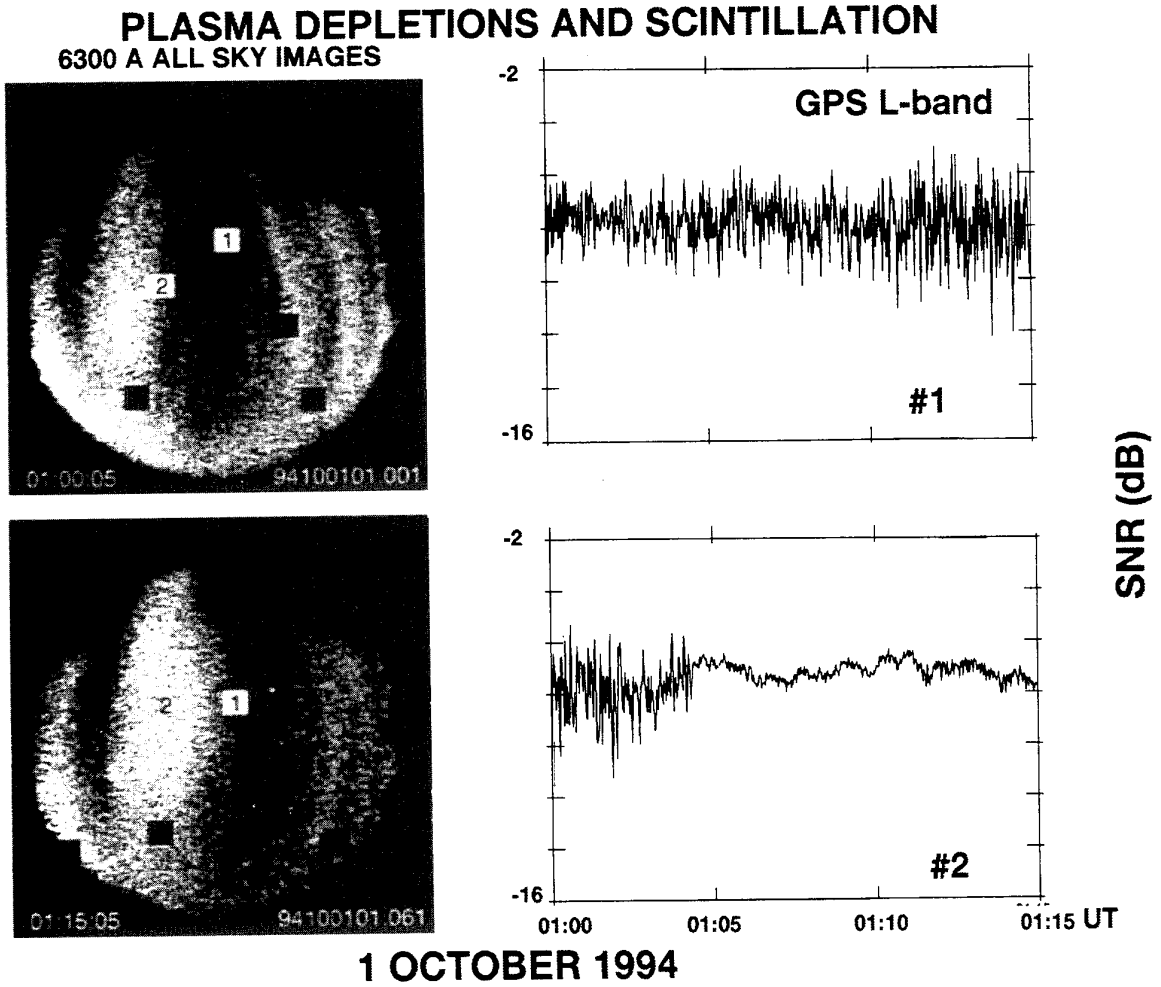

Figure 4. Concurrence of GPS scintillation with passage of raypath through large-scale equatorial plasma depletion containing turbulence; note #2 stops scintillating on exiting depletion.

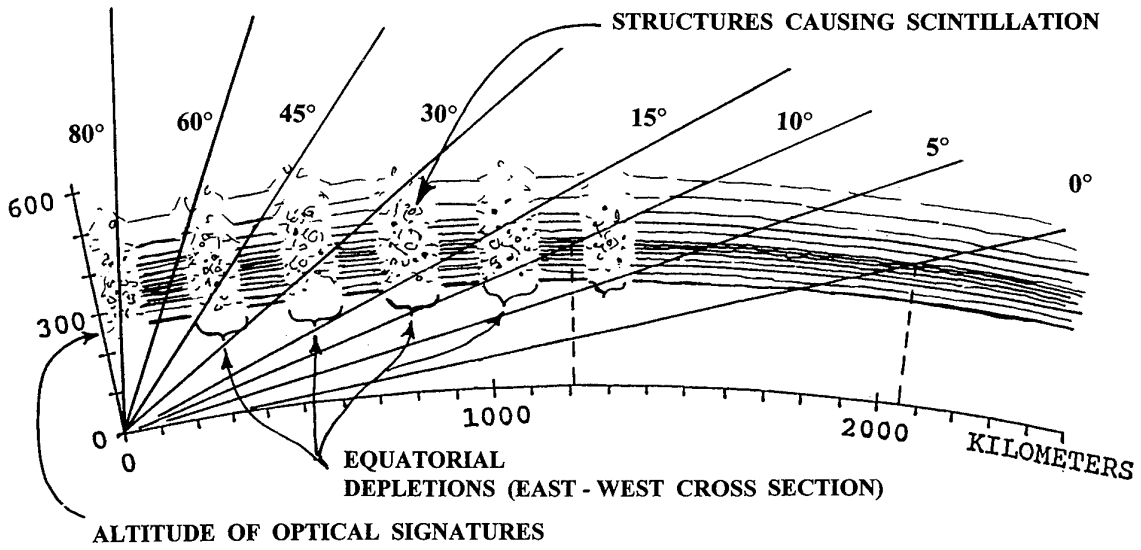

Figure 5. "Venetian-Blind" effect of equatorial plasma depletion ionospheric turbulence structures on trans-ionospheric RF signals. Shows east-west cross-section of structures. Overhead, north and south paths may avoid turbulence.

lation suggests that, at least at solar maximum, some systems may experience reduced availability of GPS satellites to support GPS integrity processing requirements [7].

3.2 Total Electron Content

Ionospheric total electron content, (which is defined as the integrated quantity of electrons contained in a 1 m^2 cross-section column along the raypath traversing the ionosphere, and measured in "TEC units" of $1x10^{16}$ electrons/m^2) produces signal delay and refraction that causes range and angle errors that apply to surveillance and GPS navigation. Due to the longer path length in the ionosphere, the range and angle errors are about three times greater at low elevation angles, where surveillance acquisition is often performed, than at zenith. This geometry may be seen in Figure 5. (Off-zenith or "slant" TEC measurements are usually geometrically scaled down to the equivalent TEC that would have been seen looking directly up from below the point where the raypath penetrates the ionosphere. These values are referred to as "equivalent vertical TEC".) The signal delay caused by TEC is also frequency dependent; this frequency dispersion can cause pulse distortion in wideband radars [9] with negative impact on range resolution. Table 2 summarizes and compares some of these TEC-related effects for radars at UHF and L-band frequencies. Diurnal and short-term TEC variations, as discussed below, often differ significantly from statistical model predictions, resulting in reduced accuracy for systems that use simplified correction models, such as GPS single-frequency navigation.

4. ENVIRONMENTAL VARIABILITY

The ionospheric effects described above show great temporal and geographic variation. Temporal variations include general cyclical effects with diurnal, seasonal, or solar cycle periods. Around the equinox periods, diurnal cycles are generally less predictable. Magnetic storms, infrequent and unpredictable occurrences lasting a few hours or more than a day, can cause high TEC values and gradients as well as scintillation effects where normally none occur. Other, very small scale disturbances (1 to 3 TEC units) may occur and pass through view at any time. Figure 6 shows an example of typical diur-

Table 2. Comparison of effects of ionospheric total electron content on radars at UHF and L-band frequencies.

UHF FREQUENCY:	430	MHz
BAND WIDTH:	1	MHz
ELEVATION ANGLE:	5	DEG.
SATELLITE ALTITUDE:	850	KM

TEC VALUE (TECu)	RANGE ERROR (m)	ANGLE ERROR (mrad)	TRACK ERROR (m)	DSPRN ERROR (nsec)
5	30	0.05	286	0.5
10	61	0.09	572	0.9
40	244	0.38	2286	3.8
80	488	0.75	4569	7.6
120	732	1.13	6851	11.3

L-BAND FREQUENCY:	1250	MHz
BAND WIDTH:	200	MHz
ELEVATION ANGLE:	5	DEG.
SATELLITE ALTITUDE:	850	KM

TEC VALUE (TECu)	RANGE ERROR (m)	ANGLE ERROR (mrad)	TRACK ERROR (m)	DSPRN ERROR (nsec)
5	4	0.01	34	3.8
10	7	0.01	68	7.7
40	29	0.04	271	30.8
80	58	0.09	541	61.6
120	87	0.13	812	92.4

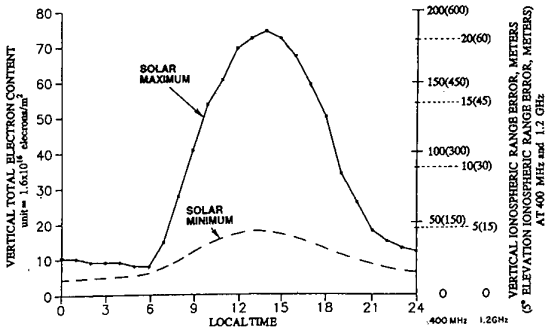

Figure 6. Example of typical diurnal TEC cycles in the middle latitudes, solar maximum and solar minimum.

nal TEC cycles in the middle latitudes, from maximum and minimum solar activity periods. (The accompanying scale shows the corresponding range errors at UHF and L-band.) Figure 7 [10] shows seasonal variation of TEC near solar maximum. Each frame represents about ten days of data. The equinox periods show less consistent cycles, the winter shows usually regular cycles with strong diurnal peaks, and the summer shows much flatter behavior. Variations caused by magnetic storms are evident in frames numbered: 280, 307, 319, and 032. Frame 32 is expanded in Figure 8. The storm effect over several days is seen in the multiple levels at about noon. Figure 9 shows a very infrequent, but interesting, disturbance caused by the passage of the moon's shadow during an annular eclipse (this is contrasted with a normal day two weeks earlier) [6].

There are also very significant variations in ionospheric behavior in neighboring "regions" of the ionosphere. Figure 10 [11] shows a general diagram of these regions. Scintillation and TEC disturbances occur more frequently in the auroral region, and occur during certain seasons or times in the polar and equatorial latitudes, but occur very seldom in the mid-latitudes. Diurnal TEC behavior is generally well-behaved in the mid-latitudes (Figure 7), shows highest values and is less regular in the equatorial latitudes and is lowest on average but most disturbed poleward of mid-latitudes, [12]. The "trough", a wide region of reduced density in the ionosphere, varies daily in its location, extent and profile and typically has high TEC gradients and associated sharp latitudinal scintillation boundaries, [10] as in Figure 2. The magnetic storm that

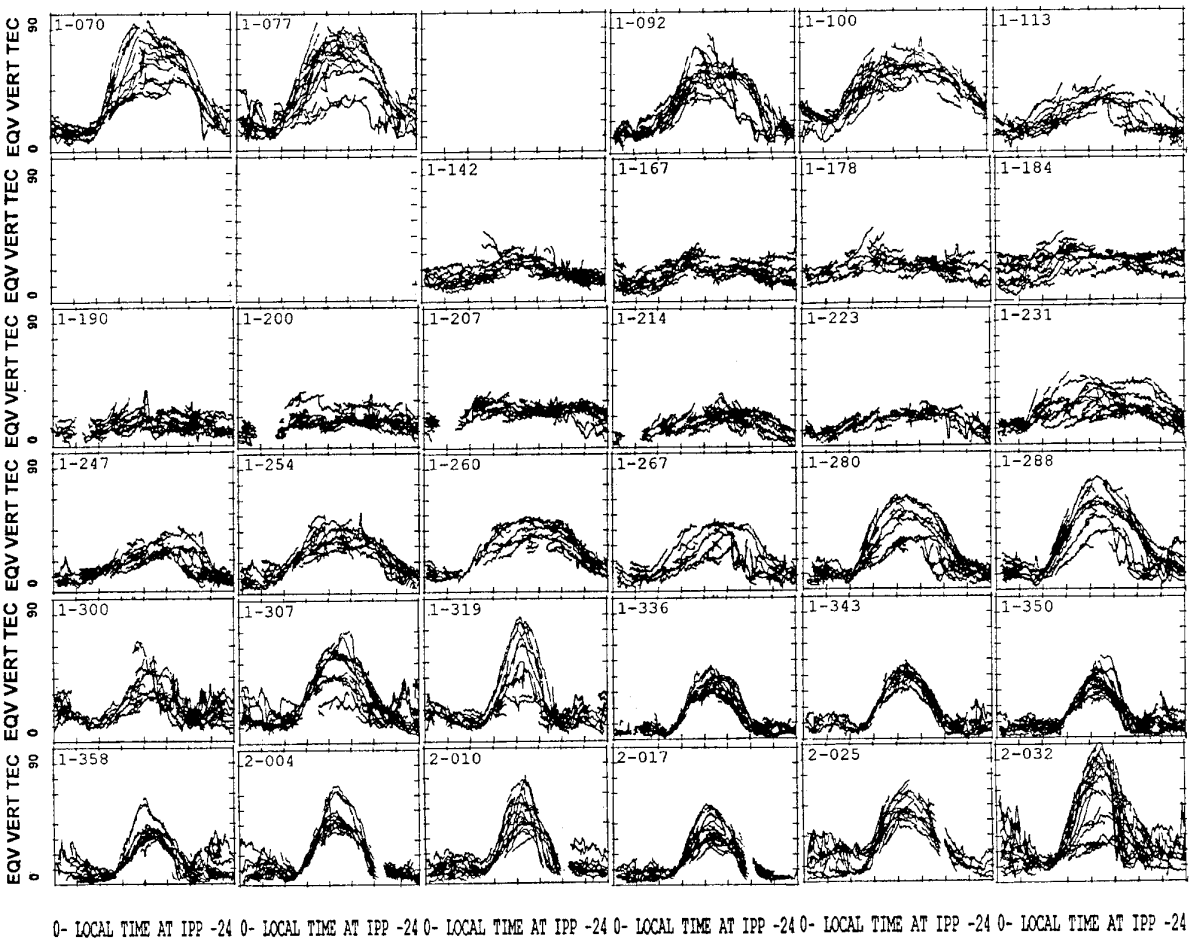

Figure 7. TEC seasonal variation, Shetland Islands, March 1991 - February 1992, (7 to 10 days of data per plot), [10].

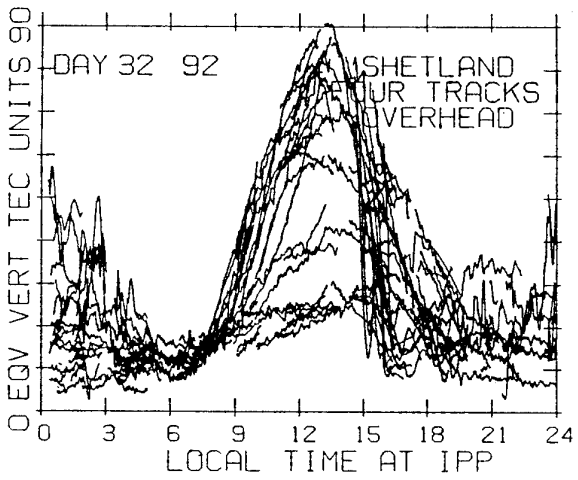

Figure 8. Expanded frame from Figure 7, showing effect of magnetic storm and the ionospheric trough region [10].

occurred during the period shown in Figure 8 moved the trough into the field of view of that station, giving a sharp vertical signature.

5. SYSTEM VARIABILITY

The operation geometry of an aerospace system may cause it to move, or simply to look, from one ionospheric region where a particular effect is not significant, to another region where the effect is very significant. Figure 5 shows, for example, that at 5 degrees elevation the point where a signal path from a ground based radar penetrates the ionosphere is more than 1500 km away in great circle distance from the radar site. This wide coverage for the region of Figure 3 is shown in Figure 11. Even in the mid-latitudes the "look-direction" variation within such a wide area produces significant variation in TEC seen by GPS, which looks like a "storm" period even for a single day of data, as in Figure 12, "all data" frame. However, when this data is separated into narrow bands of latitude and time-corrected [19], fairly regular diurnal profiles emerge - with peak values that increase toward lower latitudes, as would be expected, Figure 12 - remaining frames.

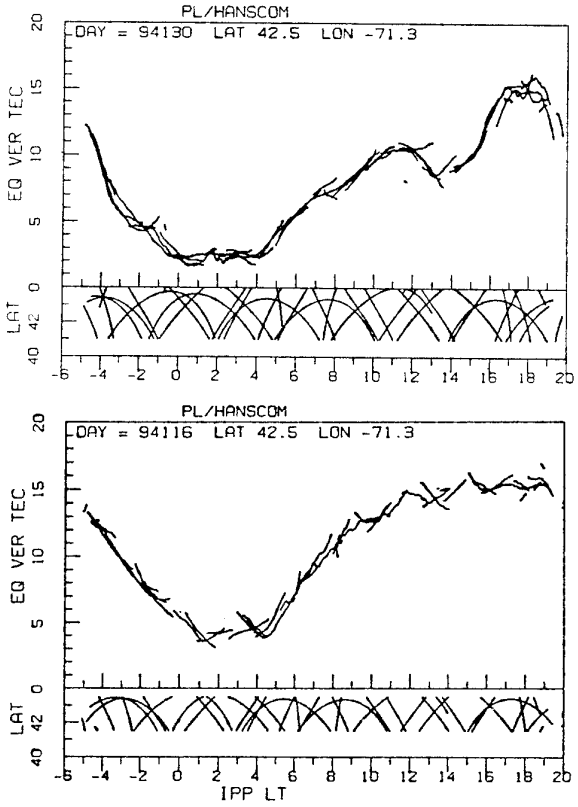

Figure 9. TEC disturbance caused by passage of the moon's shadow during an annnular eclipse, contrasted with a normal day, [6].

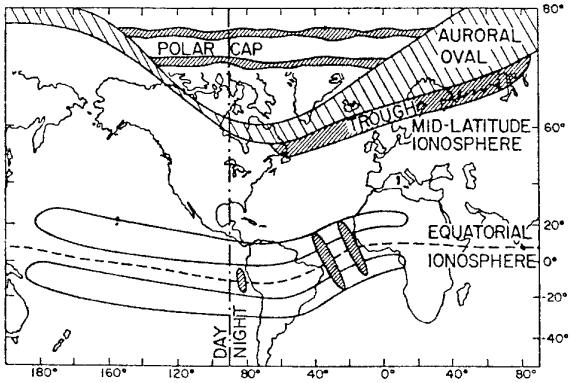

Figure 10. Geographic regions of the ionosphere [11].

Many of the design and operation parameters of aerospace systems that traverse the ionosphere have great influence on the extent to which ionospheric effects play a role in system performance. Systems such as satellite navigation, ground-based radar, space-based radar, and satellite communications will be developed with different values for parameters such as frequency, bandwidth, sample rate, signal format, and detection threshold. Similarly operational settings such as whether the system works from a stationary or a moving platform, is used in near vertical or near-horizon geometry, or covers a wide or small area, all act as filters or translators for any ionospheric effects. Table 3 illustrates how ionospheric range error due to TEC varies with system frequency and elevation angle, as well as latitude and solar cycle. This shows largest values below L-band, near the equatorial latitudes, and at low elevations.

Table 3. Examples of Variation in Ionospheric Range Error with Frequency, Region and Solar Cycle, (Typical daily peak values - vertical).

	High Elevation			Low Elevation		
Solar Cycle	Max		Min	Max		Min
Latitude	Mid	Equator	Mid	Mid	Equator	Mid
TEC Units	75	150	20	225	450	60
	- - - - - RANGE ERROR (meters) - - - - -					
VHF 150 MHz	1343	2687	358	4030	8060	1075
UHF 500 MHz	121	242	32	363	725	97
L 1500 MHz	13	27	4	40	81	11
S 4000 MHz	1.9	3.8	0.5	5.7	11.3	1.5
X 8000 MHz	0.5	0.9	0.1	1.4	2.8	0.4

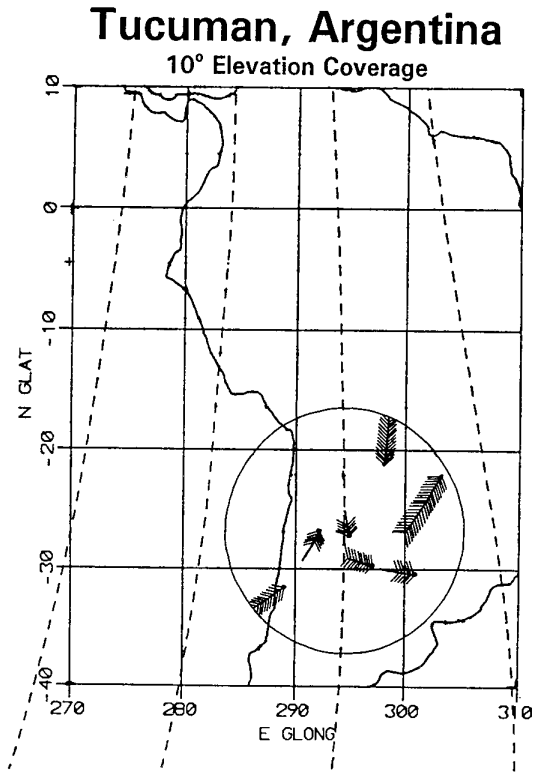

Figure 11. Geographic region covered in the observations of Figure 3, showing 1 hour of satellites' tracks, with onsets of scintillation (hash marks).

The bandwidth of a system affects whether frequency dispersion of ionospheric effects (as noted above for surveillance radars) will influence the system. Narrower bandwidth systems are less affected but there is potential to lose signal lock if the system cannot track rapid ionospheric phase variations. This can occur for some configurations of GPS receivers, for example. Detection thresholds influence the amount of data lost due to ionospheric fading or the quantity of erroneous bits introduced by enhancements. The rate of scintillation or the slope of a TEC gradient (the range rate) introduced by the ionosphere is a function of the velocity of the *signal raypath* through the ionosphere. The components of this velocity include the motions of the system segments above and below the ionosphere, as well as drift of the ionospheric structures themselves. Only in the case of a ground station locking on a geostationary satellite are these rates entirely governed by the ionosphere. GPS ground stations can experience multipath errors from the antenna environment that are comparable to the ionospheric errors [13], but techniques exist to mitigate this [14]. As a final point, the altitude of the system segments is also important, since the major contributions to ionospheric effects come from the 250-450 km altitude range, but some level of effects exists between 100 and 1000 km.

6. MITIGATION OF IONOSPHERIC EFFECTS

Mitigation of ionospheric effects must consider and adapt to the function, mission and specifications of the individual system. It may be possible to measure or model and correct for the effect. Another approach is to design the system to have capability to overcome the effect. It may also be preferable to "work around" the effect operationally, for example by using adjunct systems. This approach often requires being able to detect or predict the conditions that must be avoided. Table 4 lists some typical function, mission, and specification examples.

Table 4. Examples of system function, mission and specification which should be examined in seeking to mitigate ionospheric effects.

Function	Mission	Specification
What does system do?	Why does it do this?	How well must it do it?
Measure:	Track satellite	Range accuracy
range	Update orbit	Position accuracy
doppler	Image space object	Dwell time
radar cross section	Resolve space	Resolution
spatial pattern:	objects	Data rate
amplitude	Identify space	
phase	object	
Detect signal	Image ground	
Acquire signal	Detect ground	
Recover information	targets	
	Detect aircraft	
	Navigate	
	Communicate	

GPS navigation receivers measure range to several satellites, which, combined with known time and orbital information, allows calculation of receiver location. For precise range measurement leading to higher position accuracy, a second signal is received at a different frequency to allow measurement and correction of ionospheric range error. The (less expensive) single-frequency receivers cannot directly measure the ionospheric errors and thus must use other mitigation approaches [15]. A simple correction model which uses parameters downlinked from the satellite will correct for about 50% of the error, statistically [16]. A "work-around" differential-GPS (DGPS) approach obtains the difference between the true and measured position at a known site and transmits the correction to navigators via a separate link. DGPS provides the most accurate GPS positioning within the range where the navigator's ionospheric errors are essentially the same as those at the reference station. This range is expanded in some concepts by regional monitoring and modeling via a correction algorithm [17]. Techniques to use single-frequency receivers to measure the ionosphere exist, but usually depend on assumptions such as consistency of the ionospheric elevation profile [18]. A new technique developed by Phillips Laboratory (PL) to calibrate two-frequency receivers [19] is being extended to test application to single-frequency. Figure 13 shows a comparison of simulated single-frequency TEC measurements to two-frequency results. These initial tests suggest the technique will have practical value for improving DGPS and WAAS performance.

As noted above, ionospheric scintillation may reduce availability of satellites for maintaining GPS navigation integrity, particularly in the equatorial regions at solar maximum. To mitigate such effects, GPS navigation systems can be designed to monitor signal quality and alter internal

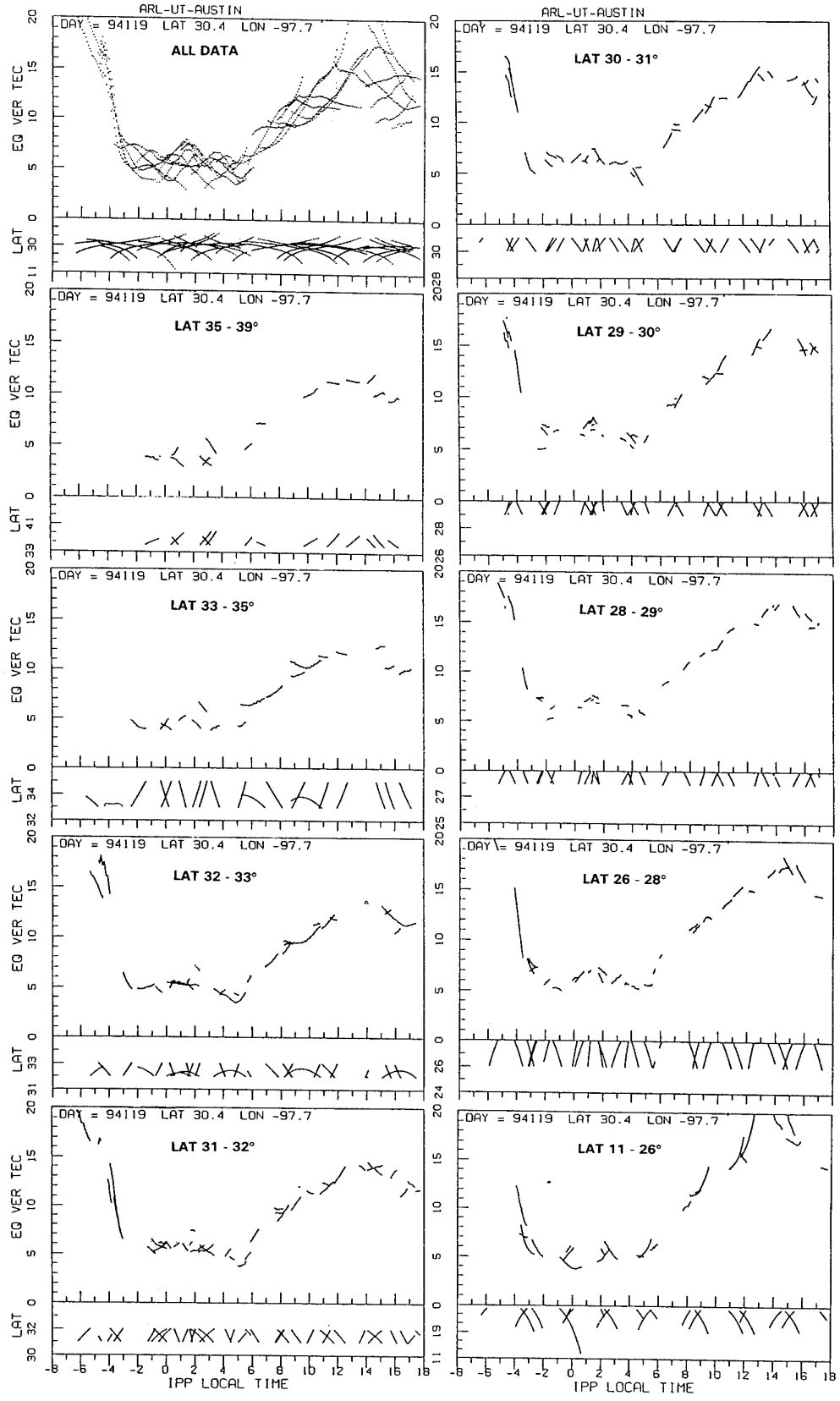

Figure 12. Latitude separation of single-station GPS TEC data from Austin, TX.

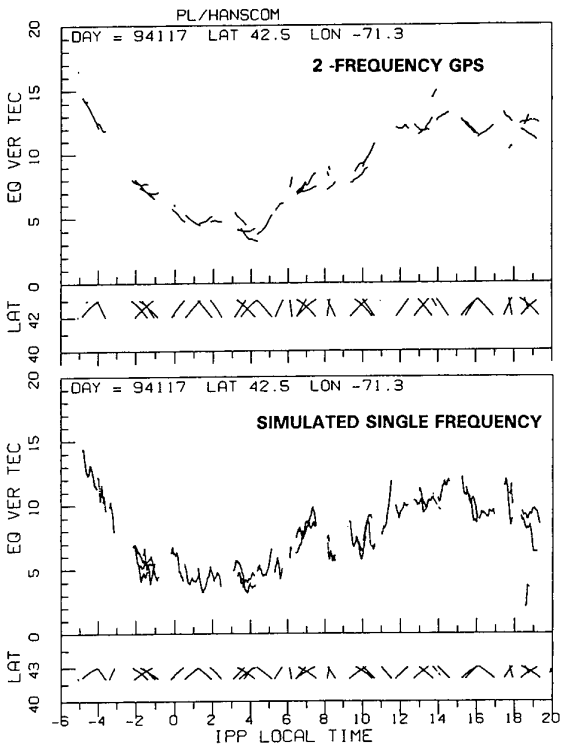

Figure 13. Comparison of simulated GPS single-frequency TEC measurements (derived using a new technique based on ionospheric self-calibration) to GPS two-frequency TEC results.

bandwidths to sustain lock. Another approach is to employ adjunct inertial systems over intervals when GPS availability is compromised. Individual system tests would be needed to determine the anticipated degree of impact on availability for known ionospheric conditions, and the extent of any degradation in navigation accuracy during use of an adjunct system.

For satellite communication systems scintillation is the major ionospheric effect. Some form of time, frequency or space diversity may be used to overcome scintillation. Also, if the system has sufficient power and antenna gain, this can reduce or eliminate any loss from scintillation fading. Use of coding and interleaving can add time diversity to the link and overcome periodic fades. Message throughput can be improved 20-30% without coding to 90-100% with coding [20]. Procedures that format messages in short blocks with error-detection capability, and repeat the blocks, have been shown to significantly reduce error rates [21]. These mitigation techniques could be used continuously on a link, but the lower throughput that results from such use makes it desirable to employ them only when required. Such scheduling requires knowledge of when and where scintillation is occurring or likely to occur.

PL has developed a Remote Access Scintillation Warning System (RASWS) that monitors scintillation conditions on satellite transmissions and can identify satellite paths that remain clear. At present this research instrument is being used in proof-of-concept studies for initial scintillation warning, [5].

There is also a climatological scintillation model (the "WBMOD" model [22]) that can provide the probability of scintillation occurrence for given conditions and time at any location. Current PL development efforts are directed to adapting RASWS to incorporate GPS and drive WBMOD to provide wide-area, *local* scintillation monitoring and warning. Such an enhanced system could identify the onset and location of ionospheric disturbances, identify regional boundaries and identify satellite links that remain clear. Current PL research efforts focus on identifying the physical trigger mechanisms for scintillation so that its onset and development may be inferred from real-time *global* ionosphere models. Clearly, these advances in scintillation warning will also benefit surveillance and navigation systems.

Surveillance systems currently require correction for ionospheric range errors in such missions as satellite tracking. The wide area of coverage of ground-based radars (1500 km radius for 5 degree elevation) typically reaches into adjacent ionospheric regions. This means that simple mitigation approaches have limited accuracy, particularly for radar sites outside the central mid-latitudes. For example, mitigation that depends solely on GPS range error measurement [23] will be most effective near-vertical but accuracy will degrade off-vertical due to GPS' wide geographic spacing. This can be seen in Figure 11, where nearly two entire quadrants of the region receive no updates for more than an hour.

Many systems employ monthly climatological forecasts from an ionospheric model [24] referenced by radar measurements of ionospheric errors using "sphere-like" targets. The model provides a good statistical estimate of variations within the coverage region, to interpolate between limited radar updates. However, such models also suffer from reduced accuracy as they are applied near or in the more dynamic ionosphere regions such as the trough. Figure 14 shows an example of a

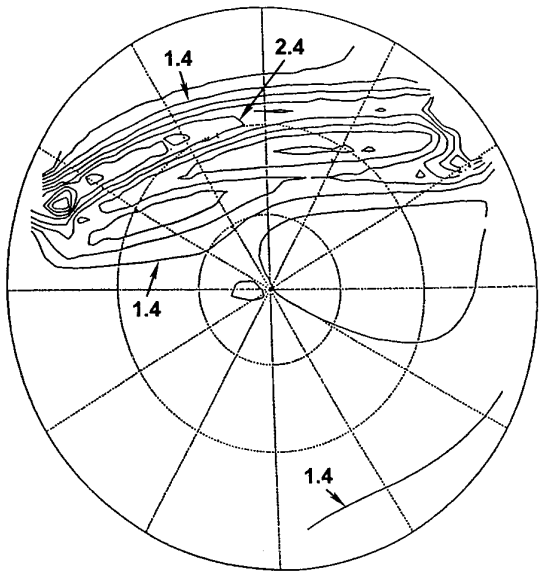

Figure 14. Example of a sky map of the impact of the ionospheric trough region on range error corrections from a model. In the middle of the trough the correction is too great by a factor of > 2.4.

sky map of the impact of the ionospheric trough region on range error corrections from a model. In the middle of the trough the correction is too great by a factor of > 2.4. Figure 15 shows a comparison of one model's climatological predictions to GPS measurements at solar maximum near the north of the mid-latitudes, [10]. Model accuracy can be seen to be quite variable. Accuracy can be enhanced by increased quantity of updates, providing better geographic and temporal reference. Although these updates help, they cannot make a climatological model accurately reflect regional variations. Figure 16 [6] gives an example of this application.

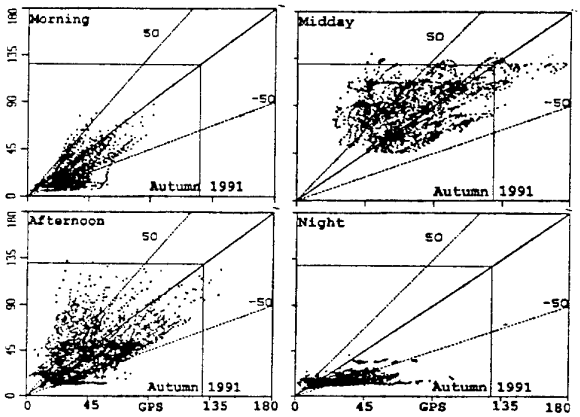

Figure 15. Comparison of the Bent model's climatological predictions of ionospheric TEC vs GPS measurements at solar maximum at a northern mid-latitude site, [10].

New measuring systems that monitor ionospheric range error are being developed by the USAF [6]. These measurements may be linked to region-adapted ionospheric models for improved surveillance correction, providing good mitigation in local region of the monitors. For systems with a wider mission, corrections outside the reach of a local monitor are required. Correction of ionospheric range errors over such wide areas requires a global-scale model that can account for the special character of each region. When provided with real-time inputs from global networks of ionospheric sensors such models can deliver good mitigation to horizon and at ionospheric region boundaries. The Parameterized Real-time Ionospheric Specification Model (PRISM), developed at PL, has these capabilities and is scheduled to become operational during 1995 at the USAF 50th Weather Squadron, in Colorado.

7. CONCLUSIONS

The ionosphere is a factor in all RF systems that involve links between ground/air and space at or above 100 km altitude, and frequencies up to at least 4 GHz. The variation of the ionosphere and its interaction with each system's function and mission must be clearly examined to determine if degradation can occur. Any important ionospheric degradation of aerospace RF system function needs to be promptly detected, differentiated from other problem sources such as jamming or system failures, and mitigated if possible. Several mitigation schemes are now in use. Two-frequency GPS navigation incorporates ionospheric measurement. Single-frequency GPS uses statistical models or adjunct differential techniques for mitigation. In communication, special equipment and signal formats can reduce message errors. Ground-based surveillance

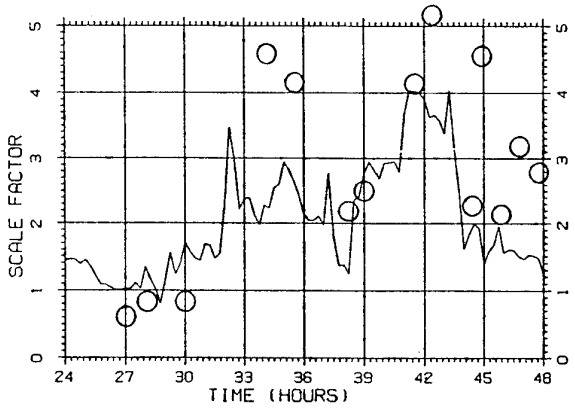

Figure 16. Ionospheric range error correction scale factors calculated by the COBRA DANE radar vs scale factors derived from on-site GPS TEC measurements, [6].

radars mitigate some of the ionospheric errors using climatological models updated by radar measurements. Mitigation improvement efforts are using improved measurement techniques (GPS) and modeling. Local measurement-warning systems can also be used to measure and correct range errors. They can also monitor the onset and location of ionospheric disturbances, to identify paths that remain clear for surveillance and satellite communication. To improve accuracy, such systems must be coupled to local ionospheric models. Corrections outside the reach of a local model may be obtained from global networks of ionospheric sensors providing real-time input to global ionosphere and space weather models. Whenever ionospheric impacts on system performance are found to occur, operators must assure that these are clearly differentiated from occurrence of system failures or jamming, and carefully recorded to support system planning and mitigation development. To aid such activity it may be appropriate for operators of certain critical aerospace systems to be provided with special training and regular ionospheric weather briefings.

8. ACKNOWLEDGEMENTS

The authors wish to thank Dr. Edward J. Weber of the Phillips Laboratory Ionospheric Applications Branch for use of the optical data in Figure 4, and Dr. David S. Coco of the Applied Research Laboratories, The University of Texas at Austin, for the GPS measurements of Figure 12.

9. REFERENCES

[1] Bishop, G. J., J. A. Klobuchar, Lt Col A. E. Ronn, and Capt M. G. Bedard, "A Modern Trans-Ionospheric Propagation Sensing System", *in* "Operational Decision Aids for Exploiting or Mitigating Electromagnetic Propagation Effects", AGARD CP 453, May 1989, Paper 19.

[2] Basu, S., E. MacKenzie, and Su. Basu, "Ionospheric Constraints on VHF/UHF Communication Links During Solar Maximum and Minimum Periods", Rad. Sci., *23*, 361, 1988.

[3] Tsunoda, R.T., and E.J. Fremouw, "Radar Auroral Substorm Signatures", J. Geophys. Res., *81*, 6148, 1976.

[4] Groves, K.M., "Nonlinear Ionospheric Propagation Effects on UHF Radio Signals, *in* "Physics of Space Plasmas (1991),

SPI Conf. Proc. and Reprint Series, No.11" T.Chang et al. eds. Sci. Publishers, Cambridge, MA, 1992.

[5] Basu, S., G.J. Bishop, and J. Larson, "Turbulence in the Upper Atmosphere: Effects on Systems", AGARD Sensor and Propagation Panel Symposium, Rome, Italy, May 1995.

[6] Bishop, G.J., D.O. Eyring, K.D. Scro, S. Deissner, D.J. Della-Rose, W. Cade, N. Ceaglio, and M. Collello, "Air Force Ionospheric Measuring System Supports Global Monitoring and Mitigation of Effects on AF Systems", *in* "Proceedings of ION GPS-94", The Institute of Navigation, Washington, DC, September, 1994.

[7] Bishop, G.J., S. Basu, E.A. Holland, and J.A. Secan, "Impacts of Ionospheric Fading on GPS Navigation Integrity", *in* "Proceedings of ION GPS-94", The Institute of Navigation, Washington, DC, September, 1994.

[8] Aarons, J., and S. Basu, "Ionospheric Amplitude and Phase Fluctuations at the GPS Frequencies", *in* "Proceedings of ION GPS-94", The Institute of Navigation, Washington, DC, September, 1994.

[9] Klobuchar, J. A., "Ionospheric Effects on Earth-Space Propagation", AFGL-TR-84-0004, 27 Dec. 1983, ADA 142725.

[10] Bishop, G. J., I. K. Walker, C. D. Russell, and L. Kersley, "Total Electron Content and Scintillation Over Northern Europe", *in* "Proceeedings of the 1993 Ionospheric Effects Symposium", Alexandria, VA, May, 1993.

[11] Bishop, G.J., D.S. Coco, C. Coker, E.J. Fremouw, J.A. Secan, R.L. Greenspan, and D.O. Eyring, "GPS Application to Global Ionospheric Monitoring: Requirements for a Ground-Based System", *in* "Proceedings of ION GPS-92", The Institute of Navigation, Washington, D.C., Sept. 1992.

[12] Bishop, G.J., T.W. Bullett and E.A. Holland, "GPS Measurements of L-Band Scintillation and TEC in the Northern Polar Cap Ionosphere at Solar Maximum", *in* "Proceedings of 11th International Beacon Satellite Symposium", URSI Beacon Satellite Group, University of Wales, Aberystwyth, July, 1994.

[13] Bishop, G.J., and E. A. Holland, "Multipath Impact on Ground-Based Global Positioning System Range Measurements: Aspects of Measurement, Modeling and Mitigation", *in* "Proceedings of AGARD EPP 53rd Symposium", Oct 1993, Paper 29.

[14] Bishop, G.J., D.S. Coco, P.H. Kappler, and E.A. Holland, "Studies and Performance of a New Technique for Mitigation of Multipath Effects in GPS Ground Stations", *in* "Proceedings of 1994 National Technical Meeting", The Institute of Navigation, Washington, D.C., Jan. 1994.

[15] Hoffman-Wellenhof, B., H. Lichtenegger, and J. Collins, "GPS Theory and Practice", Springer-Verlag Wein, New York, 1992.

[16] Klobuchar, J. A., and P. H. Doherty, "The Statistics of Ionospheric Time Delay for GPS Ranging on L1", *in* "Proceedings of ION GPS-90", The Institute of Navigation, Washington, DC, September 1990.

[17] El-Arini, M.B., C.J. Hegarty, J.P. Fernow and J.A. Klobuchar, "Development of an Error Budget for a GPS Wide-Area Augmentation System (WAAS)", *in* "Proceedings of 1994 National Technical Meeting", The Institute of Navigation, Washington, D.C., Jan. 1994.

[18] Qiu, W., G. Lachapelle and M. E. Cannon, "Ionospheric Effect Modselling for Single Frequency GPS Users", *in* "Proceedings of 1994 National Technical Meeting", The Institute of Navigation, Washington, D.C., Jan. 1994.

[19] Bishop, G.J., A. Mazzella and E.A. Holland, "Self-Calibration of Pseudorange Errors by GPS Two-Frequency Receivers", *in* "Proceedings of 1995 National Technical Meeting", The Institute of Navigation, Washington, D.C., Jan. 1995.

[20] Johnson, A.L., "Special Course on Interaction of Propagation and Digital Transmission Techniques", *in* NATO AGARD Report No. 744, Copenhagen, Denmark, October, 1986.

[21] Johnson, A.L, "The Effect of Polar Scintillation on UHF SATCOM Message Throughput", TTCP Space Communicatioons Panel Meeting, Defense Research Agency, Malvern England, October 1993.

[22] Secan, J.A., E.J. Fremouw, and R.E. Robins, "A Review of Recent Improvements in the WBMOD Ionospheric Scintillation Model", *in* "The Effect of the Ionosphere on Communication, Navigation, and Surveillance Systems", J.M. Goodman, ed., Naval Research Laboratory, Washington, 1987.

[23] Coster, A.J., E.M. Gaposchkin and L.E. Thornton, "Real-Time Ionospheric Monitoring System Using the GPS", *in* "Proceedings of ION GPS-91", The Institute of Navigation, Washington, D.C., Sept. 1991.

[24] Llewellyn, S. K., and R. B. Bent, "Documentation and Description of the Bent Ionospheric Model," AFCRL-TR-73-0657, AD 772733, 1973.

P. S. Cannon (UK)

Can you please quantify the improvement afforded by PRISM relative to a climatological model ?

Author's Reply

I will respond to your question with two qualifications. First, the authoritative answer should come from Dr. David Anderson, chief of our modelling branch, who is responsible for PRISM. Second, the improvement is a function of the quantity and quality of sensor data available to drive PRISM. With that said, if we assume that a climatological model will have an error of 50% in its TEC prediction (and the data in this paper shows: that could be conservative outside the central mid-latitudes), then I would expect PRISM to bring that down to 25%, and to 10% with good sensor input from the region.

ADAPTIVE INTERFERENCE CANCELLATION AS A MEANS OF COPING WITH THE COMPLEXITY OF THE TARGET ARRAY AND THE PLATFORM ENVIRONMENT IN MODERN AND FUTURE COMMUNICATIONS ELECTRONIC WARFARE SYSTEMS

R. Horner and D.R. Thwaites
Siemens Plessey Systems, Grange Road
Somerford, Christchurch, Dorset BH23 4JE
United Kingdom

BASIC PRINCIPLES

The basic principle of adaptive interference cancellation is very simple, it is the removal of an unwanted interfering signal by algebraically adding a replica of the unwanted component which has precisely the same amplitude and opposite phase. This is shown in Figure 1.

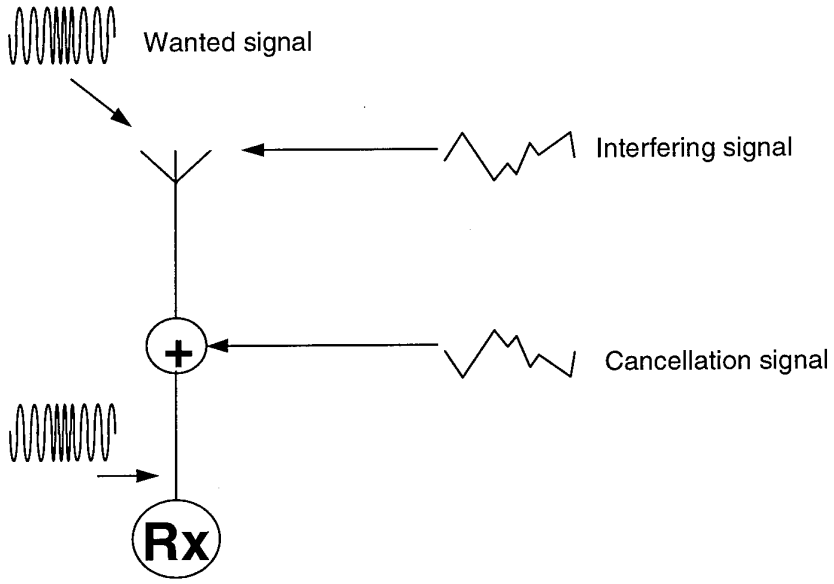

Figure 1. Adding an antiphase version of the interfering signal

In this example the wanted and the unwanted interfering signals are added to each other at the receive antenna where they form a composite signal. The cancellation signal is of exactly the same amplitude as the interfering signal but it is in the opposite phase. The result of adding it to the composite signal is that it cancels out the interfering component and leaves only the wanted signal at the input to the receiver.

The technique of interference cancellation has two major applications:-

The elimination of interference from emitters which are co-sited with the receiver for example on an aircraft or other tactical platform (co-sited interference cancellation).

The elimination of interference from emitters which are remote from the receiver (remote interference cancellation).

Remote interference cancellation employs a second antenna to acquire the interfering signal and one application of the technique is illustrated in Figure 2.

Paper presented at the AGARD SPP Symposium on "Environmental Factors in Electronic Warfare Related to Aerospace Systems" held in Pratica di Mare AFB (Rome) Italy, from 8-11 May 1995, and published in CP-573.

Figure 2 Remote interference cancellation

Co-sited interference cancellation is used to eliminate interference from emitters on the same platform as the receiver and is achieved by acquiring a sample of the interfering signal from a hard wired coupler in the antenna feed of the interfering transmitter. This is illustrated in Figure 3.

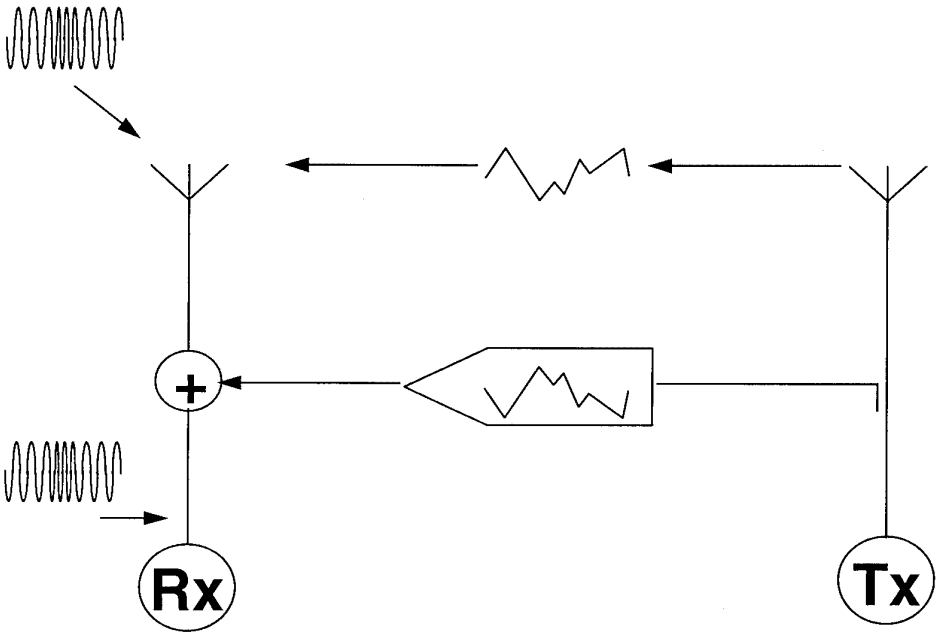

Figure 3. Co-sited Interference Cancellation

The principle of applying Interference Cancellation in these two situations is not new. It has been used in a small number of practical systems for many years. However, the advent of communications EW systems capable of exploiting broadband signals has created new areas of demand. The particular case of airborne and land based systems on small platforms can

result in systems which are completely inoperable without adaptive interference cancellation.

This paper introduces the techniques of adaptive interference cancellation and describes a practical solution fielded with a major tactical system.

EXAMPLE OF AN EARLY APPLICATION

Interference cancellation has been applied in narrow-band systems for many years. One particular example was applied to a transatlantic satellite station at Goonhilly Down, Cornwall, England which was suffering from interference from a French TV broadcast station 100 miles away in northern France. A system using Plessey hardware was installed and operated successfully for many years. This application, which is illustrated in Figure 4, used a second (smaller) antenna to receive, selectively the TV signal. After adaptive adjustment of phase and amplitude, this signal was then injected into the receive path to obtain the desired cancellation.

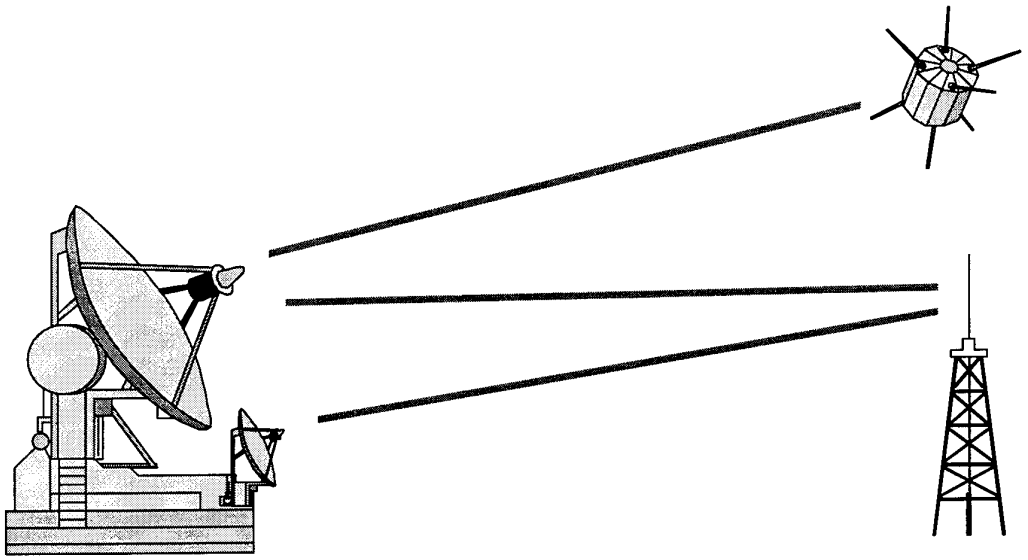

Figure 4 - Example of Interference Cancellation

APPLICATION TO MODERN COMMUNICATION EW

Some of the most modern communications EW systems are vulnerable to severe interference problems in that they often combine broadband, sensitive receive systems with agile transmitters on a single platform.

Communications ESM systems designed to counter frequency agile communications need to employ wideband front end tuners coupled to fast analogue to digital converters operating at a convenient IF. The digitised wideband IF signals can then be spectrally processed to detect, direction find or otherwise exploit agile and conventional Signals of Interest (SOIs). Tuners with several MHz of instantaneous bandwidth are often employed in such systems in order that a substantial portion of the communication band can be processed, either continuously or at a high revisit rate. Practical A/D converters limit the instantaneous dynamic range to typically 65dB so that a single strong interfering signal in the passband of the front end tuner will severely degrade the system detection threshold. Tactical ESM sensors of this type need to communicate their interception data with decision makers and other sensors to exploit the raw data. This necessitates transmitters using Electronic Protection Measures (EPM), preferably using transmissions which are not unique in terms of radio signature. This typically implies that common battlefield communications systems, such as VHF hoppers, will be preferred for inter-site communication. Without the benefit of interference cancellation, the sensitivity of the ESM may thus be degraded or the system designer must find costly alternative means of communicating between sensor sites.

The use of multiple transmitters, possibly multiplexed into a single transmitting antenna to reduce visual signature, further adds to the difficulties of the EW system designer. Multiple

cancellation systems can be readily configured to deal with this problem.

Another example where interference cancellation is valuable is where agile or wideband jammers are used on a platform which requires to receive in the same band or even in a separate band. Interference from the on-board jammer can be so high that essential communications reception is not possible due to receiver blocking or due to sideband noise form the local transmitter.

HIGH PERFORMANCE CO-LOCATION CANCELLERS

Principles

The basic principle of interference cancellation was outlined earlier in this paper. A high performance, practical implementation will now be described. As noted above, the fundamental concept of interference cancellation is to add an equal amplitude, opposite phase component of the interfering signal into the receive path requiring cancellation. To make this a practical technique, the canceller must be *adaptive* to compensate for changes in the amplitude, frequency and phase of the unwanted interference received by the victim antenna. An automatic feedback control loop is used to maintain the desired anti-phase condition for high cancellation ratio.

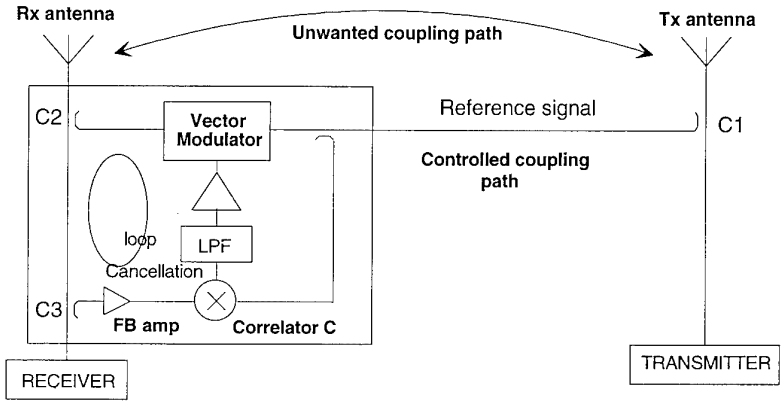

Figure 5 - Principle of Adaptive Co-location Cancellation

The basic approach to adaptive cancellation is illustrated in Figure 5. The diagram shows the unwanted coupling path between the co-located transmit and receive antennas. In an ESM system the receive antennas would typically be broadband and would feed broadband, sensitive RF tuners for signal intercept and/or direction finding. At VHF, for example, the isolation between transmit and receive antennas on a small platform could be in the region of 25dB so that the interference level at the receive antenna would be a high as 0.2watt with a 50watt transmitter power. This would clearly affect the ability of the system to detect target SOI which could be 130dB lower than the interference level.

A controlled coupling path is introduced by taking a sample of the transmitted signal using a passive coupler (C1) inserted into the transmitter feeder. The signal taken from coupler C1 is often called the 'reference' signal. The reference signal in the controlled path is weighted by a vector modulator which precisely controls the amplitude and phase so that the desired mutual cancellation is obtained at coupler C2 in the receive path. A third coupler (C3), also placed in the receive path, samples any interference residue. After amplification, this residue is correlated with a small proportion of the reference signal to produce a negative feedback control signal to the vector modulator. Additional DC gain is provided in the loop as shown. The total gain in the loop determines the degree of interference cancellation which is provided. The low pass filter is a most important element as this determines the dynamic characteristics of the cancellation loop.

Path matching

There are certain paths in the canceller system which require matching for correct system operation and optimum performance. Firstly, it is essential that the two paths from the transmitter reference coupler (C1 in Figure 5) to the

correlator inputs are matched across the operating frequency band. The relative phase angle of these paths must also be chosen to give negative feedback. This is generally achieved by including a short delay cable within the cancellation hardware, the delay being chosen by semi-automatic production test.

Matching is also required external to the cancellation hardware. This is because the cancellation process involves two separate transmission paths, one of which is controlled in magnitude and phase, via the vector modulator and the other which is uncontrolled via the antenna to antenna coupling. As the loop is adaptive and the vector modulator can provide a cancellation signal at any phase, an unmodulated (CW) interference signal will be cancelled whether or not these paths are matched. Since the vector modulator is frequency independent, it cannot compensate any frequency dependence of the paths which would become apparent with a modulated interference signal. The simple solution is to incorporate a length of RF cable to group delay match the unwanted coupling path and the controlled coupling path. The cancellation loop will then set the correct magnitude and phase for cancellation of the modulated signal with priority to the frequency of maximum energy.

The effect of imperfect matching, which may arise due to antenna site reflections or other effects, is to limit the cancellation depth for wide bandwidth interfering signals. An example of cancellation null depth versus frequency offset, for a group delay mismatch of 2ns, is shown in Figure 6. It can be concluded that excellent cancellation can be achieved without difficulty for typical communication signal bandwidths.

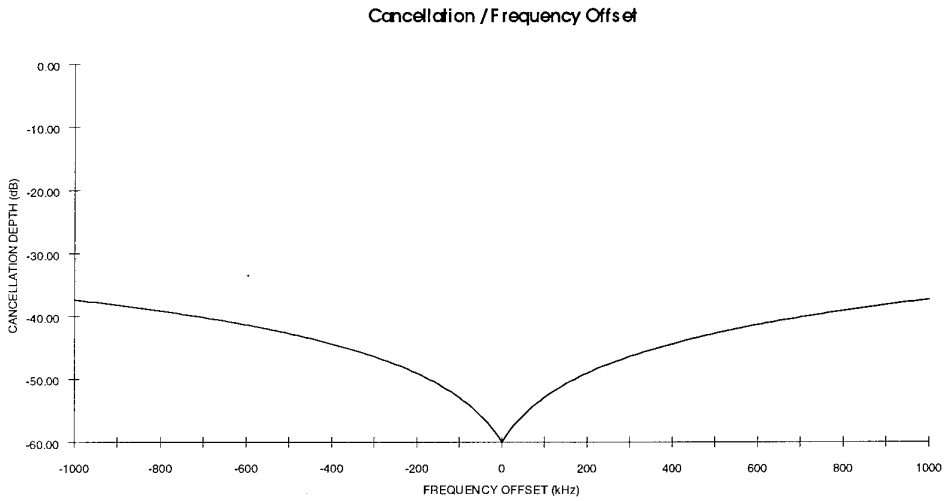

Figure 6 - Example of Cancellation Depth vs Frequency for 2ns Delay Mismatch

Static Characteristics

The negative feedback correlation loop process, when used as shown in Figure 5, exhibits a rather different static cancellation characteristic to that usually associated with more common applications. This is because the transmitter reference, applied to both the vector modulator and the correlator, is of constant magnitude when the transmitter has reached its maximum steady state level. In principle, the loop gain is equal to the square of this reference voltage multiplied by the gains and losses within the loop. The loop gain and hence the cancellation ratio is then a constant, better than 60dB is achievable in tactical environments. DC offsets in the correlator and associated circuits modify the cancellation characteristic, tending to give a constant residue of interference at the output for changes in the interference level. This characteristic tends to match the needs of the system designer as the canceller can be designed to provide a specified maximum interference residue.

In a typical VHF application, for example, the interference residue would be chosen to be less than -40dBm, which is well below the level at which serious non-linearity or blocking would be expected in the RF tuner.

Dynamic Characteristics

The speed at which the cancellation loop settles after a large change in the transmitter amplitude or frequency eg when an agile transmitter hops, is determined by the closed loop bandwidth. This is the product of the open loop gain and the open loop cut-off frequency. The cut-off frequency is set by the low pass filter at the correlator output. In order to achieve unconditional stability, the loop is maintained at first order, by setting a low pass filter cut-off frequency which avoids secondary break points in the open loop response. These break points are, typically, introduced by the vector modulator because of its need for high power handling.

A desirable feature in the dynamic response of the loop is that it should track the rising edges of the interfering waveform at the onset of each transmission. The speed of the cancellation process depends on loop gain which, as noted above, is proportional to the square of the reference signal voltage. Hence during the early part of the rising edge, the loop gain will be small and the resulting loop speed unacceptably slow. This is countered in Siemens Plessey Systems (SPS) cancellers by special, proprietary techniques which lead to canceller settling times of better than 50us being achieved with production units.

BENEFITS OF THE SPS APPROACH TO CANCELLATION

Cancellation speed : SPS cancellers, using patented adaptive loop techniques, can readily achieve cancellation speeds of better than 50us. As the rise time of typical hopping transmitters will often exceed this, it is generally the case that the cancellation loop settles well before the interfering transmitter reaches its maximum power. This means that the transient seen at the receiver is of very short duration and of such low power level that it remains below the level of any disturbance to normal ESM function. It should be noted, in particular, that this performance is achieved without a priori knowledge of the hopping pattern. This avoids the need for any modification to existing transmitters.

Interfacing : Figure 5 illustrates that the only interface required to the interfering transmitter is to take a sample of the output power by the introduction of a standard passive directional coupler. This will have minimal effect on the effective transmitter output power, often causing less than 1dB reduction. Connection to the receive path is also very simple, as the interference cancellation unit only needs to be inserted in series with the feeder from the receiver antenna. This means that cancellers can be retro-fitted to existing, installed systems without modification.

Receive Path Noise and Distortion : It is vital in ESM receive systems that front end linearity is beyond reproach. A particular advantage of the approach described is that the receive path is not affected by the canceller except that a small insertion loss in incurred due to the passive directional couplers (C2 and C3 in Figure 5). A second important aspect is that the receive path is passive so that noise and distortion, such as would be caused if amplifiers were inserted, are avoided. It is also easy to guarantee that cancellers have reproducible receive path characteristics which is important where several receive channels must be phase matched for DF.

Flexibility : The coupling ratio of C2 determines the trade off between receive path insertion loss and the maximum interference signal which can be cancelled. This provides the designer with considerable flexibility in the configuration of the cancellation system. To illustrate the trade-off, some examples are given in Table 1 :

Coupling Ratio of C2 (dB)	Receive path insertion loss (dB)	Maximum interference signal level (dBm)
10	1.5	20.5
6	2.3	25.3
3	4.0	30.0

Table 1 - Insertion Loss/Interference level trade-off

MULTI-LOOP/MULTI-CHANNEL CONFIGURATIONS

The previous description of the basic adaptive canceller, together with Figure 5, described the hardware required to protect one receive path from one source of interference. This case,

termed a '1 on 1' configuration, is illustrated in a simplified form in Figure 7.

Other configurations can readily be constructed and two examples of more complex systems are shown in Figures 8 and 9. These configurations use additional hardware building blocks which are almost identical to those used for the simple 1 on 1 case. The additional cancellation functionality may also be required to protect a very wide frequency range receiving system from transmitters operating in several different communications bands and with differing power levels. Hence a flexible and modular approach to hardware realisation is required.

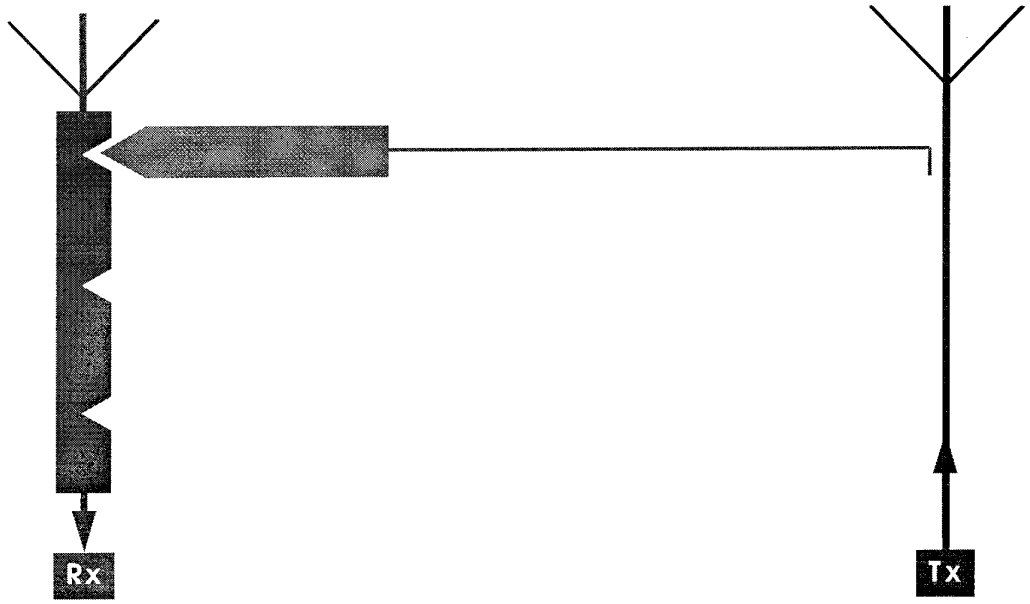

Figure 7 - Outline of a 1 on 1 Canceller Configuration

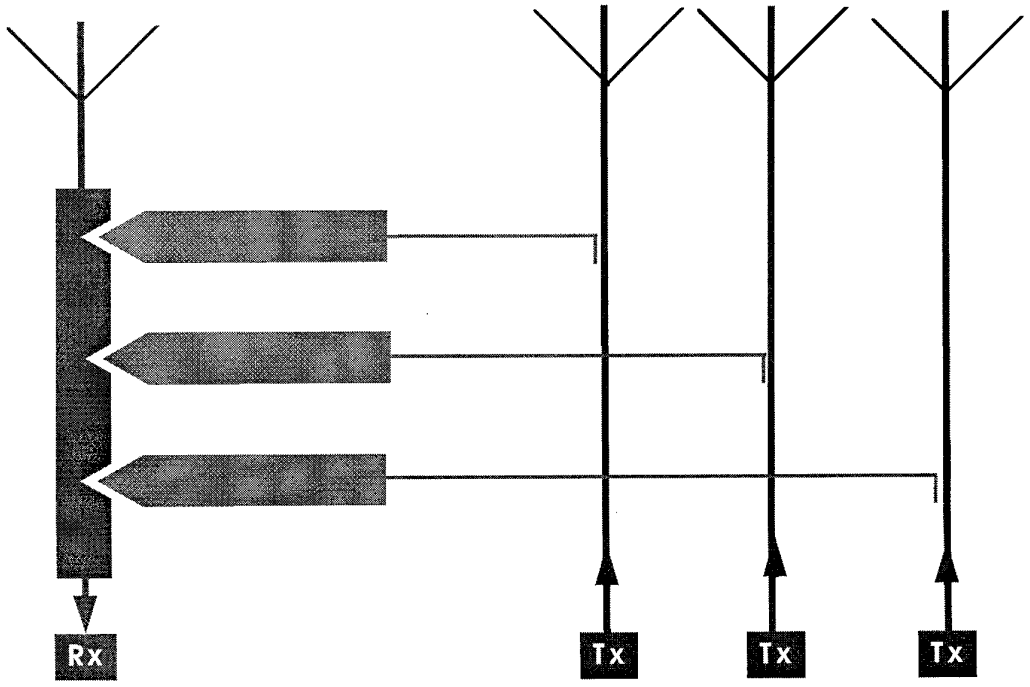

Figure 8 - Outline of a 3 on 1 Canceller Configuration

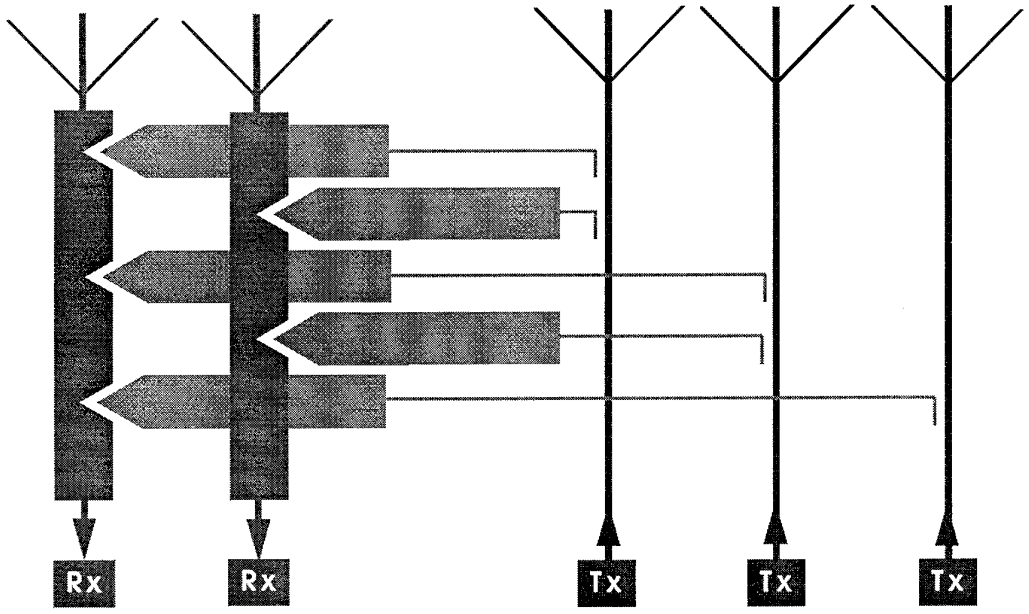

Figure 9 - Outline of a 3 on 2 Canceller Configuration

HARDWARE IMPLEMENTATION

SPS have built canceller systems in a variety of forms to suit specific requirements. The preferred approach, which is used in the Siemens Plessey 'INCAN' product, is to build systems in a modular form in which the essential cancellation functionality is realised in the minimum number of module types consistent with retaining the flexibility to meet a wide range of system configurations.

Referring to Figure 5, the key adaptive elements of the cancellation loop (vector modulator and correlator with associated loop filter and DC amplifier) are constructed in a 'weight' module. The circuit elements associated with the receive path (couplers C2 and C3 and the feedback RF amplifier) are built in a 'combiner' module. This leads to a very convenient split of functionality as the elements of the weight module are independent of the overall configuration. The combiner module, however, contains the elements which typically require minor adaptation to suit different configurations. Reference to Figures 7, 8 and 9 will show that the combiner module is where the weighted cancellation signals are added into the receive path. In addition, the combiner contains coupler C2 which determines the insertion loss/interference handling trade-off.

The INCAN combiner and weight modules are both constructed in milled alloy cases for good RF screening and for physical protection. Module size is approximately 9x10x0.6inches. The standard weight module of this size actually accommodates two independent weight circuits, to provide the cancellation functionality for two interference sources for one receive path. RF connectors are fitted to one end of the modules. Both module types are also fitted with a D connector for the input of DC power and the output a Build In Test (BIT) signal. The BIT function operates continuously and does not interfere with system operation in any way.

The modules can be plugged into an 8x9x18inch INCAN mainframe chassis, constructed of milled alloy panels electron beam welded together to give a very rugged form of construction with excellent EMC performance. The modules are firmly clamped into the chassis by wedgelocks. Internally, the chassis contains a backplane for module DC and BIT interconnections. The rear section of the chassis is used for module RF interconnections which are generally in semi-rigid cable for excellent screening and reliability. This rear section is also used for EMC filters and other components such as power dividers used for some system configurations.

A PSU/BIT module is also fitted into the chassis and provides the DC power rails from an AC power line. This module also combines the various BIT module signals into a standard serial data format.

The standard chassis will accommodate up to eight modules so that complex configurations can be built within a single unit. Figure 10 shows a lightly populated INCAN chassis, with some modules partly extracted.

The modules are sufficiently well screened and constructed that an alternative method of construction can be used in which the necessary modules are clamped together in a sub-frame and installed within a customer supplied enclosure.

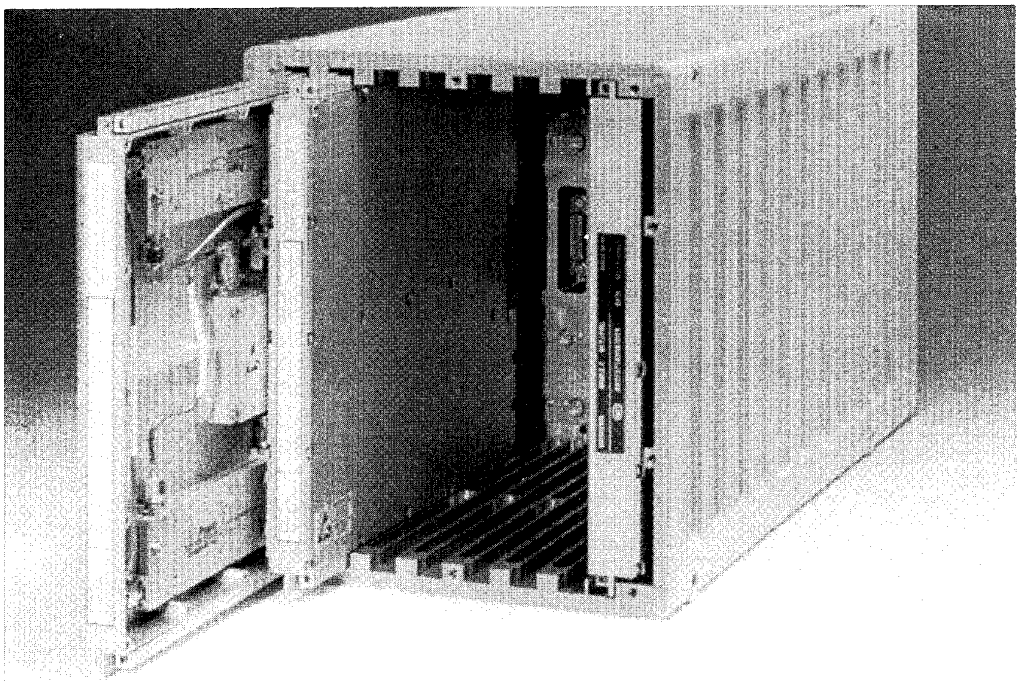

Figure 10 - Ruggedised INCAN Enclosure

PERFORMANCE IN PRACTICAL SYSTEMS

The original INCAN product, which is now in service with an advanced US Army communications EW system, provided cancellation at UHF. A summary of the key performance parameters is as follows :

- Cancellation frequency range — Greater than 225-400MHz
- Cancellation bandwidth — Greater than 100kHz
- Cancellation speed — Less than 100usec
- Max interference level — 18dBm
- Insertion loss — 1.5dB
- Phase matching between channels — Better than 1.5degrees

The equipment has been tested to a demanding environmental specification which includes operation to the above specification under severe vibration (typical of tracked vehicles and helicopters) and over an operating temperature range of -51 to +55C. Stringent EMC performance is also achieved by this equipment.

Versions of the equipment operating in other frequency bands including the VHF 30-88MHz range have also been built and delivered. These use the same modular construction and equipment size as described above.

SUMMARY

This paper has described the principles of interference cancellation. Interference cancellation is now an important part of advanced communications EW systems because of the wide instantaneous bandwidth of such systems, coupled with the increasing use of agile communications. The paper has described a state of the art military interference cancellation product which is vital to the effective performance of the complex and advanced EW system into which it is integrated.

U. Lammers (US)

You mentioned that the canceller could handle input power levels up to one watt. Does this mean that normal input stages like transistors may be used without danger of performance degradation or burn-out ?

Author's Reply

Yes, the interference cancellation equipment can protect the front-end of a receiver up to the specified maximum interfering power level. Any transients present at the input to the receiver are well below the levels at which damage could occur.

The system designer may choose to incorporate additional protection if it is considered possible that the operators may fail to switch the interference cancellation system on. This would only be required if sufficient protection was not already built into the receivers.

PREDICTION OF ANTENNA TO ANTENNA COUPLING BY USE OF A COMPUTER PROGRAM, BASED ON THE METHOD OF MOMENTS

Th. Klook
MAZ Hamburg GmbH
Germany

K.-H. Gonschorek
TU Hamburg-Harburg
Harburger Schloss Strasse, 20
D-21097 Hamburg
Germany

Introduction

On complex systems like vessels, vehicles, planes and rockets often there are used closely spaced antennas. When planning the electromagnetic compatibility of such systems the question for possible interactions between transmitting and/or receiving equipment is a major problem. It has to be clarified how critical the coupling between closely spaced antennas will be, including the question of how the antenna pattern will be influenced.
The simultaneous operation of two antennas is a very serious problem if the difference of the operation frequencies is very small. The coupling of power from one transmitter to the other (active influence) may produce malfunctions or damage the output stages.
The possible detuning of the neighbouring antenna (passive influence) is a further problem to be paid attention to.
With the help of efficient software it is possible to carry out an effective planning of the electromagnetic compatibility of such kind of systems and to support the selection of suitable antenna locations.

The computation of different cases of influences will be described, with the help of the computer program CONCEPT [4], which is based on the method of moments (MoM).

Investigated arrangement

Fig. 1 shows the arrangement for the further investigations. The transmitter S1 on the left side supplies a rod antenna of the height h1 via a matching device M1. The filter F1 is optional.
An equivalent transmitter S2 on the right side supplies a rod antenna of the height h2 via a matching device M2. The filter F2 is again optional. The distance between the antennas is l.

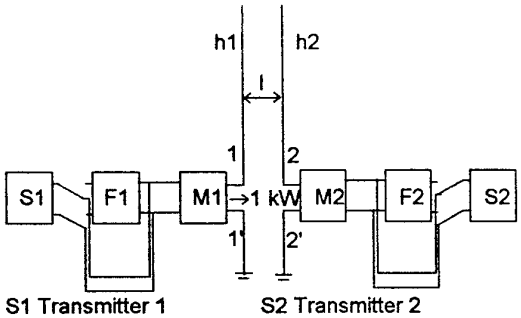

S1 Transmitter 1 — S2 Transmitter 2
F1 Filter 1 — F2 Filter 2
M1 Matching device 1 — M2 Matching device 2

Fig. 1: Arrangement of two transmitting systems

This arrangement can be transformed into a reciprocal four-pole network [2] as shown in Fig. 2. If the antenna 2 is terminated with the impedance $\underline{Z}2L$, the input impedance of antenna 1 $\underline{Z}1$ can be calculated by use of the following equation:

$$\underline{Z}1 = \underline{Z}11 - \frac{\underline{Z}12 \cdot \underline{Z}21}{\underline{Z}22 + \underline{Z}2L} \qquad (1)$$

and because $\underline{Z}12 = \underline{Z}21$, this formula can be shortened to

$$\underline{Z}1 = \underline{Z}11 - \frac{\underline{Z}12^2}{\underline{Z}22 + \underline{Z}2L} \qquad (2)$$

with

Paper presented at the AGARD SPP Symposium on "Environmental Factors in Electronic Warfare Related to Aerospace Systems" held in Pratica di Mare AFB (Rome) Italy, from 8-11 May 1995, and published in CP-573.

$\underline{Z}11$: Impedance at 11' with open circuit at 22',

$\underline{Z}12$: Relation between the open-circuit voltage at 11' and the current fed in at 22',

$\underline{Z}21$: Relation between the open-circuit voltage at 22' and the current fed in at 11',

$\underline{Z}22$: Impedance at 22' with open circuit at 11',

$\underline{Z}2L$: Load impedance at 22'.

For $\underline{Z}2$ we obtain analogous equations.

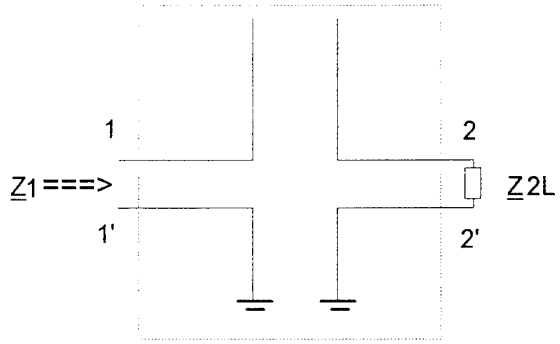

Fig. 2: Two coupled antennas simplified to a reciprocal four-pole network

In a first step the values $\underline{Z}11$, $\underline{Z}12$ and $\underline{Z}22$ have to be calculated using a computer program, for example with CONCEPT.
The antenna 2 receives the maximum power of the electromagnetic field produced by antenna 1, when the load impedance $\underline{Z}2L$ is conjugate complex to the feed point impedance $\underline{Z}2$. Furthermore the antenna 1 has to be matched to the input impedance $\underline{Z}1$, for an effective radiation.
But it has to be considered that $\underline{Z}1$ and $\underline{Z}2$ depend on each other (equation (2)). The condition for matching has to be calculated on an analytical way [3] or with an iteration procedure.

The iteration operates as follows:

1) The antenna 2 has to be terminated with the conjugate complex input impedance

   $\underline{Z}2L=\underline{Z}22^*$.

2) By use of the equation (2) the input impedance $\underline{Z}1$ has to be calculated.

3) Now the antenna 1 has to be terminated with the conjugate complex value of the calculated input impedance $\underline{Z}1$ of the last step,

   $\underline{Z}1L=\underline{Z}1^*$.

4) In this step the new input impedance $\underline{Z}2$ has to be estimated.

5) Antenna 2 has to be terminated with the conjugate complex value of the calculated input impedance $\underline{Z}2$ of step 4),

   $\underline{Z}2L=\underline{Z}2^*$,

   and a new input impedance $\underline{Z}1$ has to be calculated by use of the equation (2).

6) The steps 3) to 5) have to be repeated until no further changes of $\underline{Z}1$ and $\underline{Z}2$ occur (within a specified limit).

Simultaneous operation of two matched antennas at the same frequency

Example 1:

First a relatively simple arrangement is selected.
Two rod antennas of the same height of 10 m, with a distance of 10 m and a radius of 10 mm are modelled (Fig. 3) and computed.

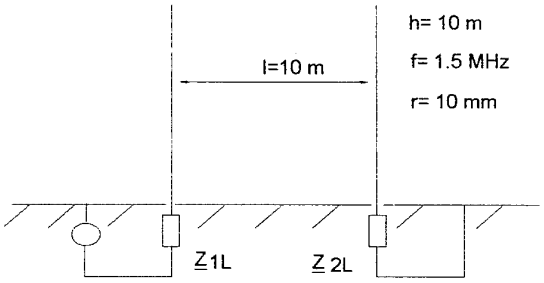

Fig. 3: Arrangement for example 1

For a frequency of 1.5 MHz the calculations yield the following values:

$\underline{Z}11=\underline{Z}22=$ (0.92-j 1077.10) Ω,
$\underline{Z}12=\underline{Z}21=$ (0.90-j 17.16) Ω.

The iterative procedure leads to impedances $\underline{Z}1$ and $\underline{Z}2$ of

$\underline{Z}1=\underline{Z}2=$ (3.297-j 1060.26) Ω.

Terminating 22' by $\underline{Z}2L=\underline{Z}2^*$ and matching the antenna 1 for an impedance of $\underline{Z}1L=\underline{Z}1^*$, seen from the antenna side, and $\underline{Z}1L=\underline{Z}_{out}$, seen from transmitter side, leads to a complete power matching of the four-pole network. ($\underline{Z}_{out}$ = output impedance of the transmitter).
Considering the matched case it is now possible to calculate the maximum power transfer from antenna 1 to antenna 2. 1 kW power input to antenna 1 results in a received power of 979 W at the port of antenna 2. In antenna 2 a feed point current of 17.23 will flow (theoretically).

From this values a decoupling of

a= 10 log (1000/979)≈0.1 dB

can be calculated.

The example 1 shows that an operation of two antennas at the same frequency is very critical, at least when the antennas are short compared to the wave length. More than 90% of the radiated power of antenna 1 can be coupled into the antenna 2 in theory.

Example 2:

Example 2 is similar to example 1. The antenna distance is again 10 m, also the radius of 10 mm has not been changed. The height of antenna 1 is now 12 m and of antenna 2 the height is 8 m. (Fig. 4).

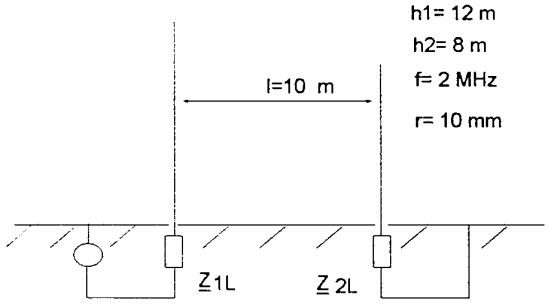

Fig. 4: Arrangement for example 2

The impedance values of this arrangement (frequency f= 2 MHz) are

Z11= (2.44-j 655.01) Ω,
Z22= (1.04-j 965.40) Ω,
Z12=Z21= (1.54-j 11.09) Ω.

The iteration procedure yields

Z1= (4.533-j 638.63) Ω,
Z2= (1.933-j 958.41) Ω.

1 kW power input to antenna 1 results in this case in a received power of 927 W at the port of antenna 2. In antenna 2 a feed point current of 21.9 A will flow (theoretically).

The decoupling is now calculated to

a= 10 log (1000/927)≈0.33 dB.

Like the last example the coupling is very critical. Investigations based on Fig. 4 for 2.5 MHz and 3.0 MHz delivers the following decoupling values:

2.5 MHz: a= 10 log (1000/821)≈0.86 dB,
3.0 MHz: a= 10 log (1000/663)≈1.78 dB.

Comparing the respective wavelength with the height of the transmitting antennas yields the following relations:

2.0 MHz: 12 m/150 m=0.08,
2.5 MHz: 12 m/120 m=0.10,
3.0 MHz: 12 m/100 m=0.12.

The comparison of this ratios with the decoupling values shows that with an increase in the electrical length of the antennas the decoupling will also increase. With other words: The coupling is more critical, when the lengths of the antennas are short.
In Fig. 5a the dependency of the decoupling from the individual height of the antennas is shown.
Furthermore the investigations in [1] have shown, that the decoupling does not increase proportional to the distance. Doubling the distance between the antennas results in a decoupling increase of only 3 to 4 dB (See Fig. 5b).

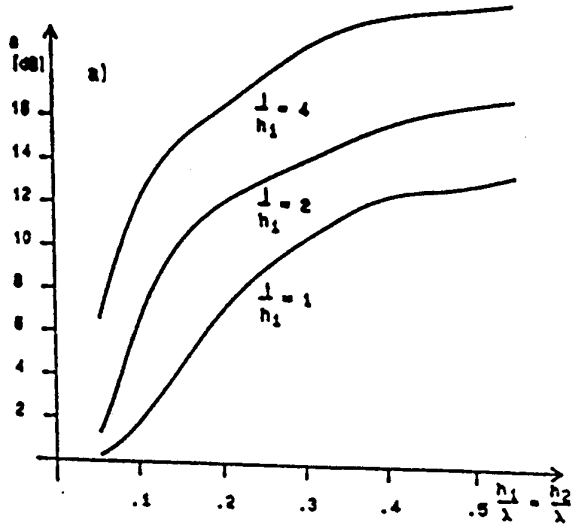

Fig. 5a): Decoupling a between two monopole antennas with the same height in dependence on their normalized heigth

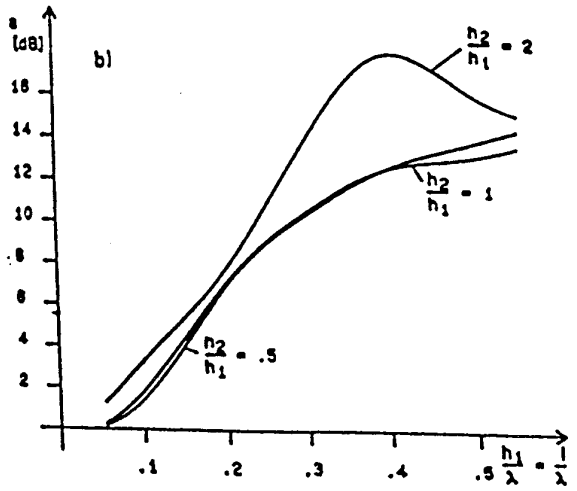

Fig. 5b): Decoupling a between two monopole antennas with different heights in dependence on their normalized distance

Operation of two transmitters with matched antennas at different frequencies

Next the example shown in Fig. 6 is investigated .

Example 3:

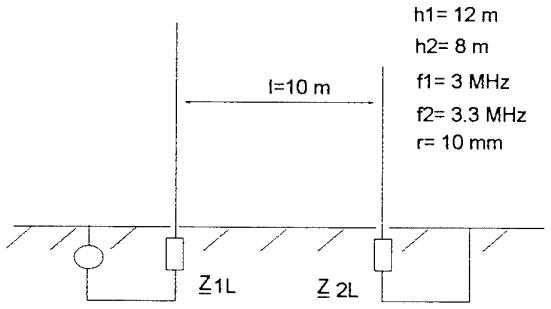

Fig. 6: Arrangement for Example 3

The difference between the frequencies is chosen to be 10%. The following values for 3 MHz (frequency 1) have been computed:

$\underline{Z}111$= (5.869-j 380.19) Ω,
$\underline{Z}221$= (2.419-j 609.85) Ω,
$\underline{Z}121=\underline{Z}211$= (3.473-j 6.15) Ω.

For 3.3 MHz (frequency 2) the following results have been established:

$\underline{Z}112$= (7.287-j 325.45) Ω,
$\underline{Z}222$= (2.963-j 542.62) Ω,
$\underline{Z}122=\underline{Z}212$= (4.207-j 5.32) Ω.

The iteration for matching of $\underline{Z}1$ and $\underline{Z}2$ has now to be carried out as follows:

1) The antenna 2 has to be terminated with the conjugate complex input impedance at frequency 2:

   $\underline{Z}2L=\underline{Z}222^*$.

2) With the equation (2) the input impedance $\underline{Z}1$ for the frequency 1 has to be established. $\underline{Z}2L$ has to be converted for frequency 1.

3) Now antenna 1 has to be terminated with the conjugate complex value of the calculated input impedance $\underline{Z}1$ of the last step,

   $\underline{Z}1L=\underline{Z}1^*$.

4) In this step the new input impedance $\underline{Z}2$ has to be estimated for the frequency 2. $\underline{Z}1L$ has to be converted for frequency 2.

5) Now the antenna 2 has to be terminated with the conjugate complex value of the calculated input impedance $\underline{Z}2$ of step 4,

   $\underline{Z}2L=\underline{Z}2^*$,

   and the input impedance $\underline{Z}1$ for the frequency 1 has to be evaluated.

6) The steps (3 to 5) have to be repeated until no further changes occur in $\underline{Z}1$ and $\underline{Z}2$.

Using this procedure the following results for example 3 are obtained:

$\underline{Z}1$= (5.463-j 379.91) Ω,
$\underline{Z}2$= (3.560-j 542.66) Ω.

The antenna 2 has to be terminated with the conjugate complex value $\underline{Z}2^*$ for the frequency 2. This antenna is surely not matched for frequency 1.
1 kW power input to antenna 1 results in a received power of 2.4 W at the port of antenna 2 and in antenna 2 a feed point current of 0.82 A will flow.
The decoupling amounts to:

a= 10 log (1000/2.4)≈26 dB.

The decoupling increases of about 24 dB compared to the simultaneous operation at the same frequency (3 MHz).
Investigating the arrangement of Fig.1 for the case of frequency 1 equal to 1.5 MHz and frequency 2 equal to 1.65 MHz leads to a decoupling of only 18 dB.
The decoupling increases from about 0.1 dB when operating both antennas at the same frequency (1.5 MHz) to 18 dB at 10 % frequency difference.

Example 4

In example 4 the case will be investigated when both antennas operate in quarter-wave resonance.

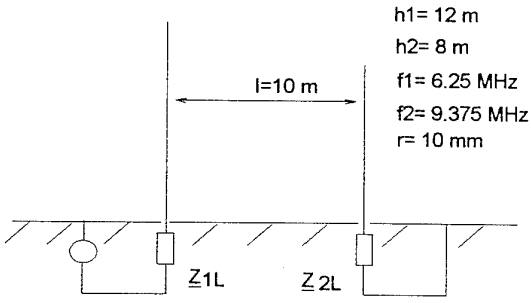

Fig. 7: Arrangement for example 4

For the arrangement shown in Fig. 7 the program computes the following values for frequency 1 (6.25 MHz).

$\underline{Z}111$= (40.068+j 21.14) Ω,
$\underline{Z}221$= (12.504-j 186.19) Ω,
$\underline{Z}121=\underline{Z}211$= (15.028-j 8.12) Ω,

and for frequency 2 (9.375 MHz):

$\underline{Z}112$= (275.93+j 431.69) Ω,
$\underline{Z}222$= (37.708+j 23.881) Ω,
$\underline{Z}122$=$\underline{Z}212$= (17.815-j 59.08) Ω.

By use of the procedure described in example 3 the following values were obtained:

$\underline{Z}1$= (38.787+j 20.720) Ω,
$\underline{Z}2$= (44.646+j 21.480) Ω.

The antenna 2 has to be terminated with the conjugate complex value $\underline{Z}2^*$ for the frequency 2. This antenna is surely not matched for frequency 1.

1 kW power input to antenna 1 results in a received power of 6.6 W at the port of antenna 2. A feed point current of 0.38 A will flow in antenna 2.

The decoupling becomes now:

a= 10 log (1000/6.6)≈22 dB.

It can be seen that despite of the large frequency difference of 50% the decoupling is in the same range as for 10% frequency shift, due to the quarter-wave resonance.

Operation of two transmitters at different frequencies, using filters

The investigations of the last chapters show that an additional decoupling is necessary. This decoupling can be performed by a transmitting filter. Nevertheless an operation at the same frequency is not allowed.
It is obvious that the filter of antenna 1 has an influence to the input impedance of antenna 2. If the matching of antenna 2 is changed a tuning of the matching device of antenna 1 will be necessary.
All possible input impedances that the matching device of antenna 1 must satisfy can be calculated from the assumption that all values of the right complex plane must be allowed as load impedances for antenna 2.
If only the imaginary axis of the impedance plane is regarded in equation (2), the result is a circle diagram in the complex impedance plane. $\underline{Z}1$ posseses all values which are enclosed by the circle.

In Fig. 8 the circle diagram for example 1 (1.5 MHz) is shown. Antenna 2 operates e.g. at a frequency of 1.65 MHz. The filter is effective.
The extension of possible mismatching can be expressed by the standing-wave ratio (SWR). The maximum SWR can be calculated by

$$SWR = \frac{Rea(\underline{Z}1)max}{Rea(\underline{Z}1)min} \qquad (3)$$

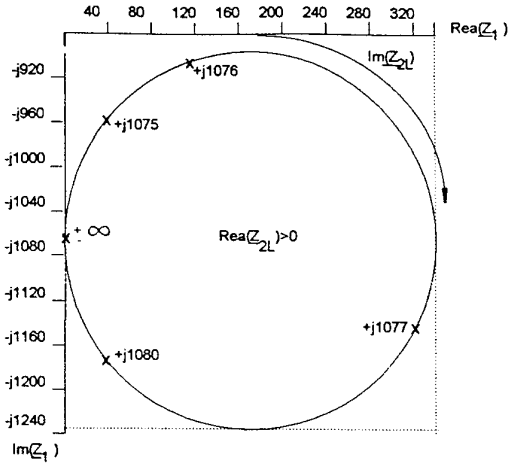

Fig. 8: Circle diagram of the input impedance for example 1

For example 1 a standing wave ratio of

SWR=340/0.9≈378

can be calculated.

From this SWR the reflection factor of

$$r = \frac{SWR - 1}{SWR + 1} = 0.995 \qquad (4)$$

can be established.

In Fig. 9 the circle diagram for example 2 and a frequency of 2 MHz is shown. The standing-wave ratio gets

SWR=120/2.3≈52,

the reflection factor becomes r= 0.96.

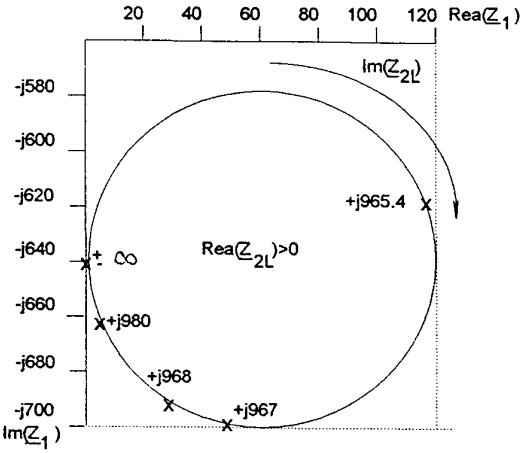

Fig. 9: Circle diagram for example 2 at 2 MHz

It must be seen that the calculated values are quite high and theoretical.
Practical investigations have shown decoupling values of less then 2 dB.

For example 2 and 2.5 MHz the SWR is about 11.5 (r= 0.84) and for 3 MHz about 9 (r= 0.80).

Fig. 10 shows the SWR in dependency of the normalized height [1] with I as parameter.

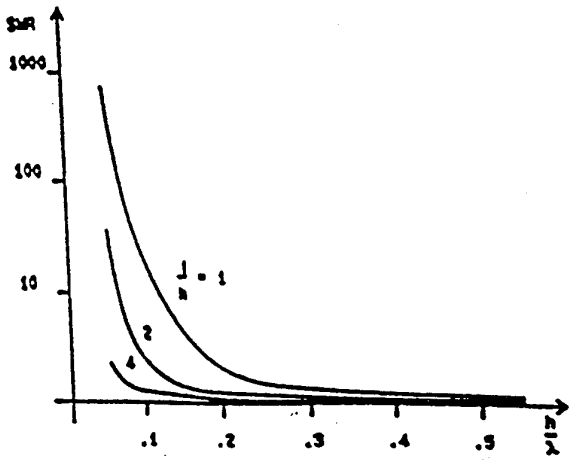

Fig. 10: SWR in dependency of the normalized antenna height

At low frequencies the SWR is very high, but only for a small range of Z2L-values as shown in Fig. 8. At high frequencies the influence becomes smaller and smaller, but for broader ranges of Z2L.

The previous treated monopole antennas were located over an infinitely conducting plane. The MoM is more powerful and able to compute coupling/ decoupling for antenna
arrangements of more complex models. In example 5 a more sophisticated model has been investigated.

Influence of the second antenna and the superstructure

Example 5

The arrangement shown in Fig. 11 shall rebuild a part of the superstructure of a ship.
Both antennas have a height of 8 m and are situated in a distance of 10 m on a support of 4 m. The antennas operate simultaneous at the same frequency of 9.375 MHz.

The investigation of the decoupling was made in the same manner as in example 1 and leads to

a= 10 log (1000/84)≈10.75 dB.

For the numerical calculation the number of unknowns in this example were 1047. The workstation HP 700 needed a calculation time of 7 minutes. The requested memory for the matrix was 19 Mbytes.

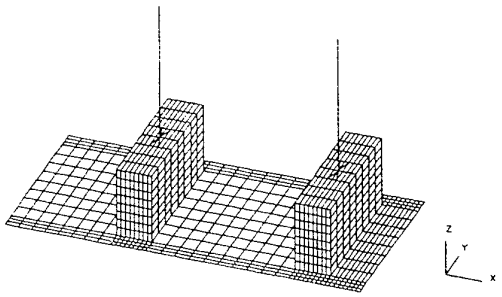

Fig. 11: Model for example 5

In the examples before the influence to the antenna pattern was not considered, but it can be shown that the antenna pattern will be influenced seriously by a parasitic radiator. Fig. 12 shows the antenna pattern for example 3 at a frequency of 3 MHz without (a) and with (b) influence of antenna 2. In Fig. 13 are shown the antenna patterns for 12-m-monopol-antenna at a frequency of 3.75 MHz, without (a) and with (b) influence of a 20-m-mast, in a distance of 5 m from the transmitting antenna. The influence of the quarter-wave resonant mast is clearly to be seen.
Fig. 14 shows the influence of the whole superstructure of example 5 and the antenna 2 to the antenna pattern of antenna 1.
All antenna patterns are linearly scaled and normalized to their maximum radiation.

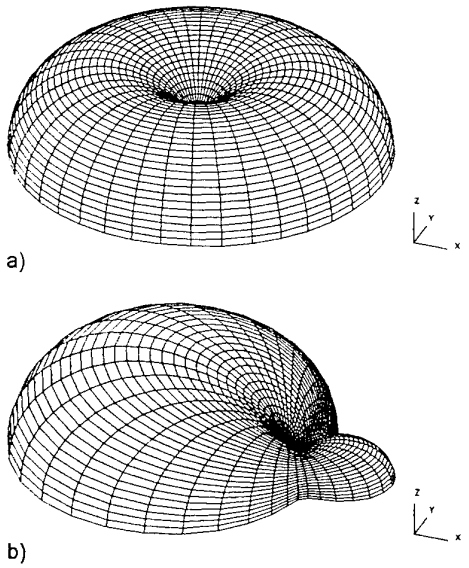

a)

b)

Fig. 12: Antenna pattern of example 3 (3 MHz)
a) without influence of antenna 2
b) with influence of the matched antenna 2

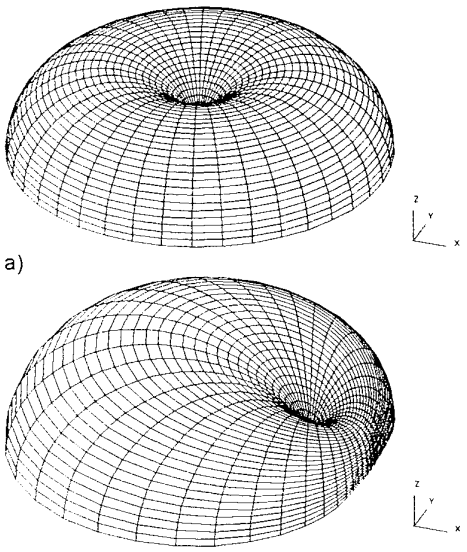

a)

b)

Fig. 13: Antenna pattern (3.75 MHz)
a) without influence of the 20-m- mast in 5 m distance
b) with influence of the 20-m-mast

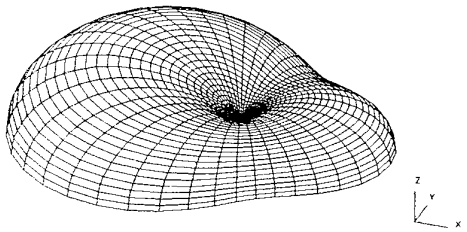

Fig. 14: Antenna pattern for example 5 (9.375 MHz) with influence of the matched antenna 2 and the structure

Summary:

It has clearly been shown, that the coupling of closely spaced antennas can be very critical. When two antennas operate at the same frequency a coupling of more than 90% is possible in theory. This coupling is able to destroy the final stages of the equipment. Therefore a tuning to the same frequency has to be avoided in any case.

Simultaneous operation of antennas in close vicinity will be connected with difficulties, even if there is a substantial frequency offset, especially in the case of resonances.

Transmitting filters permit an operation with frequency offset, but the influence of the input impedance of the second antenna is not to be avoided. In practice this is not an important influence because in low frequency range the reaction is great but only for a small range of load values. For higher frequencies the system becomes more wide-band but the reactions decrease.

Because of the presence of the second antenna the antenna pattern can seriously be influenced.

All calculations in this paper have been performed with the computer program CONCEPT. The simulation of electromagnetic field distributions by help of software can be an effective and efficient method for the planning of the electromagnetic compatibility of systems with antennas. Also complex structures can be investigated. There is not a limitation of the frequency range in theory. Only the resources of the used computer have to be considered.

References

[1] Gonschorek, K.H.:
Elektromagnetische Verträglichkeit (EMV) in Systemen mit eng benachbarten Antennen. Frequenz 38 (1984) 4, S. 78-84

[2] Mönich, G.; Kombrink, F.: Simultanbetrieb zweier Sendeanlagen bei eng benachbarten, abgestimmten Antennen. Frequenz 34 (1980) 6, S. 158-164

[3]
Beiblatt 1 zu VG 95 374 Teil 4

[4] Mader, T.; Brüns, H.-D.:
EFIE Analysis of Arbitrary Metallic Structures in the Area of EMC. 9th Int. Zurich Symp. on EMC, 1991, Contrib. 87M2

P. S. Cannon (UK)

Can you please tell me if the authors have used this technique to calculate the gain of an antenna array where two or more antennas are driven, rather than one being passive as in these examples.

Presenter's Reply

Up to now the gain of an antenna array has not been calculated for the case that two or more antennas are driven but there is no difficulty in doing this.

As long as you consider antennas with linear behaviour it is allowed to reduce the whole complex arrangement of an antenna (antenna array) and its environment to a reciprocal N-port network, using network theory for analysing the coupling between the different ports. The network elements have to be estimated with the aid of a MoM-program.

If you consider antennas with linear behaviour the law of superposition can be applied. In the first step the wanted transfer functions have to be estimated, in the second step the radiation and the gain can be calculated.

Trends and Tendencies in LPI Radar

Heiner Kuschel
Forschungsinstitut für Hochfrequenzphysik
der Forschungsgesellschaft für Angewandte Naturwissenschaften e.V.
Neuenahrer Strasse.20, D-53343 Wachtberg-Werthhoven
Germany

1. Summary

To achieve a Low Probability of Intercept is one of the most vital interests of radar developers. Different approaches to LPI radars have been made and some existing concepts are presented. The principle capabilities of LPI radar concepts are discussed and future trends are analysed with respect to ESM-system development and growing signal processing potentials.

2. Introduction

A covert radar operation in a Low Probability of Intercept mode is and will be the most effective measure against ESM detection, intelligent jamming and the Anti-Radiation Missile (ARM) threat. Most LPI-radar concepts try to reduce the transmitted peak power by stretching the signal in time and frequency in order to camouflage the specific radar signal signature. The use of a narrow beamwidth together with a low sidelobe pattern leads to a further reduction of the intercept probability. Unpredictable main beam pointing and the agility of the signal parameters as transmit-frequency, and if applicable pulswidth and pulse interval, increase the difficulties of ESM and ARM receivers in signal sorting.

Covertness in the spectral domain can be achieved by spreading the radar signal energy over a large bandwidth using a more or less noise-like wave form to make it less distinguishable from the thermal noise background. A broadband CW-signal has the least peak power but introduces severe signal processing loads. Additionally there are concepts that avoid a main beam by implementing a low gain wide angle illumination in combination with a starring multibeam receiver with highly integrating signal processing. The required radar performance as specified by range, search volume and update rate limit in general the possibility of a covert radar operation to short range radar applications.

The least probability of intercept, however, can be achieved with a so-called passive radar, offering no determined radar emission at all by the use of existing RF -transmissions. Since the covertness of passive radars is attractive, but their dependency on the availability of a satisfactory illumination can be restricting, the NATO DRG study group RSG 3 of Panel 10 has investigated the possibilities to attain good LPI characteristic and radar performance in combining a passive radar system with an active "fall back" transmitter using a covert wave form

Even if the general objective of the user is not to be identified as a radar, the first goal is not to be detected by an ESM receiver. A low probability of detection Q_D of an ESM system is influenced by several features of the radar system which determine the signal-to-noise ratio SNR_i at the location of the ESM receiver and the radar illumination sequence. A low peak power of the radar reduces the SNR_i. The narrow beam of a rotating radar antenna and a slow rotation rate reduce the probability that the radar signal is detected during the first scan of the ESM system and thus increase the search time. Increased search time and large bandwidths to be scanned, however, reduce the ESMs probability of detection.

Hence, there are several approaches to achieve a low probability of interception. Spreading the signal power over a long period or using a continuous wave (CW) and reducing the power which is transmitted through the antenna sidelobes by advanced antenna designs with narrow mainlobes are the most obvious measures. Spreading the signal energy over a large bandwidth is another approach, requiring a broadband antenna with a limited capability in sidelobe reduction. The time, an ESM system needs for search and decision can be increased by choosing a highly complex , probably a noise like waveform. Further measures to prevent an ESM system from identifying the radars emission are the use of frequency agility, PRI agility, pulse width agility, polarisation and scanning agility and the use of polyphase codes instead of pn-codes to avoid simple ESM/ARM receiver autocorrelation techniques.

The ideal LPI signal would be a noise signal with a thumb tack ambiguity function and an ultrawide bandwidth. Since the correlation of a random noise signal in the radar receiver still is a vast challenge, todays LPI radars use low sidelobe antennas and moderate signal bandwidths in a CW mode.

3. Existing LPI Concepts

The system concepts, introduced below, represent two approaches to deny hostile ESM receivers information about the radar sensor. Spreading the radar energy in time and frequency and concentrating it in a narrow mainlobe to minimise the time, the ESM system is illuminated, competes with a concept of energy distribution in time, frequency and space, where several

Paper presented at the AGARD SPP Symposium on "Environmental Factors in Electronic Warfare Related to Aerospace Systems" held in Pratica di Mare AFB (Rome) Italy, from 8-11 May 1995, and published in CP-573.

simple and inexpensive "omnidirectional" transmitters mainly result in a decrease of it's ARM vulnerability.

3.1 OLPI radar

The OLPI radar (omnidirectional LPI) /1/ of FGAN-FFM obtains its LPI characteristic through the use of low transmitted power compensated by a relatively long integration time . The idea is to distribute the signal as wide as possible in space and time to reduce the probability of being intercepted. The observation space is illuminated continuously with a phase coded CW waveform centred at about 3 Ghz. The OLPI radar is designed for surveillance of a 120° azimuth sector which is illuminated continuously with an array of 8 vertical dipoles yielding a coverage of 120° in azimuth and 20° in elevation. Thus, the 15 W CW transmit power is spread over a wide space. A multibeam antenna with 64 columns of 8 dipoles each is used on receive, yielding a 2° azimuth resolution.

Figure 1 shows the antenna pattern of the OLPI concept. The major problem in a CW radar like this is the permanent clutter from the environment which demands a high dynamic range of the receiving channels and appropriate signal processing. A long integration time in the order of 2 seconds for the radar target echoes is required to achieve subclutter visibility and thus the target resolution is limited to some hundred meters. The OLPI concept enables the use of several inexpensive transmitters which could operate alternatively or as mutual decoys.

3.2 Pilot radar

Pilot is a naval radar developed by the Philips group. The Pilot radar /2/ employs frequency-modulated continuous wave transmission (FMCW) which provides similar performance as a conventional pulse radar but limits the ESM counterdetection range to approximately 1.3 nm and thus claims to be virtually undetectable by conventional ESM receivers. The output power of 1 W can be spread over a frequency sweep of up to 50 MHz with a sweep repetition frequency of 1 kHz. The radar operates at a centre frequency of 9.375 GHz in I-band, the same band as other navigation radars, so that its signals do not clearly identify it. It is reported to enable detection of 400 t targets at a range of 15 to 20 kilometres.

Pilot can be operated with both a dual and a single slotted waveguide antenna. In the case of a single antenna for transmit and receive, a reflected power canceller (RPC) subtracts a sample of the transmitted signal from the received signal, thereby cancelling out the leakage from the transmitter. A digital signal processor using an FFT algorithm is incorporated for range computation, thus giving the pilot radar a high flexibility and good range resolution characteristics. For the future, Pilot is promoted as the forerunner of a family of LPI radar sensors.

4. LPI capability

A measure of the LPI capability of any radar is the crossover range. The crossover range is defined as the range where the radar emission can be detected by an intercept receiver. The crossover range is dependent on the effective radiated power (ERP) of the radar, the wavelength and the ESM receiver sensitivity S.

$$R_{ESM} = \sqrt{\frac{ERP * \lambda^2}{16 * \pi^2 * S}}$$

The ERP of the radar is given by

$$ERP = \frac{(4\pi)^3 * R^4 * kT_S * L(S/N)}{G_r * \lambda^2 * \sigma * T_i}$$

As an example, a generic noise radar , operating at a centre frequency of 10 GHz with a 20 ms coherent processing interval T_i, a 30 db receiver antenna gain G_r and an instantaneous bandwidth of 1 GHz , designed to detect a 2 m^2 target at 24 km range is calculated against an ESM receiver spanning a bandwidth of 500 MHz with a sensitivity S of -70 dbm. With the radar's range resolution of 0.15 m the target fluctuation is assumed to obey Swerling 0, resulting in a signal-to-noise ratio of 13 db for 90 % probability of detection and a false alarm rate of 10^{-6} . A loss of 3 db has to be taken into account since the ESM bandwidth only covers half of the radar signal bandwidth. The required ERP is calculated to be 25 W, resulting in a 26.8 km crossoverrange. Detecting the radars emission, however, in this case only means detecting another noise source and does not reveal any information about its purpose or even the radars processing parameters. The above calculation, however, shows that even the generic LPI system, applying all of the before mentioned measures to reduce the probability of being detected, can only achieve a crossover range equal to the detection range. Only if the target echoes are powerful enough like in the case of the naval radar „PILOT", where targets of several hundred square metres of RCS are to be detected, the radar power can be kept small enough to achieve as little as 1.3 nm crossover range and thus earn the name LPI.

5. Passive and Noise Radar

Since the probability of intercept is at its lowest if the emissions of a radar cannot be distinguished from environmental signals or thermal noise or, if no dedicated radar signal is emitted at all and emissions of opportunity are exploited for target detection, RSG3 has conducted a study to evaluate approaches to future ground based radars that operate in a passive mode with an active LPI transmitting mode as a fall back position.

There are several reasons to advocate the use of purely passive receivers especially on the battlefield; one of them is logistics. With a passive system using illuminators of opportunity the burden of moving a

power hungry transmitter is reduced or even eliminated. This means a cost reduction and a reduction in march time in terms of sorties transport aircraft must fly. More vital reasons are the absence of an ARM threat which makes costly ARM protection no longer necessary and a drastically reduced problem of dedicated jamming.

However so attractive these features are, the drawbacks must not be ignored. Giving up control of one's transmitter requires a versatile receiver which can work over a broad frequency band. Bistatic configurations in general have a reduced coverage compared to monostatic systems at least in the usual radar bands. Range and angular resolution are no longer constant but are dependent on the target location with respect to transmitter and receiver. The use of other radars as transmitters of opportunity requires a highly complex scanning strategy in the receiver like *pulse chasing* or a costly multi-beam antenna processing.

In a multistatic concept, by deploying several receivers at different locations and geometries, the problems of target position accuracy can be overcome. Each receiver would use the same illuminator and employ triangulation to determine target location. This information would then be feed to a central command and control location where a fire control system could be chosen to engage the target.

In the event that illuminators of opportunity are disabled or a more precise air picture is required, the system would use a transmitter which emits a random noise signal. The prime reason for this type of signal is to embed it in the general noise environment. This is intended to deny the enemy information about the source whereby the potential for electronic counter measures such as jamming or ARMs is eliminated.

5.1 Environmental conditions

The configuration is essentially a bistatic radar due to the physical relationship between the transmitter and the receiver and thus the environmental conditions of a bistatic radar have to be considered. Since the possible concepts for passive radars using transmitters of opportunity, vary over a wide frequency range from radio and TV-bands to the classical radar bands and the illuminators may also include elevated platforms, the screening and propagation situation can differ greatly. Further constraints that have to be respected are due to Doppler dead zones and the direct coupling of transmitter energy into the receiver in an area around the baseline./3/

5.2 Screening

In principle, in a bistatic or multistatic radar configuration there has to be a line-of sight (LOS) to the target from both the transmitter and the receiver stations. This condition is more restrictive than in a monostatic case, especially for ground based stations in rough terrain. Hence, the azimuthal coverage of a bistatic radar is, in general, smaller than that of a comparable monostatic one. A promising exception is the use of lower frequencies, typically VHF/UHF-band, where diffraction propagation can be exploited. Simulations with a terrain data based propagation model /4/ have shown that larger areas of coverage can be achieved with a low frequency bistatic radar where one non-LOS path can be tolerated for target detection. Figure 2 gives an example of the possible bistatic coverage of a generic site with a baselength of 41 km, antenna heights of 10m and an assumed target height of 30 m above ground for a radar frequency of 400 MHz and 1 GHz, respectively. A bistatic configuration is of special interest if the area around the transmitter and that between transmitter and receiver is to be surveyed. Here, the use of a VHF/UHF -TV transmitter as a ToO could yield large passive surveillance areas, comparable to the TV service area.

At the conventional radar frequencies screening problems can only be solved using multiple receivers or elevated platforms. Both solutions are relatively costly and thus screening may be the most restrictive constraint if low flying targets are to be detected. Mulipath propagation will more likely occur with low frequencies but mainly on line-of sight paths. It can, however, occur on both path, transmitter-target and target-receiver, which can result in up to 3 delayed target echoes compared to a maximum of 2 in a monostatic radar as shown in figure 3.

5.3 Bistatic geometry

In a passive radar which is by our definition either bi- or multistatic, the geometry is no longer circular as in the monostatic case, but it is strongly dependent on the length of the baseline between transmitter and receiver. The bistatic lines of constant signal-to noise-ratio SNR are the so called ovals of Cassini /3/. Target detection is not possible due to direct coupling in an area between transmitter and receiver which is dependent on the receiver beamwidth. The curves of constant delay of a target echo pulse are ellipses with the transmitter and the receiver as foci as shown in figure 4.

While in monostatic radar a target cannot be discriminated from clutter returns if it flies tangential to the radar, Doppler dead zones of bistatic configurations are dependent in shape and extension on the target trajectory relative to the radar baseline. Figure 5 gives some examples of bistatic dead zones. As figures 2 and 5 indicate Doppler dead zones are, in general, in conjunction with the areas of improved detectability in terms of propagation losses.

5.4 Bistatic clutter

Bistatic ground clutter is not significantly different from monostatic clutter, except from the region between transmitter and receiver where specular reflections of the ground may occur in a forward scatter situation. Here the value for σ_0 can increase to up to 20 dB m^2/m^2

/3/ as shown in figure 6 , where the out of plane angle varies from 0° (bistatic forward) to 180° (monostatic). The variation with polarisation is insignificant but increases with wavelength because of the surface roughness of the ground.

5.5 Bistatic target RCS

In bistatic radar configurations, the radar cross section RCS of an air target can be different from the monostatic RCS. Three different RCS regions are discriminated depending on the bistatic angle. The first is the pseudo monostatic one, where very few differences from the monostatic RCS can be recognised. The second region is called the bistatic RCS region with bistatic angles between 30 and 70 degs. In this region the bistatic RCS diverges from the monostatic due to several effects but is generally smaller than the latter. Three effects or sources of bistatic reflection are to be mentioned. First there are changes in relative phase between discrete scattering centres when they are significantly coupled. This is analogous to monostatic fluctuations, but caused by bistatic angular variation. The RCS can vary from a few dB to more than 20 dB dependent on the magnitude of coupling. A second source are reradiating discrete scattering centres. With changing bistatic angles the direction of reradiation moves along the lobing of the reradiation diagram of discrete scattering centres like corners, joints, edges etc. Those scatterers that were at a maximum at monostatic incidence generally diminish for larger bistatic angles and new maxima of scattering centres occur. Further on, new scatterers can occur which had been shadowed by target structures before. Shadowing is also the reason for a reduction of glint under bistatic conditions. Stealthy air vehicles may more likely be detected exploiting the design principle that radar energy is attempted to be scattered to directions different from the monostatic direction of illumination within a specific angular region. A third region of bistatic RCS, typically with bistatic angles around 180°, is called the forward scatter region. Here, the RCS is only dependent on the shadow area or silhouette of the target and can be many times the backscatter RCS of monostatic radar and will not be reduced by normal RCS reduction techniques as body shaping or coating with radar absorbing material (RAM).

At metric wavelengths, RAM application and shaping is less effective at all bistatic angles, however, we can only refer to monostatic measurements of a stealth target model. At least in the bistatic and quasi monostatic area of RCS, one can assume that at these frequencies the RCS will not vary much with the bistatic angle since it is rather a result of resonating target dimension than of specific scattering centres.

5.6 Conclusions from bistatic environment

The above considerations on the bistatic geometry and the influences of the environment including the target aspects lead to the conclusion that only limited geometric configurations of passive radars are promising. Though the forward scatter region would yield best results in RCS and coverage it is not a preferable geometry for a passive radar receiver because of the bistatic Doppler dead zone, direct coupling and specular ground reflections.

Dependent on whether the illuminator is co-operative or not, passive radars will show best performance in air space surveillance either in the vicinity of the transmitter or of the receiver. As e.g. airborne early warning radar illumination can co-operatively be exploited by forward located passive receivers, the same receiver could alternatively make use of the transmission of non-co-operative hostile radars for target detection.

5.7 Noise radar

The random noise radar /5/ was chosen for the role as active fall back component of the passive radar because the noise-like nature of the transmitted signal makes it unusually difficult to be detected by an intercept receiver or to be repeated by a deception jammer. It provides a unique ultra-wideband approach to the problem of achieving excellent range resolution and velocity resolution without the usual ambiguity restrictions. It exhibits several features that are not obtainable simultaneously by any other existing radar system. A random noise signal is virtually indistinguishable from thermal noise and has inherently a large bandwidth which is needed for high range resolution and the transmitter does not require any critical adjustments.

Range ambiguities do not occur at any pulse repetition frequency PRF since the waveform is different from pulse to pulse. Thus velocity ambiguities can always be avoided using a high PRF. Furthermore, the range and velocity resolutions are independently controllable in the receiver and there is no range-Doppler coupling. Hence, without changing the radiated signal in any way, the size of the range cell can be adjusted according to the actual task of the radar. Small range cells for target classification or clutter reduction can as well be processed as large range cells for detection. Large and small cells can even be processed simultaneously from the same transmitted signal.

However, to benefit form the features mentioned above, severe signal processing requirements have to be met. If e.g. a long range search mode of about 200 nm is to be instrumented for a scan angle of 120 degrees and enough velocity cells to detect a target of up to mach 3, dependent on the duty factor and pulse repetition rate, several hundred thousand shift register states for delay and some two to three million crosscorrelators are required.

The key problems in transmitting, receiving and processing a noise waveform are the ultra wideband

antenna, the high speed storage of the transmitted signal and its correlation with the received signal. Several technologies have been monitored and are briefly described in the following.

A periodic structure can be the basis for an ultra wideband antenna concept. The structure becomes equal to itself by a particular scaling, D, of its dimensions. Thus it will have the same properties in the sense of beam pointing direction, beamwidth and impedance at frequency D·f as at f. The characters of this antenna are periodic with the logarithm of frequency with period, log(D). These so called log-periodic antennas can be used singly or in arrays . They can also be used to exite a parabolic reflector. The properties of this latter antenna will not be completely independent of frequency as beamwidth will be proportional to wavelength.

Digital correlators are manufactured by several companies and are either designed for correlation or filtering of digital signals. The devices vary in speed and complexity but are all restricted to some tens of MHz bandwidth. However, most of them are cascadable for the processing of broadband signals. It is possible to correlate for a target, using a replica of the transmitted signal, where the replica has been significantly degraded reducing it to a 1 bit data stream. A moderate loss resulting from this degradation may be tolerable, however, if clutter rejection processing and the discrimination of multiple targets is desired, it is important to maintain the dynamic range of the target returns.

Acoustic charge transports (ACT) utilise acoustic waves propagating near the surface of a piezoelectric semiconductor to transport charge packets or signal samples from a source to a drain. The device is basically an extremely accurate high speed memory which can provide a coherent RF signal. It is constructed using a piezoelectric GaAs substrate and consequently can be integrated with other GaAs components such as high speed attenuators, switches and digital RAM. Sampling rates of the devices are in the region of 200 MHz and although this may be acceptable for some radars, a true noise radar will need considerably higher speed capability.

Another technique for storing a wideband signal is a fibre optic delay with low loss, low signal dispersion, excellent EM compatibility, immunity to RF interference and stability to temperature changes.

Doppler processing can very effectively be carried out using FFT devices which are available for a variety of processing tasks.

6. Generic approaches

6.1 Candidate design for passive/noise radar

A candidate design for a wideband passive/noise radar has been proposed by RSG 3 /5/ as an experimental system consisting of a wideband noise diode filtered by a 1 Ghz wide bandpass selected from a bank of filters with different centre frequencies for transmission. A wideband CW TWT like the ones used in EW applications can provide output to a circulator followed by a wideband antenna.

A fibre optic delay best provides a replica of the noise waveform for use in the receiver correlator. This link supports the „linear" transmission of the noise (around the centre frequency) and provides the proper delay so that targets at some predetermined range can be detected. The link consists of a direct modulated laser, the required line of fibre cable and a photo detector demodulator.

The receiver front end accesses the received signal through the circulator with low noise amplification before mixing. An agile local oscillator with the chosen centre frequency beats the incoming received signal to provide an output of 1 GHz. A 1 GHz bandpass filter follows the mixer with additional amplification preceding the receiver correlation stages.

The correlators, however, form the largest burden in the processing cycle. If the whole signal bandwidth of 1 GHz is used for target resolution, 67 correlators are used to span a target 10 meters long and 6667 correlators are required for each kilometre of range to be observed. Channelization could, for example, reduce the speed at which the correlation process must operate but the product of the number of channels multiplied by the number of correlators will remain unchanged if minimum processing losses are a goal.

6.2 VHF/UHF passive radar using broadcast transmitters as ToO

The use of broadcast stations as ToOs offers some advantageous properties that could be exploited in a passive radar. First of all, broadcast services are very likely to be operating during the periods of interest and, since they are more or less omnidirectionally transmitting, no pulse-chasing has to be applied. According to their task of serving a wide area of ground based customers, however, broadcast transmitters often have antennas which are tilted towards the ground, causing as well a multipath null at low elevations as high clutter returns

A possible system approach could consist of five or more separate receiver channels, one for the reception of the direct signal of the ToO and two other channels for the simultaneous processing of a sum and a difference signal for target direction discrimination. Dependent on the demands for mobility, the antenna would be an array of 12 or more dipoles or Yagis, arranged in two rows of 6 horizontally spaced elements. The two remaining channels will be used for elevation

discrimination and to avoid multipath. The fixed antenna array allows beam steering within the beam width of one antenna element, typically 60 deg. For the reduction of clutter, MTI processing will be applied. The ToOs that could be used range from commercial radio stations with signals of about 20 kHz bandwidth (range resolution 7,5 km) to TV signals of 5 MHz bandwidth (range resolution 30 m), where different sets of antenna arrays would be used.

The reference channel is fed by a Yagi antenna with high gain. A line-of sight from the passive radar receiver to the ToO is not required. The detection range is very much dependent on the effective radiated power (ERP) of the ToO and its antenna position and tilt. Thus, long range systems, using distant high power ToOs for the detection of targets in the forward scatter region are possible, as well as short range systems for the detection of targets either within the close environment of the ToO or the receiver.

For the processing of a signal of 5 MHz bandwidth, 1000 correlators are used if 30 kilometres of radar range are to be surveyed.

The fall back active transmitter would, if necessary, transmit a CW signal with a modulation which resembles a communication signal and thus camouflages the application. While such a waveform does not prevent detection it is possible to produce a signal which can be exploited for radar purposes but is unlikely to be identified as a radar signal. The use of several transmitters alternatively for illumination of the same observation space could be an additional measure to irritate an ESM receiver and increase the radars survivability.

7. Conclusions

The possible trends for future LPI radar techniques as analysed by NATO study group RSG 3 of panel X are pointing into two different directions, basically influenced by the radar band of operation. The choice of radar frequency, however, is subject to a variety of parameters. Desired radar properties like detecting stealth air targets is one of them.

If the detection of stealth targets is a major task of a radar with low probability of being intercepted, the exploitation of VHF/UHF radar properties may be attractive enough to deal with the disadvantages inherent to metric wavelength like reduced mobility and vulnerability to jamming. In conflict situations, ToOs like TV and broadcast stations may well be in operation and their emissions could be used for target detection if proper siting of the receiver is possible. Increased bistatic coverage even against low flying targets and a target RCS which is less reduced by stealth techniques, together with low cost components can make this passive radar configuration a somewhat exotic but nevertheless viable early warning sensor. If a more precise air picture is required or the ToOs are no longer available, one or more active transmitters would provide illumination. Since at VHF/UHF frequencies only limited bandwidths can be achieved and thus possible time-bandwidth-products are restricted even with a CW signal, the radar signal will hardly be undetectable or noise like. To camouflage the application of the emission by imitating a communication signal could be a promising approach that matches the passive receivers capabilities.

At the conventional radar frequencies, other radars are available as ToOs. these will usually scan a well defined search volume and thus, the passive radar either has to fill its search volume with multiple beams or, if the scan sequence of the ToO is fixed, can apply some form of pulse chasing technique. However, both of these techniques are difficult and costly to implement. The noise like transmission of a fall back active component is comparably easy to generate but the reception and processing of the target echoes rely on emerging correlation techniques and the requirements for a noise radar receiver do not match well with those of a passive microwave receiver using other radars as ToOs.

Nevertheless, covert operation, inherently high range resolution and ideal ambiguity function would make a microwave noise radar an attractive candidate for use in future air defence systems. In addition the size of the equipment would be suitable for mobile operation. Regarding emerging techniques in signal and data processing, which would be suited for this application, are expected to reduce in cost, noise radar should not be neglected for future LPI radar developments since an indistinguishable waveform is the only true approach to covertness.

8. References

/1/ Wirth, Omnidiretional Low Probability of Intercept Radar, Paris 89 Int. Radar Conf.

/2/ Pengelly, Philips' Pilot covert naval radar, Int. Defense Review 9/1988

/3/ Willis, Bistatic Radar, Artech House 1991

/4/ Kuschel, Mono- and Bistatic Radar Coverage Including Diffractive Wave Propagation, AGARD Conf. Proc No. 407 ,Ottawa 1986

/5/ NATO AC243 Panel 10 RSG3 Report on Passive/Noise Radar, tbp 1995

NOTE: The question relating to this paper is printed in the classified supplement.

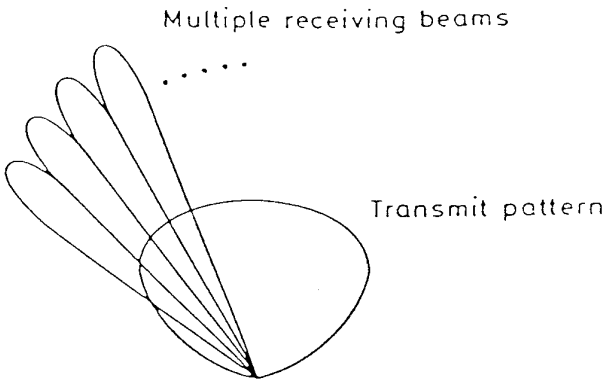

Figure 1: OLPI antenna pattern

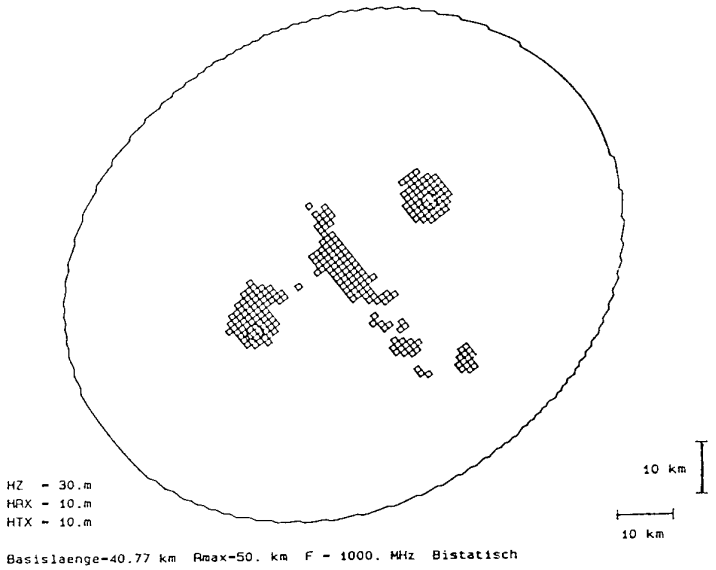

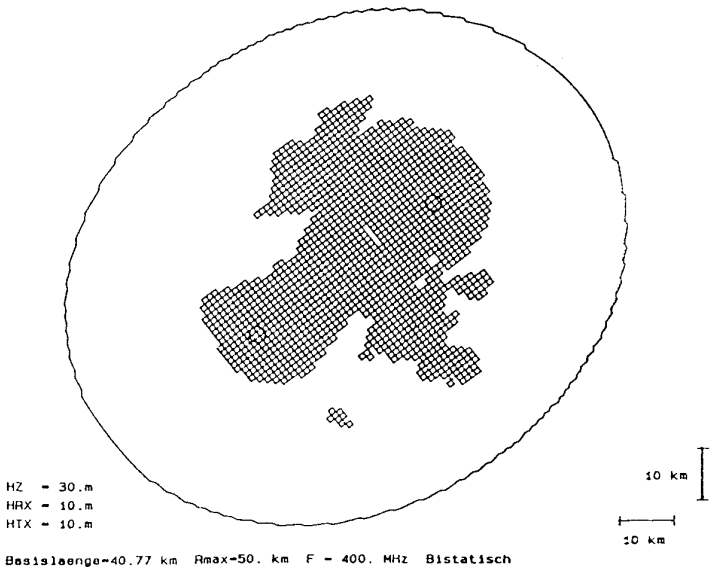

Figure 2: Bistatic radar coverage at 1 GHz and 400 MHz, respectively.

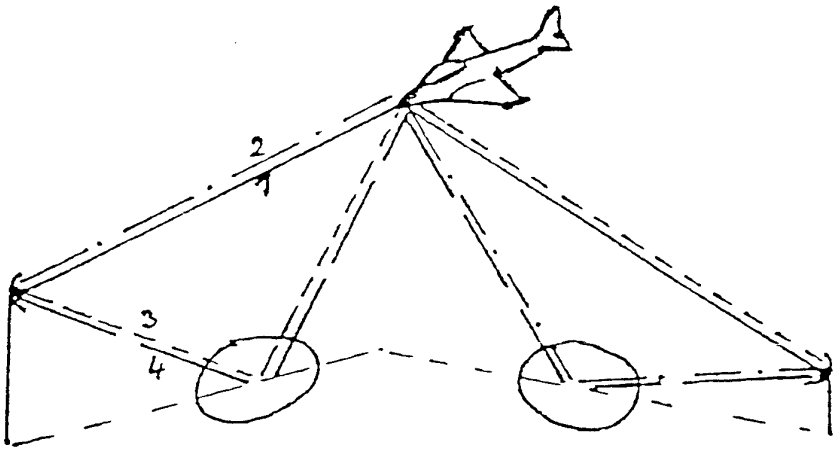

Figure 3: Bistatic multipath geometry, delayed Echoes through paths 2,3 and 4.

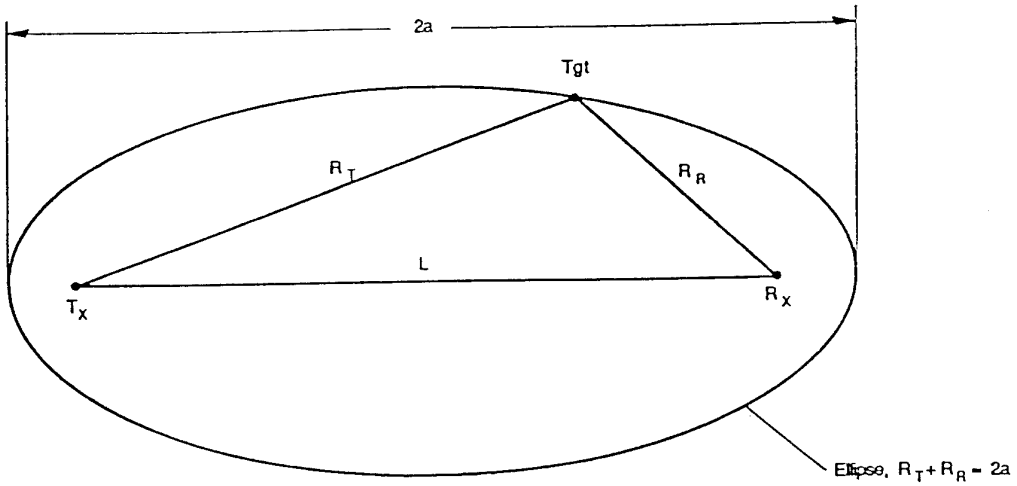

Figure 4: Ellipse of constant range sum with bistatic plane in the plane of the paper.

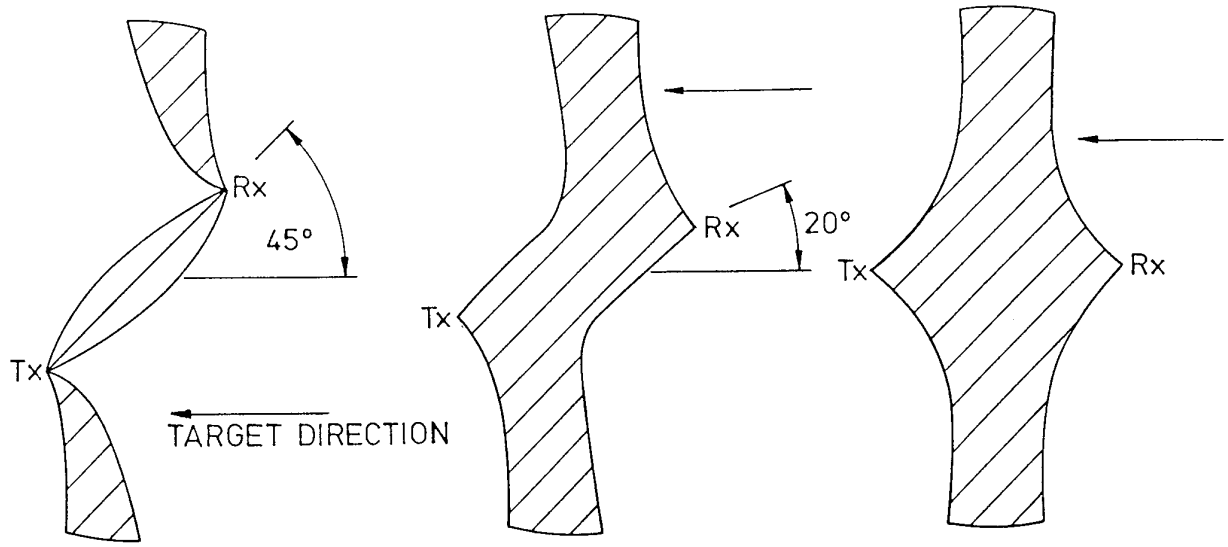

Figure 5 : Doppler dead zones for different target directions with respect to the bistatic baseline

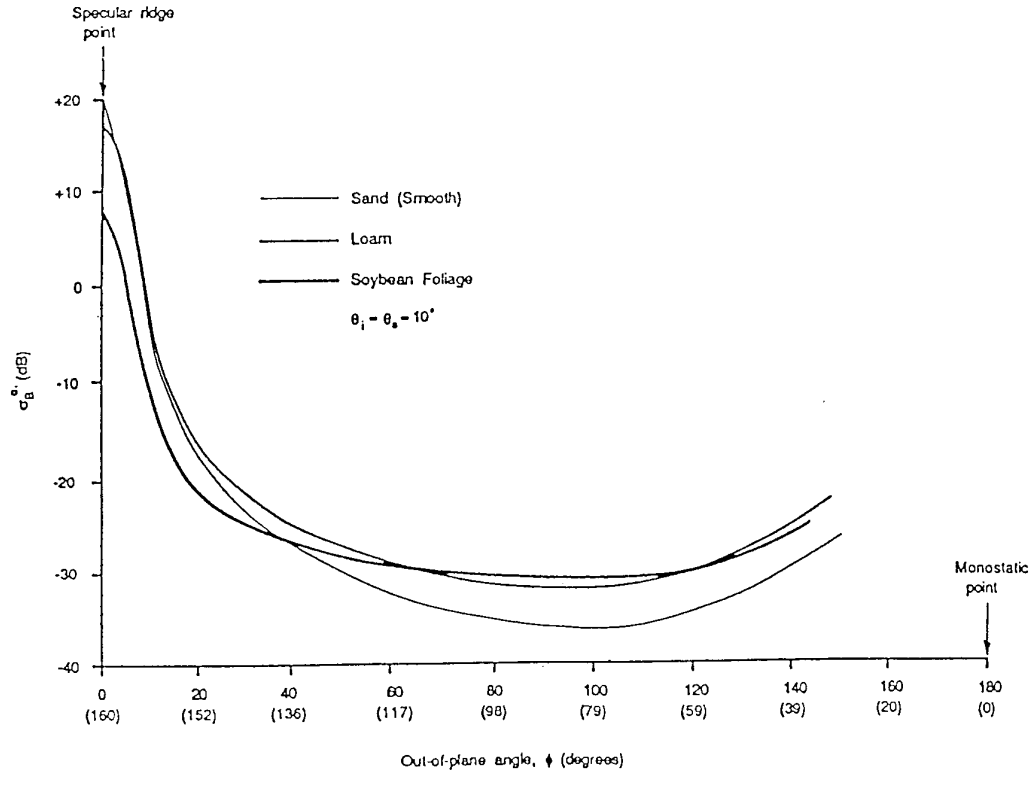

Figure 6: Out-of-plane, horizontally polarized, σ_B^o data at 10 GHz. (Courtosy of Ohio State University) /3/

Modelling of Guided Missiles and Numerical Simulation of their Interaction with RF Waves

Jürgen Nitsch
Hans-Joachim Vogel
Wehrwissenschaftliches Institut für Schutztechnologien - ABC-Schutz,
P.O. Box 1142, D 29623 Munster
Germany

Abstract

RF coupling into guided missiles is described on the basis of rough analytical estimates and of the application of the numerical MoM code CONCEPT. Coupling is maximized by resonant excitation in the external and internal resonance region of the missile and mainly takes place via slots in the surface of the missile and via the fins and stabilizers which act as antennas. In the senses of norms (∞-(peak) and 2-norm (i.e. ~ square root of energy)) a damped sinusoidal waveform in general produces a response which is much larger than that due to a decaying exponential waveform.

I. Introduction

Weapons that direct energy on targets have been extensively explored for the last two decades. Their main advantage is that they attack at nearly the speed of light. One category of directed energy weapons (DEW) are the microwave (High Power Microwave ≡ HPM) or RF energy weapons which have the advantage over other DEWs in the fact that microwaves do not face a serious propagation issue. Today HPM sources are available which produce peak powers in excess of a gigawatt, and also HPM technology for effects testing is mature enough to be applied in laboratories. However, an HPM weapon system still requires some time of investigation and modification of a large inventory before it can be deployed in the field.

The hierarchy of HPM directed energy effects ranges from burnout of or lethal damage to enemy electronic systems to the deception or spoofing of the enemy system into mission failure. This last mission is very akin to electronic warfare (EW) at higher power levels, and therefore broader classes of targets can be attacked, in distinction to EW techniques which are very target-specific.

The distinction between HPM directed energy and EW can be seen in terms of a trade-off between the power level and the sophistication of the attack. EW uses sophisticated techniques at much lower power to deny any opponent effective use of communications and control and has become expensive due to the threat diversity and the electronic countermeasure / electronic counter-counter-measure competition.

HPM can access new generic effects and lead to less threat-specific attacks. An intermediate region has developed in which features of both HPM and EW are combined known as *smart rf directed energy* (RFDE). These techniques use repetitive microwave pulse formats with amplitude and frequency modulation and pulse shape control.

Since coupling of electromagnetic (e-m) waves into targets varies (a.o.) rapidly with frequency, the use of frequency-agility in RFDE is of special importance. The coupling can vary by orders of magnitude at frequencies only perhaps tens or at most hundred MHz apart. It is the goal of this paper to investigate the interaction of RF waves with guided missiles, especially in their resonance regime.

Our paper is organized as follows: In Section II the general interaction schema of e-m waves with a target is briefly described. Sections III

Paper presented at the AGARD SPP Symposium on "Environmental Factors in Electronic Warfare Related to Aerospace Systems" held in Pratica di Mare AFB (Rome) Italy, from 8-11 May 1995, and published in CP-573.

and IV deal with the outer and inner transfer functions of a generic as well as of a real missile. The system's response to resonant and unipolar waveforms is investigated in Section V. Section VI concludes our paper.

II. The General Interaction Schema

The interaction of an incident plane e-m wave with a complex electronic system is quite complicated in its details. However, one can use e-m theory to characterize the *form* that the response takes and rely on measurements or numerical calculations to evaluate the parameters in the appropriate models. Such a model might be the singularity expansion method (SEM) which explicitly exhibits the various resonances of a system as poles in the complex-frequency plane. For signals in the interior of a system, say on the circuit level, there are, in general, many resonances associated not only with the exterior envelope of the system, but also with the transfer functions through cavities, cables, etc. to the interior. As indicated in Fig.1 the response V_i (say a voltage) at some interior port of interest is approximated as a product of various transfer functions [1].

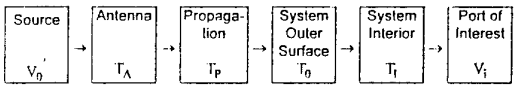

Fig.1: Factorization of transfer function from source to system.

$$V_i \cong V_0' \cdot T_A \cdot T_P \cdot T_0 \cdot T_I \qquad (1)$$

Here the equivalent source peak voltage V_0' (about a MV) is multiplied with the transfer functions for a radiating antenna

$$T_A = \frac{f_s A^{\frac{1}{2}}}{cR_0}[m^{-1}] \qquad (2)$$

a propagation path

$$T_P \approx 1 \qquad (3)$$

the response of the system outer surface (in an order of magnitude sense)

$$T_0 \approx 1 \quad (\text{ or some other constant }) \qquad (4)$$

and the system interior T_I. The final result then reads

$$V_i \cong V_0' \cdot \frac{f_s A^{\frac{1}{2}}}{cR_0} T_0 T_I$$

$$= E_0 \frac{f_s A}{cR_0} T_0 T_I \qquad (5)$$

where now f_s denotes the frequency of the radiating source, A the aperture area, c the speed of light, R_0 the distance from the antenna to the system, and E_0 the peak tangential electric field on the aperture. In order to obtain the order of magnitude for the perturbation voltage V_i one still has to (numerically) calculate or to measure the outer and interior (or the product of both) transfer functions. This will be done in the subsequent sections. Nevertheless, it is possible to define the main features of a canonical system response [1] as illustrated in Fig.2.

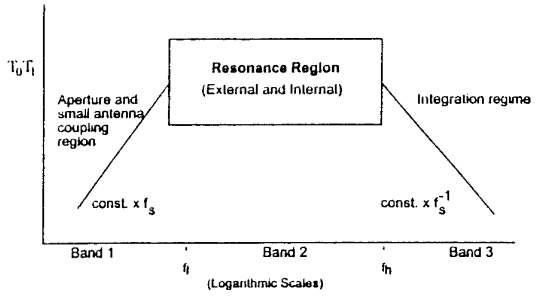

Fig.2: Canonical system response as a function of frequency.

Here we combine T_0 with T_I to form a composite transfer function from incident fields to response at box inputs. Also significant changes of T_0 in the resonance region are now admitted and observed in the product $T_0 \cdot T_I$.

The frequency spectrum is divided into three bands indicating regimes of different kinds of interaction. At low frequencies apertures and small antennas are usually differentiators [2]. As frequency is increased outer and interior resonances occur. These can be associated with a characteristic dimension l of the object (l may be, e.g., the circumference or the length of the target). The first resonance may appear at f_l where this is half-wave or even quarter-wave resonant. As one goes up in frequency shorter

wires, cavities, and apertures become important [2] and establish some high resonant frequency f_h of interest. Between the frequencies f_l and f_h the transfer functions $T_0 \cdot T_I$ exhibit resonant behaviour with order-of-magnitude variations.

Above f_h the various wires act as integrators [2]. Also at these frequencies fields almost penetrate frequency-independent into the system's interior, so the transfer funtions $T_0 \cdot T_I$ should go roughly like f^{-1} (or may fall off even with some higher power). One might estimate f_h based on the smallest typical resonant dimension of the system as of the order of some gigahertz.

In the following sections we apply a MoM code to calculate T_0 and $T_0 \cdot T_I$, respectively.

III. Interaction with System Exterior

In this section we discuss the main features of the interaction of an electromagnetic wave with the exterior of a system. This involves finding the shortcircuit surface currents and charge densities on its surface, these being the parameters that drive small antennas and apertures. Since we direct our interest to the e-m interaction with a missile we start with a very simple generic model, regarding the missile as a conducting cylinder with hemispherical endcaps. The geometrical parameters are adjusted to those of a real missile. The radius r_0 of the hemispherically endcapped cylinder is 0.07m and its overall length L=1.14m.

III.1 *Quasi-Static Current- and Charge-Densities*

At low frequencies for which the wavelength $\lambda >> L/2$, the quasi-static approximation may be used. We are still below or in the first band of Fig.2. Consider a broadside incident plane wave as shown in Fig.3 illuminating the endcapped cylinder.

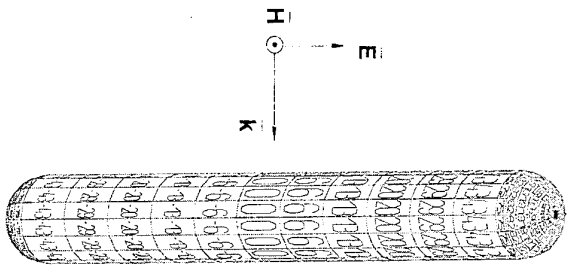

Fig.3: Real part of the quasi-static charge desity distribution.

Then the induced surface charge densities and current densities can be calculated as [2]

$$\rho(\varsigma, s) = \frac{\varepsilon_0 E^i(s)}{(1-\alpha_0)} \sqrt{\frac{1-e^2}{1-e^2\varsigma^2}}\varsigma \qquad (6)$$

with

$$\alpha_0 = \frac{1}{e^2}\left[1 + \frac{1}{2}\frac{1-e^2}{e}\ln\left(\frac{1-e}{1+e}\right)\right] \qquad (7)$$

and

$$J_\varsigma(\varsigma, \phi, s) = \frac{2H^i(s)}{(2-\alpha_0)}\cos\phi + s\varepsilon_0 r_0 \frac{E^i(s)}{2(1-\alpha_0)}\sqrt{1-\varsigma^2} \qquad (8)$$

$$J_\phi(\varsigma, \phi, s) = \frac{2H^i(s)}{(2-\alpha_0)} \sqrt{\frac{1-e^2}{1-e^2\varsigma^2}}\varsigma \sin\phi \qquad (9)$$

$$(-1 \le \varsigma \le 1 \;\; ; \;\; 0 \le \phi \le 2\pi)$$

Fig.4: Real part of the quasi-static surface current density.

The above solutions refer to a prolate spheroid with its coordinates (ξ, ζ, ϕ) and also present approximate solutions for our endcapped cylinder. The eccentricity is denoted by $e\,(= \sqrt{1-4(r_0/L)^2}\,)$, and s is the complex frequency.

The charge density does not depend on the angles and changes sign in the middle of the cylinder. In Fig.4 we clearly recognize the $\cos\phi$-dependency of the dominant component

J_z of the current density along the cylinder. J_φ becomes noticeable at the endcaps. Also remarkable is the fact that J_z for lower frequencies mainly depends on the incident magnetic field, whereas with increasing frequencies the electric field begins to contribute proportional to the frequency. Thus at higher frequencies where the E-field becomes dominant we are in the differentiating branch of our interaction schema in Fig.2.

III.2 Complex Resonance Frequencies of an Endcapped Cylinder

With increasing frequencies we approach more and more towards the resonance regime of the exterior body of our missile model where the quasi-static approximation is no longer valid. Now more exact methods are necessary, like e.g. SEM [3] or MFIE [4] (=Magnetic Field Integral Equation) to calculate fields, currents, and voltages. In the SEM-Ansatz the quantities in question are expanded with respect to their poles (in the complex plane) and in terms of weighted eigenfunctions. If one, however, is only interested in the location of the poles, i.e. in those frequencies where resonances occur and in the resonant attenuation of the corresponding excitation modes, the principle of phase matching of surface waves can be applied [5]. We refer to the results obtained by the use of the „phase-matching condition" for surface waves along the meridian and circumferential ones of a cylinder with hemispherical endcaps [5]. Selected results are listed in Tables 1 and 2. Table 1 schows some complex resonance frequencies of TM_{1n} and TE_{1n} modes of meridionally propagating surface waves when the cylinder is excited by axially incident waves.

TM_{1n}	n=1	n=2	n=3	n=4	n=5
s_{1n}^{TM}	127.6	250.1	371.7	492.5	613.9
[MHz]	-j 17.1	-j 36.2	-j 47.8	-j 56.6	-j 64.2

Table 1a: Natural frequencies of TM_{1n}-modes corresponding to meridionally propagating surface waves.

TE_{1n}	n=1	n=2	n=3	n=4	n=5
s_{1n}^{TE}	108.5	213.1	326.0	440.6	557.2
[MHz]	-j124.8	-j145.3	-j162.3	-j176.7	-j189.6

Table 1b: Natural frequencies of TE_{1n}-modes corresponding to meridionally propagating surface waves.

In Table 2 resonant frequencies corresponding to circumferential modes are given. They appear in the case of broadside incidence.

TM_{1m}	m=1	m=2	m=3	m=4	m=5
s_{1m}^{TM}	340.4	978.1	1619.3	2265.9	2917.3
[MHz]	-j446.1	-j570.2	-j660.3	-j731.9	-j791.9

Table 2a: Natural frequencies corresponding to circumferential TM_{1m}-modes.

TE_{1m}	m=2	m=3	m=4	m=5
s_{1m}^{TE}	297.4	893.6	1504.0	2124.1
[MHz]	-j871.1	-j1147.3	-j1349.2	-j1513.6

Table 2b: Natural frequencies of azimuthal TE_{1m}-modes.

Looking at the imaginary parts of the resonance frequencies for the first TM and TE layer in Table 1 one recognizes a move to higher attenuations with increasing n (=the number of wavelengths spanning a close meridional path). Also the damping of TE_{1n}-modes are stronger than the corresponding TM_{1n}-modes.

In the case of circumferential modes (see Table 2) one again observes that TE_{1m}-modes are stronger damped than TM_{1m}-modes, but also that the attenuation is almost an order of magnitude higher for azimuthal modes compared to those that propagate axially. This may mainly attributed to the greater curvature of the azimuthal paths.

In order to calculate a resonant current distribution for the hemispherically endcapped cylinder we used the numerical MoM code CONCEPT [6]. For a head on illumination at

440 MHz the wavy current structure is seen in Fig.5.

Fig.5: Current distrubution in the resonance region; f=440 MHz.

In Fig.6 we display the frequency dependency of the magnitude of the magnetic field at a point located 0.3 m in front of the top endcap.

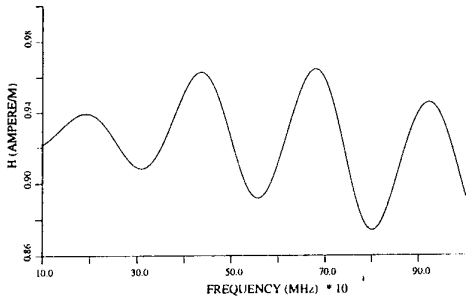

Fig.6: Magnitude of the magnetic field at a point near the top endcap.

The incident fields are normalized to 377 V/m and 1 A/m. Maxima and minima in Fig.6 correspond to resonance frequencies which in individual cases may be assigned to certain modes with the aid of Tables 1 and 2.

III.3 *Further (exterior) Resonance-Frequencies: Slot- and Fin-Resonances*

Besides the exterior body resonances of a missile we also have to take into account those which are due to outer structures of the missile. Fins, stabilizers, antennas and slots of the missile in many cases establish the connection between exterior and interior excitation and serve as main coupling paths to the inside. This coupling is most effective if, e.g., fins and slots are excited with their resonance frequencies.

Considering the slots as ($\lambda/2$)-antennas one obtains for a slot of the length l_S=0.1 m the resonance frequency f_S=1.5 GHz.

The treatment of a fin as (($\lambda/4$)-antenna (one end open, the other short circuited inside) leads to a fin resonance (length of the fin:l_F =0.055 m) of f_F=1.36 GHz. If one, however, assumes that two opposite fins are conductively connected via an half-arc inside the missile one finds a lower resonance frequency of 500 MHz.

Our final missile model (see next section) also contains a circular opening (radius=0.035 m) at the top end. Its (circumferential) resonance frequency turns out to be 1.36 GHz.

Of course, one has to be aware that an arbitrary e-m irradiation of a system does not necessarily excite every substructure. On the other hand, the responses of those parts of a system which are excited interfere to a very complex and complicated entire response, in a way that not any detail can be found in a result of an idealized calculation.

IV. Interaction with System Interior

Next we consider the internal interaction. Since there are always cavities in the system interior we first present the formula for resonance frequencies of a cylindrical cavity of length L and radius r_0.

$$f_{mnl}^{TM;TE} = \frac{c}{2\sqrt{\varepsilon_r \mu_r}} \sqrt{\left(\frac{l}{L}\right)^2 + \left(\frac{a_{mn}^{(')}}{\pi r_0}\right)^2} \qquad (10)$$

These frequencies correspond to TM(a_{mn})- and TE(a'_{mn})-modes, respectively, and the parameters $a_{mn}^{(')}$ denote the n^{th} root of the Bessel functions (resp. their derivations) of m^{th} order. They are available from tables in text books. For L=1.14 m and r_0=0.07 m we list some selected resonance frequencies in Table 3. For smaller cylinder-radii these frequencies increase, whereas the insertion of some material

(e.g. absorber material; $\varepsilon_r \geq 2$) shifts the frequencies to lower values.

f_{011}^{TM}	f_{111}^{TM}	f_{111}^{TE}	f_{112}^{TE}	f_{211}^{TE}
1.64GHz	2.61GHz	1.25GHz	1.28GHz	2.08GHz

Table3: Cavity resonances of a cylinder.

For our investigation in this section we consider a more realistic missile model (shown in Fig.7) with four slots in the upper part, four steering fins passing through the slots, a flat lower end and a circular opening (for the seeker head) at the front end.

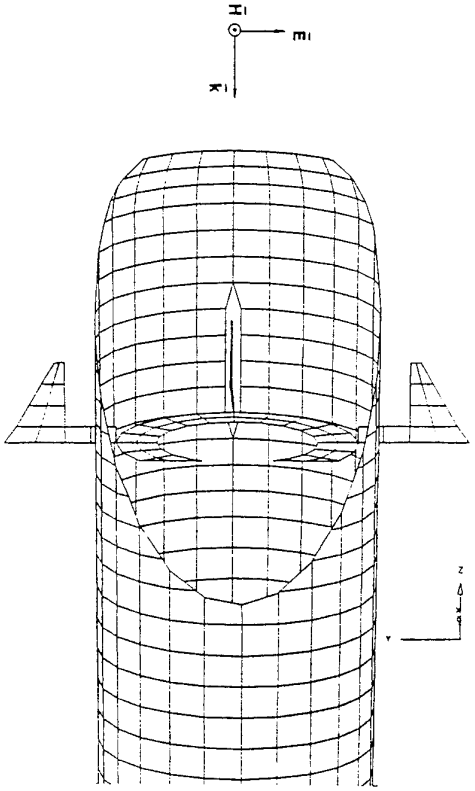

Fig.7: Missile model.

This still simple missile model is further completed at the end of this section by dividing it into three compartments (see Fig.11) with an additional cylindrical tube in the middle compartment to garantee a protected feed-through of conductors. Three of them are indicated in Fig.11. They are short circuited at both ends and run from the middle to the rear compartment through small ducts in the partition. The missiles are excited by a head on illumination. The incident linearly polarized E-field is chosen to be parallel to one fin-pair to maximize the excitation of these fins. All fins end at a concentric metallic ring inside the missile. This ring has no conducting contact to the wall of the missile and an interior circular opening of radius 0.04 m.

In Figs.8 and 9 we exhibit resonances for the magnitudes of the magnetic and electric field calculated in the frequency band from 1.25 GHz to 2.00 GHz in the middle of the missile.

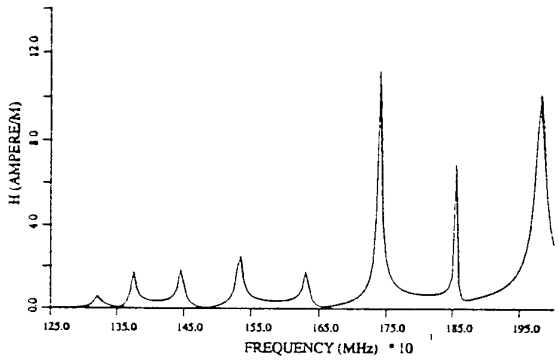

Fig.8: Maximal magnitude of the H-field in the middle of the missile.

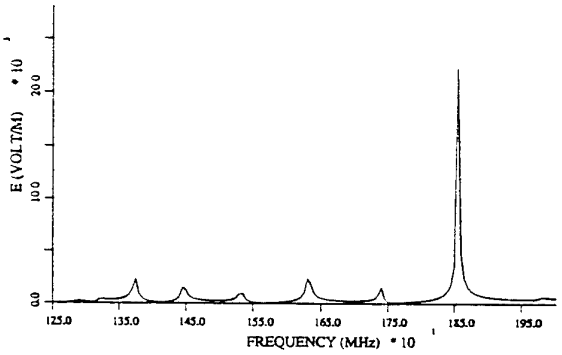

Fig.9: Maximal magnitude of the E-field in the middle of the missile.

Most of these resonances are correlated with cavity modes whereas some of them also may have their origin from the structure elements of the missile like the apertures and antennas. It is conspicuous that above 1.75 GHz the resonance peaks increase considerably up to a

multiple of 10 (compared to the magnitude of the incoming field) for the magnetic field and even to a multiple of 60 for the electric field. The lower resonance-amplitudes for frequencies below 1.75 GHz may be due to the facts that the missile is not closed at the front end, that the local field point in the middle is very special and that fields with higher frequencies can penetrate more easily into the missile. The seeker-head aperture causes an intensive coupling between interior and exterior fields and thereby the resonance frequencies are shifted (usually to lower values), and the corresponding peak values for the fields decrease remarkably.

In Fig.10 we demonstrate the *local* periodicity of the magnitude of the electric field at f = 1.855 GHz inside the missile along its axis, starting at the rear end at 3 cm from the end cap and ending at the front end 3.3 cm from the seeker aperture plane.

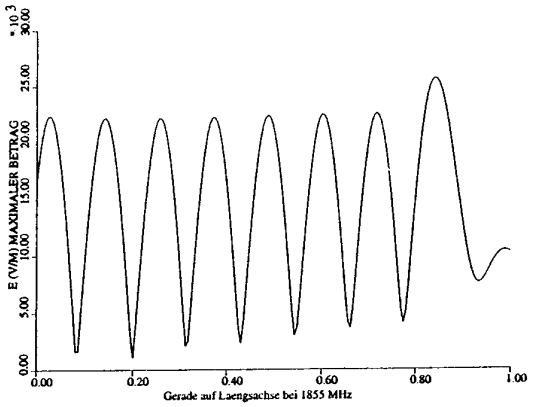

Fig.10: Maximal magnitude of the E-field along the missile axis at f = 1855 MHz.

If this straight line is parallely shifted towards one fin slot the field strengths decrease and at the height of the slot its presence and action becomes visible.

Finally, we refer to the missile configuration shown in Fig.11 to evaluate the short circuited currents at the front endings of the wires.

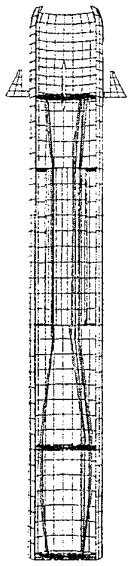

Fig.11: Missile model with three conductors.

The presence of the conductors inside the missile now causes quite a different class of resonances: quasi-TEM resonances. These resonances occur in common with cavity resonances, in general at lower frequencies f_{wire}.

$$f_{wire} = n \cdot v/(2l_{wire}) \qquad (11)$$

($n = 1,2....$; l_{wire} = length of the wire;
v = propagation speed of the corresponding TEM-mode).

Moreover, TEM-resonance peaks as a rule are higher than those which are originated in cavities.

Since the length of the cables in our missile model is approximately 0.88 m, TEM-resonances appear at following frequencies: 170.5 MHz; 341 MHz; 511.5 MHz; 682 MHz; 852.5 MHz, 1.023 GHz, etc. To obtain these numbers it was assumed that $v \approx c$ (= speed of light). In Fig.12 the short circuited current at the front end of the furthest right conductor is represented in the frequency regime between 150 MHz and 1.6 GHz. As expected we recognize well pronounced TEM-resonance peaks which increase with increasing frequency. In addition one observes a double or triple peak-structure due to the interaction between the cables. This interaction (via the impedance- and admittance-matrices) causes

the removal of degenerated TEM-eigenresonances [7].

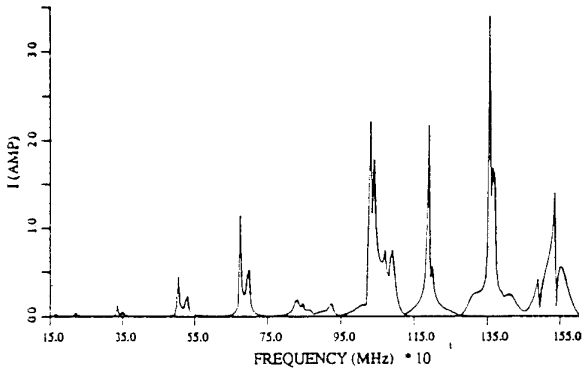

Fig.12: Magnitude of the current at the front end of the furthest right conductor.

The investigation of our simplified missile model has brought out mainly two kinds of natural modes: The transmission line modes (quasi-TEM) associated with cables, and cavity modes appropriate more to the empty volume away from the cables. The transmission line modes tend to be more important at lower frequencies while the cavity modes tend to be more important at higher frequencies. In order to remove these unwanted oscillations which can lead to serious pertubations in real systems, one can apply appropriate damping techniques. These techniques rely, e.g., on suppressing resonances by the use of more (2-3 dim.) dimensional resistor arrays, preferably positioned at field maxima for cavity modes, and by loading the conductors with resistors and (in some cases) inductors at the locations of current maxima [8].

V. Comparative System Response to Resonant and Unipolar Waveforms

From the results of our foregoing sections it should be obvious that the maximum system response is usually achieved by selecting the incoming waveform as an approximate sinusoid of sufficient cycles to „ring up" the resonance response. What happens, however, if one illuminates the system with a pulsed sinusoid which is not tuned to a resonance? Usually, the resonance structure of a missile of a possible enemy is not well known. Therefore, it might be more appropriate to choose a waveform with a different temporal shape, like, e.g., a (short) impulse-like waveform. But how strong is the interaction with the system then?

Let us assume the system is excited by an external pulse of the general shape

$$A(t)\cdot\sin(2\pi f_c t) \qquad (12)$$

with an envelope A(t) (e.g. an exponential function or a Gaussian) and the carrier frequency f_c which may be detuned or tuned to an inner resonance frequency. In case that f_c is detuned (lying between two resonances) and the response is caused by a "long" (narrow-banded) pulse we find that the interior perturbation quantity, say a voltage $V_i(t)$, follows the outer excitation [9]:

$$V_i(t) = A(t)\cdot\sin(2\pi f_c t+\varphi)\cdot\sqrt{\sum_l \frac{a_l^2}{(f_c^2-f_l^2)^2+\left(\frac{\gamma_l}{2\pi f_c}\right)^2}} \qquad (13)$$

The response caused by a "short" (but still detuned) pulse is quite different:

$$V_i(t) = -\pi\sum_l \frac{a_l}{f_l}\left|\tilde{A}(f_c-f_l)\right|\cos(2\pi f_l t+\varphi_l)e^{-\gamma_l t/2} \qquad (14)$$

This is more like a beat with a longer duration (comp. to (13)) due to the fact that the broader-banded spectrum of the Gaussian

$$A(t) = \exp\left\{-(t-t_0)^2(\pi p)^2\right\}u(t) \qquad (15)$$

(p = bandwidth parameter)

covers some resonance frequencies and thus initiates the interference of different (freely ringing) modes. The magnitudes (in the sense of norms) of both responses, however, are almost comparable [9] and correspond to the magnitude of the system response when the system is excited by a unipolar waveform [10].

Now let the carrier frequency f_c be tuned to some interior resonance frequency. Then the ratio $R_{1,m}^{(\infty)}$ of a matched response to the excitation in ∞-norm sense gives [10]

$$R_{1,m}^{(\infty)} \cong |T_c| / (-\Omega_c) \tag{16}$$

where $|T_c|$ denotes the magnitude of the pole strength of the transfer function at $s=s_c=\Omega_c+j2\pi f_c$.

For a decaying exponential waveform the response compared to the excitation gives

$$R_2^{(\infty)} \cong |T_\infty| \tag{17}$$

where T_∞ can model the regions of ω for which the transfer function is small (like the valleys between the peaks (resonances)). For a significant resonance peak at f_c the ratio of (16) and (17) becomes

$$P \equiv |T_c| / \left((-\Omega_c)|T_\infty|\right) >> 1 \tag{18}$$

indicating that the tuned oscillatory waveform is much more effective than the exponential one. An analogous estimate for the ratios of the 2-norms (proportional to the square root of energy) $R_{1,m}^{(2)}$ and $R_2^{(2)}$, respectively, leads to

$$R_{1,m}^{(2)} / R_2^{(2)} >> 1 \tag{19}$$

which under certain conditions also approaches P [10].

In summary, we have seen that in the senses of the ∞-norm (peak) and 2-norm the damped sinusoidal waveform (in general) produces a response which is much larger (more than a factor of 10) than that due to a decaying exponential waveform, if the oscillatory waveform is tuned to a resonance peak of the system. If the damped sinusoid is detuned from the resonance, then the responses are comparable. Thus for maximizing the response an oscillatory waveform is in general preferable. If, however, resonance frequencies are not well known then one might choose a broad-banded impulse-like excitation with a high amplitude.

VI. Concluding Remarks

This paper gives an example of rough analytical estimates and numerical simulation of microwave coupling into missiles. The numerical simulation is a cost effective tool to study e-m coupling, especially in cases where an actual measurement is too much involved.

The fin system and apertures of a missile are identified as very efficient penetration paths into all compartments of a missile. "Resonance-coupling" is most effective. Outer resonance structures modulate the interior ones (outer (body-)resonance peaks are much broader than interior ones). At resonance frequencies interior field strengths are a multiple larger than the incident fields.

For realistic pulse shapes (impulse-like waveform) the coupling of an illuminating microwave to the inside of a missile falls short of the theoretical maximum (tuned sinusoid excitation) by a factor of approximately 10. However, a narrow-banded signal tuned to the lower part of the resonance region of a small missile runs a high risk to achieve only a poor response because it may miss the sparse resonance peaks in that frequency band.

Of course, the application of a numerical simulation to complex systems has its limitations and does not replace an experiment. On the other hand, it serves as one basic tool to facilitate the interpretation of physical processes, and in many cases we find very good agreements of the numerical results with measurements. In the subsequent paper [11] this is convincingly demonstrated.

References

[1] C.E. Baum, "Maximization of Electromagnetic Response at a Distance", IEEE Trans. Electromagnet. Compatibility, Vol.34, No.3, pp. 148-152, 1992.

[2] K.S.H. Lee (ed), "EMP Interaction: Principles, Techniques, and Reference Data", Hemisphere Publishing Corp. (Taylor&Francis), 1986.

[3] C.E. Baum in **Transient Electromagnetic Fields**, L.B. Felsen (ed.), "The Singularity Expansion Method", Springer-Verlag, Vol.10, p. 130ff, 1976.

[4] R. Mittra in: **Transient Electromagnetic Fields**, L.B. Felsen (ed.), "Integral Equation Methods for Transient Scattering", Springer-Verlag, Vol.10, p.73ff, 1976.

[5] H.M. Überall, "Resonant Attenuation in Electromagnetic Wave Scattering from Conducting Elongated Objects", IEEE Trans. Electromagnet. Compatibility, Vol.35, No.4, pp.466-472, 1993.

[6] T. Marder, "Berechnung elektromagnetischer Felderscheinungen in abschnittsweise homogenen Medien mit Oberflächenstromsimulation", Doct. Thesis, TU Hamburg-Harburg, 1992.

[7] J. Nitsch, R. Sturm, H.D. Brüns, and H. Singer, "Splitting of Degenerate Eigenvalues in Coupled Two- and Three-Conductor Lines", EMC Proceedings of the 8th International Zürich Symposium, 87P2, 1989.

[8] C.E. Baum, "Damping Transmission-Line and Cavity Resonances", Interaction Note 503, May 1994.

[9] M. Magg, J. Nitsch, "HPM Coupling to Generic Targets: CW - VS Pulse Coupling", Proceedings of the EMC Symposium, Zürich, pp.361-367, March 1995.

[10] C.E. Baum, "Comparative System Response to Resonant and Unipolar Waveforms", Interaction Note 509, November 1994.

[11] J. Bohl, A. Kaiser, "Experimental HPM Susceptibility, Exploitation of Smart Munitions", AGARD/NATO, 3rd Symposium organized by the SPP on **Environmental Factors in Electronic Warfare Related to Aerospace Systems**", Rome, 8-11 May 1995.

EXPERIMENTAL HPM SUSCEPTIBILITY, EXPLOITATION OF SMART MUNITIONS

J. Bohl
DIEHL GmbH & Co.
Fischbachstr. 16
Department M-ELK
D-90552 Roethenbach
Germany

A. Kaiser
WWD Bwf-ABC Schutz
Humboldstr
D-29623 Munster
Germany

SUMMARY

Direct experimental exploitation and investigation of smart munitions are necessary to determine and analyze the coupling mechanisms from an outside electromagnetic field to the inside of the smart munitions where it can interact with the electronical guidance and control components as well as with the wiring. This interaction can lead to upsets on critical signals or/and to resonances on the signals. Numerical and analytical investigations are conducted prior to the experimental irradiation tests. For first approaches, direct injections of currents (normalized to the outer electric field) at the potential coupling paths (apertures and antennas) are applied to measure the resonances transferred to the inside of the munition. These test results are used as a basis for experimental exploitations at the live system with a defined simulated flight condition exposed to an electromagnetic field. The important point here is that not all coupled resonances cause a reaction/degradation in the guidance and control loops of the complex systems.
The final step is now to conduct 6-DOF-system simulations using the measured signal degradations caused by the exposure of the smart munition to an electromagnetic field. And here we can now see what kinds of interferences can be compensated by the closed loop control circuits and where the real critical parameters of an electromagnetic field are to interfere and damage the smart munition.
These results have to be used for hardening the own (friendly) systems but it also enables to prepare a system specification for a HPM defense device against smart munitions.

1. INTRODUCTION

The development of weapon systems with steadily increasing effectiveness made it necessary to apply highly sophisticated electronics, computers and sensors. On one side, these highly performed subsystems ensure that the mission of smart ammunitions can be fulfilled even under very critical circumstances like bad weather, fog, wind, a.s.o. but on the other side, these systems are now also more vulnerable against electromagnetic environments.

Paper presented at the AGARD SPP Symposium on "Environmental Factors in Electronic Warfare Related to Aerospace Systems" held in Pratica di Mare AFB (Rome) Italy, from 8-11 May 1995, and published in CP-573.

Exactly this point leads to two major aspects concerning the threat against smart ammunition. Firstly, the systems must be hardened against the commonly defined electromagnetic smog mainly to ensure the safety of the explosives but also against HPM sources. Secondly, the interference possibility of those smart ammunitions can be used to combat those systems.

Both ways of thinking require the knowledge of how a system can be interfered, which coupling mechanisms from the outside to the inside of a smart system concerning electromagnetic fields exist and what effects they have on the incorporated electronics, computers and sensors.

The development engineer has to know about the potential electromagnetic threats and how these threats in combination with the design and construction of the various missiles interact negatively with the missile's mission.

The design of a HPM-weapon system has to be specified according to the systems and their performances which have to be combated. The counter measurement aspects against such a HPM-weapon system leads to the hardening aspects for the friendly smart ammunition arsenals.

And this is the point at which the German MoD has established a fundamental research program. For selected smart ammunitions, the coupling mechanisms, the interferences on the guidance and control components including navigation platforms, signal processing units with µ-processors, seeker and control actuation systems will be investigated but the most interesting point is to indicate the degradation of the missile's mission according to different kinds of interferences.

Phenomenology is the domain of HPM research concerned with the understanding and analysis of how EM energy interacts with a target. As part of this effort, a test assessment process has been designed and implemented to test a live missile in simulated flight. This process equals to "systems functional response testing" as depicted in figure 1-1.

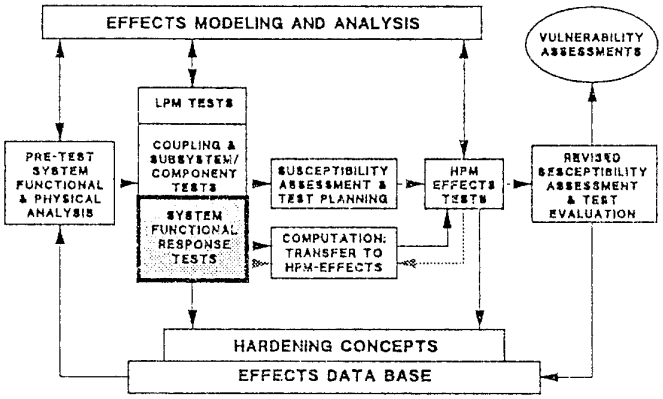

Figure 1-1: System Functional Response Testing

2. EXPLOITATION METHOD

A test methodology (figure 2-1) was created beginning with an analytical interference assessment regarding the most critical frequencies the smart ammunition does respond best to according to its design like fuselage, wings, fins, slots (back and front door coupling possibilities), followed by an numerical simulation of the surface currents and the surface charges as a response to an electromagnetic field depending on the field parameters like frequency, polarization, field strength and angle of incidence.

Experimental investigations are followed. Here we distinguish between investigations on not powered systems and live systems at a defined simulated flight condition (programmed flight, target seeking phase or target tracking phase).

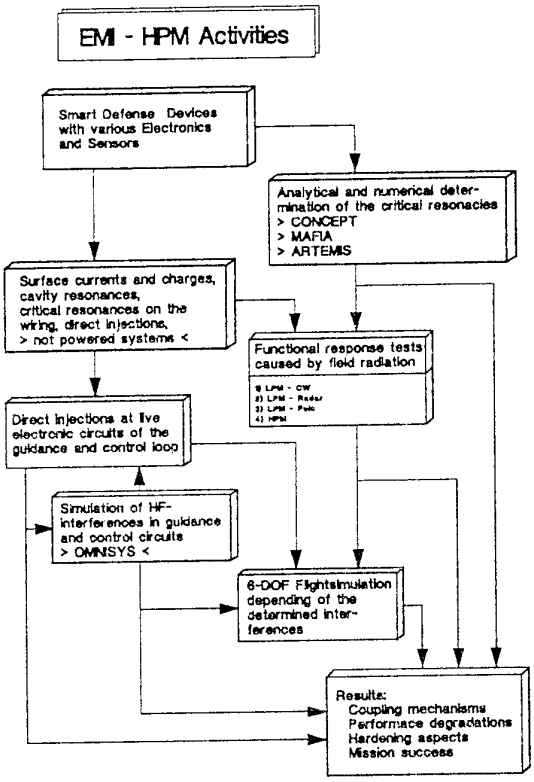

Figure 2-1: Exploitation Method

The investigations on not powered systems determine transfer functions from the outer field as well as from the surface currents to the internal field and to the resonances and induced currents on different signal wirings.

The tests with the not powered systems are distinguished between field radiation and direct injection tests of the electrical or magnetical field equivalent.

These investigations are helpful and necessary to limit the investigation efforts at live system tests where the concentration of the test runs is based on the information received from the analytical and numerical as well as from the experimental investigations conducted with not powered systems.

The functional response tests offer a non-invasive approach for a distinct measure of power-on functional degradation caused by incident radiation. These tests are critical to discover previousely unrecognized critical points within the system by means less apt to interfere electromagnetically with the normal function of the system.

Direct injection tests with live subsystems are conducted to analyze the transfer-functions and interference mechanisms and finally the detection of the descenerable signal (MDS) depending on the frequency.

The functional response tests with the live systems are conducted under various conditions beginning with low power microwave - continous wave (LPM-CW) field irradiation. These tests ensure a non disturbant investigation of the system. The following low power microwave puls/radar irradiation tests use the determined critical field parameters like carrier frequency, modulation frequency, polarization and angle of incidence from the LPM-CW tests. The aim is to analyze the additional system behaviours caused by pulses instead of CW.

The final possible irradiation investigation can be conducted with high power microwave (HPM).

These tests are critical to the hardware because it can lead to burn outs of and damages to the electronical devices. But this is very expensive. Nevertheless the tests are necessary to see the behaviour of the smart systems under a realistic battle field scenarios and also to analyze the non-linearities of these systems.

The last but one of the most interesting steps within the test sequence is the 6-DOF (six degree of freedom) flight path simulations where the degradation of the flight path and the degradation of the hit probability of the smart munitions are shown depending on the determined interferences.

The overall investigation results can be summarized to the determination of
- the coupling mechanisms
- the performance degradation of the various electronical subsystems (guidance and control systems)
- hardening aspects of the "friedly systems"
- defense aspects against "unfriendly systems"
- the mission success depending on the electromagnetic field conditions exposed to the smart munitions.

3. DIRECT INJECTION

3.1 FREE FIELD SIMULATION

If - with reference to figure 3.1-1 - the current at the end of the wire is considered to give information about the system's internal resonances when illuminated, we can measure the transfer function

$$\underline{TF}_{total}(f) = \frac{\underline{I}_{wire}(;f)}{\underline{E}_{free\ field}(;f)} \left[\frac{A}{V/m}\right]$$

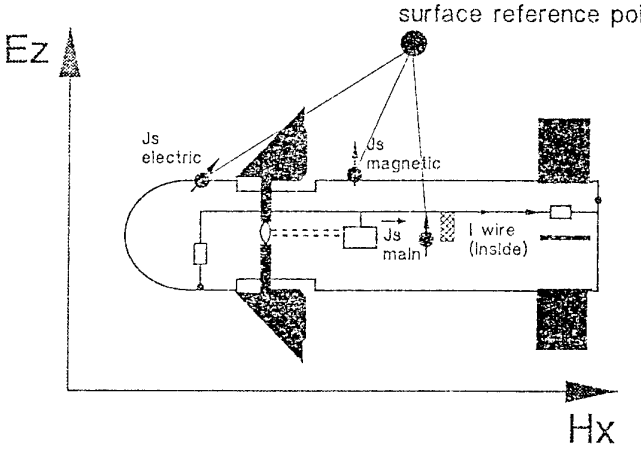

Figure 3.1-1: Simplified model of a missile exposed to vertically polarized EM-field.

The socalled total (matrix) transfer function TF_{tot} represents the wire's complex current normalized to the outer electric field the missile is exposed to. Usually, the free electric field is measured in absence of the device under test (DUT). Therefore, we cannot distinguish between inner (cable-, cavity-, ...) and body-resonances. But we can split the total transfer function into an interior on referenced to a surface reference point and an outer surface (reference point) to free field transfer function. As illustrated in figure 3.1-1, at the reference point, the measured current density on the surface can be the interface for both kinds of transfer functions (assumed that I_{wire}, J_F and E are represented by one vector component only.

$$\underline{TF}_{tot}(f) = \frac{\underline{I}_{wire}(f)}{\underline{J}_F(f)} \cdot \frac{\underline{J}_F(f)}{\underline{E}_{free\ field}(f)}$$

inner transfer funcion outer transfer funciton

Thus, the total transfer function can be represented as the product of the interior and outer to get the total one. If we consider the inner transfer function to unveil the system's inside behaviour (resonances), the outer one can be regarded as a "weight funtion" whose resonances are mostly related to the missile's body structure (length, diameter, fin or wing length, ...). This weight function usually does not show high Q resonances due to the missile's outer curved structure (radiation losses). In most cases, one can calculate it easily using analytical or numerical tools. In order to detect the missile's critical (interior) frequencies (high Q resonances) we should focus on the inner transfer function.

3.2 DETECTING CRITICAL FREQUENCIES BY THE DIRECT "INJECTION"

So far, all tests have shown that (back door) coupling into a missile's interior takes place due to the imperfectness of the missile's shielding. The missile - in general - offers two coupling paths (mechanisms) for the electromagnetic wave.

Apertures (mainly a magnetic field coupling): openings (seeker, cooling, external supply), and slots.
Antennas (mainly an electric field coupling): not massed wings and fins capable to transport current into the interior (see figure 3.2-1).

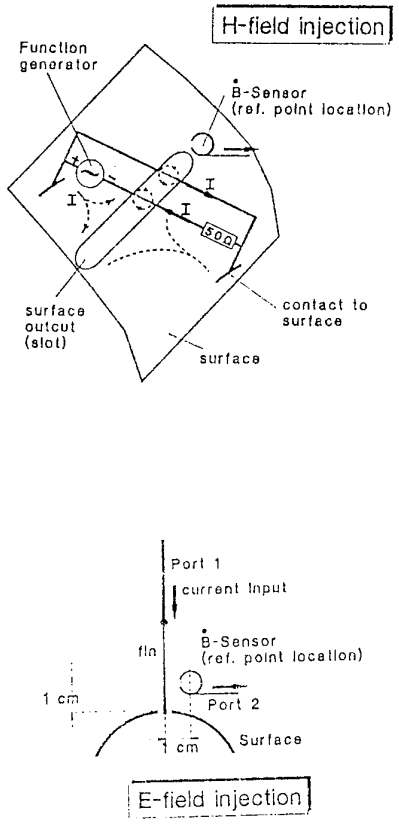

Figure 3.2-1: Direct field injection methods (in principle)

When illuminated, both mechanisms (paths) occur simultaneously. The magnetic field penetrates the missile through the slots. The electric field will preferrably excite $\left(\lambda/4\right)$-antennas.

Since we want to use the direct injection technique we have to simulate the magnetic field and the electic field in separate experiments using different injection techniques and tools.

a.) Regarding the slot couplings such a tool could be (magnetic field) a small loop or wave guide mounted above the slot (see figure 3.2-1). Actually, we used the small 50 Ω matched wave guide depicted in figure 3.2-2 which was driven by a frequency generator.

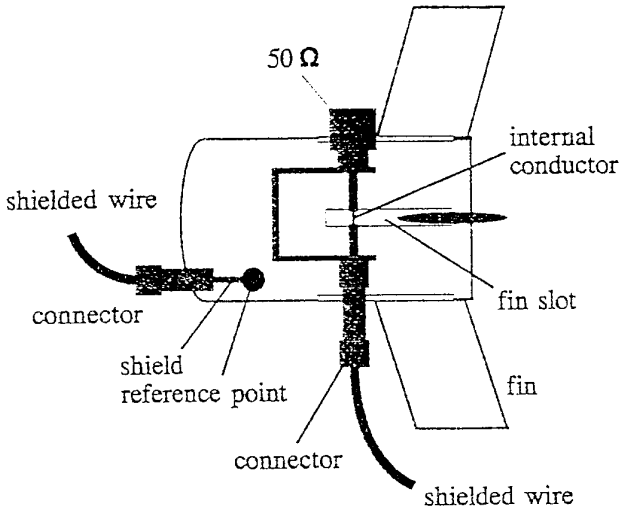

Figure 3.2-2: Magnetic field injection loop

The construction of the magnetic dipole loop is very similar to the common sensor technique where the gap in the middle of the loop allows the magnetic flux (derivation) to couple into. The symmetry of the loop's shielding minimizes the electric field portion. In a distance of few centimeters from the loop the surface reference point has to be established. This point serves as reference for the current density occurring in the transfer function

$$\frac{\underline{I}_{wire\,magnetic}(f)}{\underline{J}_{surface magnetic}(f)}$$

and for further calculations, respectively. A recommended location for the reference point could be the far end of the slot.

The orientation of the injection loop (and, of course, the adequate reference location) depends on the polarization of the free field illuminations as shown in figures 3.1-1 and 3.2-1 have to be applied. In the case of

horizontal polarization the loop has to be turned by 90° degrees.
The "loop injection method" has to be applied to all slots which are considered to be a potential POE (Point of Entry). But, in many cases missiles are built very symmetrically and even one slot magnetic field injection could be sufficient to detect the critical frequencies caused by the magnetic field penetration.

b.) As far as orientation, POE identification, and symmetry is concerned, the above mentioned also applies to the injection into antennas, like fins and wings.

As shown in figure 3.2-3 the antenna (fin) was driven directly by the frequency generator. Since the fin is not connected to the missile's hull, the applied current can flow into the interior.

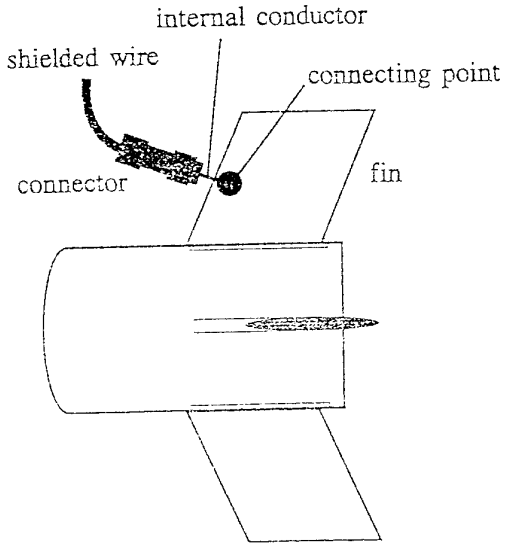

Figure 3.2-3: Electric field injection

One technical solution to inject current is depicted in figure 3.2-4 where the fin acts somehow like a λ/4 antenna in free space.

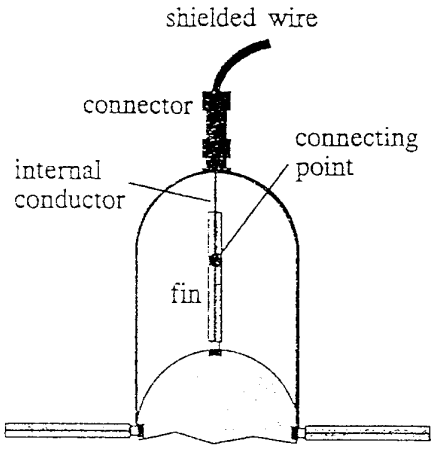

Figure 3.2-4: E-field injection

Another solution which generates more current at lower frequencies is shown in figure 3.2-2. Again, a reference point has to be chosen to build the transfer function

$$\frac{\underline{I}_{wire\,electric}(f)}{\underline{J}_{surfaceelectric}(f)}.$$

In many cases both injection methods and different POE's to inject into, require different reference points. Since, for the final result, a summation of all so far acquired transfer functions is necessary to set the "simultaneous" one, we have to choose one of the reference points to be the main one. Only the transfer functions are main ones and remain unchanged if they are built with that corresponding reference point's surface field measurement. Each other transfer function has to be adjusted by multiplying with its correction transfer function

$$\frac{\underline{I}_{ref.Fpoint}(f)}{\underline{J}_{Fmain}(f)}$$

c.) Example for superposition (summation): We assume that only two transfer functions (one magnetic, one electric) were acquired According to figure 1, three reference points were chosen (ref point electric, ref point magnetic and the main ref point).

$$TF_{simul\,tan}(f) =$$

$$\frac{\underline{I}_{wire\,electric}(f)}{\underline{J}_{Sref.point\,electric}(f)} \cdot \overbrace{\frac{\underline{J}_{Sref.point(electric)}(f)}{\underline{J}_{F\,main}(f)}}^{correction\,function} +$$

$$\frac{\underline{I}_{wire\,magnetic}(f)}{\underline{J}_{Sref.point\,magnetic}(f)} \cdot \underbrace{\frac{\underline{J}_{Sref.point\,magnetic}(f)}{\underline{J}_{S\,main}(f)}}_{correction\,function} =$$

$$\frac{\underline{I}_{wire}(f)}{\underline{J}_{Smain}(f)}$$

If we had chosen one reference point only (e.g. the main one for all measurements) no correction would have been necessary at all. The correction functions can be measured by illumination of the missile or by calculation with numerical tools. Building the correction functions over the electric free field

$$\frac{\underline{I}_{Fref.point(electric/magnetic)}}{\underline{E}_{free\,field}}$$

we get the weight function. Multiplication with this weight function directly yields the total transfer function

$$\frac{\underline{I}_{wird}(f)}{\underline{E}_{free\,field}(f)}$$

when applied to <u>all</u> injection transfer functions.

For upper bound estimation a low impedance as a (reciprocal) constant factor can be applied to get the total transfer function built over the electric free field e.g.

$$\frac{\underline{I}_{Sref.point(electric/magnetic)}}{\underline{E}_{free\,field}} = 1/50\Omega^{-1}$$

can be considered to be reasonable).
Figures 3.2-5 to 3.2-8 verify that the direct "field injection" is an appropriate method to detect the critical frequencies of a missile.

Data in figures 3.2-5 and 3.2-8 was acquired during a real test when both methods - illumination and direct "field injection" - were applied.

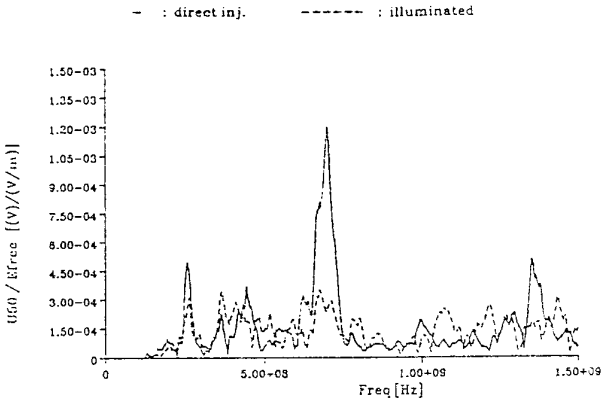

Figure 3.2-5: Illumination method versus direct "injection" (superpositioned). Voltage at the wire's 50 Ω end (U50)/ Electric free field (Efree). CAS W2

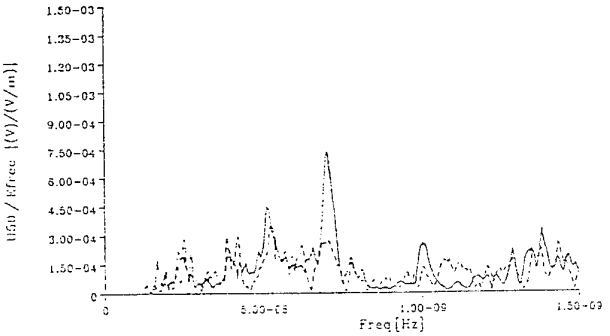

Figure 3.2-6: Illimination method versus direct "injection" (superpositioned). Voltage at the wire's 50 Ω end (U50)/Electric free field (Efree). CAS W1.

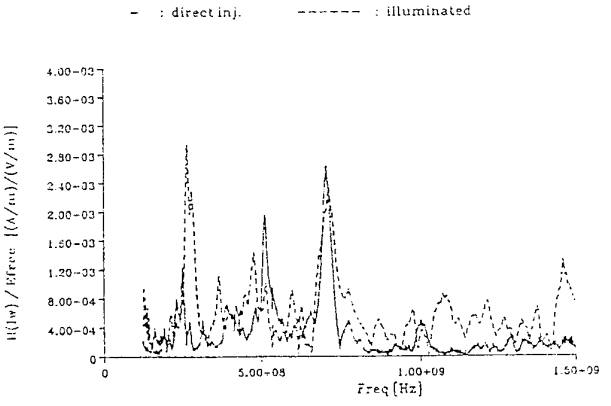

Figure 3.2-7: Illimination method versus direct "injection" (superpositioned). Magnetic field of wire's current (H(Iw))/ Electric free field (Efree).CAS W2.

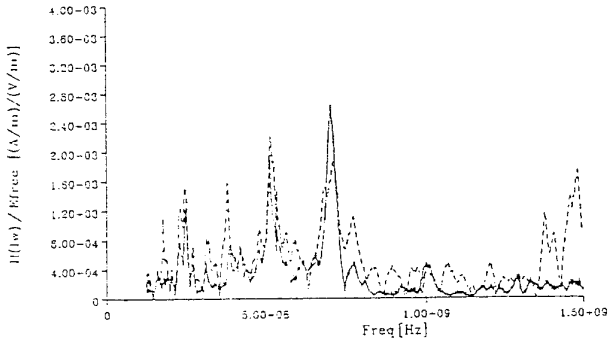

Figure 3.2-8: Illimination method versus direct "injection" (superpositioned). Magnetic field of wire's current (H(Iw))/ Electric free field (Efree). CAS W1.

SUMMARY

(1) The total transfer function actually consists of an inner transfer function and a weight transfer funcion.
(2) The inner transfer function unveils the system's critical frequencies if acquired completely.
(3)The outer transfer function emphasizes or suppresses the magnitudes of the inner ones.
(4) The inner transfer function can be built by summation of the electric field injection transfer funcion and the magnetic one, respectively.
(5) The outer transfer funcion can be easily calculated by using analytical or numerical tools and code. For upper bounds estimation a low impedance consideration (reciprocal) will sufficiently yield the total transfer function built over a free electric field.
(6) To get a complete set of inner transfer functions each POE has to be identified. Into each identified POE injection has to be made using the adequate injection method. Depending on the prior coupling mechanism, slots have to be exposed to a magnetic field, antennas to an electric one. Since fins are usually not connected to the missile's hull, they can act like λ/4 antennas.

4. FUNCTIONAL RESPONSE TESTS, FREE FIELD ILLUMINATION

The functional response tests with live smart munitions only determin the functional degradation caused by incident radiation. Not all critical resonances cause an interference in the guidance and control loops. Furthermore it is essential for the most systems that they show degradations only if the carrier-frequency is modulated. And these effects can only be demonstrated with live systems.

4.1 TEST PROCESS DESCRIPTION

The planning and preparation for HPM functional response tests is critical in ensuring that the limited test time is used efficiently. The IPAS missile, as shown in Figure 4.1-1 is composed of several subsystems, each of its critical signals had to be monitored during irradiation to determine if functional degradation was induced. This required the design of a unique fiber-optic signal monitoring system.

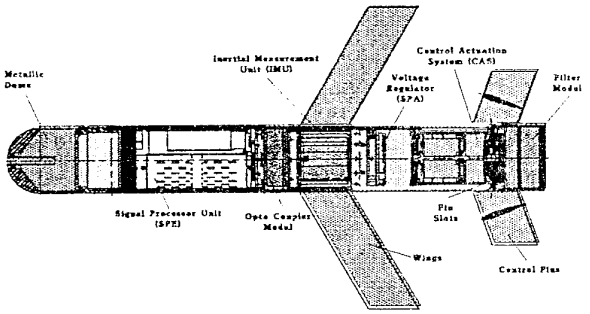

Figure 4.1-1: IPAS Test Missile with Sub-Systems

The opto-coupler module (OCM) was the part of this system responsible for the conversion of electric signals. The light signals could then be transmitted, via fiber-

optic cables, without RF (radio frequency - specific subset of the EM spectrum) perturbation, to the receiver for reconversion to electric signals. This system provided the non-invasive tool to observe the missile reaction to RF irradiation. The OCM, as seen in the figure, occupied the space which would operationally house the warhead. The filter module replaced the short-life thermal batteries and acted as an interface between the missile and the external power supply. The compartment forward of the signal processor unit (SPU) typically houses the seeker, but was not a part of this series of tests.

Due to limited space within the missile, the number of monitored signals had to be minimized because each required its own electro-optic converter. Therefore, only the primary signals of each subsystem were selected and most dealt primarily with flight control and navigation, as accuracy is key to mission success. During the tests, the missile software ran in a continuous loop to keep the missile in a simulated level-flight condition. This condition corresponded to a constant voltage value for all monitored signals, thus, effects due to irradiation could be observed by a deviation in the voltage. Six signals monitored the outputs of the inertial measurement unit (IMU) directly, whereas the next five monitored the corresponding angular rate or acceleration as computed by the SPU from the IMU output. From these rates and accelerations, the SPU determines if any control input is required to maintain level flight. If so, it sends commands to the control actuator system (CAS), i.e. any of the four independently-controlled actuators of the control fins. Any fin movement is, in turn, sensed by its corresponding potentiometer, which provides a position feedback signal back to the CAS internal control loop. The IMU would then sense the resulting flight changes. Since the signals were monitored at various points throughout the control loop process, the tester could more readily pinpoint the disturbance source(s). The test was set up as illistrated in Figure 4.1-2.

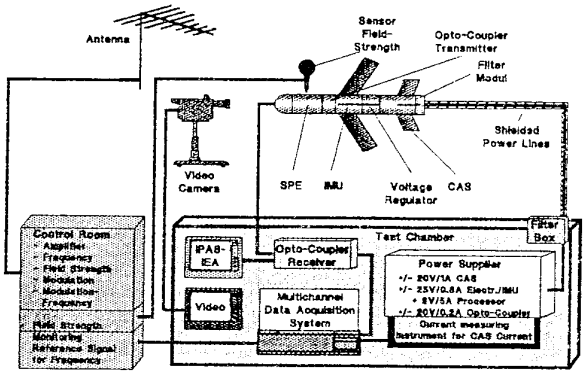

Figure 4.1-2: Test Setup

The irradiation parameters (frequency, polarization, angle of incidence, modulation, and field strength) were all regulated from the control room, which was shielded from the large anechoic chamber by a RF-shielded wall. The remainder of the setup was in the anechoic chamber itself. The IPAS missile rested upon a combination wooden table and stand to prevent unwanted reflections. Extending out of the aft end of the missile were the shielded power supply cables leading to the shielded test cabin. In this manner, the power supply lines were decoupled from the missile. Coming out of the front end were the fiber-optic cables to relay the transmitted signals to the opto-coupler receiver within the test cabin. The receiver reconverted the signals to their corresponding voltages and sent them to the data acquisition system (DAS: strip chart recorder and/or PC). The CAS current was directly monitored by current probes to identify any surges or losses in power. The digital modem signal was displayed on the computer monitor (IPAS-IEA) and allowed the missile operators to properly power up the system and to monitor SPU status. An additional indication of system effect was established via a video camera system with monitors both in the test cabin and control room.

To ensure all desired parameters were thoroughly investigated, the various trials were typically done in a manner consistent to the test flow diagram depicted in Figure 4.1-3. Occasional departures were necessary to probe a little deeper in some areas.

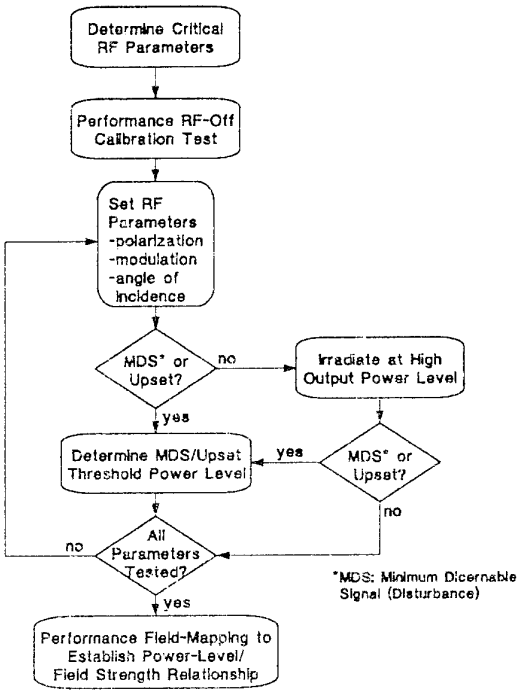

Figure 4.1-3: Test Flow Diagram

As can be seen, determining the critical RF parameters was the first step. This was done by utilizing the results of earlier analytical, numerical, and experimental investigations provided by participating organizations. The experiments were done on a non-powered, passive missile to measure body, appendage, and aperture resonances as well as those associated with specific points, cables, and volumes internal to the missile. Results provided insight as to the frequencies, polarizations, and angles of incidence where susceptibilities may occur, not necessarily where they will occur. Also, there was only limited indication of the field strenghts or modulation required to achieve an adverse effect. Instead, these investigations were used as a predictive toll and to limit the test parameters of the functional response tests to a manageable level.

The next step was to perform an RF-off calibration test because the signals are never as constant as they are supposed to be, even without radiation. This was accomplished by simply powering up the missile and running the DAS for about thirty seconds. With the heart of the test process now ready, the irradiation could start at a moderate output level that corresponded to approximately 150 V/m field strength. This was done to avoid damage to especially sensitive subsystems.

At this point, the difference between "minimum discernable signal" (MDS) and upset should be explained. MDS, as the name implies, is the smallest discernable deviation from the normal operating signal, in this case, the previously measured calibration signal. This is actually more difficult than it sounds due to natural variations from calibration to calibration. Therefore, it is often easier to wait for a "real" upset, and work backwards with the power level to find the MDS. Of course, first an MDS or upset had to be found and if none was detected at the moderate power level, the level was increased to maximum, which was anywhere from 300 to 600 V/m depending on the frequency and corresponding amplifier available. If, at both the moderate and high power level, no disturbance was recorded, irradiation was performed with the next set of RF parameters.

If an effect was detected, the next step was to determine the MDS and upset threshold power level, which could be done simultaneously. The power level in this case refers to signal generator outpout levels expressed in decibels with respect to milliWatts (dBm). This was accomplished by fixing the frequency and adjusting the power level digitally upwards during irradiation, noting the power required for both MDS and upset.

After the thresholds had been determined for all detected effects, the final step was to

determine the field strength, at each critical frequency, corresponding to each of the tested power levels. The technique used to do this is called "field-mapping" and was accomplished by running the tests with only the field probe in the test area, recording the readings from the control room. The field strengths are dependent on the antenna used, probe type, probe-antenna separation, and polarization. Therefore, when documenting these measurements, it is important to record the test conditions and measurements concurrently.

4.2 FUNCTIONAL RESPONSE TESTS/ LIVE SYSTEM

The guidance and control loops/components with the required wiring are the basis for the data acquisition during the functional response tests with live systems. All relevant signals are recorded for later data reduction and data analysis together with the irradiation parameters of the electromagnetic field. The figure 4.2-1 illustrates the complex guidance and control elements of a smart munition.

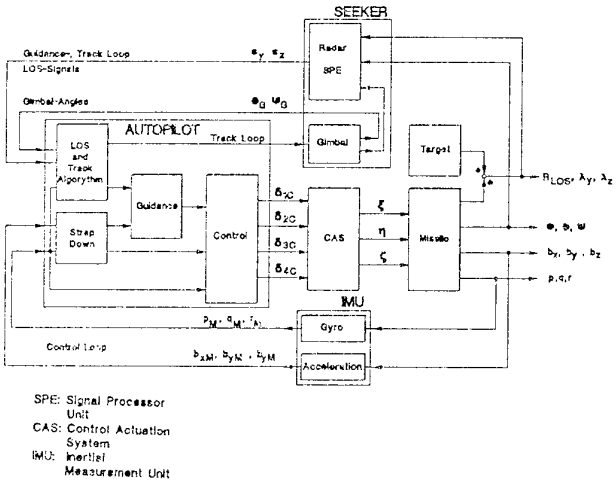

Figure 4.2-1: Structure of the guidance and control loop

The first part of the investigation was conducted without the seeker. The nose was exchanged with a dielectric dome. This ensured that only the back door effects of the fins, fin slots, wings and missile structure were considered.

The experiments on the live IPAS munition showed that it could only be affected via the control fins and their corresponding structural slots. The modulation type and its frequency played the critical role in interfering with the missile electronics; without modulation, the electronics of the system were not susceptible. The fins emulated one-sided short-circuited dipoles as described. Due to the negligible fin slot dimensions, nearly all system interference was caused by fin resonance. the measured interference of the missile's signals showed rather large attenuation between the CAS and the front of the missile.

Figure 4.2-2 shows the MDS for the four fin deflection signals. The figure 4.2-3 shows the CAS current as a function of the frequency and the field strength of the electromagnetic field. Figure 4.2-4 shows the upset levels of the four fin deflection signals.

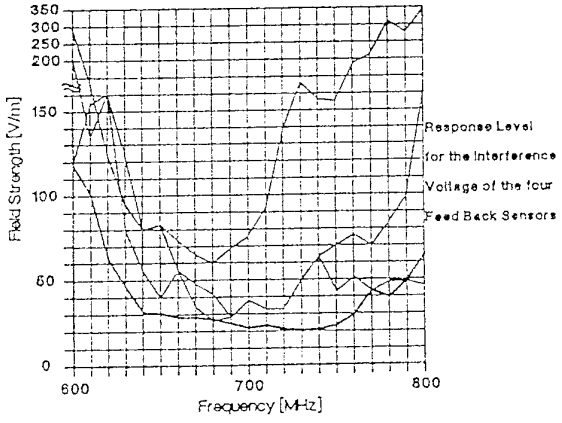

Figure 4.2-2: MDS for the fins

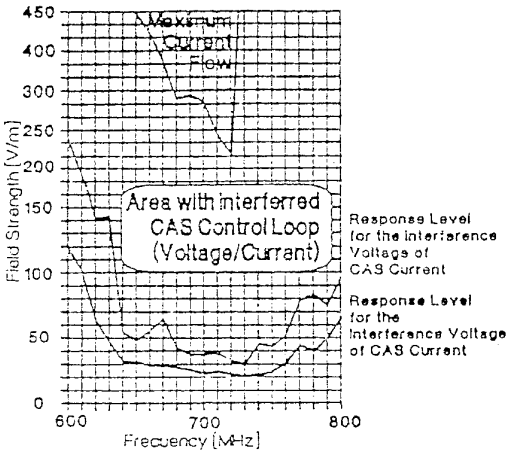

Figure 4.2-3: Current of the CAS

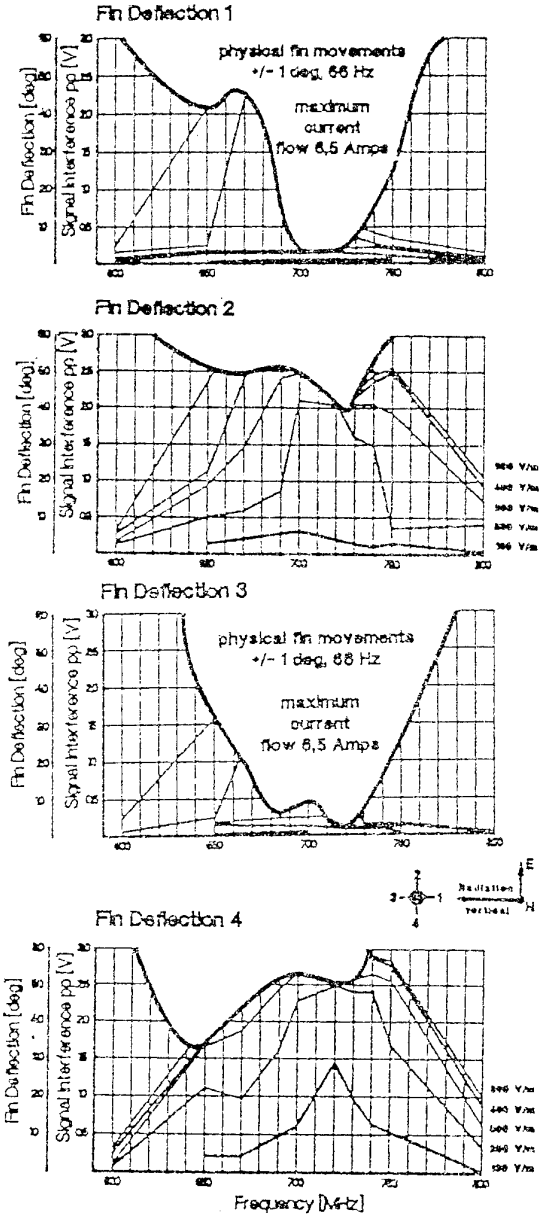

Figure 4.2-4: Upset levels of the fin deflection signals

The λ/4 predictions gleaned from the physical dimensions of the fins matched the frequencies of the measured electronic susceptibilities to a very large extent. Also, the results of wire (cable) and cavity resonance tests, performed on the passive/inactive missile by other organizations, compared favorably with the live, active missile IPAS investigations (figure 4.2-5). However, not all predicted and measured resonances of the passive munition caused an interference of the operating system electronics. That is why live system tests with activated electronics are essential to this type of assessment.

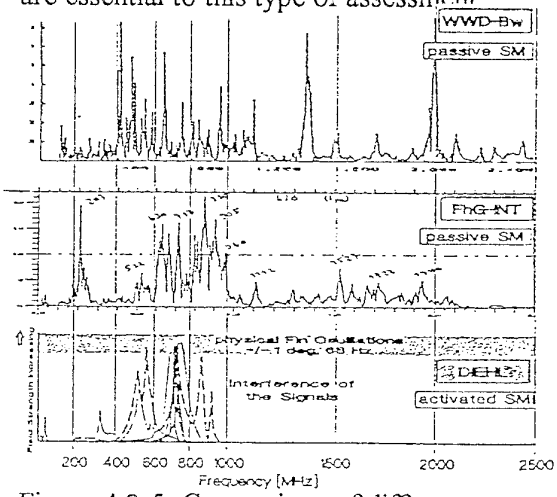

Figure 4.2-5: Comparison of different investigation types at CAS fin deflection (Cavity resonance and wire resonance at passive system; fin deflection at live system - all illuminated)

5. COMPARISON BETWEEN DIRECT INJECTION AND FUNCTIONAL RESPONSE TESTS AT LIVE SYSTEMS

The test results from the direct injection of the electrical and magnetical field equivalent at the fin and the fin slot show resonances at about 600 to 750 MHz on the fin deflection wire. This is also valid for the radiation investigations at the not powered systems (ref. figure 3.2-5 to 3.2-8) But there are also resonances in the

lower frequency range at 500 MHz and 250 MHz.

The functional response irradiation tests with the live smart ammunition show a susceptibility in a frequency range between 600 and 800 MHz only (ref. figure 4.2-2 to 4.2-4).

But the very important point is that the CAS-signals could only be interfered with a modulation frequency (66 Hz best on the carrier frequency).

This means that the resonance frequency at the various guidance and control systems alone can not necessarily degradate the performance of the system. Only the modulation frequency leads to an interference in the subsystems.

Another point is that not all resonances transferred to the inside of the smart ammunition lead - even with various modulation frequencies and wave forms - to a disturbance or interference of the system summary.

> Investigations at the not powered system are necessary to determine all possible resonance frequencies which might be critical to the system (basis for further investigations).
> Only the investigations at the live systems are able to detect the radiation parameters which are critical to the system and where interferences on critical guidance and control signals happen.
> Both methods together with the initial analytical and numerical approaches are important to be conducted to get a complete picture about the interference possibilities of such complex systems.

6. FLIGHT PATH SIMULATION

To determine if any of the observed effects translate into a mission effect, the flight path performance must be evaluated by a system simulation which considers the measured level of signal interference. The final portion of these investigations, a real-time six-degree-of-freedom (6-DOF) simulation, showed performance effects due to the irradiation of the munition. The most sensitive, "final-homing" phase of the missile's flight path was considered in this evaluation. During the simulation, actual measured response signals were directly input at various points in the guidance and control system for four cases of affected-subsystem combinations as shown in figure 4.2-1. The greatest sensitivity was found in the track loop of the guidance and control system.

a. CAS only

Oscillating resonances within the control loop, as discovered during testing, have little effect on the flight path. The system simply averages these oscillations out and proceeds to the target. However, these oscillations do cause an increased current flow in the power amplifiers which are only designed to withstand this increased flow for a few seconds. Any damage to the actuator power amplifiers will immediately interrupt the fligth mission as depicted graphically in figure 6.1.

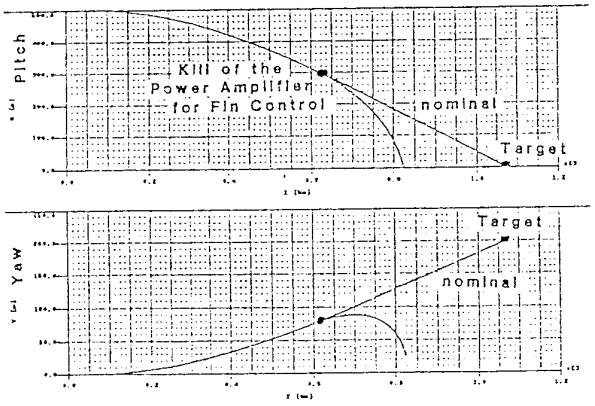

Figure 6-1: Degradation of the Final Homing caused by a burn out of a CAS-amplifier

b. IMU only

The oscillations alone had a similar effect as that of the "CAS only" run for the same reasons.

c. Combined CAS and IMU

Even with combined CAS and IMU interference, the flight path showed little degradation, as depicted in figure 6-2, due once again to the oscillating characteristic of the interference signals. On the other hand, an effective disturbance would be one which produces a signal offset or shift. Such CAS and IMU disturbances could provide a strong enough influence on the track loop to upset the mission.

d. Theoretical gimbal/seeker

A theoretical simulation affecting the seeker in addition to the CAS and IMU showed a definite loss of target as shown in figure 6-3. Even a three percent deviation of the seeker gimbel signals caused this to happen.

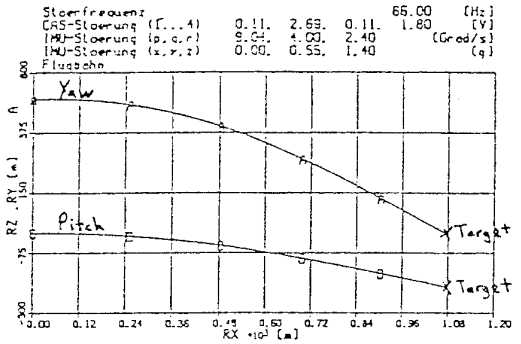

Figure 6-2: Combined CAS and IMU interferences

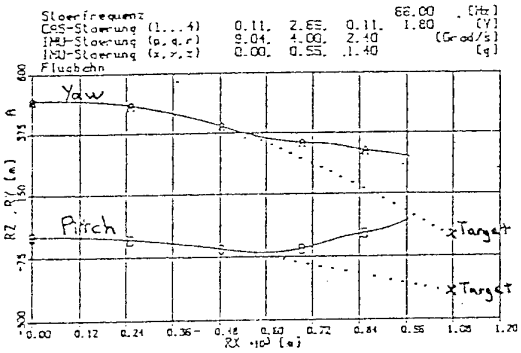

Figure 6-3: Theoretical gimbal/seeker section

7. CONCLUSIONS

The tests and simulations described herein provide the feasibility of using an HPM weapon against an attacking smart munition or smart missile as well.

Investigations of such complex systems require all investigation steps beginning from the analytical an numerical approaches followed by investigations at the not powered system (overstressing leads to a disturbance of the highly sophisticated systems) to determine all existing resonances depending on the test parameters.

The investigations with live systems show, based on the previous results, where the real interferences at the guidance and control systems are.

But only the final flight path simulation (6-DOF) with considered subsystem interferences can show if and with which field parameters it is possible to degradate the mission of smart munition.

The investigation of a variety of smart munitions/missiles lead to a data base which is the basis for hardening the own (friendly) systems against the threat of HPM-systems and also for creating a specification how a HPM defense device must be designed for optimized effects on the future battle field.

U. Lammers (US)

In terms of the previous paper your approach is a high-power, but low-sophistication attempt to throw the weapon off course, such as by burning out a part of the guidance system. What is the rationale for doing this, rather than interfering with the seeker at its operating frequency and at much lower power ?

Author's Reply

It is correct that we mainly investigated back-door - rather than front-door - coupling which will become an object of our future experiments. Since it was our goal to test the action of potential HPM-weapon systems we laid emphasis on the interference at resonance frequencies of possible targets. A broad band excitation with high power increases the ability of perturbing unknown systems. Moreover, the operation with high power has the advantage that the engagement radius becomes essentially increased if the target is irradiated at one of its operating frequencies.

MEASUREMENTS OF GPS AND LORAN PERFORMANCE IN AN URBAN ENVIRONMENT

Lance C. Miller, David Vaurio, Albert Giambalvo, Sherman Karp
Science Applications International Corporation
4001 N. Fairfax Drive
Suite 300
Arlington, VA 22203
United States of America
Phone: (703) 525-0081
Fax: (703) 524-1643
Email: lmiller@dsto.saic.com

1. SUMMARY

During the summer of 1994, the Advanced Research Projects Agency funded an experiment to collect extensive radionavigation data in the New York City area. The participants are listed under the Acknowledgments. The data includes the accuracy and availability of the Global Positioning System (GPS) and LORAN-C, the increased availability of both GPS and LORAN by adding a precise oscillator input to the receivers, and a comparison of electric field (E-field) and magnetic field (H-field) LORAN signal availabilities.

Analysis of the data shows: (1) in the deep urban canyons of Wall Street, the availability of LORAN (either E or H field) is higher than that of GPS; (2) in almost all scenarios, the LORAN magnetic field signal is easily detectable and has repeatable phase characteristics. In contrast, the LORAN electric field signal strength is frequently attenuated and undetectable, especially in the Wall Street area and under the elevated train tracks in the Bronx; (3) when corrected for propagation anomalies, the inherent repeatable accuracy of LORAN is 7-10 meters rms with under 100 meters rms potentially obtainable in an operational differential mode; and (4) the availability of radionavigation fixes can be enhanced in these urban areas by the integration of LORAN and GPS navigation information and by the use of a precise oscillator which allows a geographic fix to be made by receiving as few as two time of arrival broadcasts, e.g. one GPS satellite and one LORAN station.

2. BACKGROUND

This paper is an extension of the final report [1] of this project. This paper contains some data described in reference [1] and provides further analysis on the effect of antenna location.

LORAN is a ground-based, all-weather navigation system whose coverage includes the complete continental United States of America and selected coastal areas worldwide. It has a repeatable accuracy of 18 to 90 meters [2]. LORAN operates at a frequency of 100 kHz which corresponds to a wavelength of about 3000 meters. Due to the LORAN operating frequency, it was expected that its long wavelength would allow the LORAN signals to penetrate deep urban canyons.

GPS is a satellite-based, all-weather system with almost world-wide coverage. Its accuracy is 10 to 100 meters subject to selective availability. GPS operates at around 1.2 and 1.5 GHz which corresponds to about a 30 cm wavelength. It was thought that this shorter wavelength might be attenuated or even blocked in an urban environment.

The experiment's overall purpose was to determine the feasibility of using GPS and/or LORAN for tracking and geo-location applications in an urban environment. Individual objectives included: measuring GPS and LORAN availability in an urban environment; evaluating a LORAN H-field antenna; evaluating a new digital LORAN receiver; determining the benefit of using a precise oscillator with GPS and LORAN receivers; and, measuring the repeatability and accuracy of LORAN. Also, since some of the tracking applications could require covert placement of the antenna(s), a study was conducted to determine the effect of antenna location on the availability of GPS and LORAN. Next is a summary of the two radionavigation systems, LORAN and GPS.

3. SCENARIOS

A total of five different scenarios was completed. The scenarios were picked to represent different aspects of an urban environment. The three main scenarios included the tall buildings in the Wall Street area, the relatively more open streets, smaller buildings, elevated train tracks, and power lines of the Bronx, and a higher speed scenario in the vicinity of the large metallic structure of the George Washington Bridge. Fifteen runs of each of these three scenarios were completed in order to obtain statistically significant data. Two other scenarios were added during the data collection. The Third

Paper presented at the AGARD SPP Symposium on "Environmental Factors in Electronic Warfare Related to Aerospace Systems" held in Pratica di Mare AFB (Rome) Italy, from 8-11 May 1995, and published in CP-573.

Avenue scenario was added and consisted of tall buildings, but had wider streets than the Wall Street scenario. The van did not have to make any turns in this scenario which allowed the use of the one-axis H-field antenna with the LOCUS receiver (described later). In order to evaluate GPS under foliage, two scenario runs were completed on a tree lined drive along the Hudson River.

4. DATA COLLECTION HARDWARE

A mobile experiment van was obtained on loan from the FAA Technical Center in Atlantic City, NJ. Laptop computers were used for logging the data from the receivers. All of the hardware listed below was installed in the van.

4.1 Ground Truth Device

Ground truth position was recorded as a baseline for comparison of the GPS and LORAN fix accuracies. The ground truth sensor was a Terrafix dead reckoning system that measured distance traveled by counting speedometer pulses. At every street intersection, the latitude/longitude were known and, therefore, served as locations to recalibrate the dead-reckoning system. The data from the Terrafix device was processed and recorded on a laptop computer in latitude/longitude format. The ground truth rms error was about 5 meters.

4.2 GPS Receivers

The van was outfitted with 2 Magnavox GPS receivers. One was a 6 channel and one was a 12 channel receiver. The data recorded from the GPS receivers includes time (UTC), latitude, longitude, satellite number, azimuth and elevation to satellite, and tracking code.

4.3 LOCUS LORAN Receiver/Cesium Clock

The LOCUS LORAN Receiver is a digital LORAN receiver which accepts a precise oscillator input. In this experiment, a Cesium-based oscillator was used as the input. The receiver was configured to make the typical three station TDOA fix unless only two stations were available. In this case, the receiver made a two station TOA LORAN fix utilizing the Cesium oscillator. Most of the data collected with the LOCUS receiver was from the E-field antenna. LOCUS did supply an H-field antenna, but it was only a one-axis antenna. Therefore, every time the van turned at a corner, the loop needed to be realigned. This setup was deemed unfeasible for most of the tests. However, the Third Avenue scenario permitted the van to drive in a straight line for the entire scenario enabling some H-field LOCUS data collection. This receiver was designed to be a monitoring receiver rather than a tracking receiver which means that the algorithms may not have been optimized for tracking a moving vehicle. The LOCUS data included time, latitude, longitude, LORAN station signal strengths, signal-to-noise ratios, envelope to cycle differences, and time differences for the different LORAN signals.

4.4 HP89410 Vector Signal Analyzer

The HP89410 Vector Signal Analyzer was configured to act as a virtual LORAN receiver. An electric field 18 inch whip antenna was fed into one channel, while an omni-directional loop (H-field) antenna was fed into the second channel. This H-field antenna was an aviation crossed loop antenna developed in the former Soviet Union. Using an externally provided GRI trigger, a magnetic heading sensor, and a ROM look-up table, a logic circuit switched in the appropriate loop with the appropriate phase to produce the correct composite signal. The HP89410 measured the signal strengths and phases of Seneca, Nantucket, and Carolina Beach LORAN signals as well as the noise strengths for both antennas.

5. RESULTS

5.1 GPS and LORAN Fix Availabilities

Using the GPS and LOCUS data, an overall fix availability as a percentage of scenario distance (in meters) was found for each scenario. The data from all of a scenario's runs was merged into one file and an overall availability was calculated. Figure 1 shows the availability results for the Bronx Scenario with the 12 channel GPS receiver and the LOCUS LORAN receiver. Recall that the Bronx scenario is a suburban type of environment with mostly 1 and 2 story buildings. The LOCUS availability is with the receiver using the E-field antenna. The categories of fix availabilities are 3D and 2D GPS with and without the receiver utilizing a precise oscillator, the LOCUS receiver with and without a precise oscillator, and an integrated GPS/LORAN fix. The integrated GPS/LORAN was calculated using the LORAN TOAs and GPS pseudo ranges. For GPS, a PDOP of 3 was used which corresponds to about 100 meter accuracy. From Figure 1, it can be seen that a 3-D GPS fix without a precise oscillator could be made over about 40% of the total distance of the scenario.

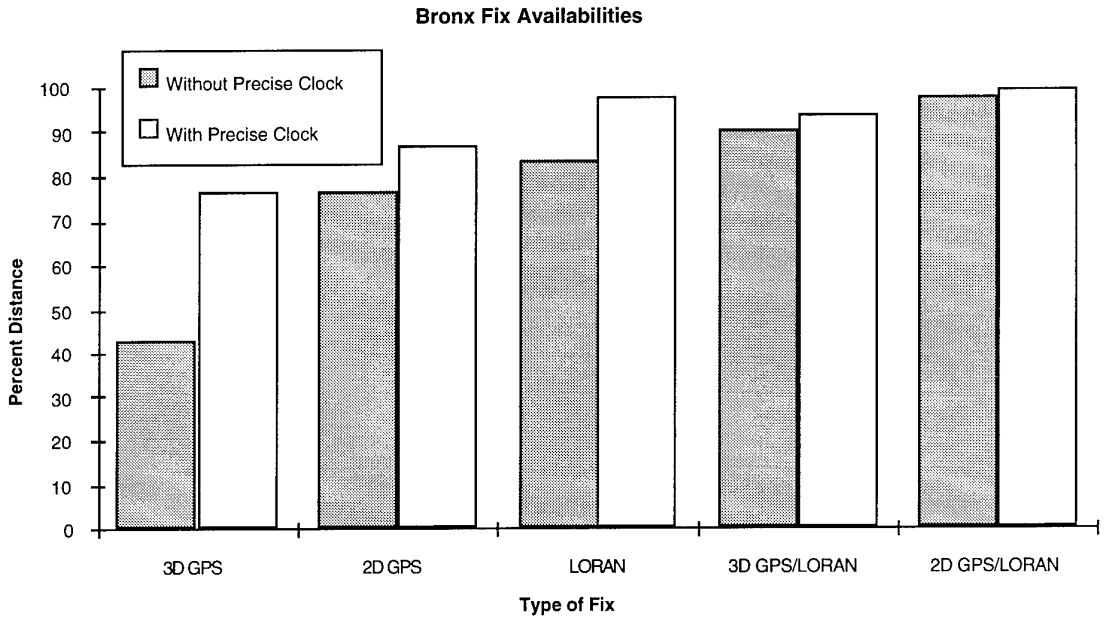

Figure 1. Radionavigation Fix Availabilities for Bronx Scenario

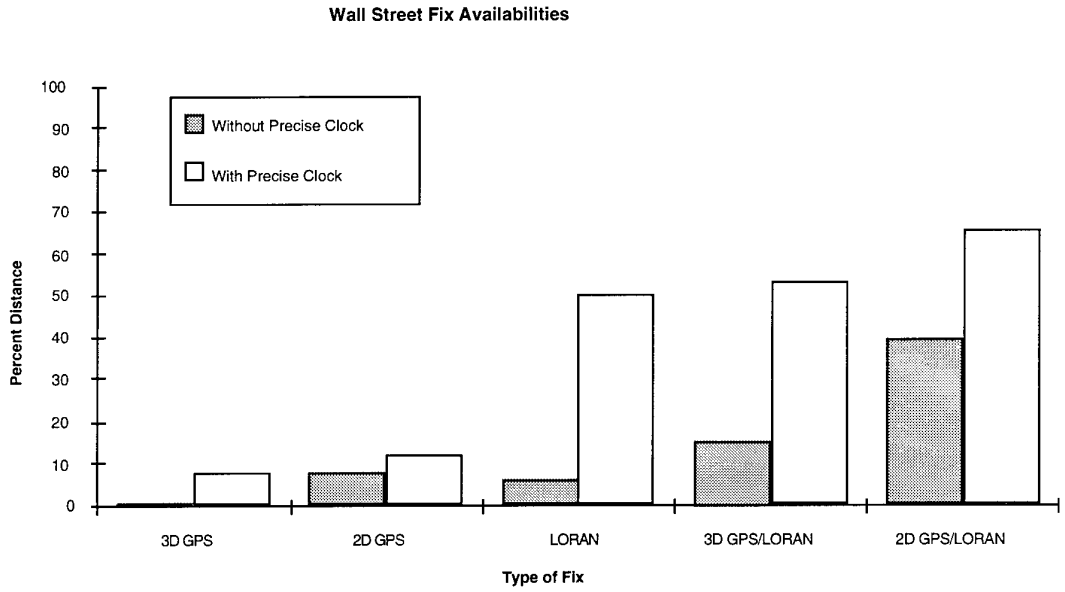

Figure 2. Radionavigation Fix Availabilities for Wall Street Scenario

Figure 2 shows fix availabilities for the harsher environment of Wall Street. Again the 12 channel GPS receiver and a PDOP of three were used. Also, the LOCUS availability is an E-field availability. Without a precise oscillator, GPS and LORAN fix availabilities are below 10% which means that while driving this scenario, one could expect to make a fix no more than 10% of the total driving distance if a precise oscillator input is not used with the receivers.

Recall that the HP89410 also collects LORAN data from E and H-field antennas. From the HP89410 data, an SNR was calculated for each LORAN station. This SNR was compared to a theoretical

SNR threshold that a typical LORAN receiver can track. The theoretical threshold was set to be -4 dB. If the HP89410 measured SNR was above this threshold, then the station was said to be trackable. This availability was calculated as a percentage of time not distance due to the data format. When this analysis is applied to the HP89410 data for Wall Street, Figure 3 shows the results. Notice that the E-field signal is less than 10% available as was expected from the LOCUS data in Figure 2. However, the H-field availability without a clock is over 50%, while the H-field availability is over 90% when a precise oscillator is used. There are two reasons the HP89410 E-field availability is not exactly the same as the LOCUS E-field availability shown in Figure 2. One reason is that our SNR threshold was conservative, that is the LOCUS receiver could track signals below the -4 dB threshold that was used for the HP89410 data. Also, Figure 3 shows the availability as a percent of time while Figure 2 calculates availability as a percent of distance.

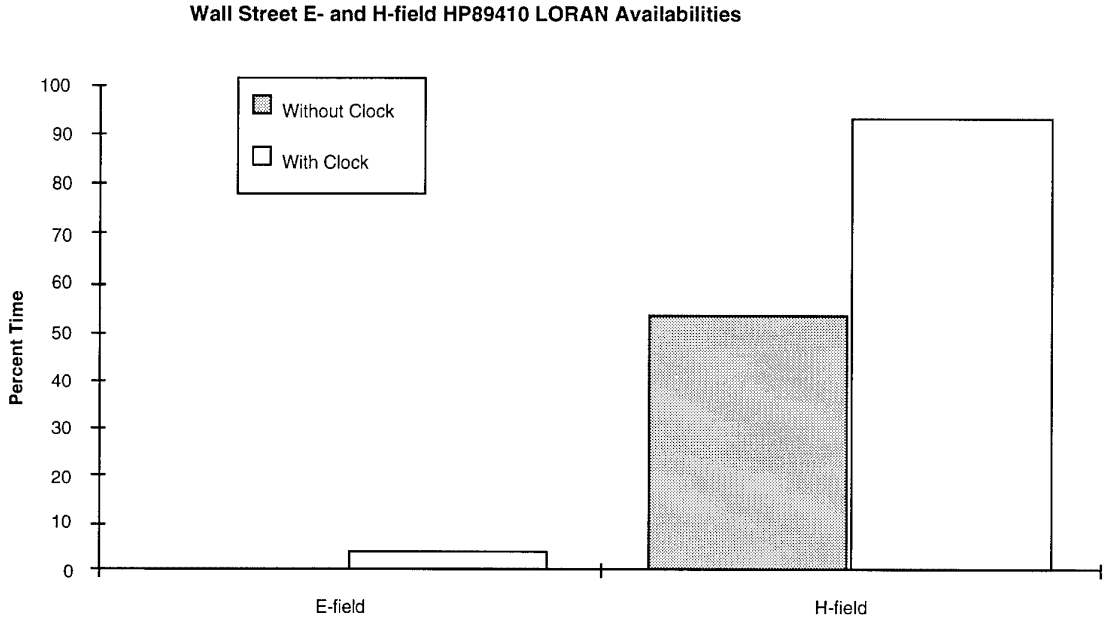

Figure 3. HP89410 LORAN Fix Availabilities for Wall Street Scenario

Now that the H-field LORAN signals have been shown to be trackable even in the harsh environment of Wall Street, the next question is how accurate and repeatable are those LORAN signals?

5.2 Inherent Repeatable Accuracy of LORAN

During one evening of the July-August tests, the experiment van was parked on Governor's Island in New York away from the urban environment and LOCUS LORAN data was collected overnight. From the latitude/longitude fixes generated by the LOCUS receiver, LORAN was calculated to have a 2DRMS (95%) repeatable accuracy of 7.25 meters (see Figure 4). This is consistent with data observed a decade ago in the U.S. Coast Guard R & D Center's Harbor Monitor Survey. Because the three LORAN stations in the 9960 MXY triad are almost equally spaced around the horizon, the PDOP is at the best possible value. Therefore, 7.25 meters is the absolute best repeatable accuracy of LORAN and cannot usually be achieved at other locations within a LORAN chain. So how repeatable is LORAN in the urban environment?

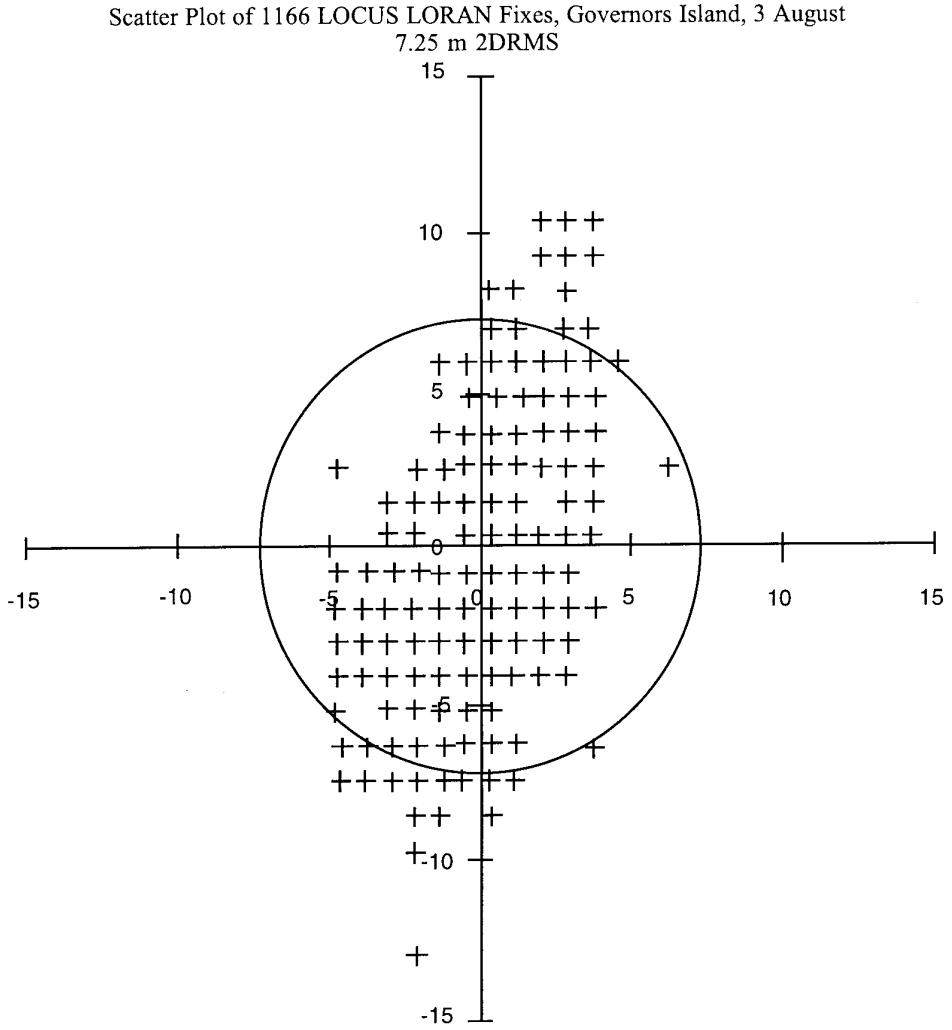

Figure 4. LORAN Fix Repeatability on Governor's Island

5.3 LORAN Phase Repeatability

Figure 5 shows the latitude/longitude fixes of ground truth, 12 channel GPS, and LOCUS LORAN for Run 4 of the Third Avenue scenario. The LOCUS fix was made using the 1 axis magnetic loop antenna. There is a bias offset of the LOCUS fix and the ground truth. It is believed that this bias is caused by the fact that the LOCUS receiver did not have an additional secondary factors (ASF) table. The ASF tables remove biasing in the LORAN signal due to changes in soil conductivity due to seasonal weather variations, day/night temperature variations, and local weather activity. Although the bias exists, it can be seen that the LORAN fixes do follow the ground truth and GPS fixes.

Figure 6 shows the same latitude/longitude fixes for run 2 of the Foliage scenario. Again, except for the bias, the LORAN fixes followed the ground truth and GPS fixes.

A LORAN receiver uses the phase information of the signals to make a fix. Therefore, to determine the repeatability of LORAN, the repeatability of the signal phases needed to be determined. Using the HP89410 LORAN phase data from the magnetic loop antenna, Figures 7 and 8 show the phase shifts relative to ground truth as a function of distance into the scenario for different LORAN stations. Theoretical phases were calculated from the ground truth data. These theoretical phases were compared to the HP89410 measured data and a phase shift was calculated. If there were no phase shift (measured phase equals theoretical phase), there would be a straight horizontal line at 0 microseconds.

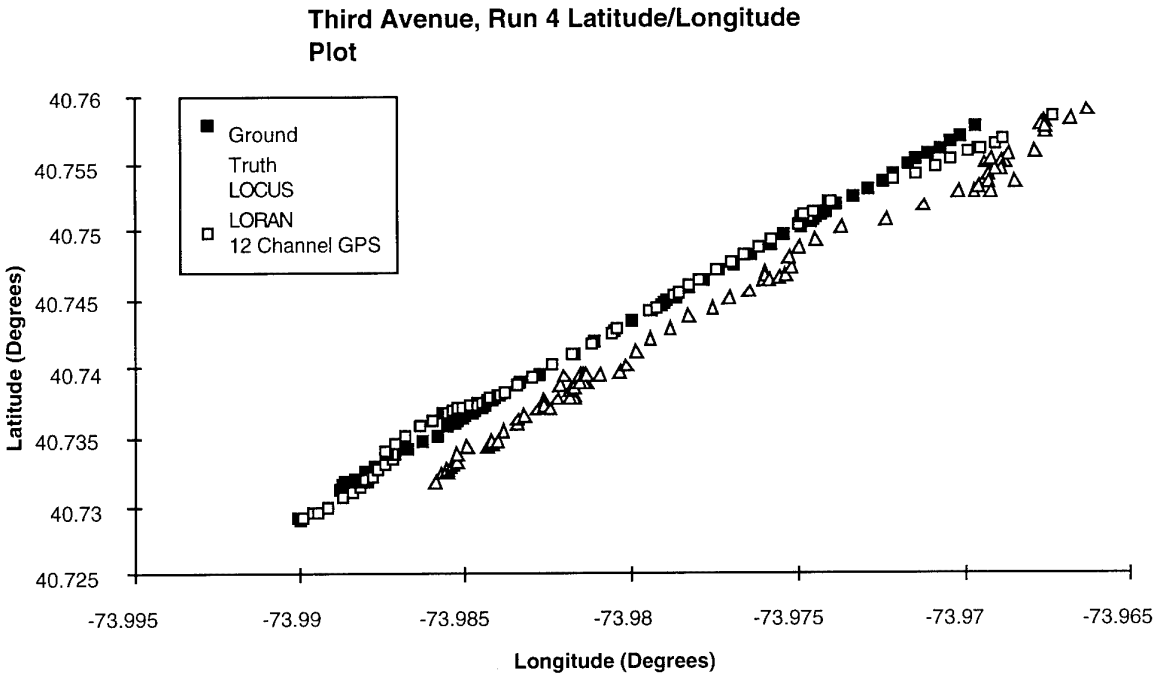

Figure 5. Third Avenue Latitude/Longitude Plot of Fixes

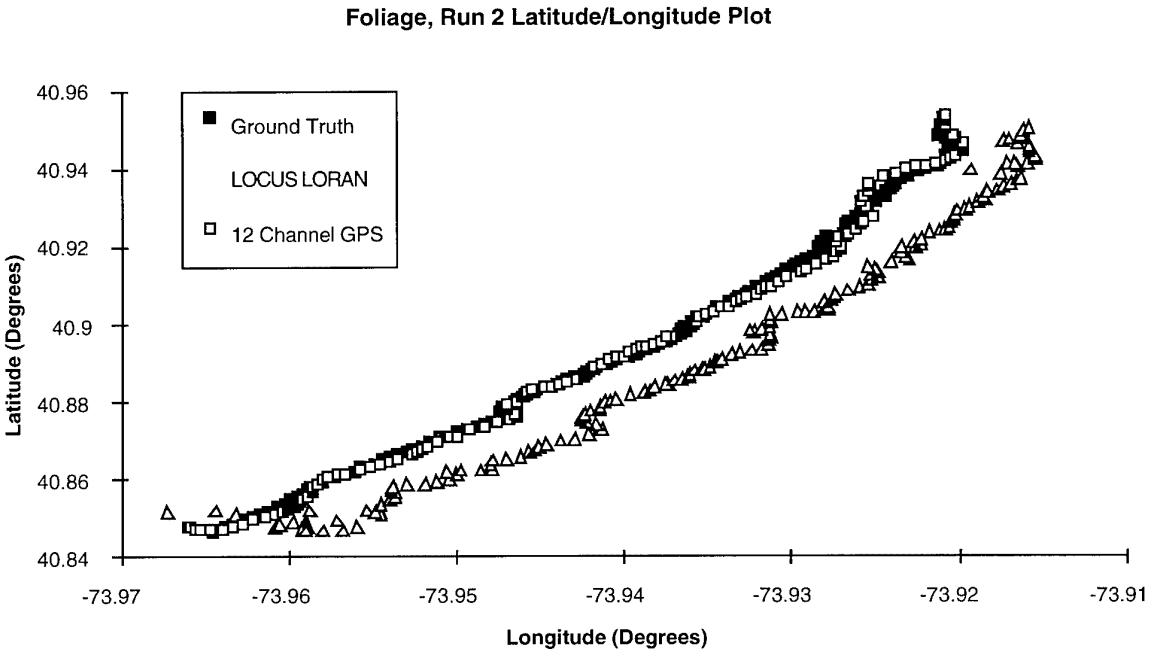

Figure 6. Foliage Latitude/Longitude Plot of Fixes

Figure 7 shows the Seneca LORAN station phase shifts in the Wall Street scenario for 9 of the Wall Street runs. From the graph, it can be seen that the phase shifts are very repeatable. The rms error for the Seneca phase shifts corresponded to about a 53 meter rms error. Figure 8 shows the phase shifts for the Nantucket LORAN station. There is a large phase shift at about 1500 and 2500 meters into the

scenario. For the Wall Street Scenario, a few streets were traversed more than once for a scenario run. At 1500 and 2500 meters into the scenario, the same point on the same street was being traveled. This large phase shift would throw the LORAN fix off by a few hundred meters. However, it is believed that the phase shifts always exists at this location.

Buildings in the urban environment cause phase shifts. If a one-time mapping of phase shifts could be made, this known phase shift could be subtracted out of the data and the LORAN fix would become more accurate. The mapping would only have to be done again if a new building were constructed or an old building demolished.

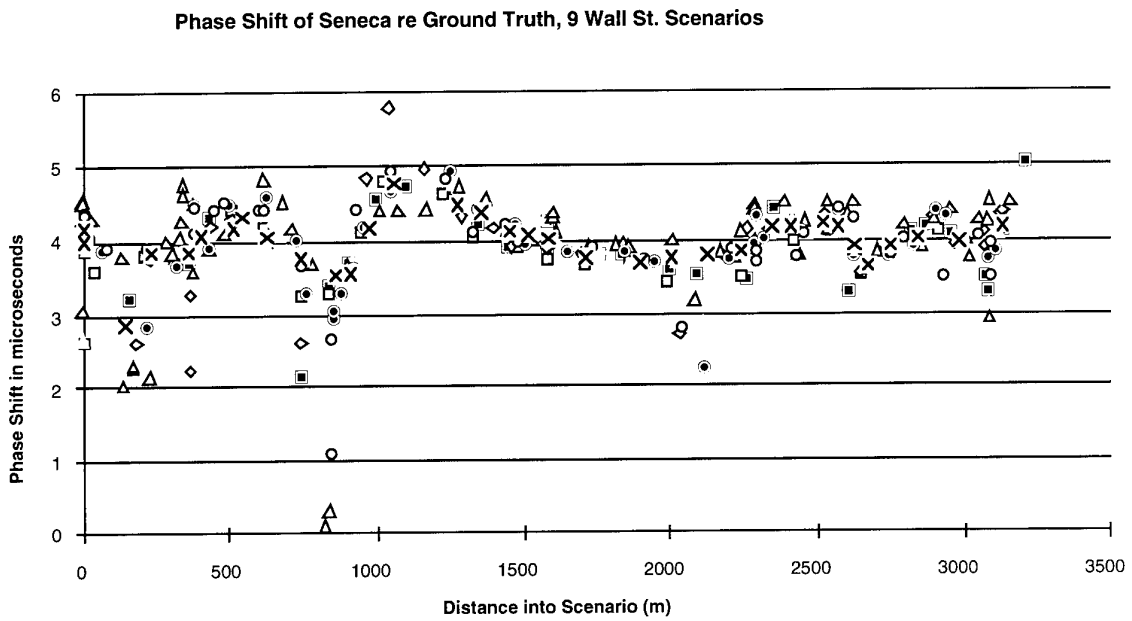

Figure 7. LORAN Phase Shift of Seneca Station for Wall Street

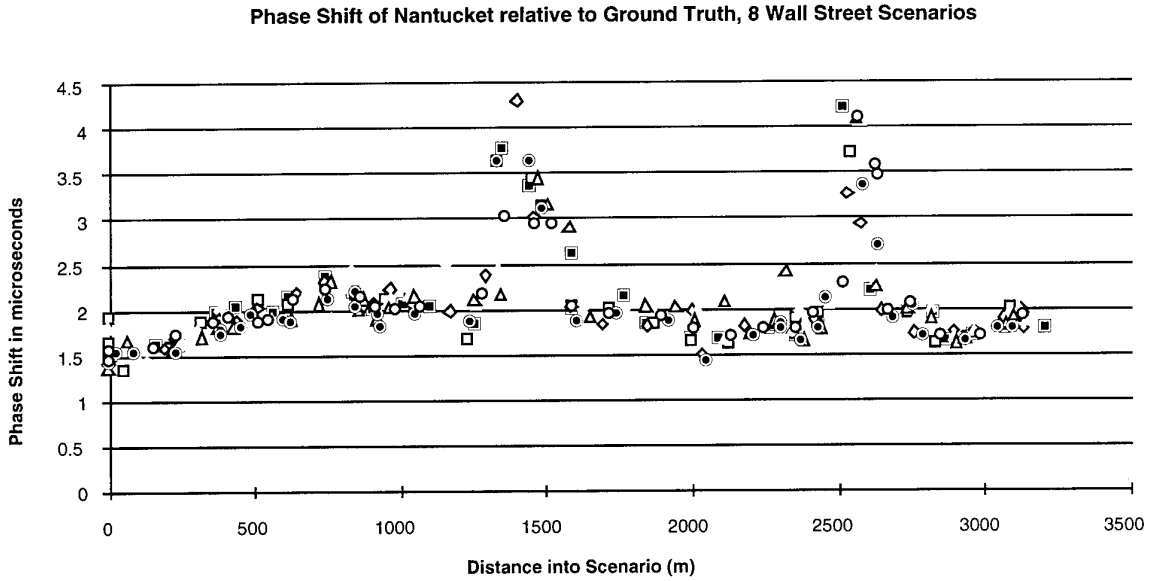

Figure 8. LORAN Phase Shift of Nantucket Station for Wall Street

5.4 Effect of Antenna Location

One geolocation application is vehicle tracking. Therefore, the location of the radionavigation antennas is important especially for covert vehicle tracking which requires the antennas to be hidden. The effect of covert antenna placement was measured in tests at the U.S. Coast Guard Academy.

The HP89410 was used to record the LORAN signal from a Navy omni-directional magnetic loop (H-field) antenna. The H-field antenna was chosen due to its success in the urban environment. The antenna was placed at various locations under the van. The signal strengths and noise strengths were recorded for each location. Also, a nominal value for the LORAN signals was measured with the antenna on the roof of the van (theoretically the optimum antenna placement). When the antenna was placed under the rear or middle of the van (away from the engine) the LORAN signal drop was found to be less than 1 dB compared to the roof value. However, as the antenna was moved closer to the engine, the noise increased enough to drown out the LORAN signals.

Two 12 channel Magnavox GPS receivers were used to collect GPS antenna location data. One antenna was located on the roof while the other antenna was placed at various locations under the van. Both receivers simultaneously recorded data for five minutes at each location.

From the data analysis, it was determined that with the antenna placed under the vehicle, regardless of location, satellites above 50 degrees elevation are masked by the vehicle. As a result, the data from New York City was re analyzed for several elevation masks. Figure 9 simulates the masking of the higher elevation satellites by re-calculating the availabilities of satellite signals in the Bronx scenario for elevation masks of 90, 70, 50, and 30 degrees. An elevation mask of 90 degrees corresponds to no elevation mask at all. Typically when discussing GPS, an elevation mask eliminates satellites below a certain elevation rather than above an elevation as is meant here. Therefore, Figure 9 is called an inverse elevation mask plot to keep the two types separate. It should be noted that these availabilities are as a percent of total scenario time rather than distance like the previous GPS availabilities. Also, no PDOP is taken into account in computing these availabilities. The abscissa of the graph is number of satellites tracked. Four satellites are needed to make a 3-D GPS fix without a precise oscillator. Therefore, with no inverse elevation mask, a 3-D GPS fix could be made about 80% of the time in the Bronx scenario. As the inverse elevation mask increases to 50 degrees (blocking out satellites above 50 degrees), the 3-D GPS availability decreases to less than 50%. The conclusion is that a GPS antenna needs to be hidden somewhere other than under a vehicle.

Figure 10 shows the same type of analysis for the Foliage scenario.

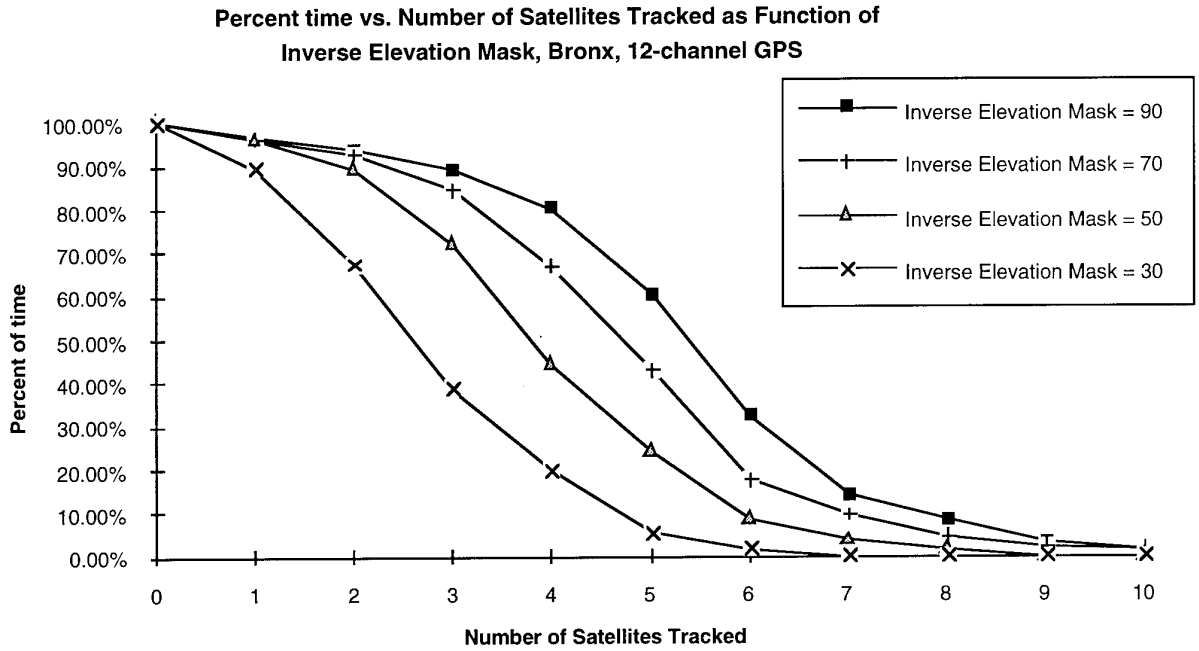

Figure 9. Bronx Scenario 12 Channel GPS Satellite Availability as a Function of Inverse Elevation Mask (in degrees)

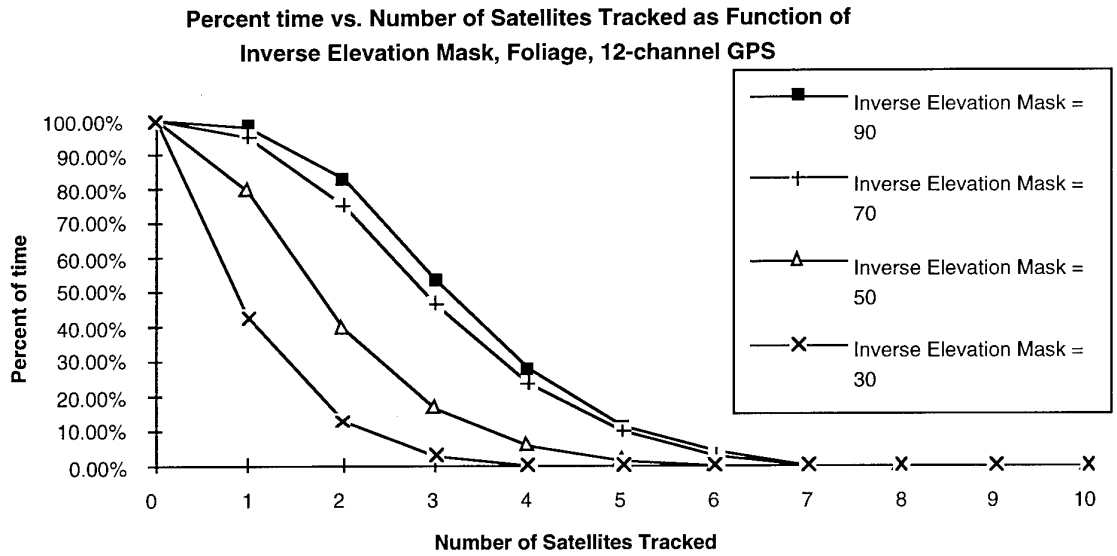

Figure 10. Foliage Scenario 12 Channel GPS Satellite Availability as a Function of Inverse Elevation Mask (in degrees)

6. REFERENCES

1. Peterson, Benjamin B. and Miller, Lance C., "Evaluation of Radionavigation Systems in an Urban Environment, Final Report", CAS Report No. 14-94, USCG Academy Center for Advanced Studies December, 1994. Submitted to NTIS.

2. "LORAN-C User Handbook", COMDTPUB P16562.5, U.S. Department of Transportation, 1992.

3. Blizard, M. M., Slagle, D.C., and Hornburg, K.P., "Harbor Monitor System: Final Report,", USCG R & D Center Report No. CG-D-17-87, NTIS ADA 183 477.

7. ACKNOWLEDGMENTS

Participants in this experiment included:

Captain Benjamin Peterson, USCGA
Dr. Mike McKaughan, USCGA
Steve Bartlett, North Carolina State University
Lance C. Miller, SAIC
Integrated Systems Research Corp. of Englewood Cliffs, NJ USA
LOCUS, Inc. of Madison, WI USA
Megapulse, Inc. of Bedford, MA USA

Also, without the generous support of the Ferryboat Maintenance Facility at the Coast Guard Base on Governors Island, completion of this effort would have been impossible.

Susceptibility Measurements on GPS Receivers

Ch. Braun
P. Guidi
H.U. Schmidt
Fraunhofer Gesellschaft INT
Appelsgarten 2
D-53881 Euskirchen
Germany

1. SUMMARY

This paper describes our low power microwave coupling measurements on hand-held GPS (Global Positioning System) receivers in the frequency range between 0.3 ... 2 GHz. The *plane wave excitation* experiments have been carried out mainly in our field coupling facility, which consists of an asymmetric triplate transmission line with maximum CW field levels of up to 120 V/m at the test position.

As test objects we examined four Standard Positioning Service (SPS) C/A-code GPS receivers of different manufacturers. The test objects were positioned in the simulator in three orthogonal orientations with respect to the external field. To maintain a high-integrity navigation, the GPS receiver must maintain lock on the satellite signal and read the data. A three dimensional position (latitude, longitude and altitude) at least requires four satellites to be in view. Failure is defined when this 3 D fix is lost.

It turned out that the GPS were most susceptible to CW fields with its internal antenna. They were less susceptible if the receiver and the GPS antenna were placed separately and linked together via a cable. Worst case effects caused GPS switch off, but no damage occurred at field strengths below 100 V/m at out-of-band frequencies. Pulse testing (width = 20 µs) the GPS always required much higher fields to cause upsets depending strongly on frequency and test object. In some cases pulsed fields of more than 2 kV/m were necessary.

2. INTRODUCTION

In recent years GPS technology is more and more used as an aid for precision positioning. Last year the US Federal Aviation Administration (FAA) has told commercial airlines that they can use GPS for navigation. GPS-based systems appear attractive as a replacement for the current Instrumentation and Microwave Landing Systems. The first widely used application of GPS for the military was the hand-held GPS receiver. Commercial markets are segmented into marine, aviation, systems integration, vehicle tracking/navigation, etc.

To evaluate the vulnerability of GPS receivers and the equipment's resistance to in-band and out-of-band interference, first investigations were started by the INT. But before reporting about our investigations, how does GPS work actually?

GPS, also known as NAVSTAR, is owned and operated by the US Department of Defense (DOD). It is a constellation of 24 satellites in six orbit lanes (four satellites per lane) in approximately 20,000 km orbits. Each satellite transmits a signal with special coding unique to that satellite. This code does allow any GPS receiver to identify the particular satellite and provide a precise time mark that will be used to determine the range to the satellite from the receiver location. It also allows each satellite to transmit on exactly the same two frequencies in L-band, 1575.42 MHz (L1) and 1227.6 MHz (L2).

Only L1 is available for civil use (encoded with the spread-spectrum C/A, or 'clear acquisition', code as well as the 'precise' or P code which is restricted to US military use). L2 contains only the P code. The signal accuracy of the C/A code is deliberately degraded by the application of a "dither", limiting its lateral resolution to 100 m in order to keep the system from being used as potential guidance for enemy missiles.

As mentioned earlier a 3 D fix requires four satellites to be in view. The receiver must be able to compute exactly the location of each of the satellites. This is done in a couple of ways. First, a general Almanac is transmitted continuously that gives the approximate location of each satellite. This transmission requires at least 12 minutes, but the data is usable for up to six month. It only provides an approximate location for each satellite so the receiver knows where to begin to look. Information that pinpoints the exact location of the satellite is transmitted about every 30 seconds. This data is referred to as the ephemeris data.

3. INT FIELD COUPLING FACILITY

All measurements reported in this paper were done with our field simulator. It was built in 1984 and served at first as a tool to carry out scale model measurements [1,2]. Since then the equipment was permanently improved and is currently used mainly for real size test objects [3].

3.1 TEM wave guide

We use an open tapered TEM cell. To enlarge the test volume, the septum was not placed in the middle, but at approximately 3/4 of the height of the cell. The design is illustrated in *Fig.3.1.1*. The simulator consists of a

- *source* (coaxial input)
- *launcher* which provides a transition from the circular coaxial output of the source to the asymmetric rectangular triplate geometry of the line
- long *pyramidal shaped section* of transmission line maintaining the width-to-plate separation ratio to provide a constant impedance (50 Ω) along the length of the line while gradually changing the cross-sectional dimension. This section is the actual simulator and includes the *test volume*.

Paper presented at the AGARD SPP Symposium on "Environmental Factors in Electronic Warfare Related to Aerospace Systems" held in Pratica di Mare AFB (Rome) Italy, from 8-11 May 1995, and published in CP-573.

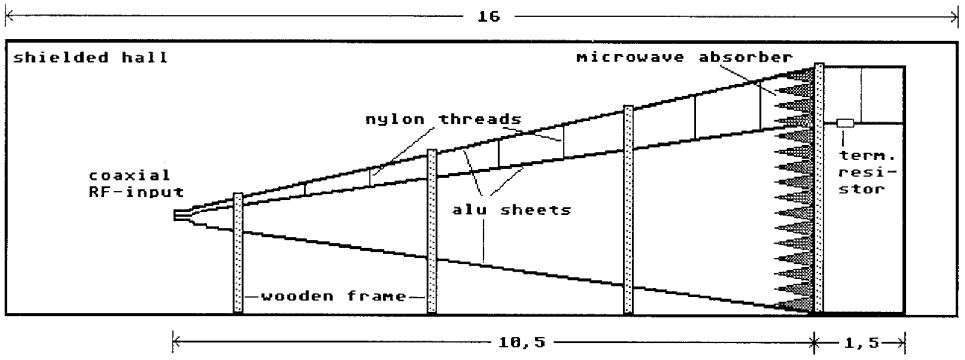

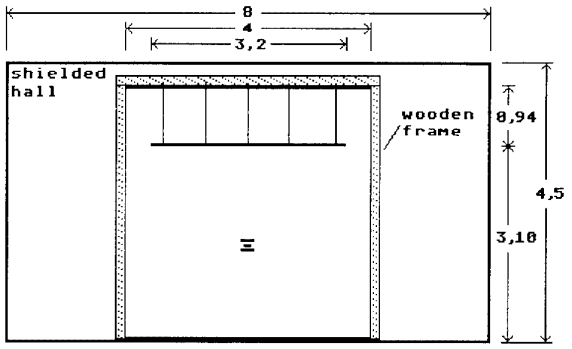

Fig.3.1.1: Side view and cross section of the TEM wave guide of the INT (units in m)

At low frequencies, a *resistor network* in series with the center conductor and equal to the characteristic impedance of the transmission line provides a matched termination for energy propagating on the line. At high frequencies, a wall of e.m. energy *absorbing material* placed across the output end of the line provides a non-reflecting termination.

The figure also shows that the maximum working volume cross section is about 3 x 2.5 m^2. Nearly the whole area under the center conductor can be used as test volume: the smaller section at the beginning for small DUTs like GPS receivers or for the calibration of field probes and the middle and the end section for larger test objects.

3.2 Measurement set-up for CW testing

The principal measurement set-up to get transfer functions of test objects is shown in *Fig.3.2.1*. The test objects can be illuminated by CW-fields in the frequency range between 100 kHz and 8 GHz. Digital tuneable sweep generators followed by power amplifiers are used to produce maximum field levels of approximately 40 V/m in the main working volume. In the front part of the simulator this leads to about 200 V/m at low frequencies.

As receiver we use two different vector network analyzers. All devices are controlled and read out via IEC-Bus by a desktop computer (HP9000). Data recording and processing are also performed with this computer or can be done by a DEC computer (VAX).

More power is needed to cause equipment malfunction or upset. Normally we use a similar measurement set-up for such tests. But in the case of the GPS receivers this arrangement did not work. It turned out, that because of the amplifier noise the GPS receivers were blocked, so they were not able to lock to the satellites data. At the outdoor measurements it was possible to increase the distance between the interference field antenna and the test objects to reduce this influence, but for the wave guide we had to replace the generator and the amplifiers by a Power Signal Source. Unfortunately the use of this source (AIL, Type 125) was awkward and time consuming. The maximum power output between 0.3 ... 1 GHz is 80 W and about 25 W between 1 ... 2 GHz.

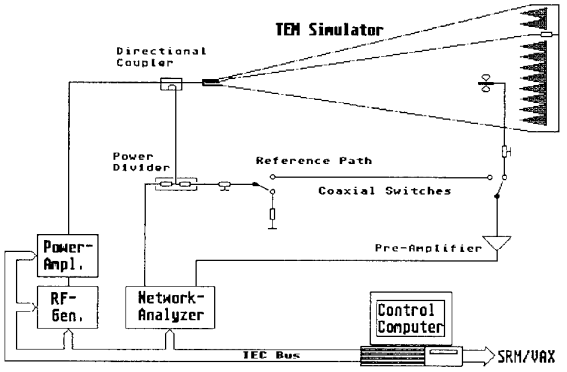

Fig.3.2.1: Principal measurement set-up to get transfer functions

The new measurement set-up is shown in *Fig 3.2.2*. By watching for upset and reading the displays of the power meter and the field strength meter close to the DUT at the moment of upset, it was possible to determine the power level and the field strength which caused the upset. The display of the GPS receiver was monitored by a video camera.

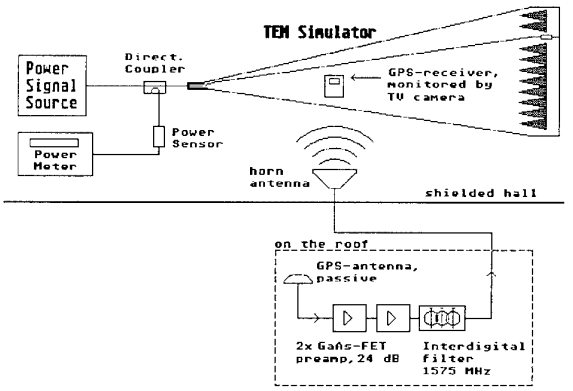

Fig.3.2.2: Principal CW measurement set-up for the GPS susceptibility tests

As the TEM wave guide is located within a shielded hall, the GPS are not able to receive any data. So we had to install a GPS antenna on the roof of our building. After pre amplifying the weak satellite signal it is transmitted inside the hall by a portable horn antenna (see also Fig.3.2.2). A further advantage of this arrangement is the possibility of positioning the DUT in each wanted direction to the interfering field without loosing the lock to the satellite signal.

3.3 Measurement set-up for pulse testing

Besides the CW experiments we also conducted pulse tests (*Fig.3.3.1*) with considerable higher power levels. As source we used the High Power Pulsed Signal Source, Model PH40KB from the LUCAS-EPSCO company, whose features are summarized in the following:

P_{max} = 35 kW
pulse width: 0.4 - 6 µs (P_{max}) and 0.4 - 25 µs (P_{red})
pulse frequency: 10 Hz - 10 kHz
t(rise) = 100 ns; t(fall) = 200 ns
plug-ins: [450 - 700 MHz (15 kW)]
[700 - 850 MHz (35 kW)]
800 - 1000 MHz (35 kW)
1000 - 1200 MHz (35 kW).

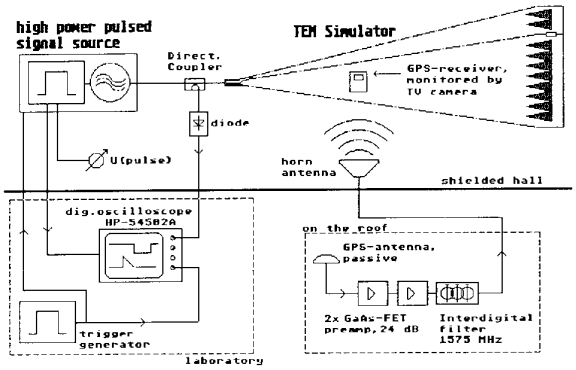

Fig.3.3.1: Principal pulse measurement set-up for the GPS susceptibility tests

As indicated the frequency range between 450 - 850 MHz is soon available to us, furthermore we intend to extend the range above 1200 MHz up to higher frequencies. An output power of 35 kW at the 50 Ω input of the TEM simulator means 1300 V at the input jack and an electric field of approximately 1300 V/m in the wave guide at a plate separation of 1 m.

A further pulse source from NARDA (Model 18500B) has the following characteristics:

P_{max} = 4 kW
pulse width: 0.25 - 6 µs
pulse frequency: 150 Hz - 4 kHz
t(rise) = 100 ns; t(fall) = 150 ns
plug-in: 2350 - 2700 MHz.

For this equipment only the indicated plug-in is available. A power level of 4 kW means a field of at least 450 V/m at the same location as before.

4. SUSCEPTIBILITY MEASUREMENTS

4.1 General

Because of the importance of GPS technology and its widespread application in civil and military areas we have decided to evaluate the vulnerability of GPS receivers. It was decided as well to investigate commercially available devices, as they were easily obtainable. The results of the following measurements are transferable only for commercial GPS receivers, because there is a general difference between military and civil GPS systems, with the military systems having some interface circuit in between the antenna and the receiver to endeavour to counter jamming. In the following the first trials undertaken on four hand held GPS receivers are described.

4.2 Test objects

We have selected four different hand helds, whose most important features are summarized in *table 1*. On DUT 1 more information can not be given in this report because it was measured in another project. Besides the GARMIN GPS 75 with its rod-shaped antenna all other candidates use flat disc or rectangular-shaped antennas (*Fig.4.2.1*). In addition to the external, detachable antennas the DUT 1 and the TRIMBLE Scout both have internal antennas. While the GARMIN has a positive locking antenna connector, the DUT 1 and TRIMBLE have simple push-in connectors. The SONY Pyxis IPS 360 antenna attaches to the GPS receiver with a screw-knob.

Table 1: Features of the tested GPS receivers

Characteristics:	DUT1	GARMIN GPS 75	SONY IPS 360	TRIMBLE Scout
Channels	6	8	4	3
Int. Ant.	flat	x	x	flat
Ext. Ant.	flat	rod (det.)	disc (det.)	flat
Display	dot matrix	dot matrix	2x40 (l•c)	4x16 (l•c)
Sat. status	bars	bars	small bars	small bars
Update (s)	1	1	2	1.5
Cold start		15 min	30 min	12.5 min
Batteries	AA	4 x AA	4 x AA	4 x AA
EMI	x	x	x	FCC P.15
Dim.(mm)		82/159/37	99/175/39	84/173/33
Weight (g)		540	590	400

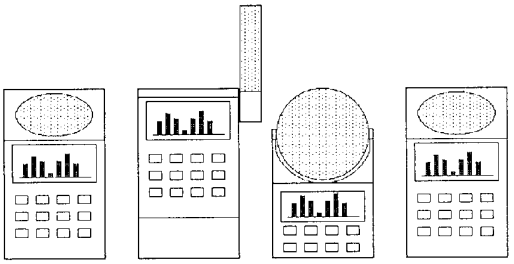

Fig.4.2.1: Schematic drawings of the tested GPS receivers (not to scale)

As shown in the drawings all receivers have nearly the same functional arrangement with the antenna at the upper part, the display in the middle and the keyboard at the lower part, where also the batteries are installed. Only the TRIMBLE tactical receiver, which is recommended also for military operations, has passed an EMI test (FCC Part 15). All devices

are powered with 'AA' batteries and have similar dimensions and weights.

The first time a GPS is turned on after a long period of disuse or having been shipped, it has to find a satellite and download the almanac that lets it know the time and date and where it should expect to find other satellites. It then begins searching for the satellites that should be visible to it and as it locks on to them it begins to calculate its position. This 'cold start' initialization typically takes between 15 and 30 minutes depending on the type of the receiver.

The GPS receivers display current location, which is constantly updated at selected intervalls (1 - 2 sec). The location is expressed in latitude and longitude, the commonly used units are degrees, minutes and seconds. A change in 1 minute corresponds to a distance of a nautical mile, whereas a change in 1 second corresponds to approximately only 31 m.

4.3 Set-up and measurements

During the trials the GPS function was monitored via the TV camera. Because we are only interested in observing an upset the GPS receiver have been switched into a 'satellite status' mode. In this mode the display shows information about satellite signals being received from the GPS satellites. Information shown on the screen for the most part includes:
- number of satellite signals currently being received
- number of the satellite transmitting each received signal
- relative strength of each received signal in the form of bars
- whether or not the receiver is able to calculate 3 D position.

The example in *Fig.4.3.1* shows the dot matrix screen of the GARMIN receiver. It is easy to read in contrast to the very short 'bars' of the TRIMBLE and SONY GPS. It was not often that the constellation of satellites were in such favourable orientations the GPS could receive more than about five for most of the time.

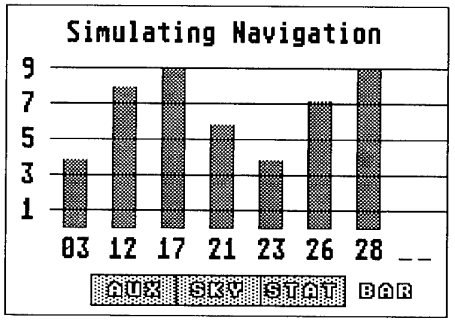

Fig.4.3.1: Typical satellite status screen of the tested GARMIN receiver

The test objects were placed on a podium of styrodur foam between the plates of our TEM wave guide at a plate separation of 0.5 m. Because of the moveable horn antenna transmitting the satellites signals it was nearly almost possible to get optimum reception.

With the GPS running the interference field was applied in increasing strength until upset was noted. The usual form of this was satellite signal strength reduction as the disturbing field was increased above a certain level and then by further increasing this level the loss of satellites signals. At this point or when the GPS indicated, that it has switched to 'No Fix' the field strength was noted. At this field strength the system was prevented from operation. This was considered as threshold. This procedure was repeated for each of the test frequencies.

As mentioned earlier the measurements in the field simulator were performed in the frequency range between 0.3 ... 2 GHz. Depending on the power signal source we got two ranges with different power levels. Between 0.3 - 1 GHz (80 W) and 1 - 2 GHz (25 W) usually the frequency was gradually increased by 50 MHz with the exception between 1.5 - 1.6 GHz, where we selected more frequencies. We are also watching the response of the GPS at L2 (1.228 GHz)

During the measurements it turned out that the response times of the various GPS to the interference fields differ. Sometimes the bars disappeared immediately at the threshold and sometimes the indicated field strength gradually decreased down to zero. To get comparable results for the receivers with these longer response times the devices were illuminated up to approximately 10 seconds.

The next two pictures (*Fig.4.3.2 and 4.3.3*) show the maximum available field strengths at the place of the test objects that can be generated with the signal source. The circles indicate the measurement frequencies. In the lower frequency range the average value is approximately 111 V/m, between 1 - 2 GHz it reaches because of the lower output power only an average of 58 V/m.

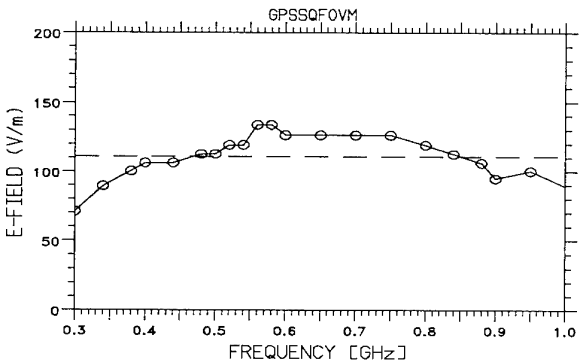

Fig.4.3.2: Maximum field strength at the test objects between 0.3 - 1 GHz (max. output power 80 W)

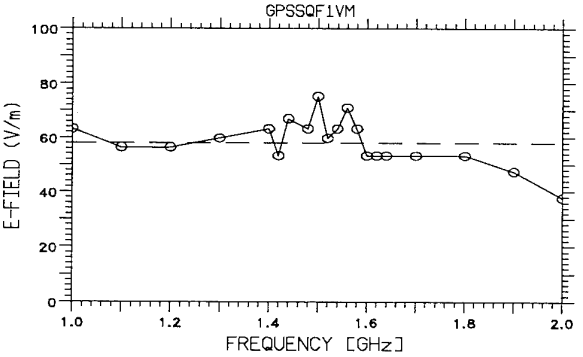

Fig.4.3.3: Maximum field strength at the test objects between 1 - 2 GHz (max. output power 25 W)

A series of tests on the four systems was performed to evaluate typical GPS receiver susceptibility to these interfer-

ence fields. First the test objects were illuminated at three different orientations to the simulator field (*Fig.4.3.4*):
- GPS horizontal (H): E-field perpendicular to the antenna surface and internal circuitry
- GPS crosswise (Q): E-field parallel to antenna surface and short end of the case
- GPS vertical (V): E-field parallel to antenna surface and long side of the case.

At each of these orientations the test objects in general were investigated in at least three different positions. In orientation H the devices were illuminated at the top (H-t), the bottom (H-b) and at the right side (H-s). In the Q orientation the field incidence was on the top, the front side (Q-f) and the rear side (Q-r); with the long side up the right side, the front and rear side were illuminated.

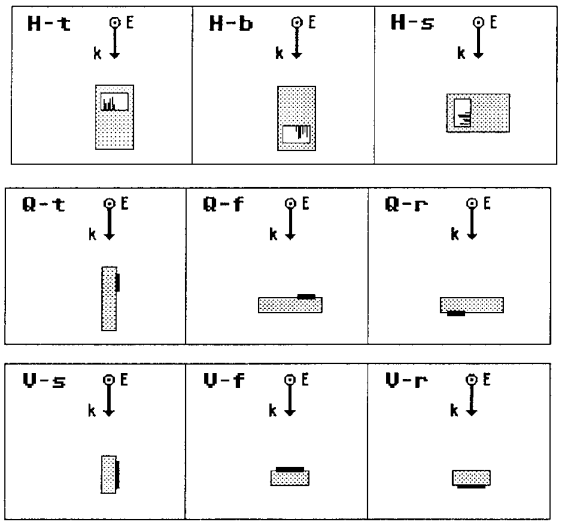

Fig.4.3.4: Different orientations (H,Q,V) and positions of the test objects to the incident interference field

These tests were useful to find out the most susceptible positions for upset. Furthermore they should indicate whether the upset is caused by the internal/attached antenna or the circuitry.

To further separate the influence of the receiving antenna and the receiver circuitry the attached antennas were removed and again connected to the receiver via a long (6 m) coaxial cable. To the systems with internal antenna a supplementary external antenna was connected which automatically switched off the internal antenna. After doing that either the receiver or the antenna was separately illuminated. In this way we are able to differentiate between the influence of 'back door' and 'front door' coupling. These tests were conducted with the external antenna placed either between the two simulator plates or mounted on the ground plane.

It should be noted that the satellite formation is asynchronous. This means that their positions, relative to a given position on earth, are not time constant, so satellites come into and fade from view. They do not even have the same configuration at the same times each day. Therefore it is also useful to ascertain whether the interference signal strength required to swamp the satellite signals would differ with variations of the received satellite signal strength.

5. CW RESULTS

5.1 General

Because of the changeable weather conditions in Germany we prefer the CW measurements in the field simulator in the shielded hall. The results in this report basically refer to these experiments. But to complete the investigations also the results from the outdoor measurements have been taken into account. Especially the experiments with the external GPS antenna and the tests in the higher frequency region between 2 - 4 GHz were performed until now only with our outdoor measurement set-up. Tests show that in principle good agreement exists between the results of these two methods. Because of the various measurements in the simulator between 0.3 - 2 GHz and the great number of disturbances in this frequency range in the following the main emphasis is put on these investigations.

The first measurements indicated that the interference field strength required to swamp the satellite signals did not differ much with the variations of the received satellite signal strengths. But since the number of the received satellites, the type number of the satellites and the satellites' signal strengths changed during the measurement on a test object, the reproducibility of the results could not be very high. Often the variation of the threshold power level was ± 3 dB, corresponding to a field strength variation at the test objects of approximately ± 35 %.

Furthermore the different response times of the GPS to the interference field aggravated the comparability of the measurement results. At some devices the bars indicating the satellites' field strength disappeared immediately at the threshold, at other GPS receivers the field strength gradually decreases down to zero.

The maximum interference field strengths were shown in Fig.4.3.2 and 4.3.3. The smallest output power level of the power signal source is 10 dBm, corresponding to a minimum field strength of 1.4 V/m at the test object in the simulator. Below this power level the signal source doesn't work. For this reason the lowest threshold we are able to get with our set-up was 1.4 V/m. Because of the limited power of the source the results given in this report only provide an incomplete threshold curve. In general the results only indicate the frequency range the GPS are most susceptible.

In the following curves the circles mark the measurement frequencies, the connecting lines only serve to clarify the curvature. The filled circles refer to the power levels and frequencies causing GPS upset, whereas the shaded circles characterize special effects occurring at the receiver. These effects did not unavoidably lead to an upset. Each curvature can be divided into three areas:
- field strengths below curve: no upset
- field strengths above filled circles (threshold): upset
- empty circles indicate highest available field strength at the GPS causing no upset; higher fields can lead to failures.

5.2 Most susceptible orientation

All devices were illuminated in the orientations shown in Fig.4.3.4. First the tests with the internal or attached GPS antenna were performed. All results show that the most susceptible arrangement was the V orientation with the E-field

parallel to the long side of the GPS receiver. As an example *Fig 5.2.1* shows the threshold values of the GARMIN at V-f and Q-f (with the short end parallel to the E-field). In both cases the GPS was illuminated at the front side.

The two curves clearly show five small regions in the V-f position where the GPS failed and only two upset regions in the Q-f position. Thresholds in the lower frequency range are about 50 V/m and below 20 V/m at the higher frequencies. To disturb the GARMIN at 520 MHz only 3 V/m are necessary, around the L1 frequency the threshold is below 1.5 V/m. The curves show clearly that the V orientation is the most susceptible arrangement.

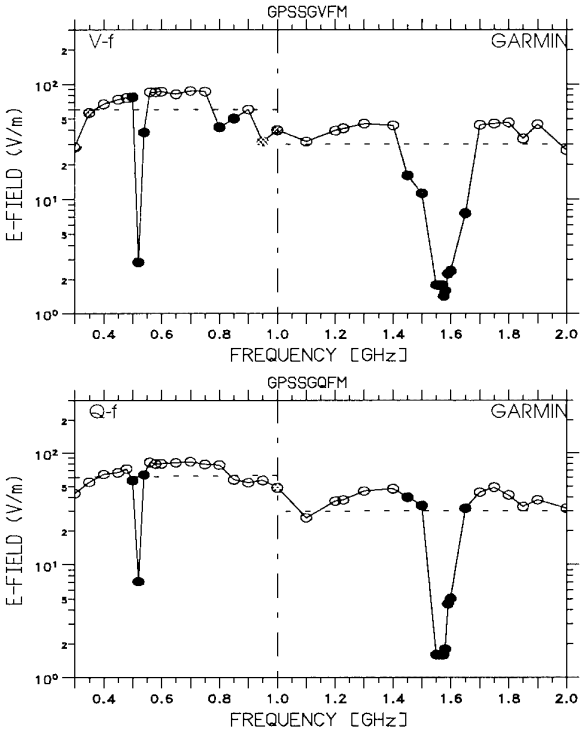

Fig.5.2.1: Threshold curves of the GARMIN in the V-f and Q-f position

Below 1 GHz in both positions special effects occurred at the GPS (shaded circles). In V-f the first two effects around 350 MHz switched off the receiver whereas the two effects near 1 GHz prevent the GARMIN to receive satellite signals. In Q-f the disturbance at 1 GHz caused the GARMIN to beep and degraded the display's contrast. Further effects are described later. The other positions in the Q and H orientation are less susceptible at all test objects.

The failures of the four GPS within the same orientation but with different positions (side, front, rear, etc.) to the interfering field show similar behaviour. For the GARMIN it can be seen in *Fig.5.2.2*, that at rear illumination upsets usually occurred at slightly lower field strengths than at front illumination. The other test objects also show few differences between these two positions.

With these results one can draw the conclusion that front illumination of the GPS receiver and therefore of the internal/attached GPS antenna doesn't increase fundamentally the upset rate. The cause for the disturbances is to be seen in the circuitry of the receiver and not in the antenna. It is therefore also obvious that the V orientation is the most susceptible arrangement, because in this case the E-field is parallel to the long side of the internal circuitry and therefore maximum coupling can occur.

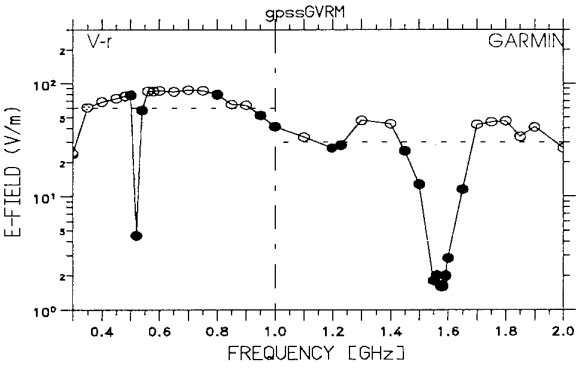

Fig.5.2.2: Threshold curve of the GARMIN in the V-r position

5.3 Critical frequencies

Nearly all of the GARMIN threshold curves show failures occurring between 520 - 560 MHz and 1.45 - 1.65 GHz. The same is true for the TRIMBLE. At the DUT1 the lower upset range is between 500 - 650 MHz. The SONY frequently failed between 450 - 1000 MHz and is therefore the most susceptible test object.

To track down all the disturbing frequencies the selected frequency steps of 50 and 20 MHz are to coarse. Nevertheless it turned out that some of the chosen frequencies are more susceptible than others, mainly in the V orientation. These frequencies are at all devices generally around 250, 300, 750 MHz and at the SONY also around 900 MHz. Naturally, in the higher frequency region the most susceptible point is always at 1.575 GHz (L1). The GARMIN is also susceptible around 1.2 GHz (see Fig.5.2.2). Besides the DUT1 all other GPS show at the L1 frequency thresholds below the earlier mentioned lower measurement sensitivity limit of 1.4 V/m.

To examine the susceptibility of the test objects at harmonic components of the L1 frequency the GARMIN and TRIMBLE were illuminated in some positions with the three additional frequencies 394 MHz (L1/4), 525 MHz (L1/3) and 788 MHz (L1/2). At these measurements between the source and the simulator a low pass filter with a cut off frequency of 500 MHz was inserted to prevent higher frequencies reaching the wave guide. The results in *Fig.5.3.1* for the GARMIN in V-s position show that at all sub harmonic components maximum susceptibility occurred.

5.4 Special effects

Usually an upset is indicated when the satellites are lost and therefore no position fix is possible. Additionally at certain frequencies between 300 - 1000 MHz some special effects occurred at all GPS receivers besides the SONY. These interference effects arising always in the V orientations and sometimes also in the Q arrangements are manifested by weak effects like contrast reduction of the display, appearance of square patterns on the display, "low battery voltage" message and other wrong messages. The worst effects are independent switching to other modes and switch off. In some cases the

effects disappeared after reducing the interference fields but sometimes the wanted mode can be attained only by reset or switch off/switch on the GPS.

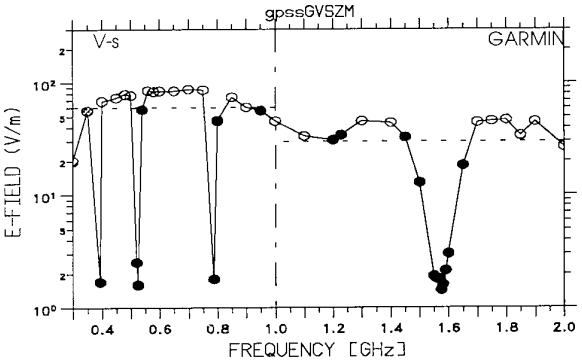

Fig.5.3.1: Threshold curve of the GARMIN in the V-s position with sub harmonic components below 1 GHz

These interference effects occurred at the GARMIN between 300 - 350 and 950 - 1000 MHz, at the TRIMBLE between 400 - 450 and 580 - 850 MHz. Unlike the GARMIN these effects did not always cause upsets at the TRIMBLE but only weaker effects like contrast reduction of the display. In *Fig.5.4.1* these two kinds of effects are depicted. The DUT1 showed these effects causing upsets usually between 250 - 500 and 540 - 700 MHz. Only the SONY did not show any special effects.

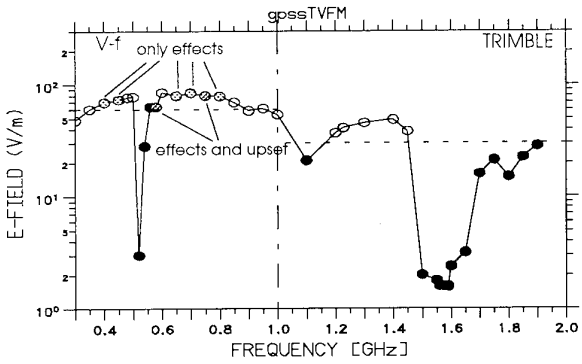

Fig.5.4.1: Threshold curve of the TRIMBLE in the V-f position with various effects

5.5 Influence of the GPS antenna

Until now all measurements have been carried out with the internal/attached GPS antenna. Now the changes were investigated caused by connecting an external or the attached antenna with the receiver through a 7 m long coaxial cable. After doing that either the receiver or the antenna was illuminated alone.

5.5.1 Illumination of the GPS receiver

These examinations were performed mainly with the DUT1 and the SONY in the outdoor measurement set-up. It was verified with the GARMIN GPS that the results can be transferred qualitatively to the simulator tests.

All results clearly show reduced susceptibility to interfering fields if only the receiver was illuminated with its antenna out of the disturbing simulator field. This reduction is illustrated in *Fig.5.5.1* showing two threshold curves of the DUT1 (V-f). It can be discerned that the DUT1 without its internal antenna is only susceptible at some frequencies around 0.52 and 1.5 GHz unlike to the usually arrangement with internal antenna. The effects around 520 MHz remained. (Because of the earlier mentioned reason only arbitrary units of the field strength are shown for the DUT1).

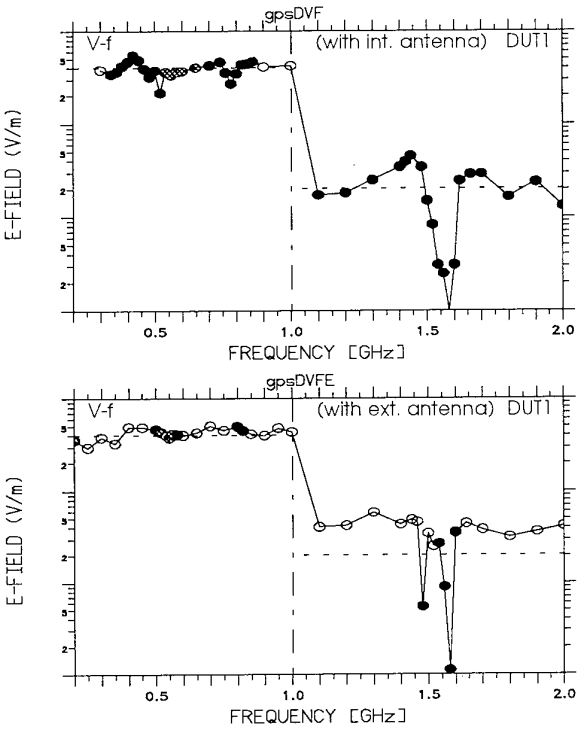

Fig.5.5.1: Threshold curves of the DUT1 in the V-f position with and without internal antenna

5.5.2 Illumination of the GPS antenna

Now the GPS antenna was illuminated in the simulator with the receiver outside the disturbing field. At the GARMIN and DUT1 upsets occurred only near 0.52 and 1.5 GHz. At the connected TRIMBLE and SONY additional upsets are observed near 250, 300, 800 and 900 MHz. It turned out that generally the GPS is less susceptible if only the antenna is illuminated and not the receiver with its internal circuitry.

The different antenna types of the GARMIN (rod and flat disc) show no significant differences regarding to the receiver sensitivity and to the susceptibility to interference fields.

5.6 Conclusions

At the end of the CW measurements on four hand-held GPS receivers the following summary can be given:

- The GPS are most susceptible if the electric field is parallel to the long side of the receiver box.
- The GPS are most susceptible with its internal/attached antennas. They are less susceptible if the receiver and the GPS antenna are placed separately and linked together via a coaxial cable. Illumination of either the receiver or the antenna caused less upsets.
- The GPS are most susceptible at the L1 frequency and its sub harmonic components.
- There is no significant dependency of the GPS's susceptibility on the satellite signal strengths.

- Below 1 GHz some weak effects occurred (e.g. wrong messages) not always causing upset. Worst effects caused switch off.
- At our tests between 0.3 - 2 GHz it turned out that the SONY and TRIMBLE were most susceptible to interference fields, whereas the DUT1 had less problems with upsets. The resistance of the GARMIN to disturbances was average.
- To cause out-of-band upsets a disturbing field level of 20 ... 60 V/m is sufficient, depending on the frequency. In band and sub harmonic-components upsets can be initiated at field strengths below 1 V/m.
- Between 2 - 4 GHz measurements have been carried out only at the DUT1 and SONY in the outdoor set-up. Failures occurred between 2.1 - 2.4 and at 3.1 GHz (Δf=100 MHz) with and without the internal antenna.
- CW field strengths below 100 V/m at out-of-band frequencies are not sufficient to damage electronic devices in the GPS. Perhaps in band and sub harmonic components frequencies at these field levels may cause destruction.

6. PULSE RESULTS

6.1 General

Until now we have carried out pulse measurements on the four GPS receivers only in one of the most susceptible V orientations. As mentioned earlier for these investigations a high power pulsed signal source is available to us. This source is able to generate power levels up to 35 kW between 800 - 1200 MHz, corresponding to a maximum field strength of about 2600 V/m at the test objects.

We started the examinations with a constant pulse width of 20 µs. This width enables us to make use of the entire power level at single shot operation, but at a repetition rate of 1 kHz, we also applied, the power was reduced. The test procedure was similar to the CW tests. At each of the five selected frequencies the pulsed power level was increased until upset occurred. After the single pulse thresholds we determined the multiple shot (1 kHz) thresholds.

In the subsequent curves the filled circles again point to the upsets whereas the blank circles indicate 'no failure'. The number next to the circles refer to the kind of the disturbance and the letters *s* (single shot) and *m* (multiple shots, 1 kHz) to the number of pulses.

6.2 Upsets and effects

At the pre-tests we discovered by chance that the GARMIN can be switched on by itself in the pulsed interference field. This effect occurred at 800 MHz with single shots at about 280 V/m, with 1 kHz repetition rate only 220 V/m were necessary. *Fig.6.2.1* shows the thresholds at the five examined frequencies and it can be seen that all the time upsets occurred. The field strengths responsible for single shot failures are, depending on frequency, between 420 and 1370 V/m. At the GARMIN only in the higher frequency region multiple shots are applied. These upsets at 1 kHz are initiated already at 760 V/m.

Besides the switch on there is a lot of further effects at the GARMIN which are summarized below:

1) The bars indicating the satellites' field strengths disappeared. Shortly after the interfering field is off they appeared again.

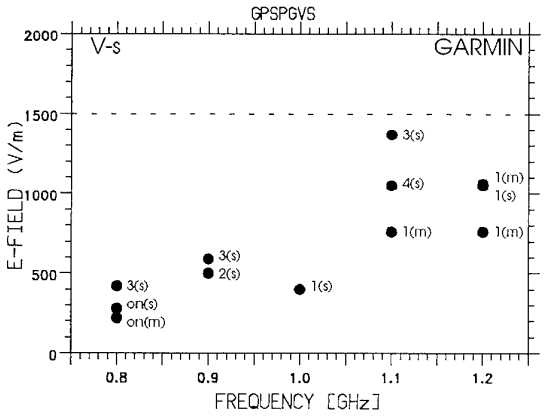

Fig.6.2.1: Thresholds of the GARMIN in pulsed interference fields in the V-s position with various effects

2) The GPS switched to another mode but returned to the initial mode after the pulse.
3) The GPS switched off and could not be switched on again. After removing the batteries and inserting again the GPS was ready for further use.
4) The GPS display is blocked, that is, the bars indicating the satellites' field strengths remained on the display although the GPS itself did not work. The same procedure as before (3) let the GPS work again. This failure is very risky because it leads the GPS user believe that his device works.

The other tested GPS show effects of similar kind. At the GARMIN it turned out further that in some cases the earlier mentioned almanac in the memory of the system was deleted (or could not be read out) after the illumination with the pulsed field, so it had to be initialized again (cold start).

As the thresholds in *Fig 6.2.2* indicate also the SONY GPS shows upsets at all the test frequencies. At this device a further worse effect appeared:

5) The GPS switched to 'status 03' (according to the manual that means an antenna disturbance). After switching off and on the batteries are nearly discharged and warm. This indicates that a high current was flowing which could destroy the integrated circuits.

For a single pulse the failure thresholds are between 470 and 1700 V/m, for multiple pulses between 470 and 950 V/m.

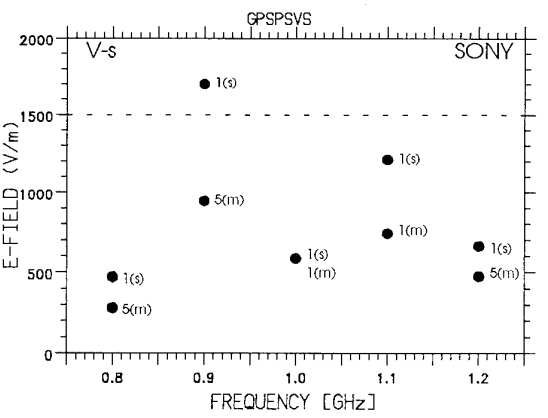

Fig.6.2.2: Thresholds of the SONY in pulsed interference fields in the V-s position with various effects

Tne DUT1 again proved to be the most resistant GPS to interference fields. Between 800 and 1000 MHz it could not be disturbed with the single pulse and at the two other frequencies 2200 V/m are necessary to cause upsets.

Also the TRIMBLE, whose thresholds are shown in *Fig 6.2.3*, was surprisingly resistant to pulsed fields. Above 1 GHz the GPS was very hard to be influenced and even fields up to 2800 V/m (single shot) did not cause an upset. Unlike at 800 and 900 MHz the TRIMBLE already failed around 320 V/m (1 kHz) and 470 V/m (s), respectively.

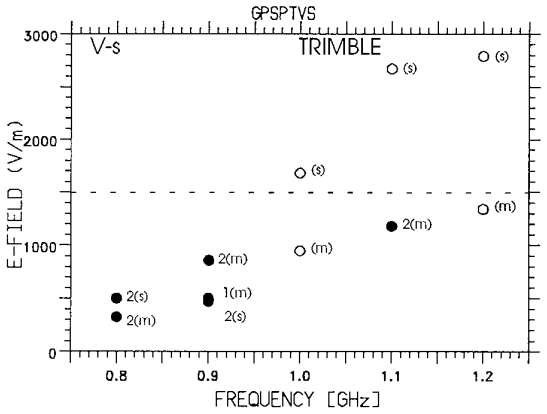

Fig.6.2.3: Thresholds of the TRIMBLE in pulsed interference fields in the V-s position with various effects

REFERENCES

[1] Braun,Ch., Graf,W., Schmidt,H.U.: "A Scale-Model Simulator for System Tests", 1992 Joint Symposia IEEE/APS, URSI, Nuclear EMP Meeting, Chicago (USA), 18 - 25 July 1992

[2] Braun,Ch.: "Design of a Broad Band Wave Guide for EMP Scale-Model Measurements ", FhG-INT (Internal Report 6/84 (in German), 1984)

[3] Braun,Ch., Guidi,P., Schmidt,H.U.: "Coupling Measurements on Intelligent Missiles at Microwave Frequencies , AGARD Meeting on High Power Microwaves, Ottawa (Canada), 2 - 6 May 1994.

Turbulence in the Upper Atmosphere: Effects on Systems

Santimay Basu and Gregory J. Bishop
Phillips Laboratory, PL/GPIA
Hanscom AFB, MA 01731
U.S.A.

Capt. John Larson
Air Force Space Command, AFSPC/SCZ
Peterson AFB, CO 80914
U.S.A.

ABSTRACT

The F-region of the ionosphere typically above 150 km at times becomes turbulent and develops small scale (<1 km) irregularities of electron density. These irregularities scatter radio waves from satellites in the VHF and UHF range and generate amplitude and phase scintillation. The magnitude of scintillation decreases with an increase of frequency but may be of concern at frequencies as high as 10 GHz. Scintillations are pronounced at equatorial and polar latitudes. The most severe scintillation is recorded over two belts, a few degrees wide at approximately 15° north and 15° south of the magnetic equator. The stations at Ascension Island, Diego Garcia, Hong Kong and Taiwan are located in this region where satellite communication links at 1.5 GHz may suffer 20 dB fades after sunset during the solar maximum period. The transmissions of GPS satellites at 1.228 GHz and 1.575 GHz are thus vulnerable. Scintillations cause message errors, cycle slips and loss of phase lock in satellite communication and navigation systems. In this paper, we first provide a summary of the climatology of scintillation with emphasis on the effects of scintillation on space systems. While the climatology of scintillation is fairly well established, the specification and forecasting of scintillation on a daily basis remains a challenging problem in view of the extreme day-to-day variability of scintillation, which is unfortunately most pronounced in the severely disturbed equatorial region. Attention is focused on this shortfall in the context of the recently formulated U.S. National Space Weather Program (NSWP) requiring the nowcasting and forecasting of the conditions on the sun, and in the solar wind, magnetosphere, ionosphere and thermosphere.

INTRODUCTION

The earth's ionosphere extends from about 50 km to above 1000 km and is a weakly ionized gas containing a large number of neutral molecules and relatively smaller number of electrons and ions. The concentration of electrons varies from 10^8 to 10^{12} m^{-3}. These are free electrons which move with their thermal speed and are influenced by the ionospheric electric field and the earth's magnetic field. It is the free electrons that affect radio wave propagation in the frequency range of 100 MHz to 10 GHz considered in the paper.

The ionosphere at times becomes turbulent when the electron concentration varies randomly with position. When radio waves from satellites traverse the ionosphere, the irregularities of electron concentration impose phase fluctuations across the wavefront. On emerging from the ionosphere, as the wavefront travels towards the ground amplitude fluctuations also develop due to diffraction. As a result, a diffraction pattern with varying amplitude and phase is developed on the ground. In the presence of a relative motion between the satellite, the ionosphere and the receiver on ground, the diffraction pattern sweeps past the receiving antenna to generate amplitude and phase scintillations. Figure 1 shows an example of amplitude and phase scintillation at 244 MHz. The data was acquired at Sondrestrom, Greenland by using a phase sensitive system using transmissions from a near-stationary polar satellite.

The severity of scintillation varies primarily with frequency, location, season and sunspot cycle. Scintillation effects decrease with an increase of frequency but may be of concern at frequencies as high as 10 GHz. The equatorial anomaly region is the worst source of scintillation. This anomaly region corresponds to two belts, each several degrees wide, of enhanced ionization density in the F-region at approximately 15° north and 15° south of the magnetic equator. During the solar maximum period, 20 dB fades at 1.5 GHz, corresponding to the GPS frequency, are often encountered in the anomaly region after sunset. However, only about 6 dB fades are encountered within a few degrees of the magnetic equator. The other active regions are located at the auroral and polar latitudes. The eleven-year sunspot cycle profoundly affects the ionosphere. During the recent solar maximum period, between 1988-1992, fade depths exceeding 10 dB at GPS frequencies were encountered at Thule, Greenland, with consequent effects on satellite communication and navigation systems. In the equatorial region, the variation of scintillation with season depends on longitude. For example, in the American sector, the occurrence of scintillation is maximum during September to April and minimum during the May to July period, whereas in the Pacific sector the occurrence is minimum during November to January and maximum during the remaining period (Ref. 1).

The global climatology of ionospheric scintillation is fairly well established. It is useful for long range planning of satellite communication and navigation systems. However, in view of the extreme day-to-day variability of scintillation, especially in the severely disturbed equatorial region, forecasts of ionospheric weather is needed for operational systems support.

Paper presented at the AGARD SPP Symposium on "Environmental Factors in Electronic Warfare Related to Aerospace Systems" held in Pratica di Mare AFB (Rome) Italy, from 8-11 May 1995, and published in CP-573.

This has been emphasized in the recently formulated U.S. National Space Weather Program (NSWP). In this document, 'Space Weather' refers to conditions on the sun and in the solar wind, magnetosphere, ionosphere and thermosphere that can influence the performance and reliability of space-borne and ground-based technological systems and endanger human life. While the NSWP deals with a wide range of effects, it recognizes that the ionospheric scintillation is a major component of space weather since it can cause the disruption of satellite communication and navigation systems.

This paper first summarizes the global climatology of ionospheric scintillation at various frequencies. These results are discussed in the context of the performance of communication and navigation systems. This section should be helpful to a user in distinguishing an outage caused by the ionosphere from malfunction of the electronic system or the satellite and in evolving strategies to combat the deleterious effects of scintillation on systems. The paper also discusses Phillips Laboratory's Space Weather initiative on ionospheric scintillation.

SCINTILLATION STRUCTURE

The scintillation structure is defined by its magnitude and frequency content. The magnitude of intensity scintillation, S_4, is defined by the ratio of the rms value of signal power fluctuations and the average signal power. The S_4 index is widely used in theoretical computations. However, the depth of signal fading in decibel (dB) is more useful to a systems engineer. Since the signal fluctuations follow Nakagami-m distribution, a relationship between the S_4 index and percentiles of fading depths in dB could be developed (Ref. 2). The top panel in Figure 1 displays a plot of signal intensity received from a satellite at 244 MHz over a 168 sec interval. The original data acquired at 50 Hz has been decimated in this plot. When the original data is processed we find that for this sample $S_4 = 0.9$ and the depth of fading exceeds 20 dB for 1 percent of the time. It signifies that if a receiving system has a fade margin of 20 dB, the signal will be buried in receiver noise for 1 per cent of the time. If the signal margin of the receiver is only 6 dB, the receiver will lose characters in messages for 10 percent of time. The standard requirement for a commercial link is much more stringent requiring that signals should not fade below the receiver margin for 0.01 percent of time. In this paper, we shall quote figures corresponding to 1 percent level. In addition to causing message errors and data losses, cycle slips occur when the fade depth exceeds the fade margin of the system. The cycle slips cause abrupt changes in phase resulting in loss of phase lock in systems incorporating phase lock loops.

Figure 1 also shows that the signal intensity fluctuates in a random manner. The structure of scintillation is defined by its power spectrum which provides information on the relative power density of different signal frequencies that constitute the signal fluctuations. The diffraction process suppresses intensity fluctuations below the Fresnel frequency, $f_F = v/(2\lambda z)^{1/2}$ where v is the relative motion between the satellite, the receiver and the ionosphere, λ is the wavelength of transmission, and z is the distance between the receiver and the irregularity layer in the ionosphere. In the case of a geostationary satellite, typically $v = 100$ ms^{-1} and for $z = 350$ km, $f_F = 0.1$ Hz at 250 MHz. In the case of an orbiting satellite $v = 3$ kms^{-1} and $f_F = 3$ Hz. The form of the irregularity spectrum and the diffraction process dictates the manner in which the power density decreases above and below f_F. Typically the power density decreases as f^{-3} at fluctuation frequencies $f > f_F$ and decreases as f^1 at fluctuation frequencies $f < f_F$. It is to be noted that f is the frequency of fluctuation and not the frequency of satellite transmission.

The bottom panel of Figure 1 shows phase scintillations associated with the intensity fluctuations in the top panel. The phase scintillation index is simply defined as the rms value of signal phase fluctuations. Unlike intensity scintillation, the diffraction process does not suppress low frequency phase scintillation. In fact, we removed the low frequencies by using a high pass filter with a cut-off frequency of 0.01 Hz. For this sample, phase scintillation index is obtained as 4 radians. From a system perspective, phase scintillations introduce phase jitter in phase modulation. The second time derivative of phase scintillation is of concern in phase lock systems. Phase scintillations will cause loss of phase lock in systems when the second derivative of phase scintillation exceeds the bandwidth of the phase lock loop.

GLOBAL VARIATION

The global variation of scintillation at L-band frequencies (1.5 GHz) is best shown by the often used cartoon of Figure 2 (Ref. 3) which shows the locations where scintillation is most pronounced. The left-hand panel represents the case for the solar maximum period when the electron concentration in the ionosphere attains its maximum while the right-hand panel is for the solar minimum period. For each globe shown in this figure, the noon meridian (12h local time) is at the left, 18h local time is in the middle and the extreme right meridian corresponds to midnight. The latitude lines represent magnetic latitudes and not geographic latitudes and, as such, the magnetic north pole and the south pole are at the top and bottom of each globe respectively. The figure shows that scintillation activity is concentrated in the equatorial and the high latitude regions covering the auroral and polar latitudes.

In the equatorial region, scintillations do not occur during the daylight hours and abrupt onset of scintillation takes place after sunset. The worst source of scintillation is the equatorial anomaly region which corresponds to two belts each several degree wide, of enhanced electron concentration in the F-region at approximately 15° north and south of the magnetic equator. The left-hand panel shows that during the solar maximum period, scintillations at 1.5 GHz may exceed 20 dB for several hours after sunset. Ascension Island in the Atlantic, Diego Garcia in the Indian Ocean, Hong Kong and Taiwan in the Pacific are some of the locations that fall directly under the anomaly region. However, areas within a few degrees of the magnetic equator encounter only 5-7 dB fades.

The other active region is located at high latitudes. In the auroral region scintillations occur primarily during the nighttime hours. In the central polar

cap, scintillations may occur at all local times and 10 - 15 dB fades at 1.5 GHz are obtained during the solar maximum period. The right-hand panel shows that during the solar minimum period scintillations are much reduced.

SOLAR CYCLE VARIATION

Figure 3 shows the solar cycle variation of scintillation in the equatorial anomaly region. The data was acquired at Ascension Island by using 1.5 GHz transmissions from the INMARSAT satellite. The figure shows that as the sunspot number increases (bottom panel) the occurrence of nighttime scintillation increases. During the solar maximum period, nighttime scintillations at 1.5 GHz exceeding 10 dB occur 30 percent of time. The effects of scintillation on GPS satellites may be assessed from this figure since the GPS satellite transmission frequencies are 1.228 GHz and 1.575 GHz. A few scintillation studies have been made with GPS satellites (Ref. 4; Ref. 5). In Figure 4, we show a sample of scintillation data acquired with GPS satellites at 1.575 GHz. The measurements were made at Tucuman, Argentina which is situated near the anomaly region at a magnetic latitude of 12° south (Ref. 6). Although the current period corresponds to the solar minimum period, some fades attain a depth of 16 dB. Since multiple GPS satellites can be viewed from one station it offers a unique platform for the study of amplitude and phase scintillation and their effects on GPS receiving systems (Ref. 7).

Figure 4 shows the solar cycle variation of scintillation at 244 MHz recorded in the central polar cap with a near-stationary satellite viewed at a high elevation angle from Thule, Greenland. The decrease of 244 MHz scintillation in the polar region may be noted. In addition to the solar cycle variation, the diagram shows a decrease of scintillation activity during the local summer. This is a result of the healing of the irregularities by the solar ultraviolet radiation available at all hours in the polar region during the summer. It is to be noted that Figure 3 refers to measurements at 1.5 GHz whereas Figure 5 corresponds to 244 MHz.

FREQUENCY DEPENDENCE

The magnitude of scintillations decreases as the frequency is increased. In Figure 6 we show multi-frequency scintillation data acquired at Ascension Island during the solar maximum period. The bottom three panels show scintillation effects on MARISAT satellite transmissions at 257 MHz, 1.54 GHz and 3.95 GHz. It shows that when 257 MHz scintillations are driven far into saturation, 1.5 GHz scintillations attain fade depths of about 20 dB and 3.95 GHz attain fades of 5 dB. From scintillation theory, the S_4 index should vary with frequency as $f^{-1.5}$ and phase scintillation index as f^{-1}. It should be noted, however, that for intensity scintillations, the frequency extrapolation is valid only when weak scatter conditions prevail, i.e., when $S_4 < 0.6$ over the frequency range of extrapolation. This limits the frequency range over which this extrapolation is possible. This frequency range does not exceed an octave thus requiring actual measurements for frequency separations more than an octave.

FORECASTING IONOSPHERIC WEATHER

The previous paragraphs summarize the climatological behavior of scintillation and their effects on technological systems. Based on DNA Wideband satellite observations and Phillips Laboratory's time continuous scintillation observations with geostationary satellites at various equatorial sites, a climatological model, WBMOD, has been developed. This computer code can be run on a PC. Given the orbital characteristics of a satellite, the geographic location of the observing site, the day number, universal time, magnetic index, sunspot number, and frequency as input, the intensity and phase scintillation indices, and their spectra can be obtained as the output. Figure 7 illustrates the magnitude of scintillation index at 244 MHz (quantized over three intervals, $S_4 < 0.3$, $0.3 < S_4 < 0.6$, and $S_4 > 0.6$) on Day 90 during the solar maximum period at 21 UT over the footprint of a geostationary satellite, parked at 15°W. The lightly-shaded region over the footprint of the satellite represents regions where $S_4 < 0.3$, the medium-shaded region over the footprint indicates areas where $0.3 < S_4 < 0.6$, and the darkly-shaded areas around the nighttime equatorial region and the extreme high-latitude portions represent areas of intense scintillation activity ($S_4 > 0.6$).

While such a climatological model is useful as a long range SATCOM planning tool, it is unable to specify scintillation on a given night for operational systems support. The ionospheric climate and weather, especially in regard to turbulence or scintillation, can be very different owing to the day-to-day variability of scintillation. Figure 8 illustrates this pronounced variability of scintillation at the magnetic equator over a seven-day period. Near saturated scintillation at 244 MHz was recorded on four evenings whereas no activity was recorded on the three remaining nights. The causes for this variability remain unresolved.

In order to provide weather information on scintillation, a real time scintillation warning system has been developed at the Geophysics Directorate of Phillips Laboratory. Figure 9 illustrates this PC-based system. It acquires signals from a satellite at 250 MHz and makes on-line processing of the scintillation data to derive the S_4 index. A user can call up the system by telephone and receive voice message reports of the on-going scintillation activity on the SATCOM link. The calling party is given options of receiving qualitative (weak, moderate or strong) or quantitative reports (S_4 index) of scintillation activity during the past 5 minutes, 15 minutes or one hour. The system can be adapted to send the data on a datalink to a central location.

In view of the severity of scintillation activity in the equatorial region, a plan for the deployment of an array of sensors over the equatorial belt is under consideration. Figure 10 illustrates the sensor deployment plan. Each station will acquire signals from two available geostationary satellites to the east and the west. In the equatorial region, the scintillation causing turbulent regions evolve after sunset and they move eastwards with a nominal speed of 6 km/min with a lifetime of about 4 hours. Thus the system will provide not only the real time specification of scintillation over a link, it will be able

to forecast scintillations to the east of a link with a lead time of about 4 hours. It has also been planned to modulate the climatological scintillation model, WBMOD, with these sensor outputs in order that nowcasting and forecasting of scintillation can be achieved over the equatorial belt. Future programs are focused on the development of a physics based scintillation model that incorporates real time electron density model in the equatorial region with the DMSP satellite derived ionospheric electric field as the input, the plasma instability theory characterizing the strength of turbulence and the radio wave scattering theory that will define the fluctuation levels of satellite signals on ground or for communication between two space platforms.

SUMMARY

The characteristics of intensity and phase scintillation, and their dependence on frequency, geographic location and sunspot cycle have been discussed in the context of available data. The constraints of ionospheric scintillation on communication and navigation systems have been mentioned. Scintillation studies by using GPS satellites is needed to study the effects of scintillation on GPS receivers with different signal margins. In the context of the U.S. National Space Weather Program, the on-going programs on the forecast of scintillation over the severely disturbed equatorial region by using an array of scintillation sensors and scintillation model have been outlined.

REFERENCES

1. Aarons, J., The longitudinal morphology of equatorial F layer irregularities relevant to their occurrence, Space Science Reviews, *63*, 209, 1993.

2. Whitney, H.E., "Notes on the Relationship of Scintillation Index to Probability Distributions and Their Uses for System Design", Rep. AFCRL-TR-74-0004, Air Force Cambridge Res. Lab., Bedford, MA 01731, 1974.

3. Basu, S., E. MacKenzie, and Su. Basu, Ionospheric constraints on VHF/UHF communication links during solar maximum and minimum periods, Radio Science, *23*, 363, 1988.

4. Rino, C.L., M.D. Cousins, and J.A. Klobuchar, Amplitude and phase scintillation measurements using the Global Positioning System, in "Proceedings of the Ionospheric Effects Symposium", 1981, available from the Government Printing Office.

5. Wanninger, L., Ionospheric monitoring using IGS data, presented at the 1993 Berne IGS Workshop, Berne, March 25-26, 1993.

6. Bishop, G.J., S. Basu, E.A. Holland, and J.A. Secan, Impacts of ionospheric fading on GPS navigation integrity, in "Proceedings of ION GPS-94", The Institute of Navigation, Arlington, VA, September 1994.

7. Aarons, J. and S. Basu, Ionospheric amplitude and phase fluctuations at the GPS frequencies, in "Proceedings of ION GPS-94", The Institute of Navigation, Arlington, VA, September 1994.

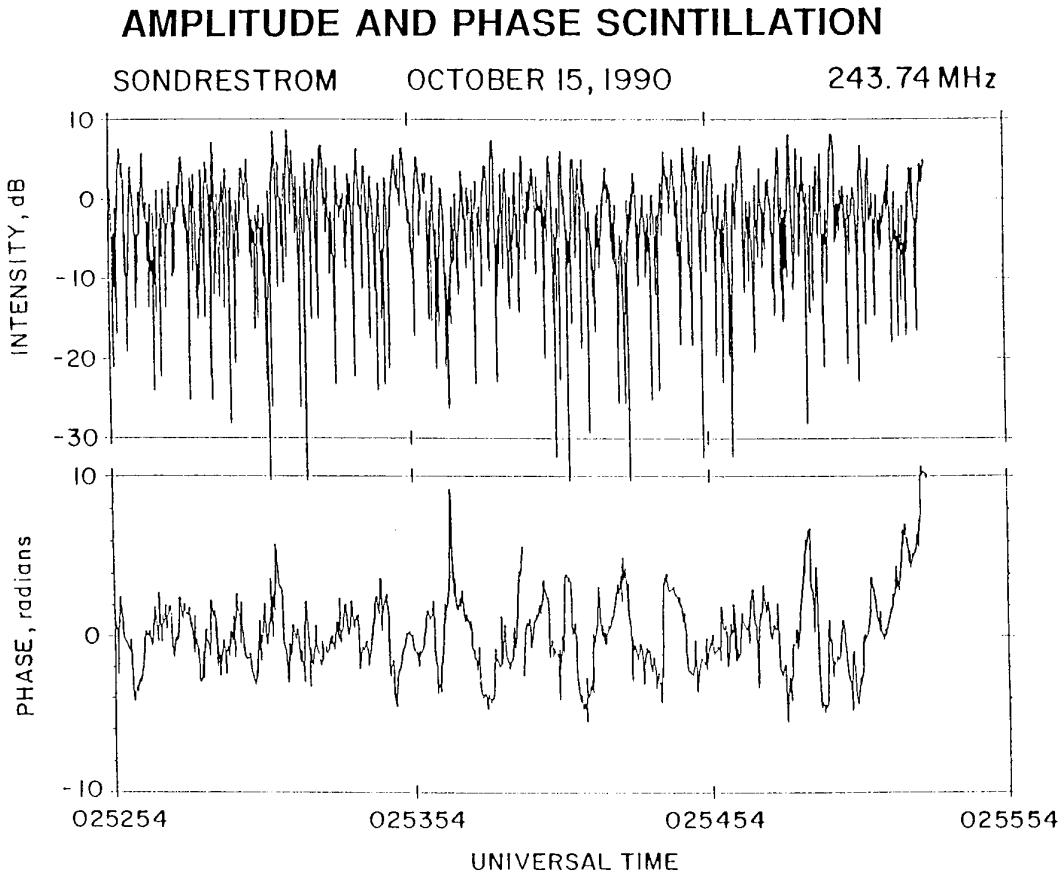

Figure 1. Amplitude and phase scintillation at 244 MHz recorded at Sondrestrom, Greenland, by using transmissions from a polar satellite in a Molniya orbit viewed at high elevation angles.

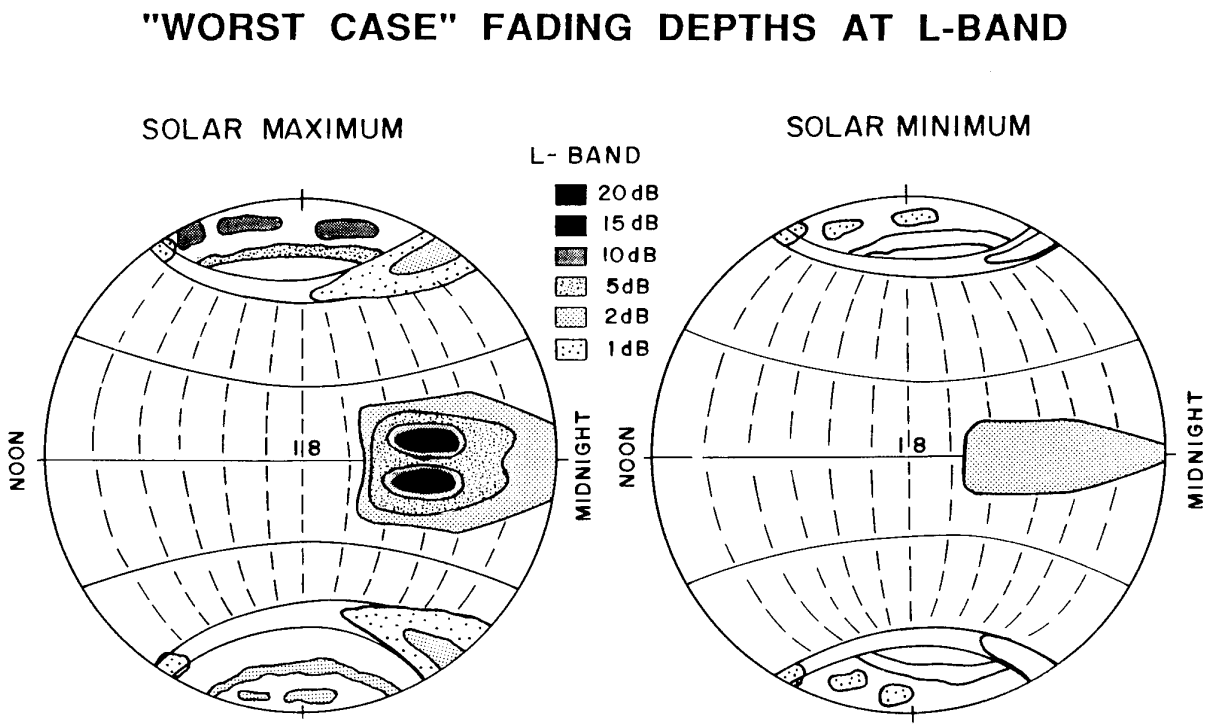

Figure 2. Global distribution of scintillation.

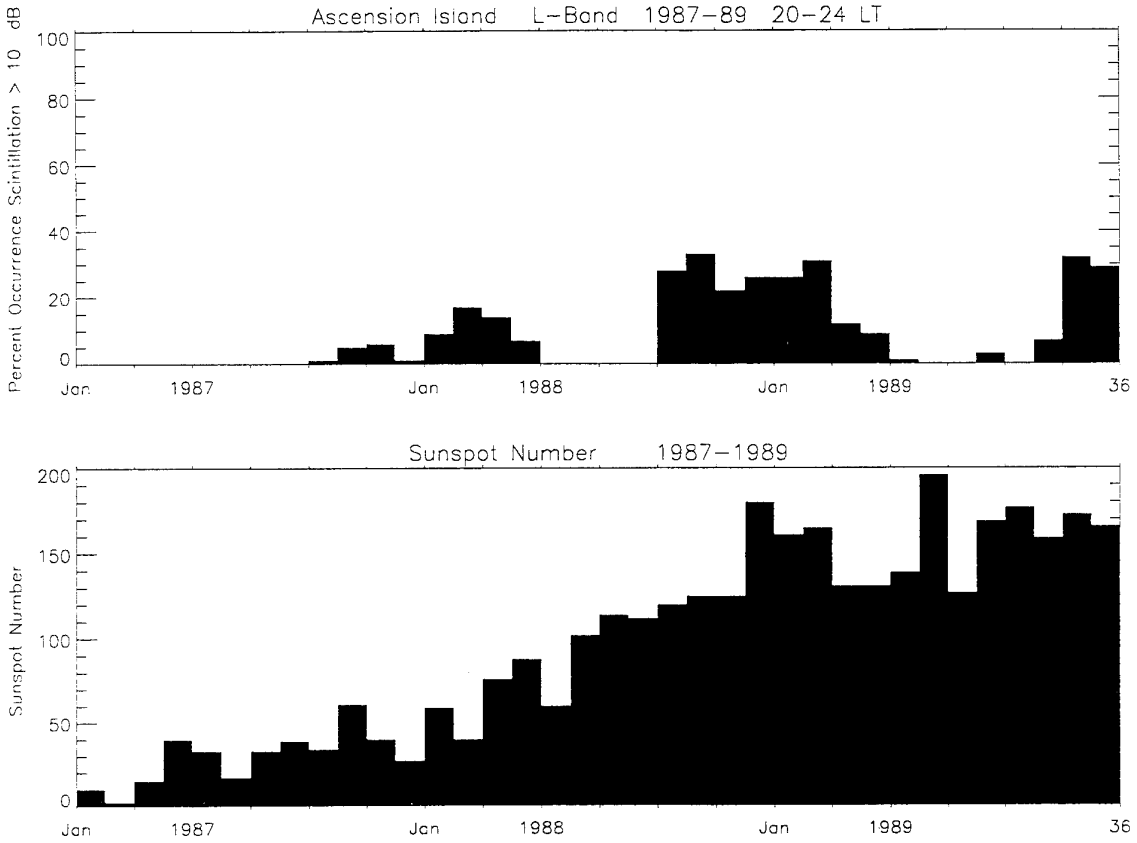

Figure 3. The variation of the occurrence of nighttime scintillation at 1.54 GHz with sunspot number obtained at Ascension Island located in the equatorial anomaly region.

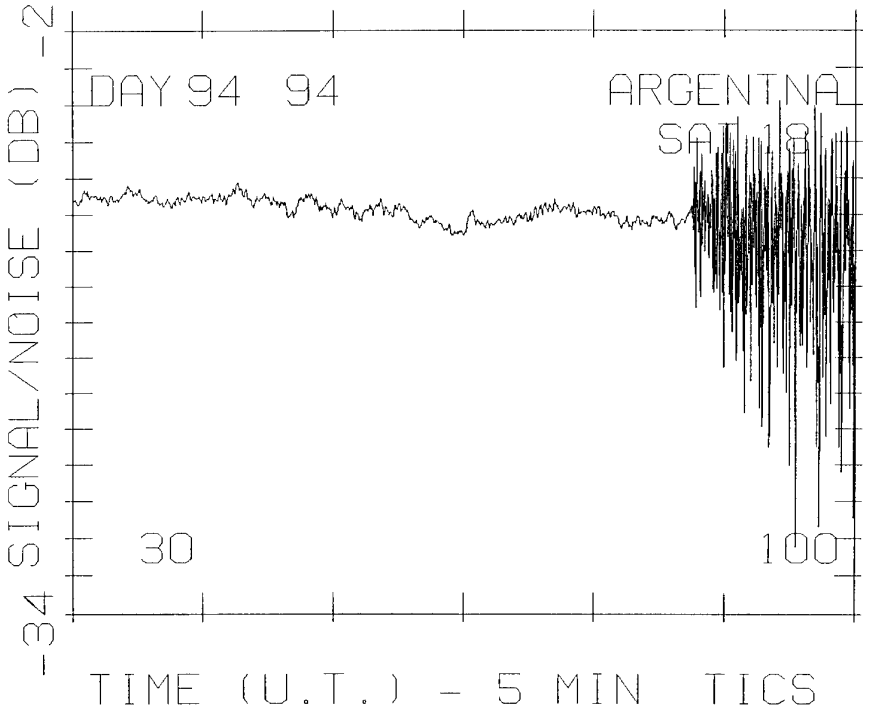

Figure 4. Scintillation of a GPS satellite at 1.575 GHz recorded at Tucuman, Argentina on Day 94, 1994.

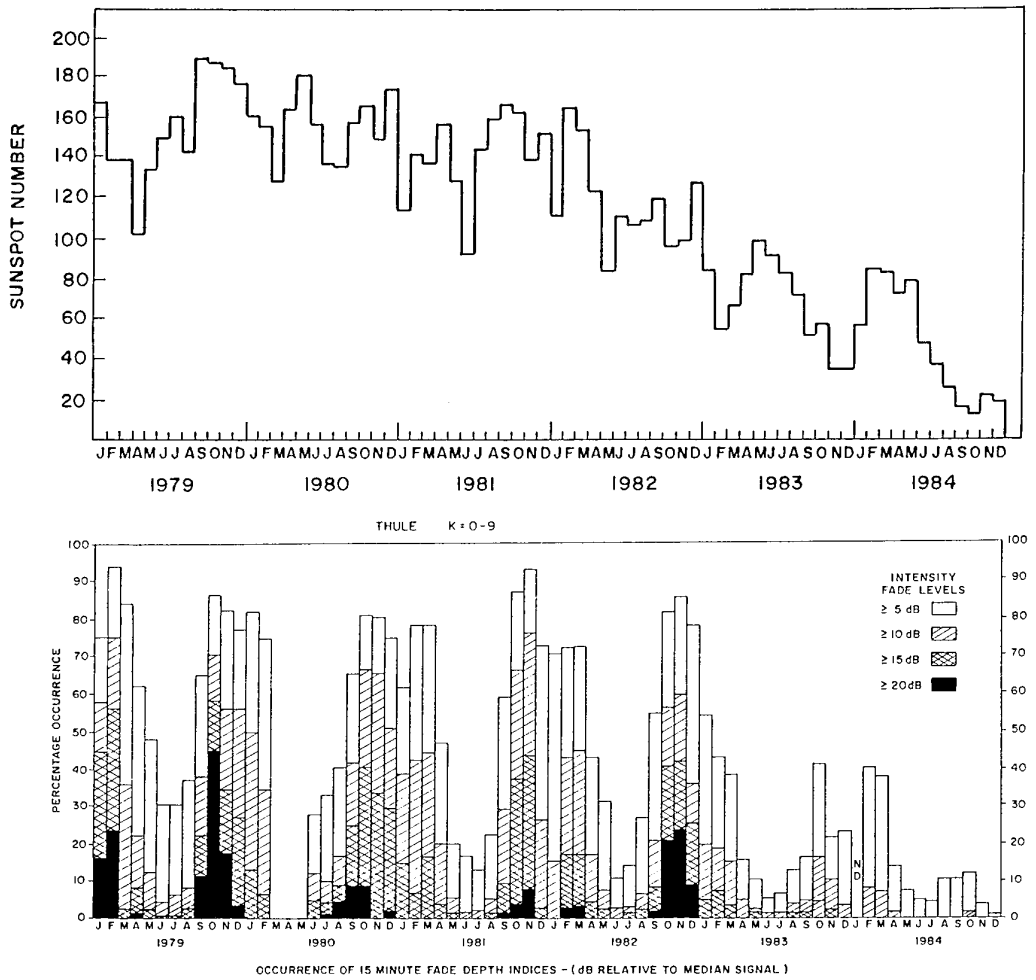

Figure 5. The variation of the occurrence of 244 MHz scintillation fades with sunspot number obtained at Thule, Greenland.

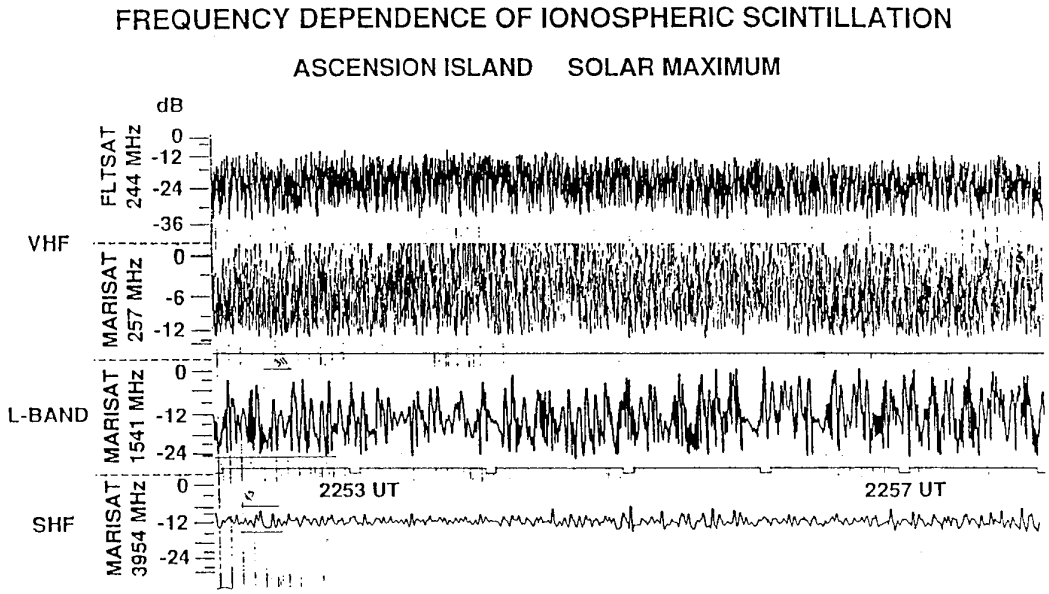

Figure 6. The variation of scintillation magnitude with frequency recorded at Ascension Island by monitoring MARISAT satellite transmissions at 257 MHz, 1.54 GHz and 3.95 GHz.

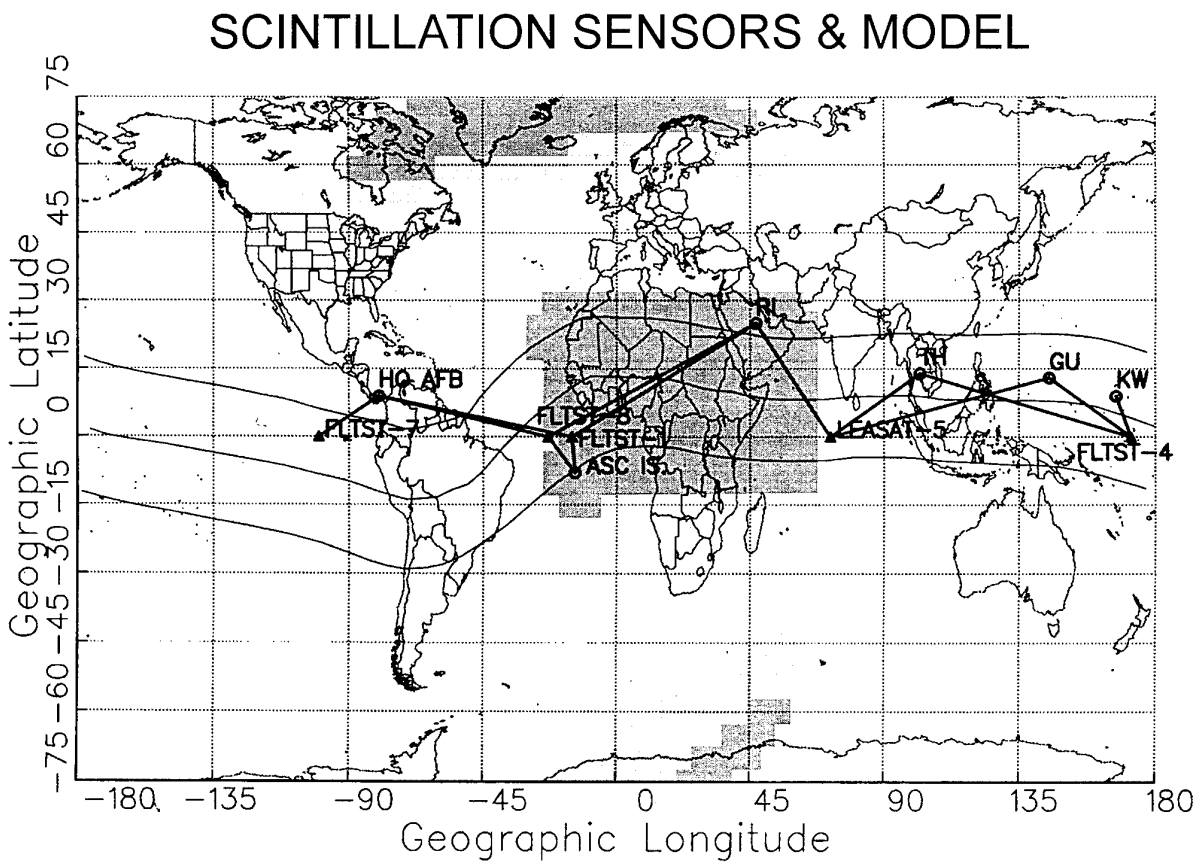

Figure 7. Distribution of the magnitude of scintillation at 244 MHz, obtained from the WBMOD scintillation model, over the footprint of a geostationary satellite at 15°W on Day 90 during the solar maximum period at 21 UT.

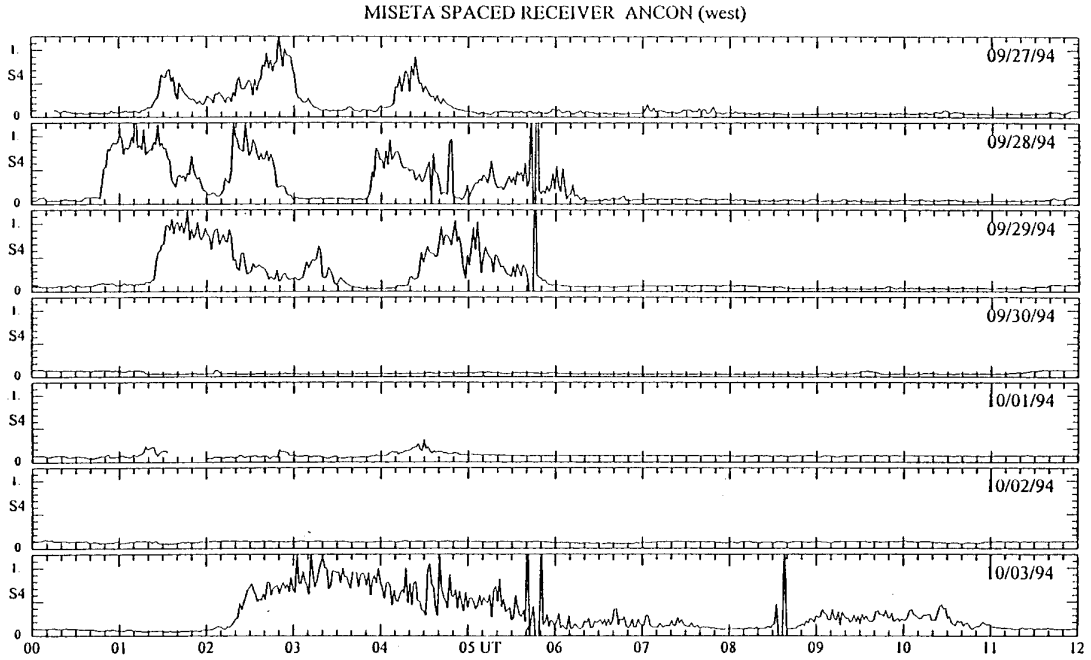

Figure 8. Illustrates the day-to-day variability of 244 MHz scintillation recorded at Ancon, Peru, located at the magnetic equator.

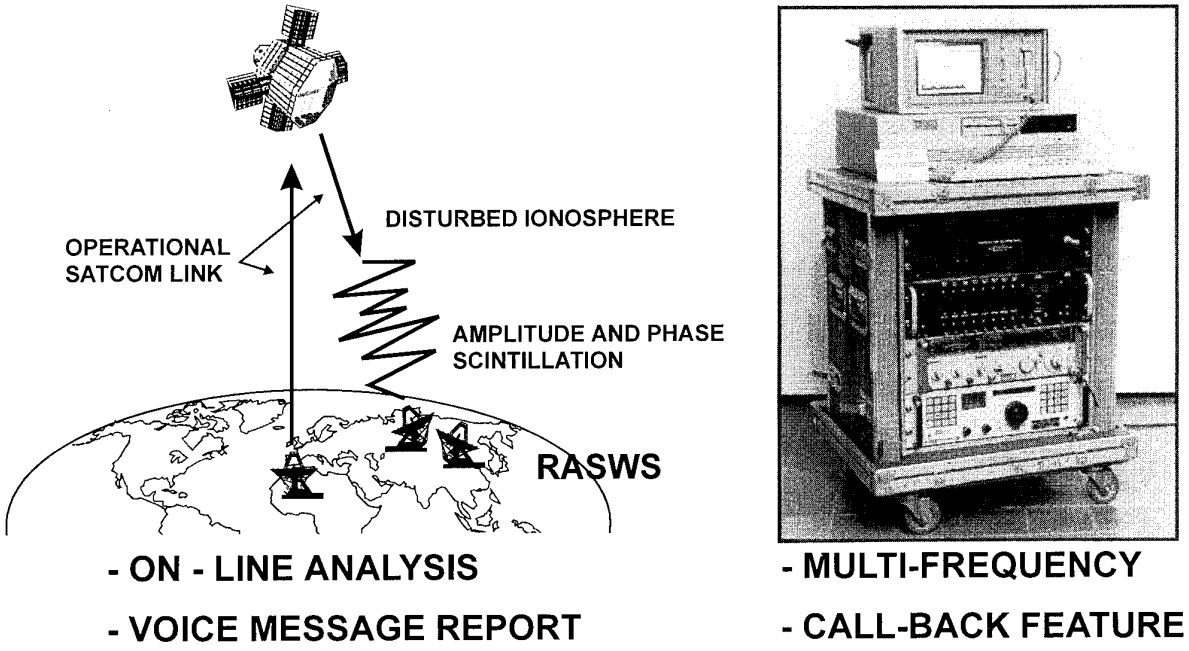

Figure 9. Real Time Scintillation Warning System developed at the Geophysics Directorate of Phillips Laboratory at Hanscom AFB.

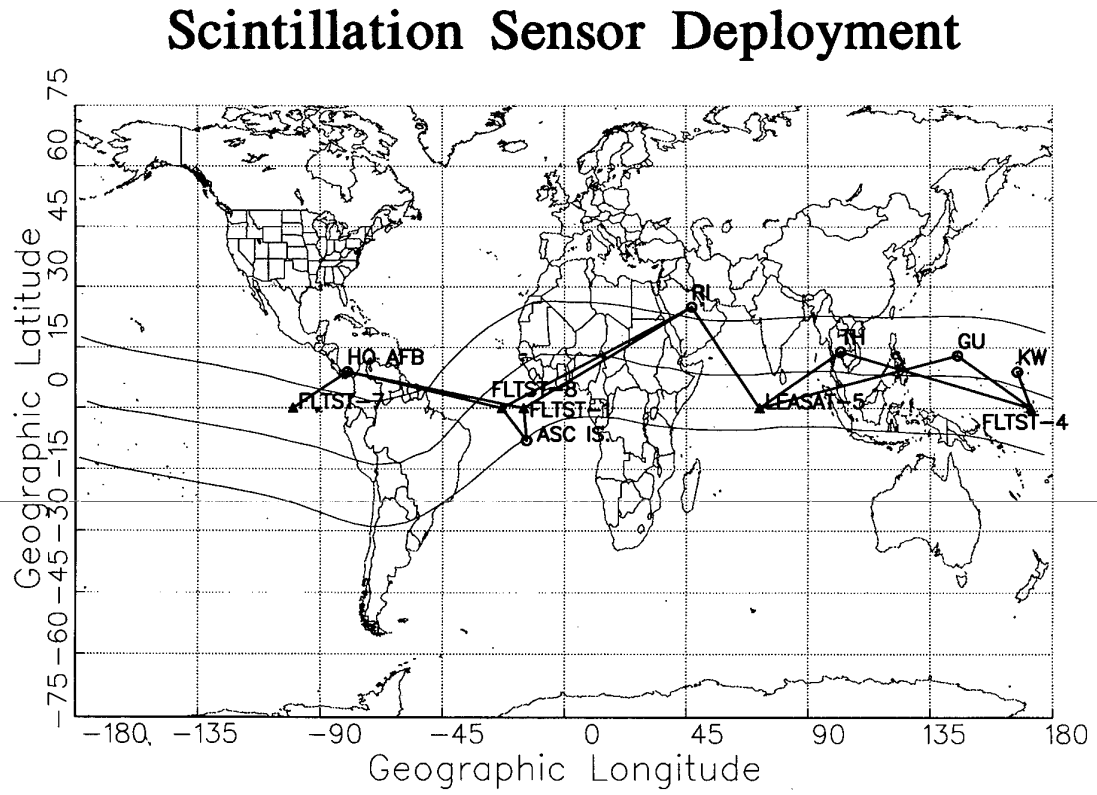

Figure 10. Proposed deployment of scintillation sensors over the equatorial region for the specification and forecasting of scintillation.

MICROWAVE SENSORS FOR MATERIAL CHARACTERIZATION

A.CAILLE
D.DERRAY
A.JULIEN-VERGONJANNE
P.GUILLON
Institut de Recherche en Communications Optique et Micro-onde
123, avenue Albert Thomas
87060 LIMOGES CEDEX
FRANCE

SUMMARY

Two sensors for a non-destructive testing of materials at low microwave frequencies are described.
One is a resonant dielectric probe acting on a quasi -TEM mode at about 1.7 GHz.
The other sensor is a microstrip system developped in the 0.5-2.5 GHz frequency range.
The Finite Element Method (FEM) leads to the determination of resonant or propagation parameters of each sensor.
The main basis of characterization methods is to compare the measurement values of the characteristic parameters of the sensors with the corresponding theoretical ones.
Several tests of dielectric and magnetic materials are presented and confirm the validity of the two methods.

LIST OF SYMBOLS

$\varepsilon = \varepsilon' - j\varepsilon''$: complex permittivity
$\mu = \mu' - j\mu''$: complex permeability
2D: two dimensions
3D: three dimensions
FEM: Finite Elelment Method
TEM: Transverse Electric and Magnetic

INTRODUCTION

Many dielectric and magnetic materials are used in new microwave applications like industrial measurements and so, characterization of their electromagnetic parameters is now necessary.
Numerous characterization methods are available at microwave frequencies. They can be generally differenciated according the measurement technique used : resonant or tansmission-reflexion .
Only few methods permit to test the materials without any machining of the samples.

We present in this article, two sensors for non-destructive testing of dielectric and magnetic materials at low microwave frequencies.

DESCRIPTION OF SENSORS

Dielectric probe

The probe is composed of a rectangular dielectric resonator metallized on three faces and inserted into a rectangular metallic box (fig.1).

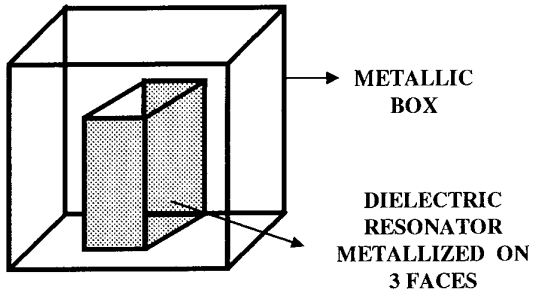

-fig 1-

The excitation of the structure is a 50 Ohm microstrip line facing one of the metallized lateral sides of the resonator.
Such a device is acting on a quasi-TEM mode around 1.7GHz.
The sample to be tested may be placed either on the non-metallized top side of the resonator or along one of its metallized lateral sides (fig.2a 2b).

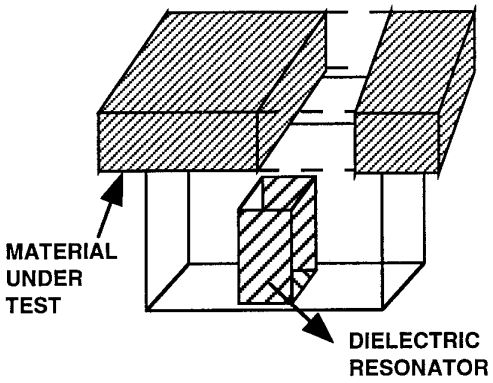

Sample on the top side of the resonator

-fig 2a -

Paper presented at the AGARD SPP Symposium on "Environmental Factors in Electronic Warfare Related to Aerospace Systems" held in Pratica di Mare AFB (Rome) Italy, from 8-11 May 1995, and published in CP-573.

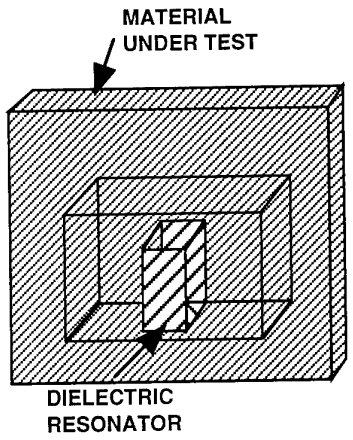

Sample along the metallized lateral side of the resonator

-fig 2b -

At low microwave frequencies , the cross section of material under test is about 5 cm^2.
Furthermore, in order to take into account contact problems, we introduce an air gap between the resonator and the tested material.

Microstrip sensor

The sensor consists of a 50 Ohm microstrip line operating in a quasi-TEM mode.
Perpendicular connectors permit to excite the TEM mode of the line (fig.3)
The transition between the excitation connectors and the microstrip line is composed of a 50 Ohm stripline.
This configuration enables us to apply the material to be tested near the microstrip line , without any contact with the conductor ribbon (fig.4).

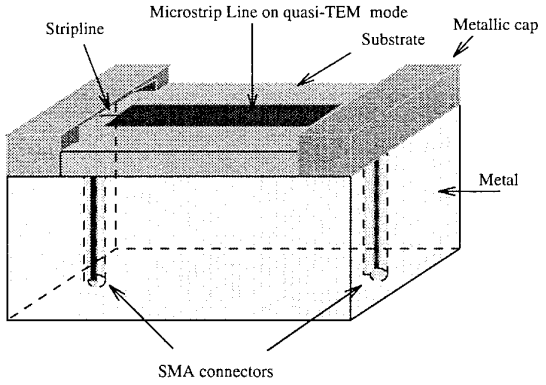

-fig 3 -

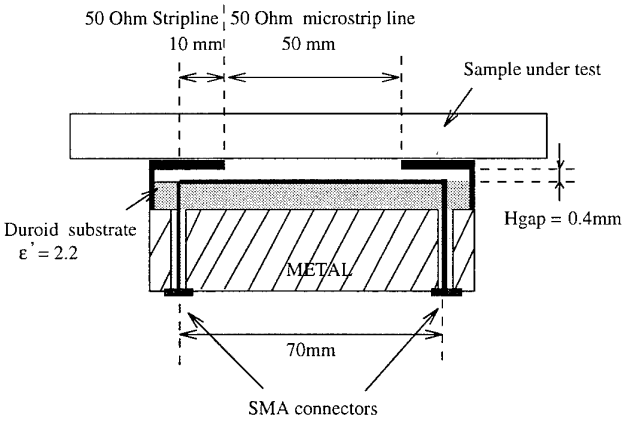

- fig 4 -

The material under test is placed on the metallic cap of the stripline transition and cover completly the microstrip line.
The material surface necessary for testing is about 15 cm^2.

THEORETICAL ANALYSIS

The Finite Element Method (FEM) performed at IRCOM leads to the characteristics parameters of each sensor.[1]
The FEM can be applied to homogeneous or inhomogeneous , isotropic or anisotropic, complex media.
This method permit to solve the vectoriel wave equations derived from Maxwell's ones.
The studied structure is divided into triangular (2D) or tetrahedron (3D) subdomains.
The exact function is approximing on each subdomains satisfaying the boundaries conditions.
There is two resolution cases :

- the forced oscillation analysis leads to the scattering parameters of the structure in the access planes and to the electromagnetic field distribution.
- the free oscillation case yields to each eigen mode resonant frequency and field repartition of studied structures.

dielectric probe

The free oscillations and complex formulation FEM applied to the dielectric probe leads to the resonant frequency f_0 and unloaded quality factor Q_0 of the quasi-TEM mode of the sensor loaded or unloaded by a sample.
So, a chart's catalog of f_0 and Q_0 as a function of electro-magnetical and geometric parameters of the sample under test have been drawn.
The comparison between the measured values of f_0 and Q_0 and the corresponding theoretical ones, permits to obtain by inter-polation on a chart, the complex permittivity or permeability of the sample.
We present fig.5 to 8 the charts corresponding to a dielectric material for the two positions of the sample described in fig.2.
The analysis of the $f_0$and Q_0 variations shows that:

- the dielectric probe do not permit low loss dielectric material characterization such as $\varepsilon'' < 10^{-3}$

- if $10^{-3} < \varepsilon'' < 5$, the resonant frequency f_0 is independant of dielectric losses. Consequently, a measured value of f_0 leads to the determination of ε' and a measured value of Q_0, to the determination of ε''.
- the sample position on the non-metallized top side of the resonator, is well-suited for determining the complex permittivity ε.

Fig. 9 to 12 show charts of magnetic materials with permittivity $\varepsilon = 5 - j\,0$.
We notice that:

- the method is not available for magnetic materials such as $\mu'' < 10^{-3}$
- if $10^{-3} < \mu'' < 0.1$ a measured value of f_0 leads to the determination of μ' and a measured value of Q_0, to the determination of μ''.
- for high loss magnetic materials such as $\mu'' > 1$, the chart corresponding to the sample position on the top side of the resonator, presents severals solutions for the permeability μ.

So, the sample position along the lateral metallized side of the resonator is a best position for testing high loss magnetic materials.

microstrip sensor

The microstrip sensor is studied by application of the FEM in the case of forced oscillations and complex formulation.
The analysis is divided in two cases:

- the uniform microstrip line acting on a quasi TEM mode is studied in 2D.
- the transition between connectors, stripline and microstrip line is analysed in 3D.

The combination of 2D and 3D studies yield to the scattering parameters of the sensor.
The comparison of the experimental and theorical values of the transmission and reflexion characteristics of the probe, have permit to fix severals theoretical parameters: the dielectric losses of the microstrip substrate and the geometric parameter hgap of the stripline structure (fig. 4).
From this, the phase transmission coefficient $\varphi(S_{21})$ versus its modulus $|S_{21}|$ of the microstrip sensor loaded with a material of complex permittivity or permeability have been plotted for each frequency of the (0.5 - 2.5 Ghz) range.
The principle of the method is to place on a theoretical chart the corresponding experimental coefficient S_{21} of the sensor loaded with a sample under test.
The complex permittivity ε or permeability μ are determined by using graphical interpolation.
Severals charts at the frequency f = 2GHz are presented.
Fig. 13 and 14 show dielectric materials case.
We have to note that:

- The sensor is suitable for dielectric materials such as $0.01 < \varepsilon'' < 20$
- For low loss dielectric materials such as $\varepsilon'' < 0.5$, the S_{21} phase is independant of the dielectric losses. So, the measured value of S_{21} phase gives ε' and the measured value of $|S_{21}|$ gives ε''.

Magnetic materials which permittivity is $\varepsilon = 5 - j\,0$, are studied on fig.15 and 16.

The charts show that the sensor permit to characterize magnetic materials such as : $\begin{cases} 0.05 < \mu'' < 5 \\ -5 < \mu' < 10 \end{cases}$

EXPERIMENTAL RESULTS

To ensure the validity of theoretical results, severals dielectric and magnetic materials have been tested by the two sensors.
The complex values of ε and μ obtained by interpolation on the corresponding charts, have been compared with those provided by a coaxial method performed at CEA/CESTA [2].
Fig.17 and 18 show the complex permittivity values obtained in dielectric material case.
For all methods, the results are similar and confirm the validity of the sensors method to determine the permittivity.
The uncertainty on the plot corresponds to the measured error of the S_{21} parameter of the microstrip sensor.
Two magnetic materials have been also tested.
One is a magnetic material such as $\varepsilon = 14 - j\,0$ and the other is a metallized on one face magnetic material such as $\varepsilon = 27 - j\,2.5$.
The different results presented fig.19 and 20 are very close to each other, for all frequencies of the 0.5 - 2.5 Ghz range.
We notice that the precision of permeability results obtained by the microstrip sensor is lowest for metallized material.

CONCLUSION

Two sensors for a non destructive testing of dielectic or magnetic materials with a weak surface of testing have been presented.
One is a resonant device around 1.7 Ghz which permits to test lossy dielectric materials on the top side of the probe and lossy magnetic materials along the lateral metallized side of the probe.
The other, is a wide-band system operating in the [0.5-2.5ghz] frequency range which is also suitable for lossy dielectric or magnetic materials.
The theoretical parameters of each sensor are calculated by the Finite Element Method.
A chart's catalog for each sample thickness in the two sensors case can be drawn and permit to obtain the complex permittivity or permeability of the samples under test.

[1] Zienkiewicz O.C., "The finite element method in engeneering Science" McGrawhill 1971 London

[2] Verdier A., Bardy N., Bonnefoy J.L., Prulhiere J.P. "Caractérisation radioélectrique de matériaux absorbants, application aux ferrites et aux agrégaires magnétiques." Journées de Caractérisation Micro-onde des Matériaux JCMM Limoges 1991 France

SAMPLE ON THE TOP SIDE OF THE DIELECTRIC PROBE

LOW LOSS DIELECTRIC MATERIAL

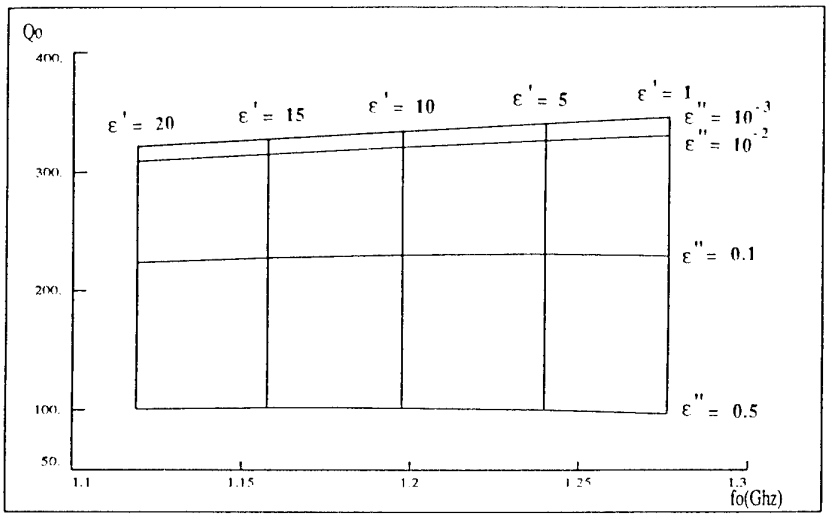

-fig 5-
Material Thickness = 3 mm

SAMPLE ALONG THE LATERAL SIDE OF THE DIELECTRIC PROBE

LOW LOSS DIELECTRIC MATERIAL

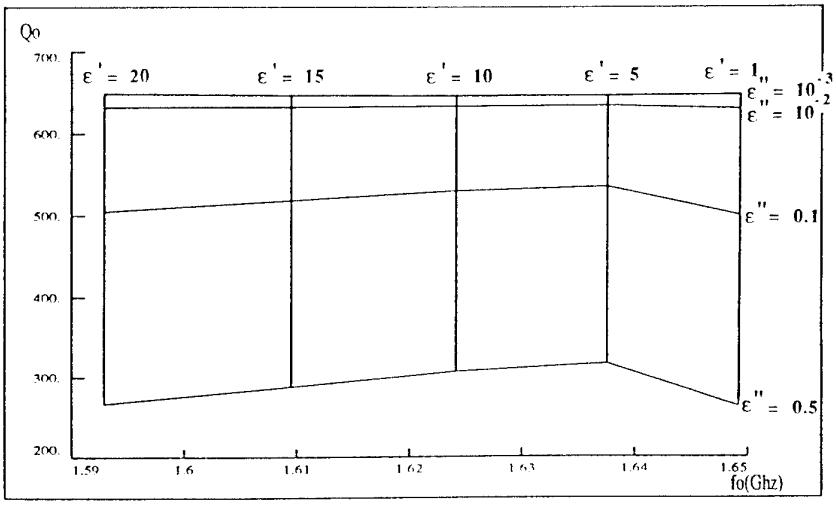

-fig 6-
Material Thickness = 3 mm

SAMPLE ON THE TOP SIDE OF THE DIELECTRIC PROBE

HIGH LOSS DIELECTRIC MATERIAL

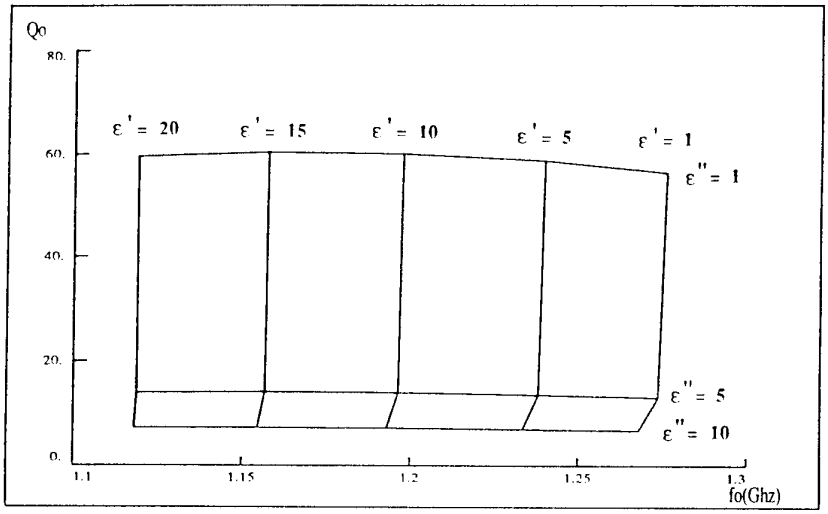

-fig 7-
Material Thickness = 3 mm

SAMPLE ALONG THE LATERAL SIDE OF THE DIELECTRIC PROBE

HIGH LOSS DIELECTRIC MATERIAL

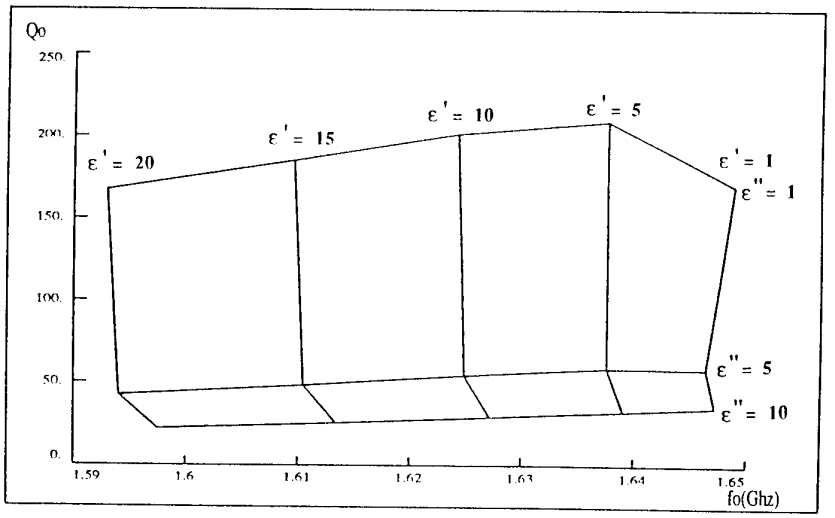

-fig 8-
Material Thickness = 3 mm

SAMPLE ON THE TOP SIDE OF THE DIELECTRIC PROBE

LOW LOSS MAGNETIC MATERIAL

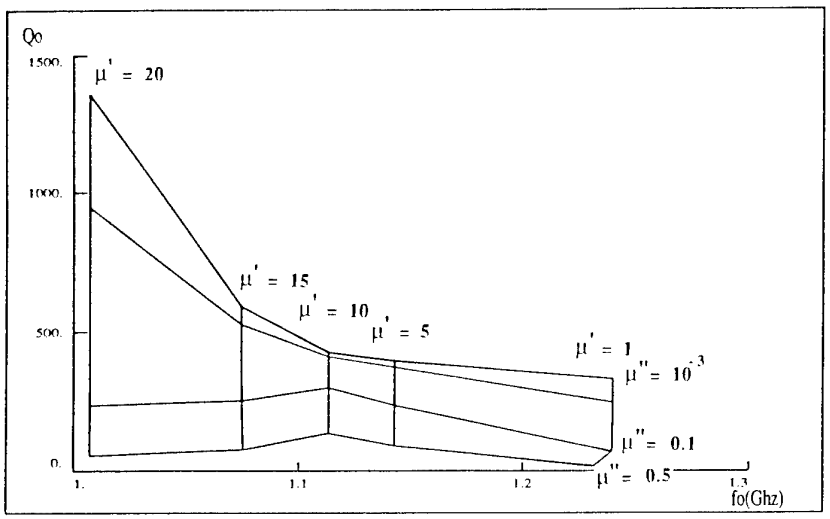

-fig 9-
Material Thickness = 3 mm

SAMPLE ALONG THE LATERAL SIDE OF THE DIELECTRIC PROBE

LOW LOSS MAGNETIC MATERIAL

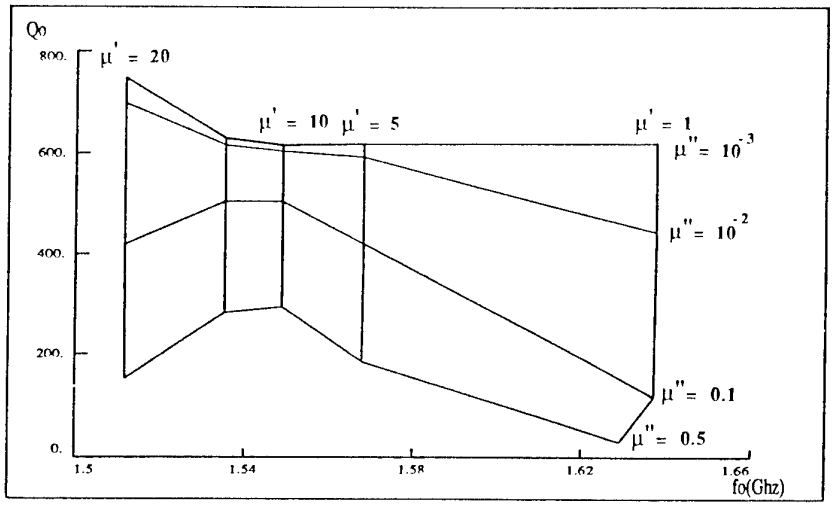

-fig 10-
Material Thickness = 3 mm

SAMPLE ON THE TOP SIDE OF THE DIELECTRIC PROBE

HIGH LOSS MAGNETIC MATERIAL

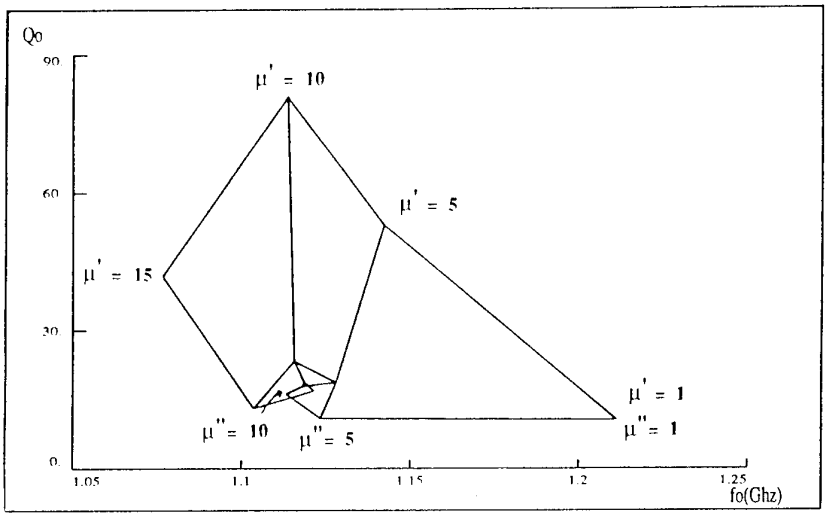

-fig 11-
Material Thickness = 3 mm

SAMPLE ALONG THE LATERAL SIDE OF THE DIELECTRIC PROBE

HIGH LOSS MAGNETIC MATERIAL

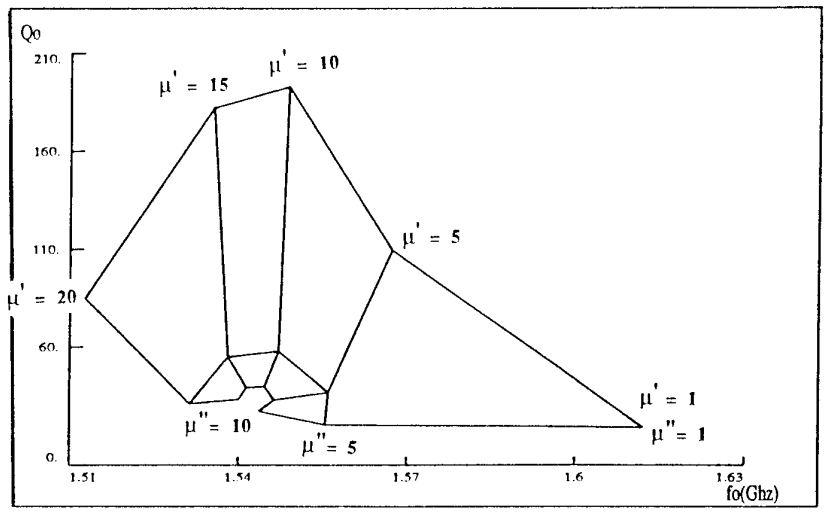

-fig 12-
Material Thickness = 3 mm

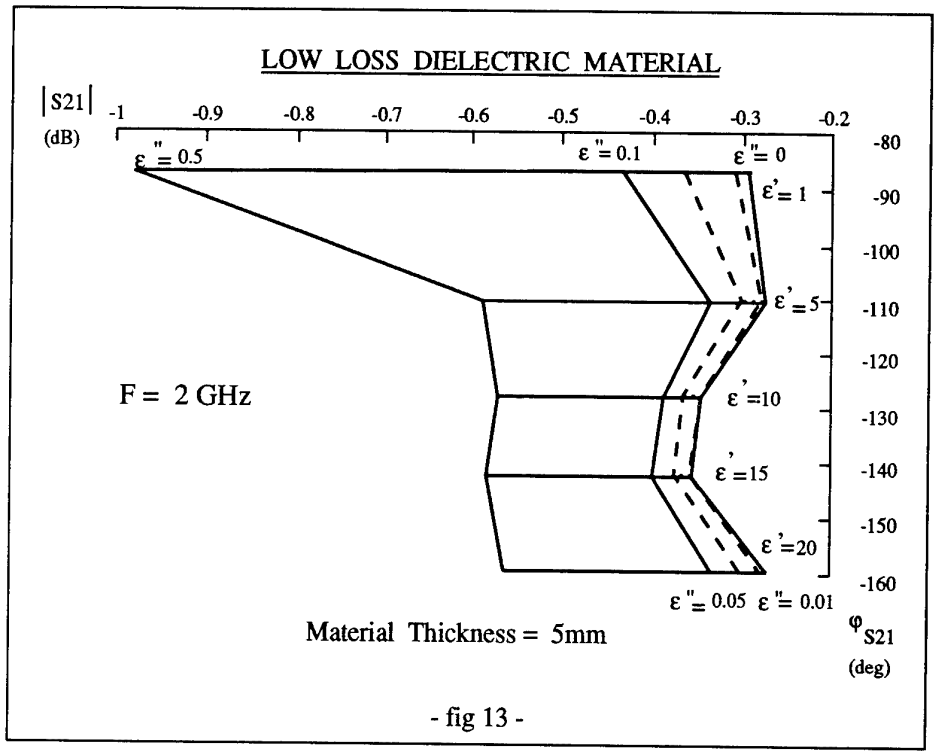
LOW LOSS DIELECTRIC MATERIAL
|S21| (dB)
-1 -0.9 -0.8 -0.7 -0.6 -0.5 -0.4 -0.3 -0.2
ε" = 0.5
ε" = 0.1
ε" = 0
ε' = 1
ε' = 5
ε' =10
ε' =15
ε' =20
-80 -90 -100 -110 -120 -130 -140 -150 -160
F = 2 GHz
ε" = 0.05 ε" = 0.01
Material Thickness = 5mm
φS21 (deg)

- fig 13 -

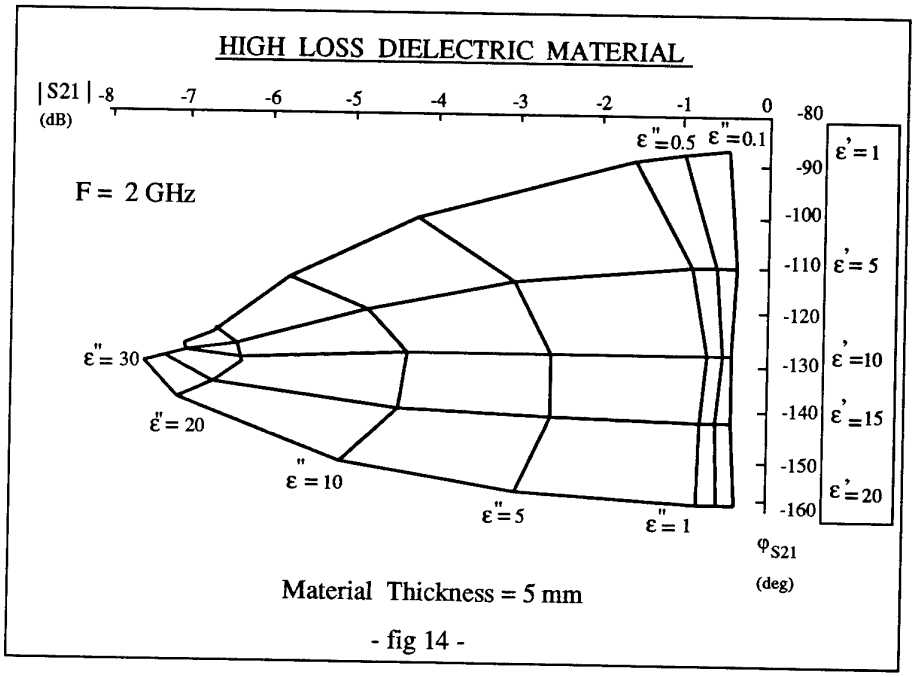
HIGH LOSS DIELECTRIC MATERIAL
|S21| (dB)
-8 -7 -6 -5 -4 -3 -2 -1 0
ε" =0.5 ε" =0.1
F = 2 GHz
ε" = 30
ε" = 20
ε" = 10
ε" = 5
ε" = 1
-80 -90 -100 -110 -120 -130 -140 -150 -160
ε' = 1
ε' = 5
ε' =10
ε' =15
ε' =20
φS21 (deg)
Material Thickness = 5 mm

- fig 14 -

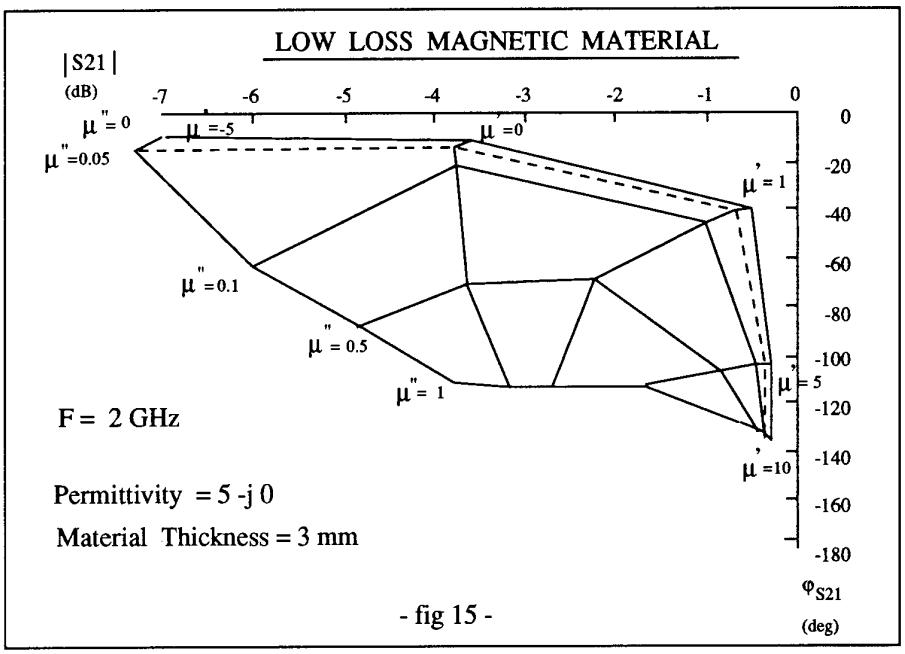
LOW LOSS MAGNETIC MATERIAL
|S21|
(dB)
-7
-6
-5
-4
-3
-2
-1
0
μ"=0
μ'=-5
μ'=0
μ"=0.05
μ'=1
μ"=0.1
μ"=0.5
μ"=1
μ'=5
μ'=10
0
-20
-40
-60
-80
-100
-120
-140
-160
-180
φS21
(deg)
F= 2 GHz
Permittivity = 5 -j 0
Material Thickness = 3 mm

- fig 15 -

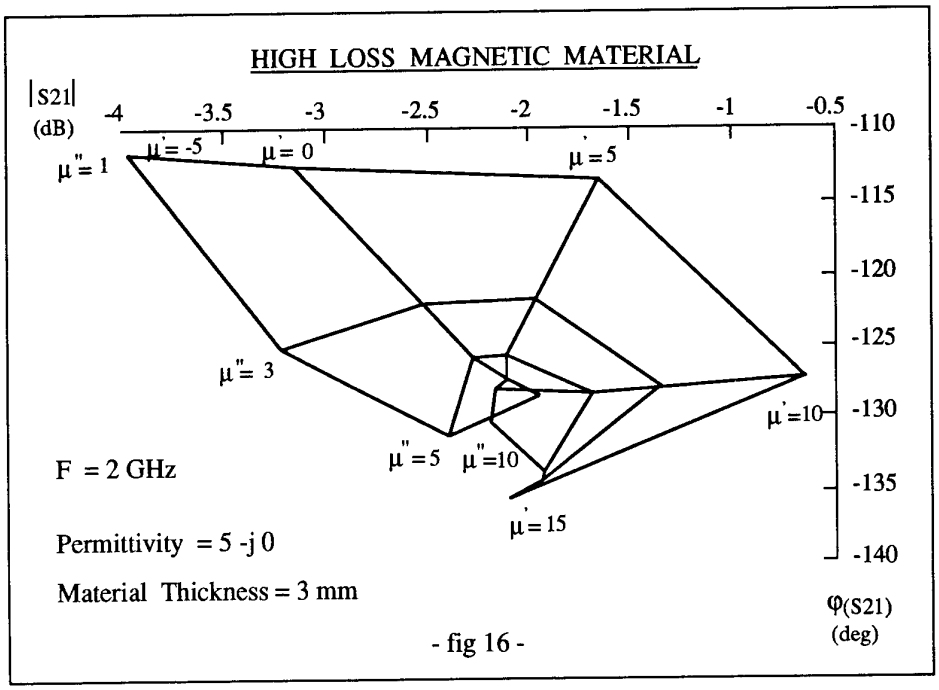
HIGH LOSS MAGNETIC MATERIAL
|S21|
(dB)
-4
-3.5
-3
-2.5
-2
-1.5
-1
-0.5
μ'=-5
μ'=0
μ'=5
μ"=1
μ"=3
μ'=10
μ"=5
μ"=10
μ'=15
-110
-115
-120
-125
-130
-135
-140
F = 2 GHz
Permittivity = 5 -j 0
Material Thickness = 3 mm
φ(S21)
(deg)

- fig 16 -

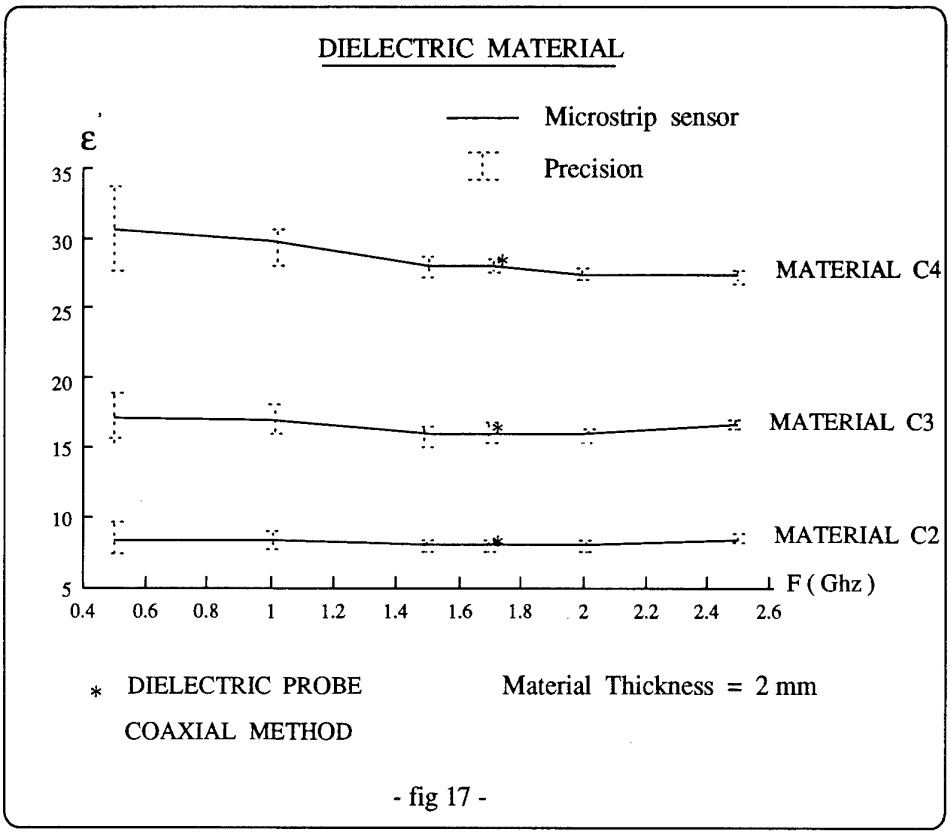
DIELECTRIC MATERIAL
ε'
Microstrip sensor
Precision
35
30
25
20
15
10
5
MATERIAL C4
MATERIAL C3
MATERIAL C2
F (Ghz)
0.4 0.6 0.8 1 1.2 1.4 1.6 1.8 2 2.2 2.4 2.6
* DIELECTRIC PROBE
COAXIAL METHOD
Material Thickness = 2 mm

- fig 17 -

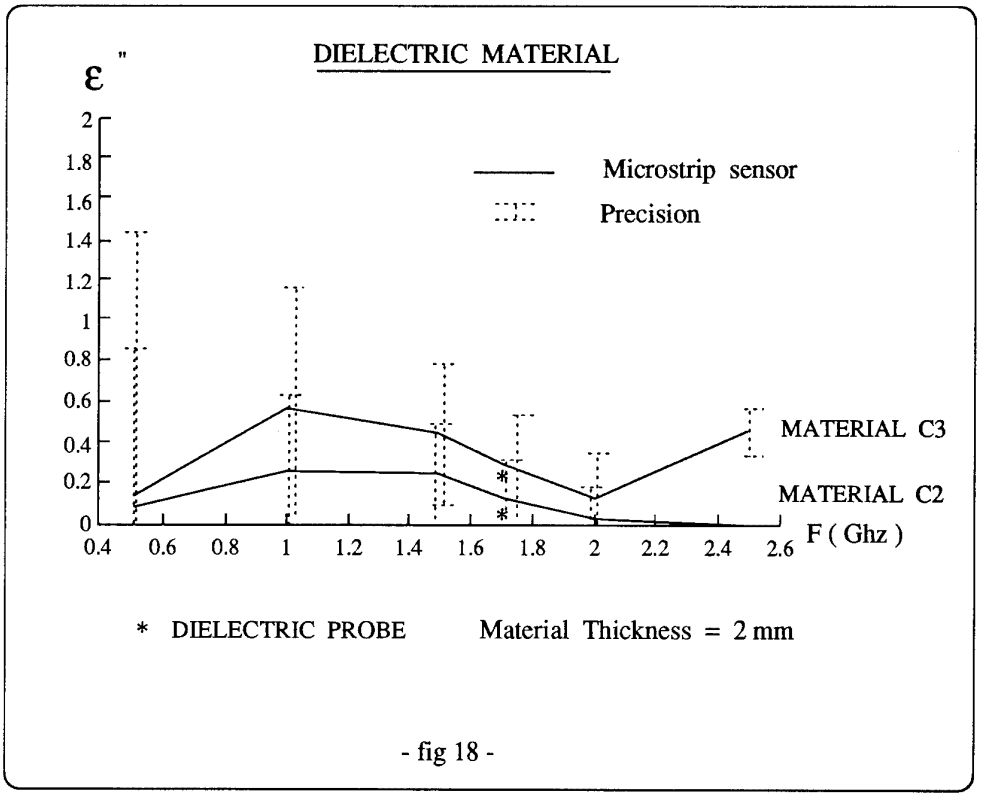
DIELECTRIC MATERIAL
ε"
Microstrip sensor
Precision
2
1.8
1.6
1.4
1.2
1
0.8
0.6
0.4
0.2
0
MATERIAL C3
MATERIAL C2
F (Ghz)
0.4 0.6 0.8 1 1.2 1.4 1.6 1.8 2 2.2 2.4 2.6
* DIELECTRIC PROBE
Material Thickness = 2 mm

- fig 18 -

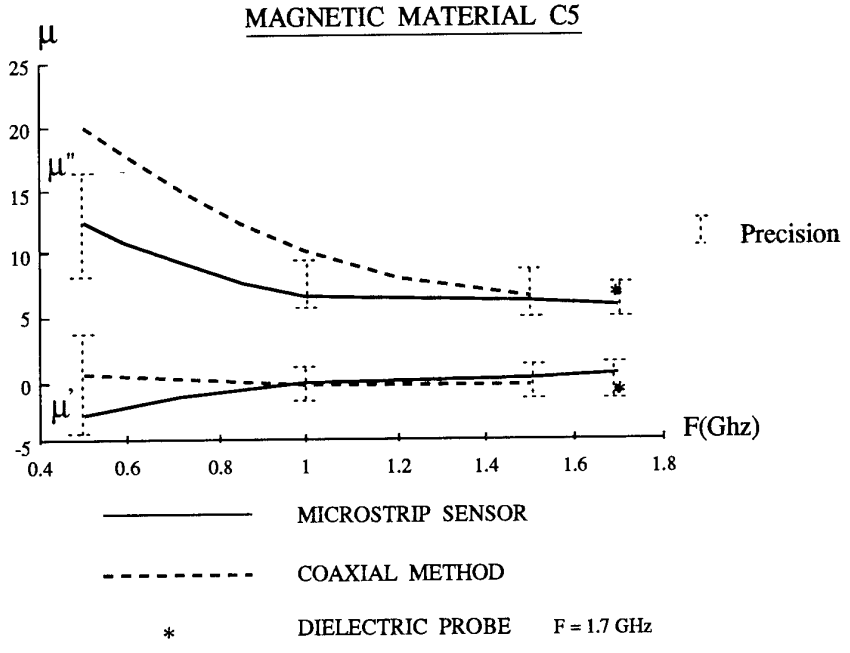
MAGNETIC MATERIAL C5
μ
25
20
15
10
5
0
-5
μ"
μ'
0.4
0.6
0.8
1
1.2
1.4
1.6
1.8
F(Ghz)
Precision
MICROSTRIP SENSOR
COAXIAL METHOD
DIELECTRIC PROBE
F = 1.7 GHz
Material Thickness = 4.75 mm

- fig 19 -

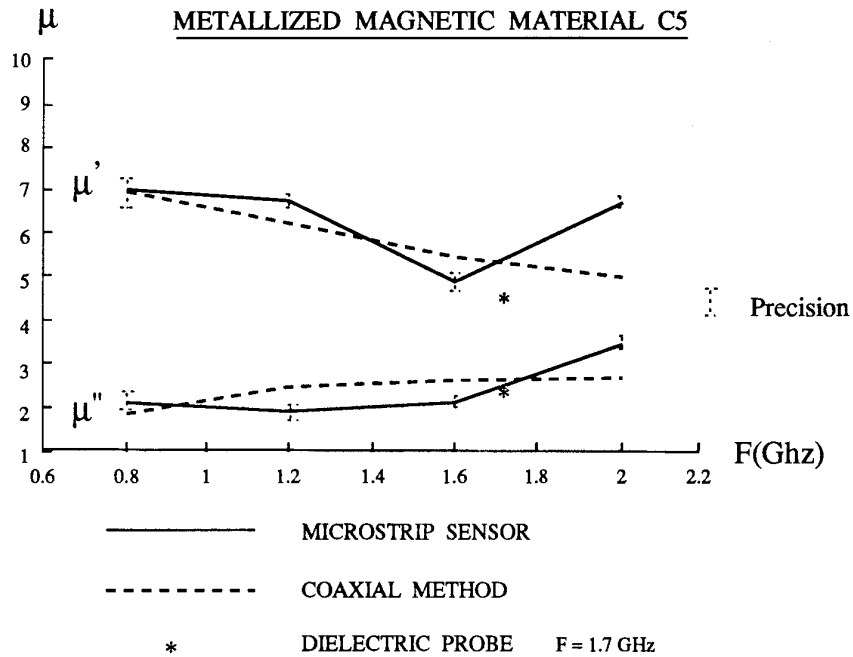
METALLIZED MAGNETIC MATERIAL C5
μ
10
9
8
7
6
5
4
3
2
1
μ'
μ"
0.6
0.8
1
1.2
1.4
1.6
1.8
2
2.2
F(Ghz)
Precision
MICROSTRIP SENSOR
COAXIAL METHOD
DIELECTRIC PROBE
F = 1.7 GHz
Material Thickness = 1.96 mm

- fig 20 -

Accuracy of computer codes that calculate electromagnetic cross sections of nonspherical particles.

J.F. Embury, J.D. Rainey and O.I. Sindoni
Edgewood Research Development and Engineering Center
Attn: SCBRD RTB
Aberdeen Proving Ground, Md 21010
USA

Accuracy of the electromagnetic cross sections of spheroidal particles computed using the discrete dipole approximation and the extended boundary condition method are checked in the high and low frequency limits and in the limit where the shape becomes spherical. We compute electromagnetic cross sections and intensity scattering matrix elements of spheroids with aspect ratios (major to minor axis ratios) up to four averaged over random orientations for a range of sizes where the major and minor axes are much greater than the wavelength and much less than the wavelength. Complex refractive indices typical of dielectric matrial in the visible and infrared spectral regions have been chosen. Accuracy is judged based on comparisons with Mie theory calculations in the limit when aspect ratio approaches unity, with the Rayleigh spheroid theory in the limit when both size parameter and phase shifts are small, with the geometric optics theory in the limit when both size parameter and phase shifts are large, and finally in the anomalous diffraction theory in the limit of large size parameter and complex refractive index near unity. In addition we use constraint inequalities involving the intensity scattering matrix elements to check the validity of randomly oriented spheroid calculations.

I. INTRODUCTION

The spheroid provides a flexible model for convex non-spherical particle shapes encompassing prolate cigar shapes approximating rods, oblate pancake shapes approximating discs and the sphere. Today there are three popular ways to compute electromagnetic cross sections of spheroids; the solution using boundary values and separation of variables [1]; the extended boundary condition method (EBCM) [2] or T matrix approach and the discrete dipole approximation (DDA) [3–5]. Here we will discuss EBCM and DDA results with emphasis on validation by cross comparisons and by comparisons with well known MIE [6] solutions in the limit of a spherical shape and the low frequencies or electrostatic solutions [6,7] for spheroids small compared to the wavelength. In addition we can check equality constraints [8] involving Mueller (intensity) scattering matrix elements in the case of fixed orientation spheroids, although this would only check the algebra relating amplitude to intensity scattering matrix elements. More importantly we can check inequality constraints [8] in the case of matrix elements averaged over random orintation. Validation at intermediate and higher frequencies should be possible using a combination of geometric optics [6] and anomalous diffraction [7] solutions to compare with the EBCM and DDA results. This effort has begun here with comparisons among the MIE, anomalous diffraction and geometric optics solutions for spherical scatterers.

II. DISCUSSION

We will be comparing the extinction, absorption and backscatter efficiencies computed for spheres in the first three figures where the cross sections are equal to the efficiencies multiplied by the geometric cross section and the units for extinction and absorption cross sections is area while the backscatter cross section is expressed as area per steradian. In figure 1 there is good accuracy in extinction and absorption efficiencies out a size parameter of about five using 8 x 8 x 8 dipoles in DDA and for EBCM we set convergence variables NRANK = 12 and NTHETA = 24. In figure 2 again using 8 x 8 x 8 dipoles in DDA the accuracy in efficiencies for extinction, absorption and backscatter are checked with backscatter error most pronounced. The effect of reducing the number of dipoles used by DDA below 8 x 8 x 8 is evident in figure 3 where significant differences in extinction and absorption efficiencies are evident for size parameters greater than about two.

The low frequency or electrostatic spheroid solution can be used to check the accuracy in the region of small size parameters. In figure 4 we see that the 8 x 8 x 8 dipole DDA calculation for an oblate spheroid converges with the electrostatic result for size parameters under 1/3. Here size parameter is defined in terms of the diameter of an equal volume sphere. The average Mueller (intensity) scattering matrix for a randomly oriented spheroid involves eight non-zero elements S_{11} , S_{12} , S_{22} , S_{33} , S_{34} , S_{44} , $S_{43} = -S_{34}$ and $S_{21} = S_{12}$ of which six are independent [6]. In the case of a sphere the same elements remain non-zero but now only four of them are independent since $S_{44} = S_{33}$ and $S_{22} = S_{11}$ in addition to $S_{12} = S_{21}$ and $S_{43} = -S_{34}$. Figure 5 presents these four non-zero independent scattering matrix elements for a sphere normalized with respect to S_{11} and computed using EBCM (NRANK = 12, NTHETA = 24) and compares them with MIE theory predictions. At this size parameter of 1.5 there is excellent agreement. Four of the six independent EBCM scattering matrix elements P_{ij} for a prolate a/b = 4 randomly oriented spheroid, are normalized with respect to P_{11} and shown in figure 6 which compares these elements

Paper presented at the AGARD SPP Symposium on "Environmental Factors in Electronic Warfare Related to Aerospace Systems" held in Pratica di Mare AFB (Rome) Italy, from 8-11 May 1995, and published in CP-573.

with those computed using the electrostatic spheroid approximation at an equal volume sphere size parameter of 0.1.

Although accuracy of efficiency factors for extinction, absorption and backscatter might be the only concern for some applications and although accuracy of all Mueller scattering matrix elements provides a basis for estimating total error of any scattering calculation, additional parameters such as asymmetry factor, single scatter albedo and backscatter to total scatter ratio can be of great concern for applications such as radiative transfer and lidar. In figure 7 these parameters have been computed for spheres over a range of size parameters using the MIE theory. In figure 8 the same calculations have been performed using the discrete dipole approximation with an 8 x 8 x 8 dipole array.

An important although not yet well known analysis [8] provides another check on accuracy. Because there are only four complex elements in the amplitude scattering matrix transforming the incident electric field into the scattered electric field and because there are 16 real elements in the intensity (Mueller) scattering matrix transforming the incident Stokes parameters into the scattered Stokes parameters, we can expect constraining conditions on the Mueller matrix elements since only seven of the elements can be independent. Without absolute phase and only relative phase information the amplitude scattering matrix has seven independent variables involving amplitude and relative phase of orthogonal polarized electric fields. Therefore we expect equations relating the amplitude scattering matrix elements to the intensity scattering matrix elements [6] will provide nine equality constraints but as it turns out this is only for a single fixed orientation scatterer. When averaging over random orientation the nine equality constraints become six inequality constraints that are actually more useful in checking validity of our DDA and EBCM calculations. Since half of the 16 Mueller matrix elements are zero for a randomly oriented isotropic spheroid and only six of these eight non-zero elements are independent [6] we find that two pairs of the six inequality constraints are identical yielding four inequalities listed below.

$$(S_{11}+S_{22})^2-(2S_{12})^2-(S_{33}+S_{44})^2-(-2S_{34})^2\geq 0$$

$$(S_{11}-S_{22})^2-(S_{33}-S_{44})^2\geq 0$$

$$(S_{11}+S_{21})^2-(S_{12}+S_{22})^2\geq 0$$

$$(S_{11}-S_{12})^2-(S_{12}-S_{22})^2\geq 0$$

We can see in figure 9 that all four inequalities, normalized with respect to P_{11} , are satisfied since all remain positive for this EBCM calculation of a prolate a/b=2 randomly oriented spheroid.

In the limit of large size parameters the theories of geometric optics and anomalous diffraction (when refractive index is close to unity) can be adapted to non-spherical shapes to provide accuracy checks for DDA and EBCM calculations. The geometric optics solution for a weakly absorbing sphere [6] is compared in figure 10 to MIE computation results with good agreement almost all the way to where the sphere becomes opaque and a second geometric optics solution independent of size parameter must be used. Additional accuracy checks provided by geometric optics include the limit value of two for extinction efficiency and the differential scattering cross section represented by a combination of Fresnel reflection (for an opaque scatterer we ignore refraction) and diffraction. Results computed using the anomalous diffraction approximation are plotted beside those computed from the MIE solution in figure 11. Even though the refractive index is not very close to unity and therefore does not strictly satisfy that requirement of anomalous diffraction theory the efficiencies are close for the larger size parameters.

III. CONCLUSION

We have presented a number of validity tests that we currently use to check the accuracy of our EBCM and DDA scattering calculations. With these tests we can adjust convergence criteria for EBCM and the number of dipoles in the three dimensional array used by DDA in order to trade off accuracy and computation time when it is an issue. Once convinced of the accuracy of EBCM and DDA we can work in the opposite direction and determine the range of accuracy of the various limit theories such as Rayleigh at low frequencies and geometric optics at high frequencies.

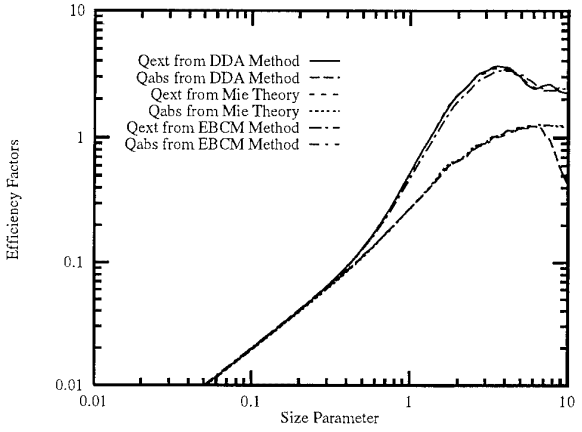

Figure 1. Extinction and Abosrption Efficiencies for Spheres with m = 1.55 +.10i. Computed using Mie Theory and the Discrete Dipole Approximation Method (DDA) and Extended Boundary Condition Method (EBCM).

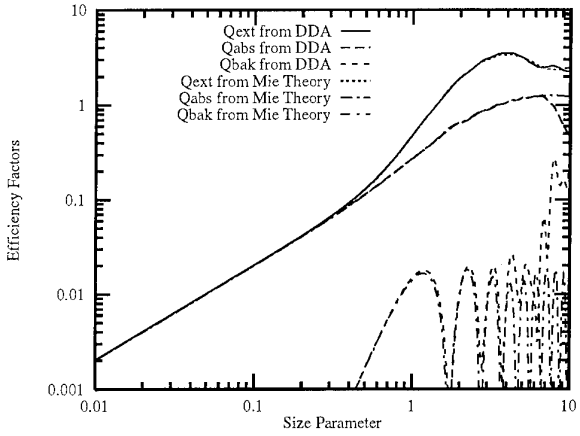

Figure 2. Extinction and Absorption and Backscatter Efficiencies for spheres with m = 1.5 + .1i. Computed using the Mie Theory and the Discrete Dipole Approximation Method (DDA).

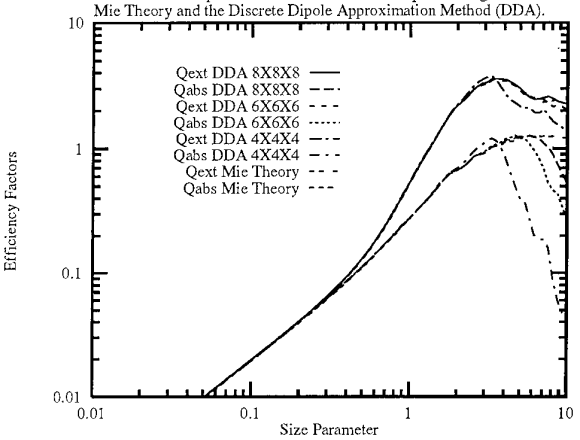

Figure 3. Extinction and Absorption Efficiencies for Spheres with m = 1.55 +.10i. Computed using the Discrete Dipole Approximation Method(DDA) and Mie Theory.

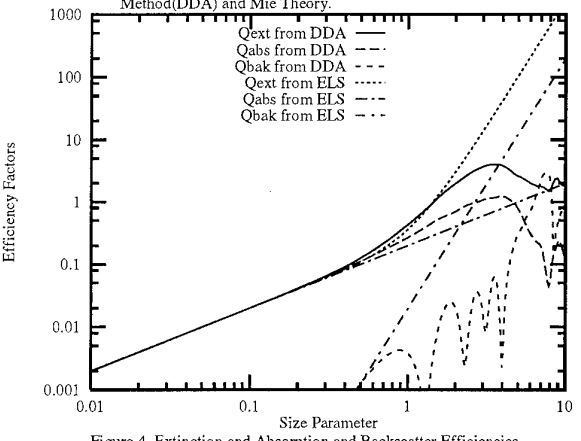

Figure 4. Extinction and Absorption and Backscatter Efficiencies for spheroids with a/b = .250 and refractive index m = 1.50 + .10i averaged over random orientation. Computed using the Discrete Dipole Approximation Method (DDA) and the Electrostatic Approximation (ELS).

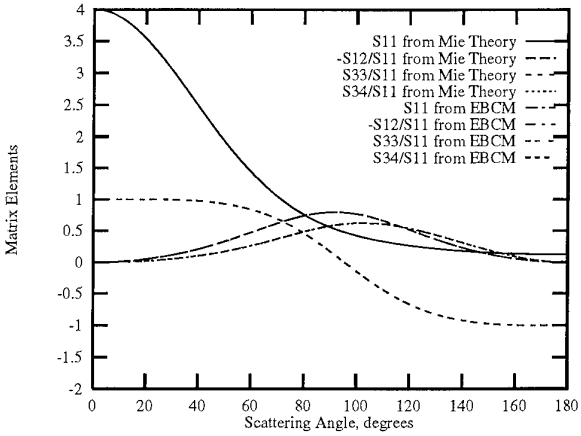

Figures 5. Scattering Matrix Elements obtained from the Mie Theory and the Extended Boundary Condition Method (EBCM) for spheres with size parameter x = 1.5 and refractive index m = 1.5 + .5i.

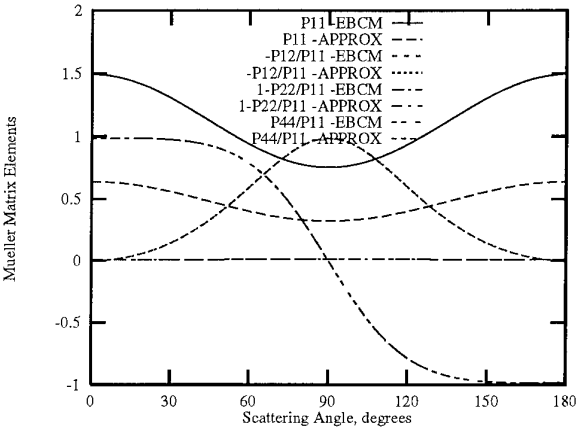

Figure 6. Mueller Scattering Matrix Elements obtained from the Extended Boundary Condition Method (EBCM) and the Electrostatics Approximation for a spheroidal particle with a/b = 4,refractive index m = 1.50 + .01i, and size parameter x = .10.

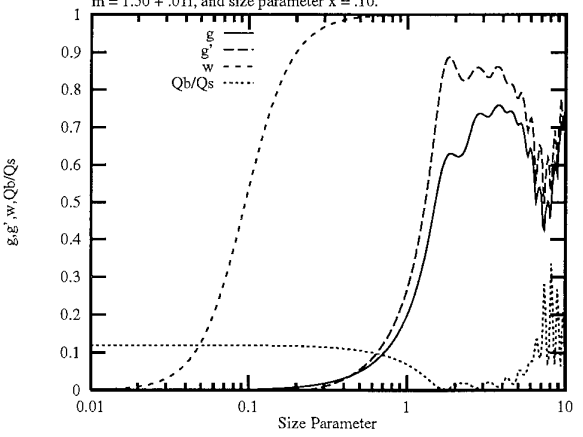

Figure 7. Asymmetry factor g,forward hemisphere-back hemisphere scatter fraction g',albedo w, and backscatter/total scatter ratio Qb/Qs computed for a sphere with refractive index m = 1.50 + .0001i by Mie Theory

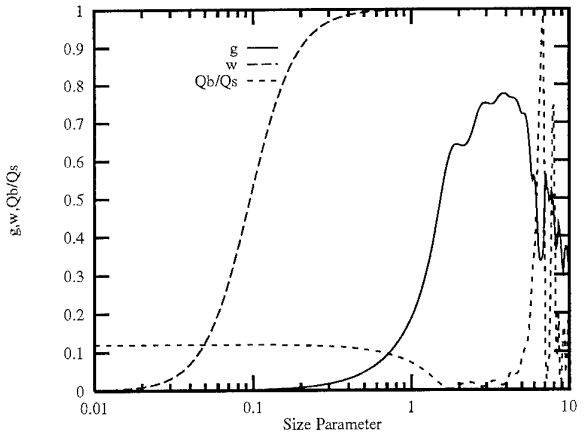

Figure 8. Asymmetry factor g, albedo w, and backscatter/total scatter ratio Qb/Qs computed for a sphere with refractive index m = 1.50 + .0001i by the Discrete Dipole Approximation Method (DDA).

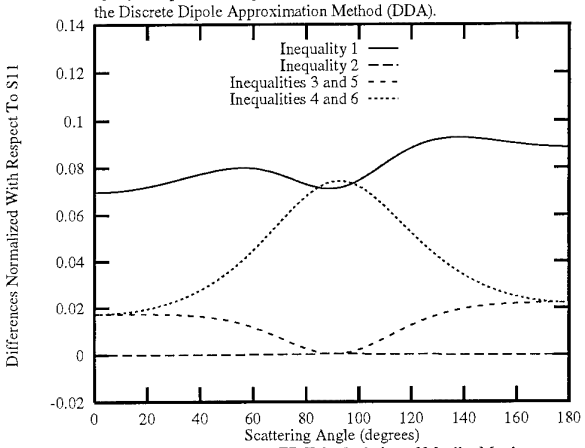

Figure 9. Validity check on EBCM calculation of Mueller Matrix Elements for Random and Fixed Orientation Spheroid with a/b = 2, m = 1.5 + .1i,and x = 1.

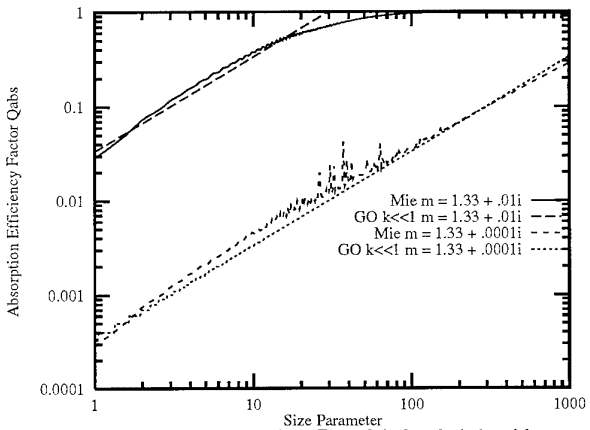

Figure 10. Absorption Efficiency Factor Qabs for spherical particles computed using Mie Theory and the weakly absorbing sphere geometric optics approximation (GO).

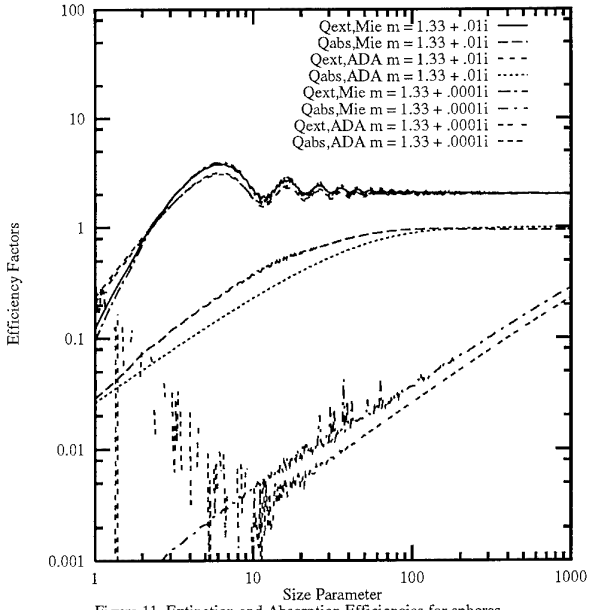

Figure 11. Extinction and Absorption Efficiencies for spheres computed using the Mie theory and the Anomalous Diffraction approximation (ADA) for 2 different refractive indexes.

[1] S. Asano and G. Yamamoto 1975, Appl. Opt. ,14,29

[2] P. W. Barber and S. C. Hill , "Light Scattering by Small Particles: Computational Methods", (World Scientific, Singapore, 1990)

[3] E. M. Purcell and C. R. Pennypacker 1973, Ap. J., 186, 705

[4] B. T. Draine 1988, Ap. J. , 333, 848

[5] B. T. Draine and P. J. Flatau 1994, JOSA A, 11,1491

[6] C. F. Bohren and D. R. Huffman, "Absorption and Scattering of Light by Small Particles ", (Wiley, NewYork, 1983)

[7] H. C. van de Hulst, "Light Scattering by Small Particles", (Wiley, NewYork, 1957)

[8] E. S. Fry and G. W. Kattawar 1981, Appl. Opt., 20,2811

R.B.Gomez (US)

(1) You did not show any error bars in your calculations. What is the magnitude of your uncertainties ?

(2) Have you performed sensitivity studies to find out what parameters are driving the results of the calculations ? That is, what is driving the accuracy of the results, size distributions, optical properties (index of refraction), shape ...?

Author's Reply

(1) There are no uncertainties in the calculations which are all theoretical, therefore the results are accurate to the 8th significative digit.

(2) Yes, we have carried out such type of studies. In general, for a single particle the shape, followed by the optical properties (index of refraction) and size determine the results. For a cloud the determination depends on the density, on the size parameters (average), the optical properties (average) and a shape factor (average).

ENVIRONMENT MODELS AND THREAT SIMULATORS - HIGH QUALITY AND LOWER COST VALIDATION OF EW SYSTEMS

M. Pywell and N. Stubley
British Aerospace Defence (Military Aircraft Division)
W392D, Warton Aerodrome, Warton
Lancashire, PR4 1AX, United Kingdom

SUMMARY:

Recent conflicts such as the Falklands campaign, Gulf conflict and Bosnia have amply demonstrated the importance of EW to Mission Effectiveness and crew Survivability. In addition to this, since world-wide defence budgets are still reducing overall, the key driver for most Customers is Affordability. To a major aircraft prime contractor such as BAe Defence, these Customer requirements mean addressing a number of issues related to establishing the minimum necessary aircraft EW suite to satisfy those requirements. A key issue in this determination is a ***precise*** definition of the radar, RF and Electro-Optic (EO) electromagnetic environment that the aircraft must operate correctly in.

This paper addresses this aspect and the tools and techniques necessary to produce aircraft EW systems that not only conform to specification, i.e. have no defects, but also have adequate performance, i.e. are 'fit for purpose'. It concentrates on the RF environment (modelling and threat simulators) as relevant to the testing of ESM/RWR/ELINT and ECM systems, although the principles are equally applicable to the EO, i.e. Infra-Red (IR) and Ultra-Violet (UV) regimes, and this is also discussed. It outlines EW System specification, describes EW environment modelling and its role in the design and validation process, covers EW Test and Evaluation (T&E) improvements, identifies shortfalls in current modelling capabilities, and gives major thrusts aimed at improving the EW development process.

It addresses the issues above in the light of BAe Defence, Military Aircraft Division's experience in the field of both RF scenario modelling in support of a number of aircraft projects and planned ESM-ECM development work using scenario and equipment modelling, two world-class RF threat simulators, state-of-the-art ECM response measurement equipment and EW data analysis tools. It develops the argument that one of the main contributors to previous/current poor press on EW systems is believed to be the lack of ***adequate*** EW scenario definition at equipment/aircraft contract signature and that such definition should appear in specifications along side electromagnetic compatibility and other environmental issues.

1. INTRODUCTION

Successful validation of complex EW systems prior to combat is a major technical goal of Industry, Government and Military Engineers alike. Adequate EW systems' performance is crucial to mission effectiveness and crew survivability and is likely to remain so for the foreseeable future. Even as current and future aircraft strive for ever lower multi-spectral signatures it is considered that a plateau will soon be reached at which point mission success and survivability will again depend largely on the capability of the vehicle's EW systems.

For a variety of reasons, EW systems world-wide have justifiably received bad publicity for many years - mainly through appearing to offer substantial technical promises which either have not been, or could not have been, realised. The methods of validating these systems, particularly ESM/ECM systems, have given cause for concern to the Customer and User alike. In particular there has appeared to be poor repeatability and substantial mismatch of results between laboratory tests and in-Service behaviour of EW equipment.

In addition, the traditional validation methods involving extensive flight trials can no longer be afforded in the light of shrinking defence budgets and there is a thrust both in the U.S.A. and Europe to move much of this work to the modelling and ground test phase, by aircraft testing in an anechoic chamber and a combination of avionic rig and threat simulator tests. This work, which includes extensive scenario modelling and the increasing use of EW equipment models, offers great promise in reducing not only the expensive flight testing phase, but also overall EW development timescales and costs.

The affordability thrust also means that the following issues must be addressed, and this paper addresses primarily the last two:

- What is the minimum necessary EW suite to provide appropriate level of aircraft survivability?
- What are the trade-offs between various factors affecting the level of complexity of that suite and how are they related?
  - Radar Cross Section vs. Altitude vs. ECM capability
  - IR Signature vs. countermeasures capability, e.g. flares
  - Use of Stand-Off or Escort Jammers vs. fully capable Self-Protection Jammer
- What is the RF/EO environment (threat and other emitters) in which mission effectiveness and survivability are required?
- How to specify, design and validate the performance of an installed EW suite with highest quality and at minimum cost.

For EW systems validation to be achieved via this relatively new and more cost-effective route there is a need for better environment and emitter models, more capable and multi-spectral threat simulators for EW test and evaluation, realistic modelling of EW equipments and high power analysis capabilities. Although RF environment and threat simulation tools have existed for some time, it is only more recently that some of the more complex issues of environment modelling, such as terrain masking, have been addressed in any detail. Recent computing power increases now enable some of these computationally intensive tasks to be conducted in real time.

2. EW SYSTEMS

A typical modern aircraft EW suite is shown in Figure 1. Its prime objective is the immediate and unambiguous identification and classification of threat RF/EO emitters, and automatic engagement of countermeasures and/or timely set-on of own weapon systems, preferably via passive targeting.

A factor in common between Radar Warning Receivers (RWR), EW Support Measures (ESM) and Electronic Intelligence (ELINT) is their function of detecting and processing radar signals. Although differences exist, in terms of this paper their main functions are effectively the same and thus hereafter the term ESM is taken to mean all three. Missile Warning (MW) systems are sub-divided into pulse doppler radar Missile Approach Warners (MAW) and passive (IR/UV) Missile Launch Warner (MLW).

Paper presented at the AGARD SPP Symposium on "Environmental Factors in Electronic Warfare Related to Aerospace Systems" held in Pratica di Mare AFB (Rome) Italy, from 8-11 May 1995, and published in CP-573.

3. SPECIFICATION OF EW SYSTEMS

Detailed knowledge of the following three items is crucial to the precise specification of EW suites, of whatever complexity:

- The RF/EO threat scenario(s), including geopolitical data to enable determination of non-military emitters in the theatre of operations for inclusion in the scenario(s),
- High quality RF/EO emitter parametric data, and
- Equally high quality operational analysis, covering tactics and the determination of Electronic Order of Battle.

This information is used to generate time ordered histories of engagements which form quantitative benchmarks of performance for the aircraft and its installed EW suite. Such benchmarks for ESM/ECM systems include pulse density (pulses per second) vs. frequency sub-bands vs. time, instantaneous dynamic range requirements vs. time, number of simultaneous pulsed and CW emitters vs. time, etc.

An ideal EW equipment specification is one where these time histories are included pre-contract, such that no ambiguity on performance issues can exist, and such that the aircraft and EW equipment suppliers can understand fully and concisely what is expected of their products, i.e. what is the definition of 'fit for purpose' for that aircraft when performing stated roles and missions. This level of specification, which requires significant modelling capability and effort, is rarely seen in specifications and less often, if ever, included pre-contract award. It is seen as an area where aircraft and EW equipment manufacturers, in concert with Defence Ministry and Air Force agencies, can enact major improvements in aircraft EW performance in terms of Affordability and reduced development timescales, balanced Survivability and Operational Effectiveness. Use of the modelling tools and techniques described later, during the Staff Target/Requirements phases of projects, is seen as a potential enabler of these major improvements.

4. EW ENVIRONMENT MODELLING AND ITS ROLE IN THE SPECIFICATION/VALIDATION PROCESS

4.1 Use of Modelling in the Specification/Validation Process

BAe Defence (Military Aircraft Division), in its role as a major aircraft manufacturer and systems integrator, has a suite of appropriate models and simulators to support the conceptualisation, design and development of whole aircraft and their systems. The two modelling tools of most relevance here are BAe's Airborne Weapon System Engagement Model (AWSEM) and the EW Evaluation System (EWES) by Data Sciences (U.K.) Ltd.

AWSEM, which runs on an IBM Model 5 Mainframe, enables operational analysts to take a Customer's threat scenario and tactical information and create an Electronic Order of Battle for input to the EWES. Figure 2 gives a block diagram of the EWES suite of programmes and AWSEM as used by BAe. Figure 3 shows the considerable computing resources required to support such modelling capabilities as EWES. Slow run times for complex scenarios has, for example, led to a 1995 EWES upgrade, *inter alia*, to a DEC Alpha main host.

4.2 Use in Validation of ESM Systems

Figure 4 shows the typical arrangement and interaction of receiver model and EW receiver equipment in the validation process, whether at EW equipment supplier, ground avionic integration rig or aircraft ground/flight test stage. This shows how emitter and scenario data is input to both the EWES tool and RF threat simulator, and how the output of each is fed into the EWES or ESM Receiver Model and real avionic equipment respectively. The output of the Receiver model and real equipment, primarily in the form of time-ordered emitter track files with associated RF parametric and identification data, is correlated off-line via use of EW Analysis Post-Processor (EWAPP) and/or comprehensive EW [test] Data Merge, Analysis, Correlation and Statistics package (DMACS). By pre-determining allowable modelling and test error budgets and pass/fail criteria, a suitable regime for the quantitative demonstration of performance to specification can be determined through the comparison of modelled data with those acquired from rig or aircraft testing of the EW system.

Where full ESM performance cannot be cost-effectively demonstrated via hardware tests, such as in the area of maximum pulse densities, it is necessary to use EWES and the receiver model as the verification tool. This requires that the receiver model is validated. This can be achieved by driving both real and modelled receivers with the same emitter scenarios and comparing their outputs.

A typical EWES 'ESPRIT' (man/machine interface) tactical scenario page is given in Figures 5 and typical outputs of the EW Scenario Generator and Analysis Post-Processor are shown in Figures 6 (pulse descriptor file for input to Receiver Model) and 7 (two commonly used analysis pages) respectively.

4.3 The Need for High Quality Emitter Parametric Data

As stated in section 3, high quality emitter parametric data is crucial to precise specification of both RF and EO EW systems. The performance and effectiveness of EW systems in ensuring survivability and first time mission success is directly related to the quality of the emitter data used in the specification and design of, and subsequent programming into modern EW systems. This level of importance is recognised world-wide and most new EW equipments are now flight line re-programmable with the latest emitter data of the highest quality. Such parametrics include primary items such as frequency, pulse width, pulse repetition rate and scan parameters, and more difficult parameters to measure and/or determine, such as pulse jitter/stagger rate/pattern, frequency agility, and modulation on pulse.

Since many radar and RF emitters occupy a fairly small portion of the total electromagnetic spectrum it is hardly surprising that many emitters have broadly similar radar/RF parametrics. This in turn poses one of the most difficult tasks for an ESM system - that of unambiguously identifying a given emitter, often in the presence of many other emitters (including the aircraft's own transmissions). Quality and validated emitter parametrics used both in the specification and design stages, ensures that the ESM-ECM receiver has a measurement capability equal to (if not in excess of) the maximum range of each parametric it is specified to handle, but also that it can use the latest 'picture' of a given emitter to form a multi-parametric 'window' to aid in the identification/classification process within the ESM.

Parametric data on Red (potentially hostile), Blue (own/friendly) and Grey (neutral/other) emitters is collected through various intelligence gathering, including interception of actual transmissions by the threat radar - the ELINT mission. Data is analysed and collated into an Emitter Data Base (EDB). These are usually of the highest national and/or NATO security classification. The data gathering, analysis and database functions are complex and costly, yet essential [1].

Such data is only released to Industry on a project by project and strictly need-to-know basis, in relation to specific EW and aircraft contracts. This poses a problem to Industry where bid preparation and other pre-contract work often requires such data to enable the determination of the level of EW suite complexity and thus the level of test effort and resources/facilities required - both of which directly impact upon the bid price. It is therefore in the interest of Governments and Industry alike that suitably sanitised data is available during the bid and pre-contract phases of a programme. Although it is possible to construct unclassified emitter databases with a reasonable level of confidence in quality/fidelity of the data, a far better solution to enable a minimum of over-specification for Industry and Services alike is believed to be the production of down-graded versions of the national database(s).

When using such data in support of EW system specification, design and validation, it is important to maintain adequate configuration control of the database. A method of assessing the impact of adding a new emitter, changed parametrics or behaviour of an emitter in a given scenario is required that gives confidence that the EW system still remains fit for purpose, as a change in parametric(s) can result in a significant change to the overall electromagnetic environment seen by the aircraft during a given mission.

4.4 EO and Combined RF/EO Environment modelling

To date most attention has been paid to radar/RF threat scenario definition, modelling and T&E facilities. The recognition that the majority of aircraft kills since the Vietnam war have been to IR-guided missiles, combined with the apparently ever-increasing use of lasers as primary or adjunct targeting systems, necessitates the development and use of EO modelling and test capabilities akin to those already well established for the radar/RF bands.

Survivability in future conflicts is likely to be best ensured when aircraft and their EW systems have the scenarios described in section 3 defined in multi-spectral terms. Such scenarios would therefore fully describe the electromagnetic environment that the aircraft must operate correctly in and would include (as a minimum) the RF bands from HF, through the established microwave band (primarily C-J band with the more recent expansion of emitters into k-band), selected parts of the upper millimetre wave band (atmospheric windows in the 90-150 GHz area), various IR wavelengths (lasers, terrestrial heat sources, IR signatures of aircraft and inbound missiles) and UV wavelengths (lasers and missile motor plumes). Should such speculative directed energy weapons as High Power Microwave, Non-Nuclear Electromagnetic Pulse and laser dazzle/damage [2],[3],[4] prove to be viable, then these too would need to be included in the scenario specifications.

These multi-spectral scenarios will enable precise specification of not only ESM, but also Laser Warners and IR/UV Missile Launch/Approach Warners, and will enable appropriate specification of multi-spectral test equipment for T&E work, particularly in the area of sensor correlation, data fusion and crew situation awareness. Such scenario definition, modelling and T&E capabilities will become increasingly important for future aircraft where affordability, lethality, flexibility, availability and survivability considerations drive aircraft manufacturers toward much more highly integrated and covert sensors/systems, and faster reaction weapons systems than seen to date. Precise specification of systems of this level of capability, authority and probable automation - especially in the EW area - is seen as a prime requirement in minimising development costs/timescales and ensuring that the aircraft is fit for purpose. This argument is seen to be equally applicable to the upgrading of current aircraft, where increased EW capability and/or integration of EW elements is popular world-wide and predicted to remain so for the foreseeable future. To support the production of such EO scenarios the same fidelity level of data on EO sources is required as for the RF/radar emitter case, see section 4.3

4.5 Modelling Shortfalls

There are seen to be three main issues at present, which affect both environment/EW equipment models and simulators used for T&E and model validation:

Emitter/threat system fidelity: Somewhere between simple simulation and reverse engineering real equipment lies a cost effective 'simulation' of, for example, a threat radar system. For EW system performance specification and testing, a radar emitter needs much more than merely being modelled as a zero scan, fixed frequency/pulse width/pulse repetition rate isotropic point source. Levels of complexity of the simulation necessary, which in many cases approach *emulation* (i.e. an accurate representation of the emitter in every way the sensor/weapon system can determine), is largely limited by computing power, both in EWES-type tools and RF threat simulators. An example is the relatively small amount of data points which can be used to represent both emitter and own aircraft ESM antenna beam patterns. Typically large values are 500k points for a sensor antenna, split between the azimuth and elevation gains vs. frequency (i.e. a maximum resolution of 1 degree, 0.25dBi and 0.5 GHz), and 4k points per full beam pattern for each emitter in the scenario (i.e. maximum resolution of 0.5 degree, 0.1dBi and 0.5 GHz).

In the U.S.A. the validation of threat simulators to be able to faithfully replicate a given threat is overseen by the CROSSBOW-S committee [5]. When extensive comparisons between the real threat and the simulator's version are complete (often >12 months per threat), they make recommendations for approval to the DoD Executive Committee on Threat Simulators, which manages and approves all DoD development of surrogate systems.

Scenario fidelity: Fidelity of the scenario is a trade-off of computing power vs. capability. To be truly representative all platforms must move correctly within the scenario, with such items as accurately modelled turn manoeuvres, 6-degrees of freedom on the own aircraft with at least 3 degrees of freedom for the 'enemy' airborne systems, terrain modelling/masking, missile fly-out models, etc. Ranges, resolutions and accuracies of all parameters within the scenario need to be at least equal to, or preferably better than those of the aircraft/EW system being modelled or tested. All engagements/tactics (which lead to EOB definition) and movement/manoeuvres of all players must be faithful representations of those contained in the specification. Current EW modelling tools and simulators cannot fully satisfy these requirements and those of emitter/threat system *emulation* in real time, although the ongoing vast increases in computing power and speeds now becoming available offer much promise.

Modelling vs. Simulator Capabilities: If the modelling system (e.g. EWES) and RF/EO threat simulator form an integral part of the specification, design and development process, then it is important, if not crucial, that their capabilities in a number of specific areas are very similar if not the same. Without this capability matching there is a real risk that correlation of results from the environment/EW equipment modelling and simulator/real EW equipment tests may not be possible without a substantial increase in the number of tests conducted or unnecessarily large error bounds and/or pass/fail criteria.

This can come about, for example, if the emitters in the scenarios within the environment model and threat simulator start at different times and/or scan positions. When merged with the energy intercept algorithms for the sensor in the respective systems, it can easily be envisaged that the pulse descriptor time history from the environment model and simulator may well be different; possibly with marked differences (including missed pulses). Thus, if marginally or substantially different pulse descriptor files are presented to the ESM model and the real EW equipment via post-antenna injection or irradiation, then differences will result in the track file reports vs. time, making the correlation of modelled and test results difficult. This can also be exacerbated if the emitter and scenario processing within the simulator is not fully synchronised with its RF generation system.

By careful consideration of these aspects it is possible to enhance repeatability, minimise these effects and thus enable an appropriate level of correlation between modelled and test results, leading to adequate validation of EW systems' performance.

Modelling Enhancements Needed: BAe has conducted extensive investigations into the requirements for modelling and T&E capabilities necessary to support the conceptualisation, specification, design and development of modern RF EW systems, and have extended some of these investigations, which are continuing, into the EO/laser arena. The items of particular interest in the RF area are listed below. Most have been taken into account in the specification of two world-class RF threat simulators, an ECM response measurement system and a comprehensive EW data analysis capability. In addition an upgrade to our EWES capability includes changes relating to modelling vs. simulator issues described above.

1. Terrain modelling: Various terrain types and surface cultures within scenario; including reflectivity aspects and sea states. *Vertical* as well as horizontal plane modelling. Grid size, terrain map input (e.g. DMA and DTED).
2. Multipath: Forward ground bounce, own transmitter vertical ground bounce. Specular/diffuse reflections = signal phase difference and thus changed amplitude at ESM. Own and other emitter multipath from aircraft in close proximity (includes need for some level of RCS modelling of aircraft involved - complex).
3. Near field effects: dependent on frequency, transmit/receive antenna size; more relevant to large aircraft or low flyers.
4. Antenna patterns: Better emitter/sensor antenna beam pattern modelling: i.e. more data points per pattern.
5. Third party tracking: irradiation of ESM by emitter which is tracking/locked on to another aircraft in the scenario.
6. Atmospheric effects: Attenuation varying representatively with frequency; rainfall rates; ducting.
7. Chaff: Eject/bloom times and stream/drop characteristics.
8. Repeatability and Correlation: Ability to specify emitter boresight start values (e.g. all North, centre of scan on velocity vector of aircraft, or random). Same/similar parameter ranges/resolutions/accuracies as threat simulators.
9. Emitters/Sensors on platforms, particularly aircraft: Current systems largely employ 'point' platforms, e.g. each aircraft's emitters/sensors exist at one point in space. Need for wire grid 'model' of (at least) own aircraft on which emitters and sensor antennas may be placed. Need substantial computing power increase to enable this.
10. Improved Modulation on Pulse: Improved fidelity needed.
11. ECM Effectiveness: Closed loop effects of own (and hostile) ECM on emitter behaviour and performance is required if quantitative metrics of survivability are to be specified and demonstrated in the future; cf. also 6.2
12. Missile Modelling: Adequate fly-out model needed for missiles with active seekers. Proportional navigation homing is suggested minimum. Model needs to be same as that used in threat simulator.

5. COMMONALITY OF EW AND EMC ENVIRONMENT PREDICTION NEEDS

5.1 Realistic Environment and Probability of Exposure

Specification of the minimum necessary RF environment(s) in which aircraft have to operate is also a key issue in the cost and development timescales of new and/or modified aircraft and their avionics [6]. Modern Electromagnetic Compatibility (EMC) specifications, which are most often based on a worst case consideration with additional safety margins, simulate conditions which rarely, if ever, occur in real life. A number contain single value field strength levels across significant parts of the RF and radar bands, even though in some sub-bands transmitters do not exist. Thus there appears the possibility for cost/timescale reductions, which could be applicable across all military platforms, if a better RF environment prediction were to exist or be developed.

The time line field strength/power density vs. frequency profile the aircraft is subjected to during its various mission types and phases, for peace- and war-time conditions, also affects RADHAZ. This is required to be known to ensure that aircrew are not hazarded and that there is no unacceptable hazard posed to on-board fuel systems and weapons/systems containing electro-explosive devices. For both EMC and RADHAZ, the item requiring determination therefore is, as for EW, the

profile of power density vs. frequency vs. exposure time, i.e. the ***probability of exposure***, and, in the case of EMC, the consequent ***probability of upset*** of avionic circuitry when the aircraft is ***actually*** irradiated with such an exposure profile.

5.2 HIRTA/EUROCAE Prediction Methods/Limitations

Currently the RF environment drivers behind EMC specifications in the U.K. are the High Intensity Radio Transmission Area (HIRTA) scheme [7] for military aircraft and the European Civil Aircraft Equipment (EUROCAE) User's Guide [8] for civil aircraft. Of late the HIRTA scheme has assisted EUROCAE Working Group 33 in the definition of the European RF environment. In each of these schemes a worst case is statically modelled where transmitters are effectively assumed to be permanently pointing their boresights directly at the aircraft under consideration. Both use equations based on optical point source theory to give far field power density (P_d):

$$P_d = \frac{\text{Antenna Gain x Mean Transmitter Power}}{4\pi \text{ x Main Beam Slant Distance}^2}$$

with appropriate near field adaptations, particularly relevant for sub-GHz emitters, and antenna radiation patterns only for sub-0.6 GHz emitters where significant off-boresight elevation and azimuth sidelobes can be encountered. Calculations, which take into account multi-transmitter sites, are translated into HIRTA exclusion zones which are simple geometric shapes (right-cylindrical for ground/shipborne emitters and spherical for airborne emitters).

With the possible exception of hovering or slow moving helicopters at very low levels, this represents an extreme worst case assessment as military aircraft moving at over 300 knots above a few hundred feet altitude are unlikely to be irradiated at any appreciable level by ground emitters for more than a few seconds in reality. The two schemes therefore, although adequate for their intended purpose, i.e. ensuring safety when in proximity to high power RF/radar transmitters, are both considered very conservative, due to:

- no modelling of emitter/aircraft relative motion,
- no modelling of emitter scan patterns,
- inadequate transmit antenna modelling, and
- only using worst case RF parametrics rather than a realistic set vs. time (e.g. *constant* illumination by a CW source is unusual, whereas mode changes between search, track, lock and back to search are more realistic).
- other shortfalls, e.g. section 4.3: terrain, multipath, weather effects and modulation on pulse.

Since the EWES environment modelling capability addresses most of the shortfalls of these other tools/techniques, it is believed that there is significant scope for its use to develop ***realistic*** environment predictions upon which an estimation of probability of upset of avionics can be superimposed to yield higher quality EMC specifications. Aspects of BAe research are currently addressing this potential.

6. EW TEST AND EVALUATION IMPROVEMENTS

The development timescales of any avionic system is dominated by the T&E process, particularly so in the case of RF/EO EW systems. Table 1 shows the typical life cycle of aircraft EW systems prior to in-service use and shows T&E elements at the EW equipment supplier and the aircraft system integrator (avionic rig and aircraft ground/flight test). Operational Evaluation flying by Air Forces just prior to service use is a further T&E element. A major internal study of EW systems integration over many years and a number of aircraft types showed that many of the problems encountered, some 85%, could have been discovered much earlier in the development process, as shown in Table 2, by a combination of better T&E tools/techniques and specification/desgin methodologies. Although this underlined the possibility of verifying the majority of EW systems performance characteristics long before flight, through a combination of modelling, avionic rig and aircraft ground tests in anechoic chambers, it also showed that there would be a continued need for EW flight testing - albeit greatly reduced.

Table 3 shows locations and techniques which can be used to support the development process. To minimise development costs and timescales it is necessary to push as much as possible of the T&E work to the top of the table. BAe Defence (Military Aircraft Division) is making much progress in enabling this by the provision of new/updated EW test and modelling capabilities.

6.1 Threat Simulators

The need for, use and availability of RF threat simulators for laboratory, chamber, flight line and test/training range is widely recognised and documented [9-13]. Such simulation ranges from signal generators, a number of which now have both very wide frequency range (e.g. 100 kHz - 40 GHz) and internal pulse/frequency modulation capability, to arguably the two most capable systems at this time - the Advanced Multiple Environment Simulator (AMES II) by Advanced Systems Development Inc., and the Combat Electromagnetic Environment Simulator (CEESIM) by Amherst Inc. Figures 8 and 9 are block diagrams of these two systems, showing the substantial complexity of the test tools required to adequately stimulate modern ESM and ECM systems.

Having recognised the value of such simulators to the T&E process it is important from a cost standpoint, as world-class RF threat simulators are multi-million dollar items, to ensure that the simulator to be used at each point of the life cycle (see Table 3) is not over-specified. Here again is seen the importance of precise definition of the electromagnetic environment and scenarios, as the complexity and specification of the simulator required is directly driven by those items. From consideration of the scenarios and environment the key cost drivers of the simulator can be specified:

- Number and frequency sub-banding of RF channels, yielding the pulse density capability (of the order of 1-10 million pulses per second for modern ESM systems [14]).
- Number of simultaneous active emitters at any time.
- 'Concurrency' (how many of what type of emitter at any time) - a significant complexity/cost driver if a number of pulse doppler radars, CW emitters and lower pulse repetition frequency emitters need to be simulated simultaneously.
- Number of emitters and platforms per scenario.
- Pulse % drop-out tolerable by the EW equipment under test.

- Tolerable noise floor/bandwidth, intra- and inter-pulse noise levels, harmonics/spurious and inter-modulation signals.
- RF Output: 4, 6 or 8 port DOA; phase interferometer array.
- Power output, both for the post-antenna injection and (amplifier/transmission system) free space irradiation cases.

6.2 ECM Response Measurement

To evaluate ECM systems it is necessary to stimulate their receiver system, either ECM-specific or the ESM in the case of some modern ESM-ECM systems, and this is achieved by use of the simulators previously discussed. For high quality T&E work it is necessary to simultaneously stimulate ESM and ECM receiver elements for both post-antenna signal injection and irradiation cases. To enable this, special simulator frequency sub-banding, output power and combining arrangements may be required, especially if the simulator can combine other on-board aircraft transmitters and harmonics/intermodulation products thus caused into its outputs.

ECM response measurement can be achieved through use of spectrum analysers and, more recently, by comprehensive and easy to use pulse modulation analysers, e.g. Hewlett Packard 5373A. However such capability is only suitable for simple ECM engagements and is manually and experience intensive. To be able to sort and recognise an ECM technique from an RF environment containing many pulsed/CW emitters as well as transmissions from other aircraft emitters, then establish that the correct technique has been engaged spatially on the appropriate threat emitter is complex and well beyond the scope of such equipment. For this task a new generation of ECM Response Measurement System (RMS) has been specified and ordered by BAe which largely automates this task for laboratory and aircraft chamber/open air trials. Once again the environment and scenarios form the backbone of the specification of this equipment. By sampling the simulator output and the ambient RF environment, and through containing a pre-defined list of ECM techniques vs. their RF parametrics, the RMS is able to quickly identify ECM transmission by direction, time and emitter being jammed.

Currently the *effectiveness* of an ECM system is very difficult to measure absolutely. Survivability is a key issue in determining mission success and fleet affordability, but its quantification is made more difficult by the many interacting items affecting it (tactics, countermeasures engagement and/or deployment, SEAD/SOJ/ESJ support levels to the raid package, and so on). To quantify the survivability of an aircraft it is necessary to develop metrics which can be realistically specified and cost-effectively demonstrated with acceptable repeatability. Modelling has a role to play here [11],[15] but it is thought that a more realistic way forward, which would probably also achieve higher credibility with air crew, may be a statistical model determination based on chamber tests of a selected number of ECM types and technologies. Determination of the metrics and qualification/measurement of aircraft performance could be achieved via a modified threat simulator and RMS, where the threat simulator output is modified by the ECM transmitted from the aircraft. This topic of *Measures of Effectiveness* has attracted much attention in recent times, particularly in the U.S.A. where the Association of Old Crows has recently completed a study for the DoD on this topic [16].

6.3 EW Test Data Analysis

As discussed in section 4.2, a comprehensive tool is required for the parametric analysis of EW test data and its correlation with simulator and/or EW environment/equipment modelling outputs. The lack of such capabilities in the past is believed to have contributed much to the apparent differences between equipment and aircraft EW test results. Such a new tool has been specified and ordered by BAe which will enable, in addition to the near real-time correlation capability of the ECM RMS (cf. 6.2), post-test analysis of aircraft avionics/EW equipment data and threat simulator data. This includes correlation of simulator-generated data with that of the EW system under test and subsequent time history and statistical analysis. Multi-parametric comparison of test and simulator data against engineer-defined correlation 'windows' can also be carried out automatically.

In combination with

- precise scenario definitions,
- capable and realistic simulation,
- the ECM RMS, and
- a controlled, anechoic chamber electromagnetic environment,

this new generation of EW analysis tool, enabled by computing advances in recent years, will enable quantitative and repeatable EW equipment, sub-system and on-aircraft tests.

6.4 The Need for Correlated EO and RF Threat Simulation

The importance of precise specification of the EO environment and scenarios is covered in section 4.4. For T&E of EO equipments there is a need therefore for the generation of appropriate stimulus for irradiation of sensors and post-sensor injection. In the case of lasers this is fairly straight forward for the post-sensor and direct irradiation of the sensor (via a closed 'hood') cases for un-installed equipment and avionic rig work.

For the future, the use of multi-spectral sensors, data fusion, knowledge-based systems and fully integrated weapons systems on aircraft mean that it will be necessary to provide co-ordinated RF/EO stimulus to the EW system, particularly of IR/UV Missile/Laser Warners and ESM-ESM, and other aircraft RF/EO sensors.

This poses a T&E problem as free space firing of lasers poses a safety hazard and there are no established IR/UV simulators akin to the well established radar/RF ones. Development work on such simulators is in progress in the U.S.A. and the Real-Time IR Scene Simulator (RISS) by Amherst Inc., which can also have UV capability, is believed to be the world leader at this time. Figure 10 gives a block diagram of the RISS. Use of such a system in conjunction with a RF threat simulator and laser irradiation and control system, will enable controlled and simultaneous multi-spectral stimulation of aircraft Forward Looking IR, IR Search & Track, passive Missile Warning Systems and Missile/Weapon Guidance Seekers. The use of such a comprehensive sensor stimulation suite in conjunction with an anechoic chamber may offer significant test quality and cost/timescale improvements on the combined aircraft ground and flight trials currently necessary to develop and clear such systems into service.

7. IMPROVED EW DESIGN/T&E METHODOLOGY

The thrusts of the previously described improved EW specification, design and T&E methodology are:

- Obtain the agreement of Government agencies on the principle of precise RF/EO EW scenarios pre-contract signature. Work with those agencies and EW equipment suppliers to support timely production of scenarios. Explore further the application of such methodology and tools to the EMC arena.
- Continue driving more of the EW system development process away from the highly expensive and time consuming flight test phase, through avionic rig, laboratory and aircraft in anechoic chamber trials, towards suitably validated modelling wherever possible.
- 1995 commissioning by BAe of EWES upgrade, transportable (1.0 MPPS) and (1.5 MPPS) RF threat simulators, transportable ECM Response Measurement System and comprehensive EW data analysis utility.
- Continue investigations of shortcomings of present modelling and T&E tools/techniques, particularly those identified herein and especially those in the area of EO threat simulation and ECM effectiveness modelling/test. Use this data to target improved capabilities to optimise development costs and timescales.
- Build on over 20 years of BAe experience of Operational Analysis, EW environment modelling and EW integration rig and aircraft trials work. Work with EW equipment suppliers to ensure affordable and mission effective EW system solutions for military aircraft, whether upgrades or on new airframes. Use of these Industry capabilities can lead, in co-operation with Government/Air Force agencies, to much increased quality specifications leading to aircraft weapon systems which are fully fit for purpose at the most affordable price.

8. CONCLUSIONS

BAe Defence Military Aircraft Division has learned many lessons from its 20+ years of involvement in EW equipment installed on its military aircraft. It has enacted most of the recommendations of internal study reports on its performance in this area and this year will augment upgraded EW environment and Operational Analysis modelling tools with major world-class EW test capabilities.

This paper has highlighted a number of the issues involved in the specification, design, development and test of EW systems and concludes that the dominant factor in many of the key areas of Affordability, Mission Effectiveness and Survivability is a precise definition of the electromagnetic environment in which the aircraft and its systems must operate correctly. A revised specification, design and development process has been described which can be used to provide evidence of performance at realistic cost and with maximum integrity. A number of potential enhancements to current generation modelling and test and evaluation tools are identified and BAe research and development work is ongoing in these areas.

With environment and scenario modelling tools and techniques in place, it is believed that Air Forces, Industry and Governments alike would all benefit from this precise and unambiguous definition of the radio/radar and electro-optic environments at the pre-contract stage for new or upgraded EW equipments.

9. ACKNOWLEDGEMENTS

The authors wish to thank BAe Defence (MAD) for permission to publish and acknowledge input/comment from: G. Slater (RMPA DASS Manager), C.D.Hinds (EF2000 DASS Manager), Dr. C.P. Loller (Head of EW & Stealth Facilities), K. Lawton (Specialist, EW Testing), K. Smith (Operational Analysis), I.P. MacDiarmid (EM Hazards Specialist) and Prof. R.J. Simpson (Univ. of Central Lancashire, U.K.). Acknowledgement is also made for material used in the paper/presentation to: Messrs. Peter Crouch, Data Sciences (U.K.) Ltd. [EWES], Larry Diamond & Joe Gorelick, Advanced Systems Development Inc. [AMES II] and Bob Cockrell & Larry Robinson, Amherst Systems Inc. [CEESIM and RISS].

10. REFERENCES

1. **Wade**, L. (Condor Systems) "The Significance of a Valid Threat Data Base to Effective Radar Warning Receivers." Presentation at Tutorial Session at 1994 Int. Symp. of the Association of Old Crows, Washington, D.C. October 1994.
2. **Audone**, B. "The Electromagnetic Threat to Future Avionic Systems." AGARD Conf. Proc. No. 417: "The Design, Development and Testing of Complex Avionic Systems," Las Vegas, U.S.A. 27 April - 1 May, 1987. [Unclassified]
3. **Cabayan**, H.S. "Current Status of High Power Microwave Effects and Simulation." High Power Microwave Systems for Defense Conference, Air Force Weapons Laboratory, Albuquerque, New Mexico, U.S.A., December 1-5, 1986 [Unclassified]
4. **Herskovitz**, D. "Killing Them Softly." J. Electronic Defense, August 1993, pp.41-46.
5. **Bolino**, J.V. *et al.* "Threat Simulator Validation", J. Electronic Defense, September 1991, p.40.
6. **Woolnough**, R.C.N. and **Pywell**, M. "The Control of RF Radiation Hazards in an Industrial and Airfield Environment." I.E.E. 9th Int. Conf. on EMC, Univ. of Manchester, U.K. , 5-7 September 1994.
7. **Elton**, L.D. RF Environment External to Aircraft. Vol.1, Issue 2a: "The Calculation of Aircraft Safe Distances for the Definition of High Intensity Radio Transmission Areas (HIRTA) in the United Kingdom." BAeSEMA report MNC 00220, September 1992. [Unclassified]. Vol.2: "Ship and Aircraft based Transmitters." March 1992. [Classified].
8. **EUROCAE USER'S GUIDE** FOR AMJ No. XX. Guidance to the Certification of Aircraft Electrical/ Electronic Systems for Operation in the High Intensity Radiated Field (HIRF) Environment. (Certification Requirements and Procedures) EUROCAE WG33 Sub-Groups 2&3. Draft Version 2.2, 4 March 1993.
9. **Fossier**, P. "MESA: Modular Interactive Electronic Warfare Simulator suited to the coverage of EW Equipment life cycle." Presented at AGARD Meeting on "Challenge of Future EW System Design," October 1993.
10. **Herskovitz**, D. "Technology Survey: A Sampling of Electronic Warfare Simulators." J. of Electronic Defense, December 1994, pp.56-66.
11. **Peccini**, M., **Veredice**, A., **Formica**, A. and **Conte**, F. "Real-Time E.W. Test Range Simulator." Presented at AGARD Meeting on "Challenge of Future EW System Design," October 1993.
12. **Stallard**, R. "Mobile EW Trials Facilities at DRA Farnborough." Presented at AGARD Meeting on "Challenge of Future EW System Design," October 1993.
13. **Hardy**, S.M. and **Lum**, Z.A. "Simulation Shadowland." J. Electronic Defense, November 1994, pp.38-47,67.

14.**Schleher**, C.D., "Introduction to Electronic Warfare." Artech House (1990). ISBN 0-89006-142-4. p.38, Tab. 1-7.
15.**Teris**, M. "Current ECM Evaluation Methods." Article in J. Electronic Defense, January 1995 supplement; adapted from "Penetrator - An Integrated EW Encounter Simulation," Topics of Engineering, Vol.V, Pub.: AIL Systems, 1994.
16.**Porter**, Rusty (AOC President): "Taking the Measure of EW's Effectiveness". J. Electronic Defense, Vol.18, No.1, January 1995, p.12 and Vol.18, No.4, April 1995, p.10.

Figure 1: Typical Aircraft EW Suite

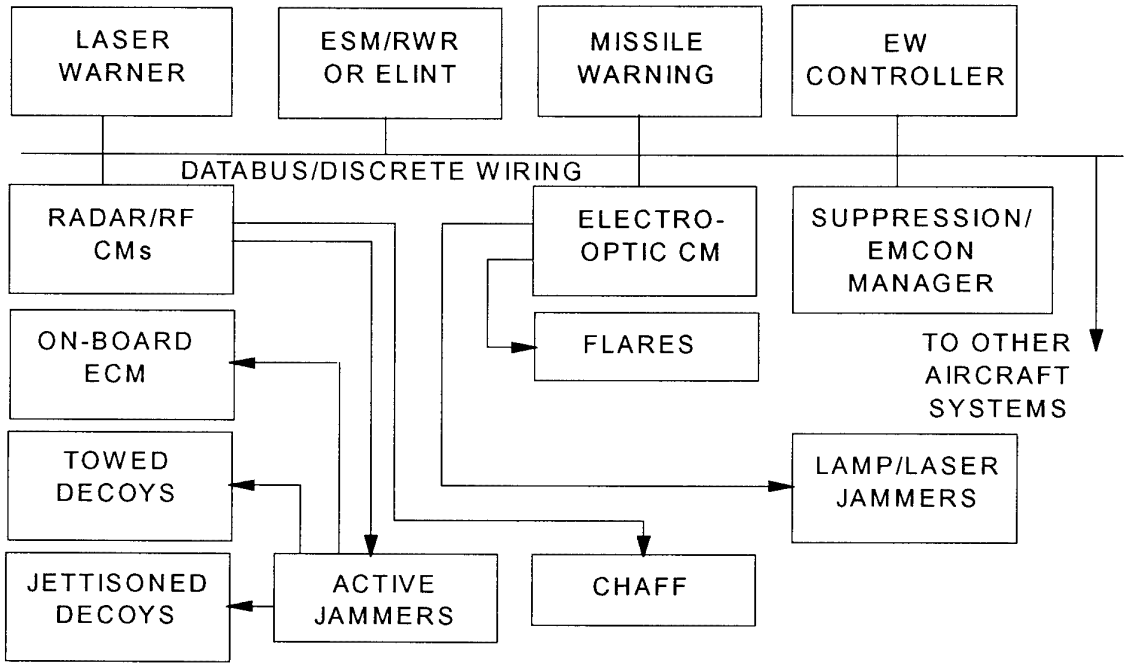

Figure 2: Block Diagram of EWES and ASWEM

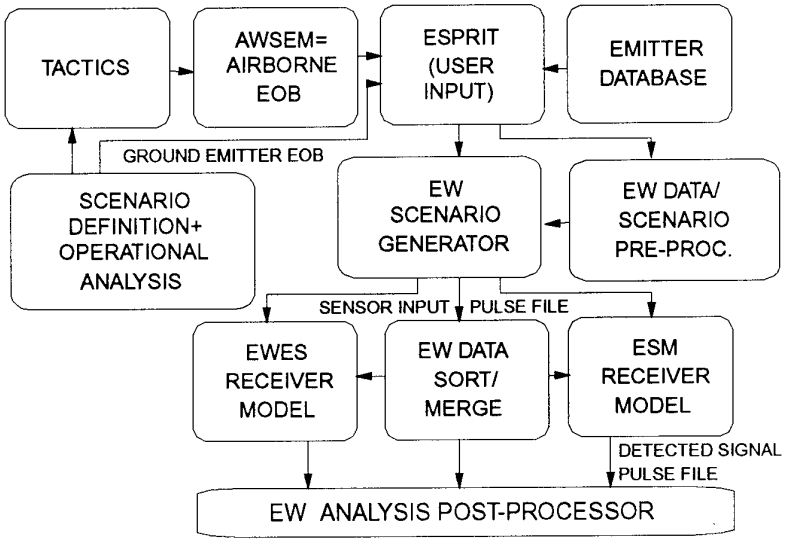

Key to Figure 2:

- Threat Scenario Definition = descriptive + initial conditions
- Operation Analysis: Tactics and engagement rules into AWSEM = Electronic Order of Battle (EOB)
- EOB comprises platform manoeuvres and events plus emitter events (e.g. mode changes)
- Enhanced Scenario Preparation Interactive Tool (ESPRIT) is prime Graphical User Interface.
- ESPRIT output = full scenario manoeuvres and EOB list for input into Scenario Generator.
- EW Data and Scenario Pre-Processors are optional.
- EW Data Sort/Merge Utility, used for very large scenarios, is also optional.
- BAe currently have all but EWES Receiver Model and Scenario Pre-Processor.

Figure 3: Computing Resources for EWES

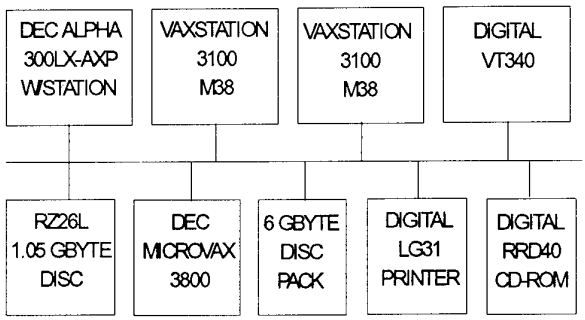

Figure 4: Use of Modelling in Validation of ESM Performance

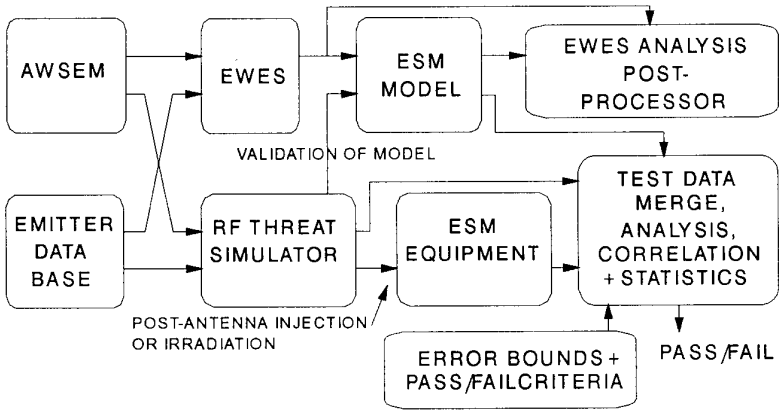

Figure 5: Typical ESPRIT Tactical Scenario Display

Figure 6: Typical EW Scenario Generator Pulse Descriptor File Listing

TYPE	ID	NAME	RF MHz	RFVAR %	LENGTH microsec	PLAT BRG degs	PLAT ELEVN degs	AMPLITUDE dBW/m**2	RANGE km	INTERVAL ms	POL ANGLE degs	RATIO %	TIME hh:mm:ss
pulse	8	FIREX	2700.00	0.0	15.00	228.45	0.0	-64.871	100.00	0.234	0.0	100.00	00:00:00.000461411
pulse	8	FIREX	2700.00	0.0	15.00	230.14	0.0	-64.560	100.00	0.230	0.0	100.00	00:00:00.000694916
pulse	8	FIREX	2700.00	0.0	15.00	231.79	0.0	-64.255	100.00	0.226	0.0	100.00	00:00:00.000924889
pulse	8	FIREX	2700.00	0.0	15.00	233.42	0.0	-64.070	100.00	0.274	0.0	100.00	00:00:00.001150917
pulse	1	REDEW	3000.00	0.0	10.00	233.54	0.0	-65.514	300.11	0.200	0.0	100.00	00:00:00.001167467
pulse	6	DETEW	7400.00	0.0	3.70	233.71	0.0	-81.633	288.47	0.420	0.0	100.00	00:00:00.001191417
pulse	5	SEATE	9350.00	0.0	20.00	234.07	0.0	-96.877	340.68	0.300	0.0	100.00	00:00:00.001241425
pulse	3	CANAB	9700.00	0.0	12.00	234.92	0.0	-88.506	200.01	2.000	0.0	100.00	00:00:00.001360138
pulse	7	VRA	15624.39	0.0	5.00	234.97	0.0	-96.671	384.73	0.650	0.0	100.00	00:00:00.001365903
pulse	1	REDEW	3000.00	0.0	10.00	234.98	0.0	-64.394	300.11	0.150	0.0	100.00	00:00:00.001367467
pulse	8	FIREX	2700.00	0.0	15.00	235.39	0.0	-64.42	100.00	0.230	0.0	100.00	00:00:00.001424470

Figure 7: Commonly Used EW Graphical Analysis Pages

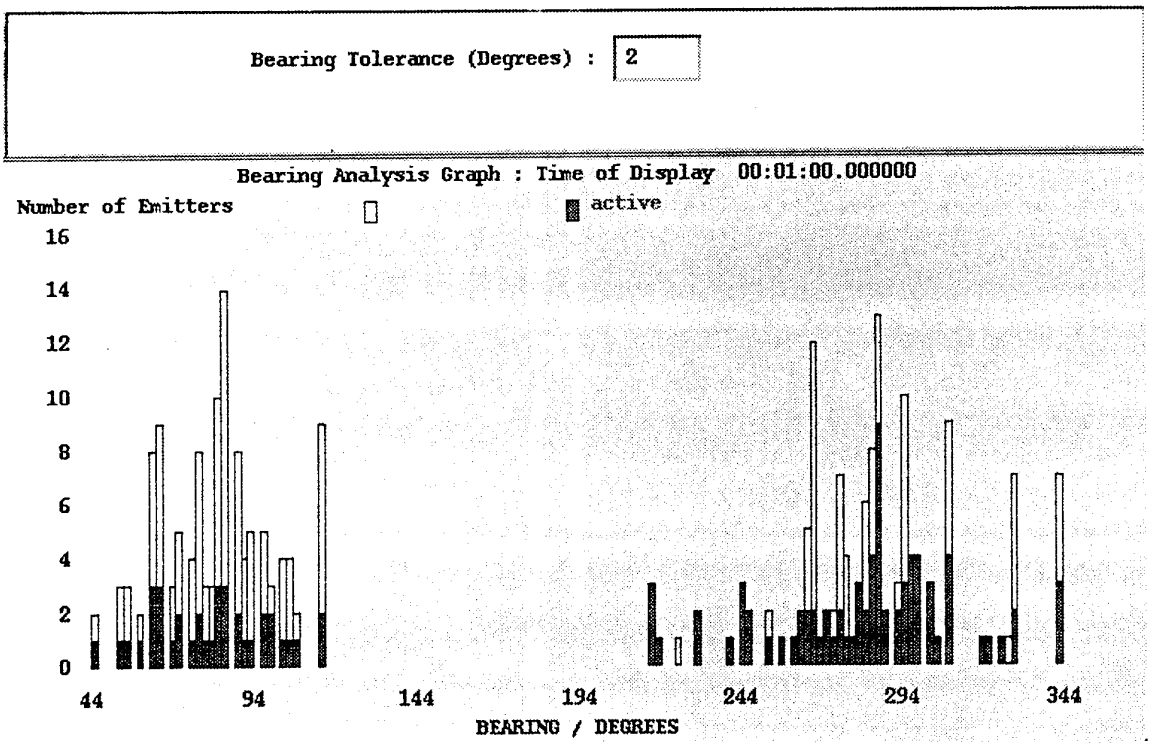

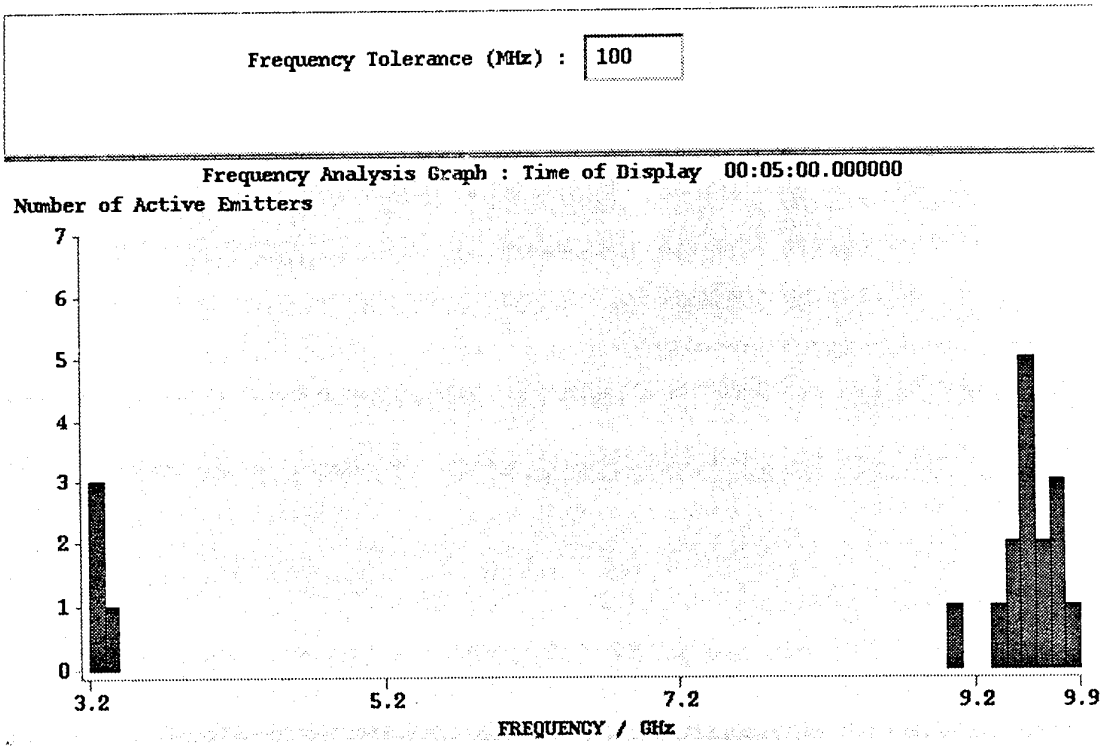

Table 1: EW Development Life Cycle:

Air Force/Government Agency	Operational Requirement
	Weapon System Specification
	Air Vehicle Specification
Aircraft Prime Contractor	System/Equipment Specifications
EW Equipment Manufacturer	Hardware/Software Specifications
	Design/Build/Code Hardware/Software
	Equipment and EW Sub-System test
Aircraft/Systems Integrator	Avionic integration rig tests; aircraft ground and flight tests.
	Corrections/Modifications and specification changes if necessary.
Air Force	Operational Evaluation leading to Initial Operational Clearance.
All parties	Changes/corrections leading to Final Operational Clearance.

Table 2: Earlier Discovery of EW Systems Integration Problems

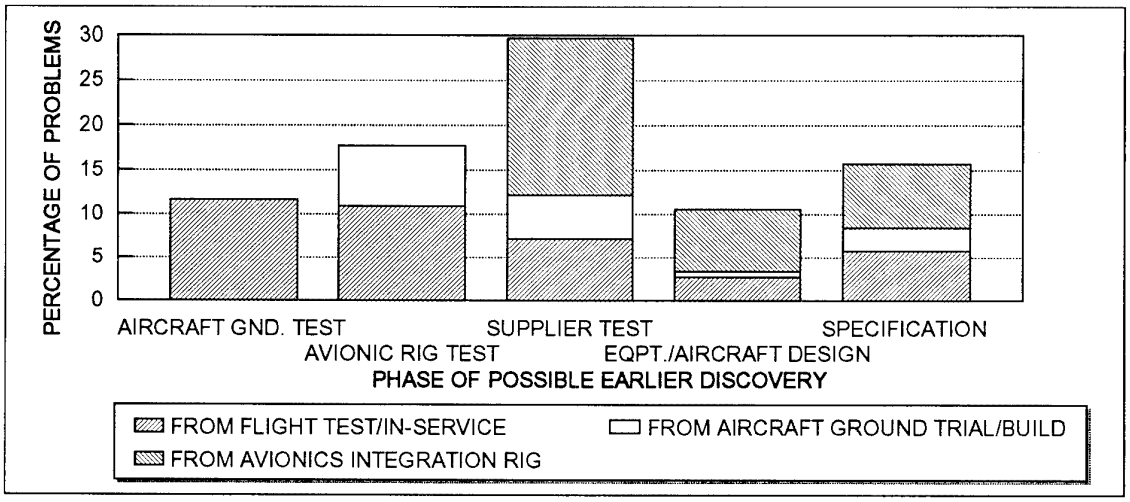

Table 3: Development Test/Evaluation Locations and Technique

Who/Where	What and How
Aircraft & EW manufacturers: Own premises.	Environment/EW equipment modelling via use of EWES-type models and proprietry/generic equipment models
EW equipment manufacturer: Own premises.	Rig test: software, hardware, equipment, sub-system. Post-sensor injection; free space irradiation; anechoic chamber.
Aircraft/Systems Integrator: Sub-System Rig, Avionic Integration Rig	Progressive integration of equipment and sub-systems into full aircraft weapon system. Post-sensor injection and limited free space irradiation.
Airfield (e.g. Warton, U.K.)	Open air EW and EMC tests. RCS measurement, DOA measurements. Free space irradiation of installed EW equipments.
Anechoic chamber (U.K.)	Whole aircraft EW tests in secure and controlled electromagnetic environment. Irradiation using RF simulator and response measurement system for ESM/ECM.
Locally (North U.K.)	Local flight trials, covering test points now yet done + confirmation of selected items tested earlier. Signal generator(s)/threat simulator + amplifier/antenna.
e.g. RAF Spadeadam EW Training Range, Aberporth , BAe's North Sea Combat Range.	U.K. Flight trials: DOA, antenna coverage, EW performance demonstration. Irradiation by simulators/emulators, real radars; often involving other platforms.
U.S. anechoic chamber, e.g. Benefield Anechoic Facility, California.	Tests where either aircraft size or test requirements, e.g. multi-aircraft, dictate out-of-U.K. tests.
U.S. EW Flight test ranges: Nellis, Eglin, China Lake, Patuxtent River.	Tests not possible with U.K./E.C. facilities, e.g. full aircraft in-flight RCS measurement and total weapon system performance in realistically dense RF environments. Free space irradiation with many emitter types and numbers.

Figure 8: AMES II Block Diagram

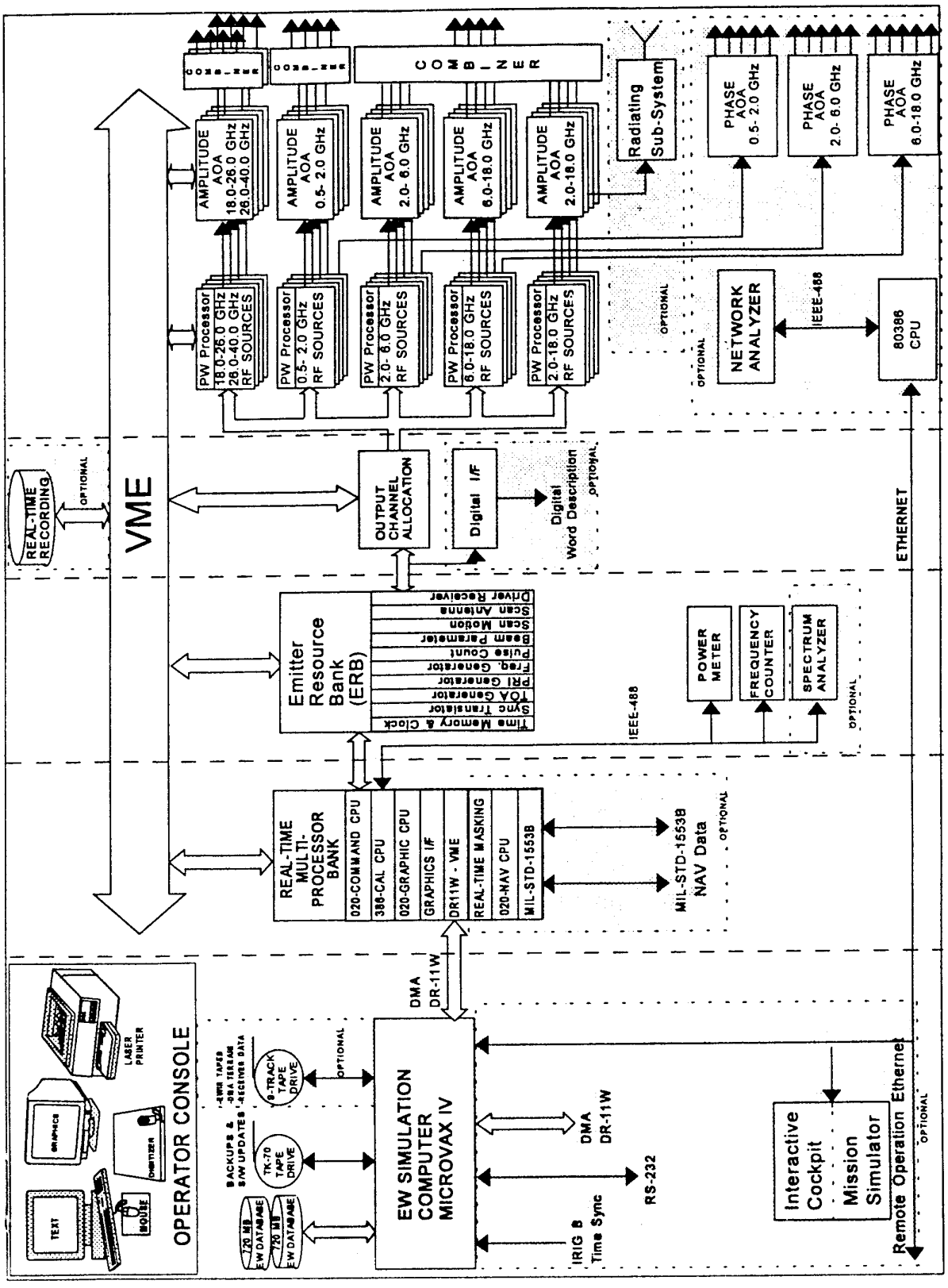

Figure 9: CEESIM Block Diagram

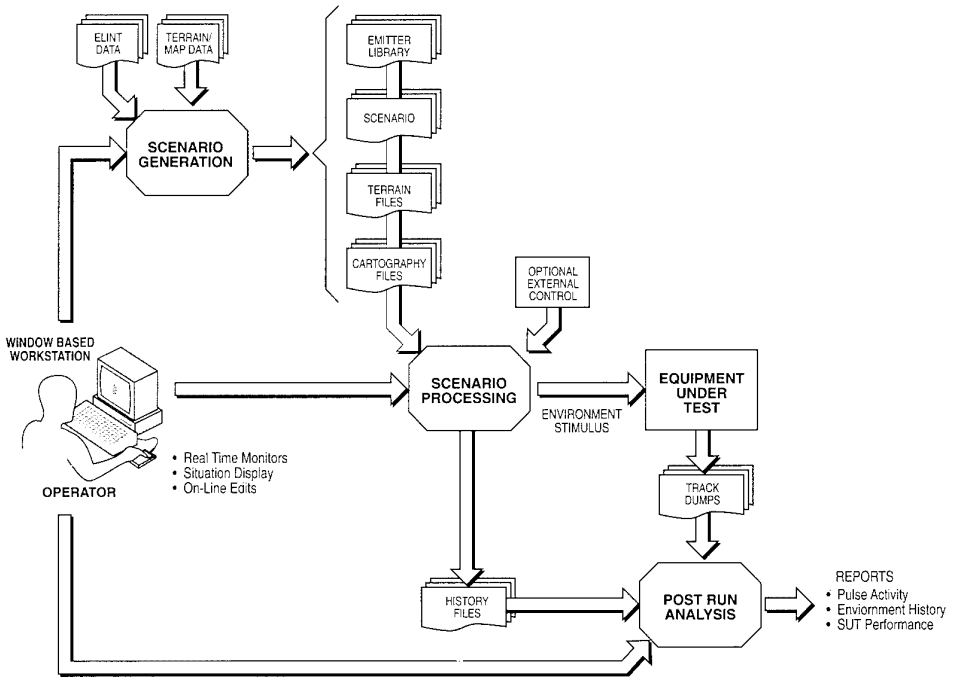

Figure 10: Real-Time Infra-Red Scene Simulation System

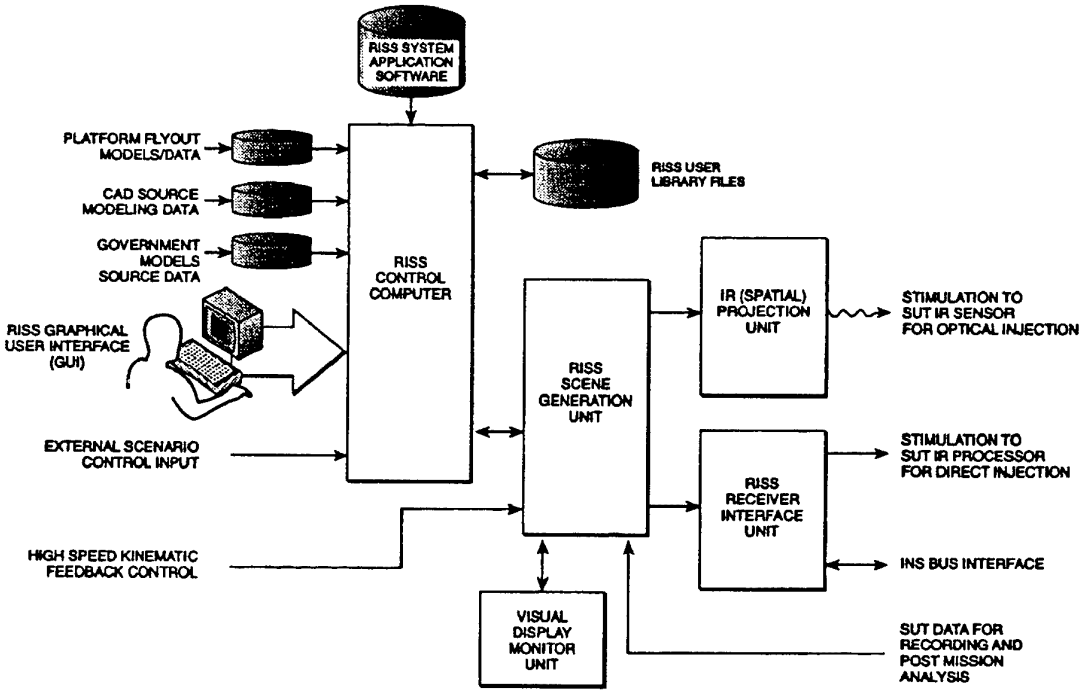

REPORT DOCUMENTATION PAGE

1. Recipient's Reference	2. Originator's Reference	3. Further Reference	4. Security Classification of Document
	AGARD-CP-573	ISBN 92-836-1028-8	UNCLASSIFIED/ UNLIMITED

5. Originator Advisory Group for Aerospace Research and Development
North Atlantic Treaty Organization
7 rue Ancelle, 92200 Neuilly-sur-Seine, France

6. Title

Environmental Factors in Electronic Warfare Related to Aerospace Systems

7. Presented at/sponsored by

The Sensor and Propagation Panel Symposium, held at Pratica di Mare AFB (Rome), Italy 8-11 May 1995.

8. Author(s)/Editor(s)	9. Date
Multiple	January 1996
10. Author's/Editor's Address	**11. Pages**
Multiple	156

12. Distribution Statement There are no restrictions on the distribution of this document. Information about the availability of this and other AGARD unclassified publications is given on the back cover.

13. Keywords/Descriptors

Electronic warfare	Adaptive systems
Terrain	Survivability
Direction finding	Vulnerability
Scenarios	Obscuration
Threat evaluation	Camouflage
Sensors	Jamming
Electronic countermeasures	Antijamming
Electronic support measures	LPI (Low Probability of Intercept)
Wave propagation	Modelling

14. Abstract

This publication reports the unclassified papers presented at a specialists' meeting held by the Sensor and Propagation Panel at its Spring 1995 meeting.

The topics covered included:

— Survey of threat and EW scenarios for aerospace systems;

— Relevant environmental effects with respect to aerospace systems in the applicable portions in the entire spectrum from optical/infrared frequencies to the ELF range;

— Environmental control (including artificial modification of propagation media);

— Aerospace system aspects;

— Advances in environment-oriented EW-analysis and modelling as related to aerospace systems;

— Environmental aspects of emerging EW-concepts and future outlook with the focus on aerospace systems.

AGARD

NATO OTAN

7 RUE ANCELLE • 92200 NEUILLY-SUR-SEINE

FRANCE

Télécopie (1)47.38.57.99 • Télex 610 176

DIFFUSION DES PUBLICATIONS

AGARD NON CLASSIFIEES

Aucun stock de publications n'a existé à AGARD. A partir de 1993, AGARD détiendra un stock limité des publications associées aux cycles de conférences et cours spéciaux ainsi que les AGARDographies et les rapports des groupes de travail, organisés et publiés à partir de 1993 inclus. Les demandes de renseignements doivent être adressées à AGARD par lettre ou par fax à l'adresse indiquée ci-dessus. *Veuillez ne pas téléphoner.* La diffusion initiale de toutes les publications de l'AGARD est effectuée auprès des pays membres de l'OTAN par l'intermédiaire des centres de distribution nationaux indiqués ci-dessous. Des exemplaires supplémentaires peuvent parfois être obtenus auprès de ces centres (à l'exception des Etats-Unis). Si vous souhaitez recevoir toutes les publications de l'AGARD, ou simplement celles qui concernent certains Panels, vous pouvez demander à être inclu sur la liste d'envoi de l'un de ces centres. Les publications de l'AGARD sont en vente auprès des agences indiquées ci-dessous, sous forme de photocopie ou de microfiche.

CENTRES DE DIFFUSION NATIONAUX

ALLEMAGNE
Fachinformationszentrum Karlsruhe
D-76344 Eggenstein-Leopoldshafen 2

BELGIQUE
Coordonnateur AGARD-VSL
Etat-major de la Force aérienne
Quartier Reine Elisabeth
Rue d'Evere, 1140 Bruxelles

CANADA
Directeur, Services d'information scientifique
Ministère de la Défense nationale
Ottawa, Ontario K1A 0K2

DANEMARK
Danish Defence Research Establishment
Ryvangs Allé 1
P.O. Box 2715
DK-2100 Copenhagen Ø

ESPAGNE
INTA (AGARD Publications)
Pintor Rosales 34
28008 Madrid

ETATS-UNIS
NASA Headquarters
Code JOB-1
Washington, D.C. 20546

FRANCE
O.N.E.R.A. (Direction)
29, Avenue de la Division Leclerc
92322 Châtillon Cedex

GRECE
Hellenic Air Force
Air War College
Scientific and Technical Library
Dekelia Air Force Base
Dekelia, Athens TGA 1010

ISLANDE
Director of Aviation
c/o Flugrad
Reykjavik

ITALIE
Aeronautica Militare
Ufficio del Delegato Nazionale all'AGARD
Aeroporto Pratica di Mare
00040 Pomezia (Roma)

LUXEMBOURG
Voir Belgique

NORVEGE
Norwegian Defence Research Establishment
Attn: Biblioteket
P.O. Box 25
N-2007 Kjeller

PAYS-BAS
Netherlands Delegation to AGARD
National Aerospace Laboratory NLR
P.O. Box 90502
1006 BM Amsterdam

PORTUGAL
Estado Maior da Força Aérea
SDFA - Centro de Documentação
Alfragide
2700 Amadora

ROYAUME-UNI
Defence Research Information Centre
Kentigern House
65 Brown Street
Glasgow G2 8EX

TURQUIE
Millî Savunma Başkanliği (MSB)
ARGE Dairesi Başkanliği (MSB)
06650 Bakanliklar-Ankara

Le centre de distribution national des Etats-Unis ne détient PAS de stocks des publications de l'AGARD.
D'éventuelles demandes de photocopies doivent être formulées directement auprès du NASA Center for AeroSpace Information (CASI) à l'adresse ci-dessous. Toute notification de changement d'adresse doit être fait également auprès de CASI.

AGENCES DE VENTE

NASA Center for
AeroSpace Information (CASI)
800 Elkridge Landing Road
Linthicum Heights, MD 21090-2934
Etats-Unis

ESA/Information Retrieval Service
European Space Agency
10, rue Mario Nikis
75015 Paris
France

The British Library
Document Supply Division
Boston Spa, Wetherby
West Yorkshire LS23 7BQ
Royaume-Uni

Les demandes de microfiches ou de photocopies de documents AGARD (y compris les demandes faites auprès du CASI) doivent comporter la dénomination AGARD, ainsi que le numéro de série d'AGARD (par exemple AGARD-AG-315). Des informations analogues, telles que le titre et la date de publication sont souhaitables. Veuiller noter qu'il y a lieu de spécifier AGARD-R-nnn et AGARD-AR-nnn lors de la commande des rapports AGARD et des rapports consultatifs AGARD respectivement. Des références bibliographiques complètes ainsi que des résumés des publications AGARD figurent dans les journaux suivants:

Scientific and Technical Aerospace Reports (STAR)
publié par la NASA Scientific and Technical
Information Division
NASA Headquarters (JTT)
Washington D.C. 20546
Etats-Unis

Government Reports Announcements and Index (GRA&I)
publié par le National Technical Information Service
Springfield
Virginia 22161
Etats-Unis
(accessible également en mode interactif dans la base de
données bibliographiques en ligne du NTIS, et sur CD-ROM)

Imprimé par le Groupe Communication Canada
45, boul. Sacré-Cœur, Hull (Québec), Canada K1A 0S7